Cyclical neurogenesis and neurodegeneration in the colonial tunicate *Botryllus schlosseri*

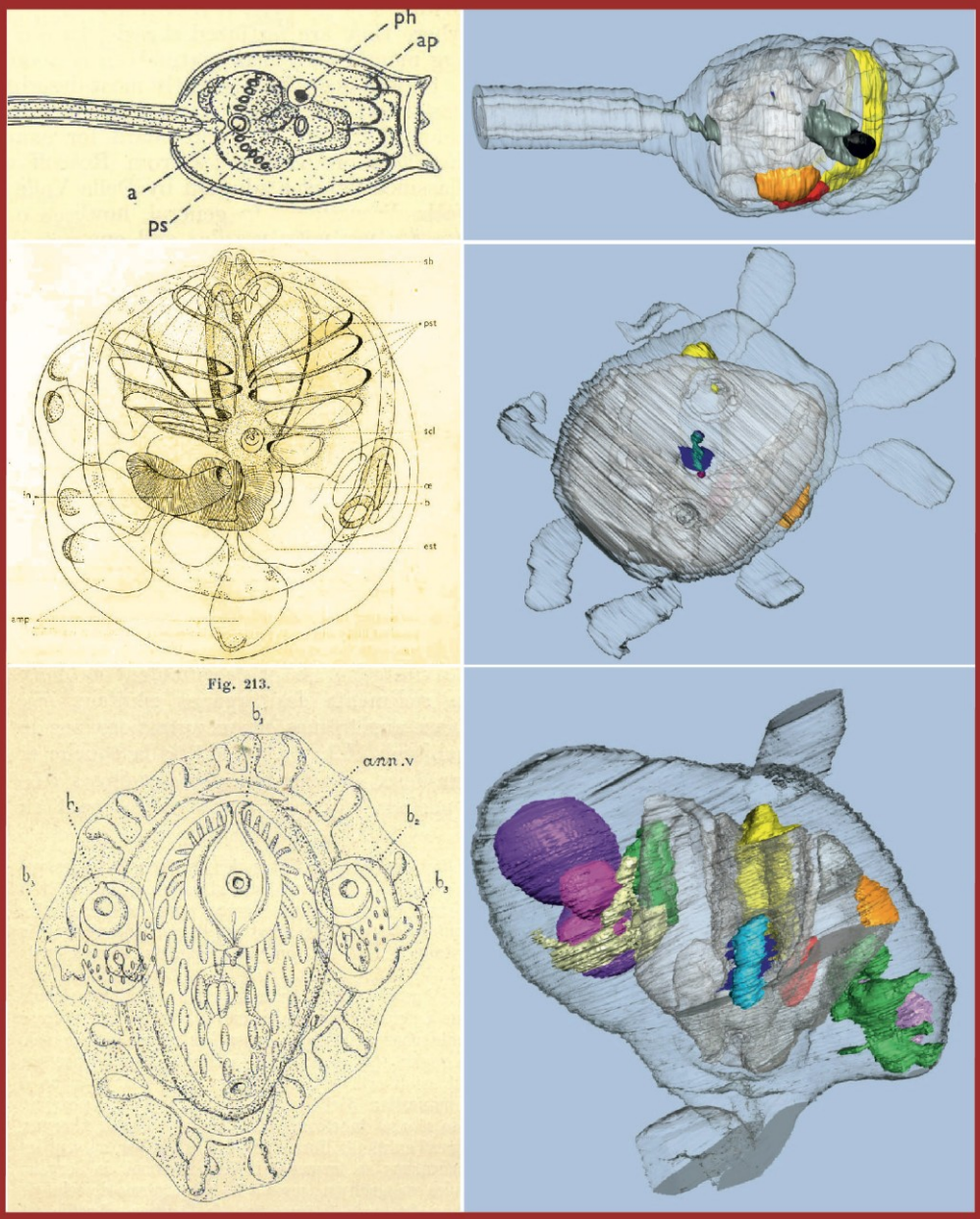

Chiara Anselmi

Cyclical neurogenesis and neurodegeneration in the colonial tunicate *Botryllus schlosseri*
Chiara Anselmi-University of Padova- PhD Thesis

Cover:

- Swimming tadpole larvae *Botryllus schlosseri*, Berril (1950).
- Oozoid of *Botryllus schlosseri*, Grassè (1948).
- Colony of *Botryllus schlosseri,* Delage and Herouard (1898).
- 3D reconstruction of swimming tadpole larva. Chapter 2
- 3D reconstruction of oozoid. Chapter 2
- 3D reconstruction of bud. Chapter 2

Università degli Studi di Padova

Head Office: Università degli Studi di Padova

Department of Biology

Ph.D. COURSE IN: BIOSCIENCES
CURRICULUM: CELL BIOLOGY AND PHYSIOLOGY
SERIES XXXI

CYCLICAL NEUROGENESIS AND NEURODEGENERATION IN THE COLONIAL TUNICATE *BOTRYLLUS SCHLOSSERI*

Coordinator: Prof. Ildikò Szabò
Supervisor: Prof. Lucia Manni

Ph.D. student: Chiara Anselmi

TABLE OF CONTENT

ABSTRACT

In this work, we studied the nervous and sensory system of the colonial ascidian *Botryllus schlosseri* during the development of embryos, buds, and in adult individuals belonging to young and old colonies. *B. schlosseri* is a colonial ascidian in which individuals (blastozooids) are organized in star-shaped systems. In a colony, sexual and asexual reproductions are coordinated and cyclical. Moreover, three generations of zooids coexist: adults (filter-feeding individuals), their buds (primary buds), and the budlets (secondary buds) produced by buds. Cyclically, during a phase called takeover, adult zooids are reabsorbed by the colony and are replaced in physiological activities by their buds that become adults. Cuncurrently, budlets mature into buds and produce a new generation of budlets.

We first reviewed historical studies concerning *B. schlosseri* with the intent of characterizing the colony life cycle and bud development. We then compared nervous system formation in two different developmental pathways, embryogenesis and blastogenesis. Since *B. schlosseri* has internal fertilization and development, we developed a method for culturing embryos *in vitro*. Using a combination of *in vivo*, confocal, histological observations, and 3D reconstructions based on serial sections, we described the embryonic development and drafted a timetable. Next, we sequenced transcriptomes of embryos and buds at several stages and illuminated the strict temporal relationship between morphogenetic events and the expression pattern of genes associated with the nervous system during the formation of the larval brain, its degeneration at metamorphosis, the adult brain formation in embryo and bud, and its degeneration at takeover.

We also studied the nervous system in adult individuals belonging to colonies of different ages. We observed that the number of brain cells changes throughout the adult zooid life following a specific trend. Transmission electron microscopy and TUNEL assays on adult brains showed that apoptosis is involved in neurodegeneration and the number of immunocytes contacting or infiltrating the brain increase in number during the adult life. Changes in brain cell number parallel changes in sensory cell number. We developed two novel behavioural experiments for *B. schlosseri*, which showed that zooid ability to respond to mechanical stimuli parallels changes in the number of brain and sensory cells. Then we compared adult individuals belonging to young and old

colonies and found that aging influences both nervous system morphology and behaviour. We analysed differentially expressed genes in brains of individuals belonging to young and old colonies and found that the old colonies exhibit a gene pattern associated with several human neurodegenerative diseases, such as the Alzheimer's disease.

Finally, we studied, the coronal organ, a mechanoreceptor located on the tentacles, in the oral siphon. We analysed its cytodifferentiation during asexual reproduction and we documented the mechanosensorial impairment caused by gentamicin at morphological and behavioural level. In mammals gentamicin can destroy both hair cells and their innervating neurons. The pre-treatment with fenofibrate, a gentamicin protector, followed by a treatment with gentamicin, resulted in no significant effect on animal behaviour. These results support the hypothesis of homology between vertebrate hair cells and tunicate coronal sensory cells.

In conclusion, the research presented here shows that *B. schlosseri* can be considered a useful model species for analysing the development of the central nervous system and sensory system, as well as its degeneration as caused by drugs, metamorphosis, takeover and aging. Additionally, the species' different developmental pathways allow for interesting evolutionary comparisons, at both the morphological and molecular level, that can help improve scientific understanding of the origin of the animal phenotype.

SUMMARY

The aim of this thesis is to present my research conducted during three years of work as PhD student in the School of Bioscience of the University of Padova (Italy). The subject of the work was to study nervous and sensory systems of the colonial ascidian *Botryllus schlosseri* during the development of embryos, buds, and in adult individuals belonging to young and old colonies. *B. schlosseri* is a colonial ascidian in which individuals (blastozooids) are organized in star-shaped systems. In a colony, sexual and asexual reproductions are coordinated and cyclical. Three generations of zooids coexist: the adult (filter-feeding individuals), their buds (primary buds), and the budlets (secondary buds) produced by buds. Cyclically, during a phase called takeover, adult zooids are resorbed by the colony and are replaced in physiological activities by their buds, the latter become adults while budlets mature into buds and produce a new generation of budlets.

In this thesis, I first present a review of the historical reports concerning *B. schlosseri* with the intent of characterizing the colony life cycle and bud development. Experiments performed to analyse variations in bud productivity, zooid growth, bilateral asymmetry (including the induction of the *situs inversus viscerum*), and the alternative budding from circulating haemocytes (vascular budding) are described. Moreovere, the results of experiments using zooid and bud removal to study the cross talk between consecutive blastogenetic generations and to induce vascular budding are discussed. The genetic experiments demonstrating that the ability of two distinct colonies to fuse or reject is controlled by a single polymorphic gene locus (BHF) with multiple, co-dominantly expressed alleles are summarised. Finally, a part describes how the ability of colonies to fuse and create chimeras has been used to demonstrate that, within a chimera, somatic and germline stem cells compete to populate niches and regenerate tissue or germline organs. Building upon the results obtained over 60 years of study, we propose that new technological advances can be used to expand the study of *B. schlosseri* traits and to understand the functional relationships between its genome and its phenotype.

I also used *B. schlosseri* to compare the nervous system formation in embryogenesis and blastogenesis, two different developmental pathways. Since *B. schlosseri* has internal fertilization and development, a method for culturing embryos *in vitro* was

developed. Using a combination of *in vivo*, confocal, and histological observations, and 3D reconstructions based on serial sections, a timeline describing embryonic development was produced. Then transcriptomes of embryos and buds at several stages were sequenced and compared. The data show a well-defined temporal relationship between the morphogenetic events and the expression pattern of genes associated with the nervous system during the formation of the larval brain, its degeneration at metamorphosis, the adult brain formation in embryo and bud, and its degeneration at takeover.

Next, I focused the attention on the nervous system of adult individuals belonging to colonies of different ages. Adult zooids at three life stages: individuals in early-cycle (*i.e.*, zooids that had just opened their siphons), in mid-cycle, and late-cycle (*i.e.*, before their degeneration and reabsorption at takeover) were mainly considered. Surprisingly, the number of brain cells changes throughout the adult zooid life, reaching its maximum in mid-cycle. Subsequently, the cell number decreases until the complete brain reabsorption during the takeover, suggesting that, brain degeneration begins during the adult life when zooids are still active. Transmission electron microscopy and TUNEL assays were used to show that apoptosis is involved in neurodegeneration in adult brain and that the number of immunocytes contacting or infiltrating the brain increase in number during adult life. Changes in brain cell number parallel changes in sensory cell number. Two novel behavioural experiments for *B. schlosseri*, never performed before, were developed and showed that zooid ability to respond to mechanical stimuli parallel changes in the number of brain and sensory cells. The comparison between adult individuals belonging to young and old colonies demonstrated that the latter are characterised by fewer brain cells and decreased behavioural responses. Differentially expressed genes in the brains of individuals belonging to young and old colonies were analysed. Interesting, the old colonies exhibit a gene pattern associated with several human neurodegenerative diseases, such as Alzheimer's disease. All these data indicate that *B. schlosseri* can serve as a useful model for studying mechanisms of adult neurogenesis and neurodegeneration.

Finally, I studied the coronal organ, a mechanoreceptor that is located on the tentacles at the base of the oral siphon. The function of this organ is to check particles entering the siphon within the seawater flow and to induce a squirting reaction when dangerous particles are detected. This reaction causes the violent expulsion of water (and particles)

form the branchial chamber. Coronal sensory cells are considered homologous to vertebrate hair cells. The coronal organ cytodifferentiation during asexual reproduction was analysed following the main phases of oral tentacle development, neurite growth toward the presumptive sensory area, coronal cells differentiation, and synapsis formation. The mechanosensorial impairment caused by gentamicin was also evidenced at morphological and behavioural level. In mammals, aminoglycoside antibiotics, like gentamicin, can destroy both hair cells and their innervating neurons. Scanning Electron Microscopy was used to investigate the morphology of the coronal organ of adult zooids in colonies treated with gentamicin and compared with a control group. Control colonies showed a continuous row of ciliated cells, the typical arrangement of the coronal organ. In treated colonies the continuity of this row was altered by scattered interruptions. The administration of gentamicin increased the absence of the squirting reaction. The pre-treatment with fenofibrate, a gentamicin protector, followed by a treatment with gentamicin resulted in no significant effect on animal behaviour. Finally, treatment with only fenofibrate did not affect zooid behaviour. These results indicate that fenofibrate has a strong protective effect on coronal sensory cell gentamicin-induced toxicity, as occurs in vertebrate hair cells and support the hypothesis of homology between vertebrate hair cells and tunicate coronal sensory cells.

In conclusion, the research presented in this thesis show that *B. schlosseri* can be considered a useful model species to analyse both the development of the central nervous system and sensory system, as well as their degeneration as caused by drugs, metamorphosis, takeover and aging. Moreover, on account of its different developmental pathways, the species allows for interesting evolutionary comparisons at the morphological and molecular level that can improve scientific understanding of the origin of the animal phenotype.

INTRODUCTION

Botryllus schlosseri is an ascidian with sexual and asexual reproduction. It belongs to the subphylum Tunicata, considered the sister group of Vertebrata within the Phylum Chordata (Delsuc et al. 2018). Its asexual reproduction (or blastogenesis) is characterized by colonies with synchronized waves of budding cycles accompanied by the regression and reabsorption of filtering adults in a phase called takeover. New adult zooids, as represented by mature buds, replace them in the colony. Buds originate from a population of somatic stem cells (Voskoboynik and Weissman 2014). Blastogenesis has been extensively studied in this species (see for review: Manni et al., 2007; 2014; Gasparini et al., 2015; Cima et al., 2015).

During sexual reproduction, which has a strict temporal relationship with blastogenesis, *B. schlosseri* produces a free-swimming tadpole larva that has features common amongst vertebrates: a notochord, a dorsal neural tube, a musculature, and gill slits (Dehal et al., 2002). Although the embryonic development of solitary ascidians has been studied in detail, less is known about the process in colonial species, as they are ovoviviparous or viviparous, with internal fertilization and development.

Ascidian larval and nervous system development has been the subject of numerous, detailed studies. Cell lineage, neuronal circuits, and homologies with the vertebrate nervous system are known and in recent years even neural crest-like cells and placodal areas have been individuated (Meinertzhagen and Okamura 2001; Lemaire et al., 2002; Manni et al., 2004; Gasparini et al., 2013; Patthey et al., 2014; Horie et al., 2018;). This nervous system is destined to regress during larval metamorphosis and be replaced by a new brain, the adult cerebral ganglion, whose origin and organization are less well studied (Manni et al., 1999; Sasakura et al., 2012). It is important to note that a similar cerebral ganglion is formed during blastogenesis in colonial ascidian (Burighel et al., 1998).

The coexistence in *B. schlosseri* of two parallel developmental processes (embryogenesis and blastogenesis) leading to the same adult form - a blastozooid in asexual reproduction, derived from pluripotent/multipotent somatic cells and an oozooid in sexual reproduction, derived from a fertilized egg - raises interesting questions. What are the relationships between these two reproductive strategies? Are there genetic pathways belonging to embryogenesis that were co-opted during the evolution of

blastogenesis? How can the same phenotype be produced from starting points that are so different? How are the larval nervous system and the adult nervous system synchronised in their development, so that at metamorphosis the latter replaces the former? How can opposing phenomena, like the degeneration of the larval brain and the contemporary development of the cerebral ganglion at metamorphosis or the degeneration of adult brain and the contemporary development of bud brain at takeover, coexist? What are the mechanisms protecting the developing brain from neurodegeneration?

Beyond the developmental processes of tunicates, answers to these questions are of great biological relevance to studies examining the evolution of the animal phenotype, regeneration, aging, and human diseases.

In search of answers, the aim of this work is to study the nervous and sensory system of *B. schlosseri* in embryo, in bud, and in adult individuals belonging to young and old colonies.

This thesis is organized in four main Chapters. The first Chapter is a review; Chapters 2-4 are organized as publications, each is introduced by an Abstract, followed by Introduction, Results and Discussion, and Conclusion. A summary conclusion chapter closes the thesis.

In Chapter 1, I reviewed over 60 years of experimental studies on *B. schlosseri* blastogenesis, in order to describe the various strategies that colonies undertake to survive and propagate. These strategies include variations in bud developmental potential, zooid growth potential, duration of generation cycle, and the number of coexisting generations and genotypes (*i.e*., the formation of chimeras). This chapter has been published in collaboration with Dr. Ayelet Voskoboynik of Stanford University (CA, USA). It is in press in the *Journal Developmental Biology* and I am a corresponding author (Manni L., Anselmi C., Cima F., Gasparini1 F., Voskoboynik A., Martini M., Peronato A., Burighel P., Zaniolo G., Ballarin L. Sixty years of experimental studies on the blastogenesis of the colonial tunicate *Botryllus schlosseri.* Developmental Biology https://doi.org/10.1016/j.ydbio.2018.09.009).

The Chapter 2 represents a paper in preparation. It presents a research that is part of a large project involving Dr. Ayelet Voskoboynik and her collaborators, in particular PhD student Mark Kowarsky (Stanford University) who assisted with specimen collection, transcriptome preparation and molecular analyses, and Dr. Kohji Hotta of the Kejo

University (Japan) and his collaborators trained in confocal imaging. This work focuses on the development of the nervous system and aims to analyse in detail the anatomical and molecular aspects of embryogenesis and blastogenesis. In this chapter, I describe the development of methods for culturing embryos and give the first account of an embryo development timetable that was subsequently produced. I analyzed transcriptomes produced for several embryogenetic and blastogenetic stages, showing that differentially expressed genes are related to the nervous system development in blastogenesis and embryogenesis, and I described common and divergent pathways between the two developmental strategies. In this project, I was personally involved in developing the method of embryo culture, defining embryo stages and preparing the timetable, and analyzing and discussing the molecular data in relation to the nervous system development. Part of these results was presented at the "9th International Tunicate Meeting", July 17-21 2017, New York (USA).

Chapter 3 considers the nervous system in adult individuals, with respect to the blastogenetic cycle, in both young and old colonies. It also represents a paper in preparation, in collaboration with Dr. Ayelet Voskoboynik, PhD student Mark Kowarsky and their collaborators at Stanford University. The chapter presents the dynamic changes of the cerebral ganglion and some sensory organs during the adult zooid life (in both young and old colonies), discusses two new behavioural tests for *B. schlosseri*, analyses the possible role of immunocytes in neurodegeneration, studies mechanisms of neuron death, presents differentially expressed genes related to the nervous system during the blastogenetic cycle, and correlates the neurodegenerative processes in young and old individuals with those occurring in human neurodegenerative diseases. My primary role in the work was planning experiments, analysing cerebral ganglion and sensory cells in young and old colonies at a confocal level, developing behaviour tests, studying apoptosis with Transmission Electron Microscopy and TUNEL, conducting statistical analysis, and analysing and discussing results. Part of the results were presented at "Neural Crest and Cranial Placodes Gordon Research Conference", February 5-10 2017, Ventura (CA-USA), and at the "7th meeting of the European Society for Evolutionary Developmental Biology (EED)", June 26-29 2018, Galway, (IR).

Chapter 4 describes the development of a sensory organ, the coronal organ, during asexual development. The organ possesses sensory cells considered homologous to

vertebrate hair cells (Rigon et al., 2018). This Chapter documents the effects of the ototoxic aminoglycoside gentamicin on coronal cells. In this research, I was involved in planning experiments with drugs, and in the discussion of data. These results have been presented to the "Symposium of Integrative Biology of Sensory Hair Cells" at the Society of Integrative and Comparative Biology Meeting in San Francisco (CA, USA) January 3-7 2018 and have been published in the journal *Integrative and Comparative Biology* in a manuscript of which I am a corresponding author (Manni L., Anselmi C., Burighel P., Martini M., Gasparini F. Differentiation and induced sensorial alteration of coronal organ in asexual life of a tunicate. Integrative and Comparative Biology 58: 317-328. DOI: 10.1093/icb/icy044).

REFERENCES

- Burighel P., Lane N. J., Zaniolo G., Manni L. (1998). Neurogenic role of the neural gland in the development of the ascidian, *Botryllus schlosseri* (Tunicata, Urochordata). Journal of Comparative Neurology 394: 230-241.

- Berrill NJ. (1950). The Tunicata, with an account of the British species. London: The Ray Society.

- Cima F., Ballarin L., Caicci F., Franchi N., Gasparini F., Rigon F., Schiavon F., Manni L. (2015). Life history and ecological genetics of the colonial ascidian *Botryllus schlosseri*. Zoologischer Anzeiger 257: 54-70

- Dehal P., Satou Y., Campbell R. K., Chapman J., Degnan B., De Tomaso A., Harafuji N. (2002). The draft genome of *Ciona intestinalis*: insights into chordate and vertebrate origins. Science 298(5601): 2157-2167.

- Delage Y., Herouard E. (1898). Traitè de zoologie concrète, vol 8, Les procordès. Paris: Schleicher Frères.

- Delsuc F., Philippe H., Tsagkogeorga G., Simion P., Tilak M. K., Turon X., Lopez-Legentil S., Piette J., Lemaire P., Douzery E. J. P. (2018). A phylogenomic framework and timescale for comparative studies of tunicates. BCM Biology 16(1): 39.

- Gasparini F., Manni L., Cima F., Zaniolo G., Burighel P., Caicci F., Ballarin, L. (2015). Sexual and asexual reproduction in the colonial ascidian B otryllus schlosseri. Genesis, 53(1): 105-120.

- Grasse, (1948). Traité de zoologie, Tome XI, Masson, Paris.

- Horie R., Hazbun A., Chen K., Cao C., Levine M. & Horie T. (2018). Shared evolutionary origin of vertebrate neural crest and cranial placodes. Nature 560(7717): 228.

- Lemaire P., Bertrand V. & Hudson, C. (2002). Early steps in the formation of neural tissue in ascidian embryos. Developmental biology 252(2): 151-169.

- Manni L., Gasparini F., Hotta K., Ishizuka K.J., Ricci L., Tiozzo S., Voskoboynik A., Dauga D. (2014). Ontology for the asexual development and anatomy of the colonial chordate *Botryllus schosseri*. Plos One 9(5): e96434

- Manni L., Lane N., Sorrentino M., Zaniolo G., Burighel P. (1999). Mechanism of neurogenesis during the embryonic development of a tunicate. Journal of Comparative Neurology 412: 527-541

- Manni L., Zaniolo G., Cima F., Burighel P., Ballarin L. (2007). *Bortyllus schlosseri*: A model for the study of asexual reproduction. Developmental Dynamics 236: 335-352.

- Manni L., Lane N. J., Joly J. S., Gasparini F., Tiozzo S., Caicci F., Burighel P. (2004). Neurogenic and non neurogenic placodes in ascidians. Journal of Experimental Zoology Part B: Molecular and Developmental Evolution 302(5): 483-504.

- Meinertzhagen I. A., Okamura Y. (2001). The larval ascidian nervous system: the chordate brain from its small beginnings. Trends in neurosciences 24(7): 401-410.

- Patthey C., Schlosser G., Shimeld S. M. (2014). The evolutionary history of vertebrate cranial placodes–I: cell type evolution. Developmental biology 389(1): 82-97.

- Rigon F., Gasparini F., Shimeld S.M., Candiani S., Manni L. (2018). Developmental signature, synaptic connectivity and neurotransmission are conserved between vertebrate hair cells and tunicate coronal cells. Journal of Comparative Neurology 526(6): 957-971.

- Sasakura Y., Mita K., Ogura Y. & Horie T. (2012). Ascidians as excellent chordate models for studying the development of the nervous system during embryogenesis and metamorphosis. Development, growth & differentiation 54(3): 420-437.

- Voskoboynik A., Weissman I. L. (2015). *Botryllus schlosseri*, an emerging model for the study of aging, stem cells, and mechanisms of regeneration. Invertebrate reproduction & development 59(sup1):33-38.

Chapter 1

Sixty years of experimental studies on the blastogenesis of the colonial tunicate *Botryllus schlosseri*

Lucia Manni[1], **Chiara Anselmi[1]***, Francesca Cima[1], Fabio Gasparini[1]*, Ayelet Voskoboynik[2], Margherita Martini[1], Anna Peronato[1], Paolo Burighel[1], Giovanna Zaniolo[1], Loriano Ballarin[1]

[1]Department of Biology, University of Padova
[2]Institute for Stem Cell Biology and Regenerative Medicine and Hopkins Marine Station, Stanford University

**Corresponding Authors*: Chiara Anselmi, Fabio Gasparini

Journal: Developmental Biology
Special Issue on Tunicates

ABSTRACT

In the second half of the eighteenth century, Schlosser and Ellis described the colonial ascidian *Botryllus schlosseri* garnering the interest of scientists around the world. In the 1950's scientists began to study *B. schlosseri* and soon recognized it as an important model organism for the study of developmental biology and comparative immunology. In this review, we summarize the history of *B. schlosseri* studies and experiments performed to characterize the colony life cycle and bud development. We describe experiments performed to analyze variations in bud productivity, zooid growth and bilateral asymmetry (*i.e.,* the *situs viscerum*), and discuss zooid and bud removal experiments that were used to study the cross-talk between consecutive blastogenetic generations and vascular budding. We also summerize genetic experiments that demonstrated that the ability of two distinct colonies to fuse or reject is controlled by a single polymorphic gene locus (BHF) with multiple, codominantly expressed alleles. Finally, we describe how the ability to fuse and create chimeras was used to show that within a chimera somatic and germline stem cells compete to populate niches and regenerate tissue or germline organs. Starting from the results of these 60 years of study, we can now use new technological advances to expand the study of *B. schlosseri* traits and understand functional relationships between its genome and life history phenotypes.

1. The history of *Botryllus schlosseri*

The second half of the eighteenth century represented the golden age for both intellectual curiosity and studies on the marine fauna and flora. During that time European physicians, philosophers and naturalists began identifying different marine species. The colonial ascidian *Botryllus schlosseri* (Pallas, 1766), commonly known as the star ascidian or golden star tunicate, was one of these newly characterized species. *B. schlosseri* was initially classified as "plantanimal" or "zoophyte" based on its sedentary nature paired with animal features (*e.g.*, contractility). Rondelet (1555) was the first to describe *Botryllus* colonies and called them *uva marina* (Fig. 1A) while Pallas (1766) and Linnaeus (1767) named it *Alcyonium schlosseri*, Gärtner (1774), Bruguière (1792), and Renier (1793) adopted *Botryllus stellatus* and, finally, in 1816, Savigny called it *Botryllus schlosseri* (Brunetti et al., 2017).

The first microscopic description of *B. schlosseri* in scientific literature dates back to 1756, when a manuscript entitled: *An account of a curious, fleshy, coral-like substance*, by J.A. Schlosser and J. Ellis, was read at the Royal Society, in London (Schlosser and Ellis, 1755-1756). They named the species *Alcyonum carnosum asteriscis, radiis obtusis, ornatum* and described the development of the buds:*...all the interstices between the stars are fill'd with eggs of different sizes, each adhering by one end to a very fine capillary filament. The smallest eggs are globular, and as they advance in size, change to an oval figure; from thence they assume the shape of one of the radii of the star*... (Fig. 1B).

The species was also described by the German scientist J. Gärtner (1774) (Fig. 1C), and by the Italian scientist L. Spallanzani (1784) who, in his diary, described it as a new animal, unknown to him, and reported his observations on the replacement of the old generation zooids by a new generation: *August, 20, 1784. This morning a new phenomenon occurred. The zoophyte collected yesterday, maintained in seawater, and observed today, did not have only six leaflets, but 12. In a day, then, 6 new leaflets appeared and these are very similar to the old ones. The zoophyte was circular and still is.* In his investigations in the North-Adriatic Sea, Spallanzani was supported by the naturalist Stefano Chiereghin (Chioggia (Italy), (1745-1820), who rendered some drawings of marine animals and, among them, a detailed illustration of *B. schlosseri* (Gibin, 1997; Fig. 1D). The naturalists Olivi (1792) and Renier (1793), from Chioggia,

also described *Botryllus*. According to Renier, buds are *eggs interspersed among the big corpuscles* (zooids), and the generation change as follows: …*the eggs of the Alcyonium, once developed, increase the number of the corpuscles and the total volume.* Renier was the first to describe the colonial vasculature: ...*the crystalline substance* (the tunic) *contains internal small vessels that communicate with small vesicles* (the ampullae) *that contain various small opaque clustered globules* (the hemocytes)… and included a detailed illustration of the colony (Fig. 1E; Gibin, 2013).

In the nineteenth century, *B. schlosseri* was described by many authors, including Savigny (1816; Fig. 1F), Ganin (1870), Giard (1872), and Della Valle (1881). Giard (1872) studied colony pigmentation (Fig. 1G), and Haeckel (1899) described the colony anatomy (Fig. 1H). Metschnikow (1869), Hjort (1893) and Pizon (1893) described the process of bud development, later re-investigated by Berrill (1941a,b; 1951), Watterson (1945), Sabbadin (1955), and Izzard (1973). In the first half of the last century, Bancroft (1903a) was the first to describe colony specificity: the ability of *B. schlosseri* to fuse or reject other colonies. Sabbadin (1955) succeeded in raising *B. schlosseri* colonies in the laboratory and began studying their life history. Classical genetic studies and fusion rejection assays performed by Sabbadin (1962) and Scofield et al. (1982) on *B. schlosseri*, by Oka and Watanabe (1957a, 1960), Taneda and Watanabe (1982a,b) and Taneda et al. (1985) on *Botryllus primigenus* revealed that the ability to fuse in *Botryllus* is controlled by a single polymorphic gene locus with multiple, codominantly expressed alleles.

Burnet (1971) suggested studying *Botryllus* as a model for the evolution of self-recognition. He wrote: *although self recognition in ascidians is not analogous to the immunological processes of vertebrates, it presents a primitive type of 'self and not self' recognition from which adaptive immunity may have evolved*.

Over the last 35 years electron microscopy (scanning, transmission microscopy, freeze-fracture techniques) (reviewed in Manni et al., 2007) has advanced the knowledge of *B. schlosseri* anatomy and development. The Weissman lab has focused on the genetic control of the fusion/rejection in *B. schlosseri.* Fusion or rejection occurs when two colonies touch, the blood vessels either fuse and create a chimera or reject forming inflammatory responses (points of rejection) (Sabbadin, 1962; Scofield et al., 1982). They determined that chimerism is a stem cell mediated phenomenon (Laird et al., 2005a) and that the biology of stem cell engraftment in *B. schlosseri* chimeras is

regulated on four different levels: first, there is fusion or rejection (Scofield et al., 1982); second, if fusion occurs, the body of one partner is resorbed (Rinkevich et al., 1993; Corey et al., 2016); third, there is competition between somatic stem cells that circulate from one chimeric partner to another for asexual whole body development (Stoner and Weissman, 1996; Stoner et al., 1999; Laird et al., 2005a; Voskoboynik et al., 2008); and fourth, there is stem cell competition among germ line stem cells (Stoner et al., 1999; Rinkevich et al., 2013). Using defined homozygous and heterozygous *B. schlosseri* lines for distinct fusibility alleles that were developed by the late Y. Saito (1985-1987), the Weissman lab described hierarchies in allogeneic resorption (Rinkevich et al., 1993), sequenced the *B. schlosseri* genome and transcriptome (Voskoboynik et al., 2013a,b), and discovered BHF, the gene that controls fusion and rejection outcomes (Voskoboynik et al., 2013b). Fusion between colonies requires at least one shared *BHF* allele while rejection occurs when no BHF alleles are shared (Voskoboynik et al., 2013b). Genetically distinct strains have somatic stem cells that, in a chimera, vary in their vulnerability to be resorbed, undergo competitions to "win" or "lose" differentiated tissue (akin to regeneration), and to win or lose germline niches (Rinkevich et al., 1993; Stoner and Weissman, 1996; Stoner et al., 1999; Laird et al., 2005a; Voskoboynik et al., 2008; Rinkevich et al., 2013).

Sixty years of research on *B. schlosseri* asexual reproduction, stem cell biology, and stem cell competition within chimeras has directed studies in mammals that revealed stem cell competition during mammalian development, aging and cancer (Weissman, 2015).

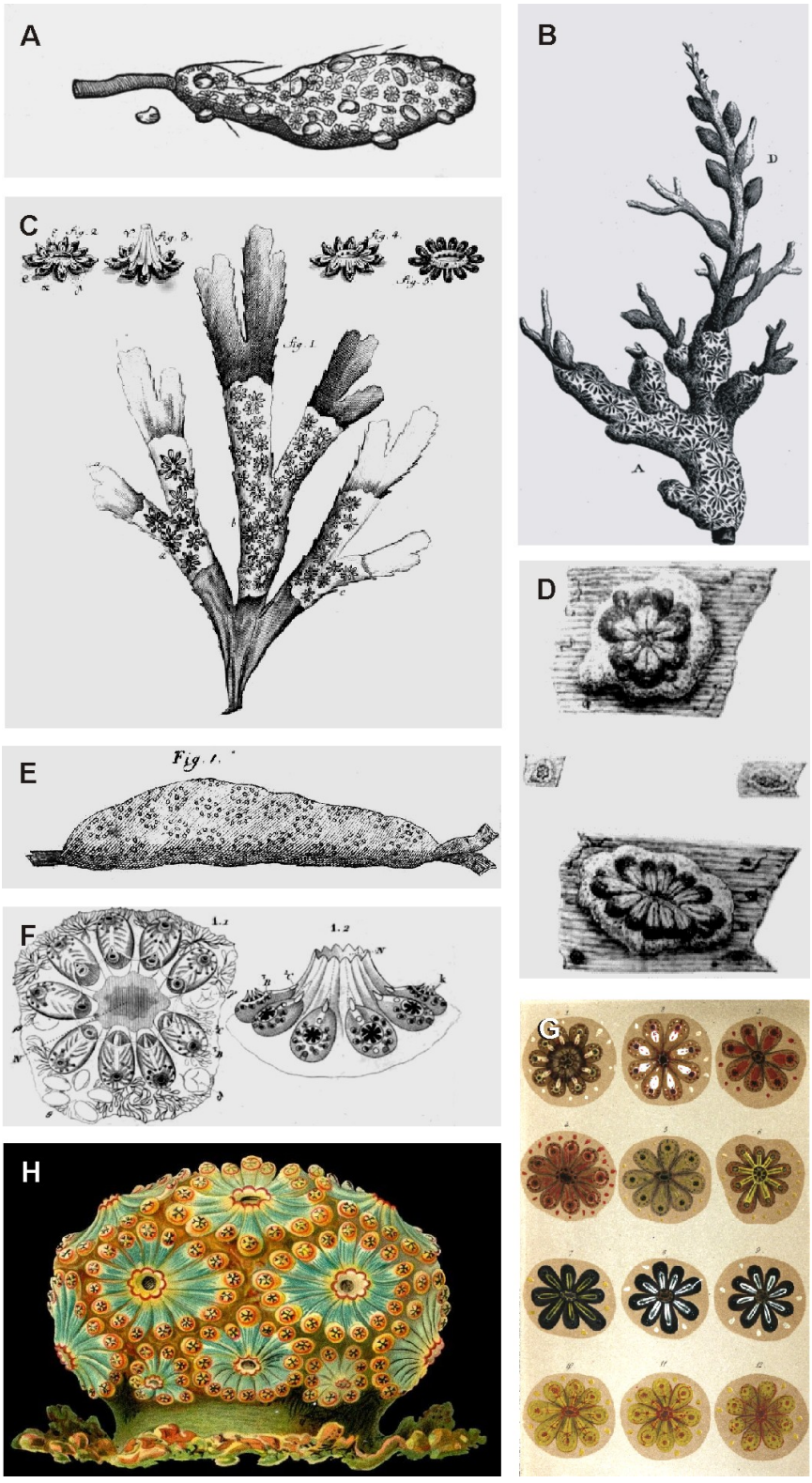

Fig. 1: Colonies of *Botryllus schlosseri*, as drawn by: Rondelet (1555) (**A**), Schlosser and Ellis (1755-1756) (**B**), Gärtner (1774) (**C**), Stefano Chiereghin (in Gibin, 1997) (**D**), Andrea Renier (in Gibin, 1997) (**E**), Savigny (1816) (**F),** Giard (1872) (**G**), and Haeckel (1899) (**H**).

2. The star ascidian: the colony and its blastogenetic cycle

A *B. schlosseri* colony begins its life as a tadpole-like larva (the product of sexual reproduction) that metamorphoses into an oozooid (the first zooid of the colony) (Fig. 2). The larva has two buds one on the right side of its body wall (formed of the epidermis, the peribranchial epithelium, and the mesenchymal derivatives between the two epithelia), the other on the left (Sabbadin, 1958). Following metamorphosis, the bud on the oozooids' right side develops into the first blastozooid (the zooid derived from asexual reproduction). Through asexual reproduction, new blastozooids are formed and arrange themselves in star-shaped systems, with a common cloacal siphon in the center. The number of individuals in a colony increases when more than one bud replaces the blastozooids of the old generation. The colony expands as a system divides into two or more systems after the development of approximately 12 or more blastozooids. All the systems of a colony are embedded in a common, gelatinous tunic and are connected to each other by vessels containing hemolymph.

Eleven, morphologically-distinguishable blastogenetic developmental stages from bud to adult zooids were introduced by Berrill (1941a) and modified by Sabbadin (1955) and Izzard (1973) (Fig. 2F). This is the reference staging method used today, and has been described in an anatomical and developmental ontology that has been recognized by the tunicate community (Manni et al., 2014). Some authors adopt the four phase (A-D) method suggested by Watanabe (1953) for the Japanese species *B. primigenus,* based on the rapid (four day) blastogenetic cycle of colonies reared in the warm water temperature of the Japanese Sea. This method cannot document zooid developmental changes and irregularities in the synchronization of the different blastogenetic generations coexisting in colonies.

Three blastogenetic generations are usually observed: the adult filtering zooids and their (primary) buds and budlets (secondary buds). Colonial developmental phases are defined by the blastogenetic developmental stages of the three generations and expressed with a formula of three numbers, separated by slashes, each number referring to the blastogenetic developmental stage of adult zooids, primary buds and budlets, respectively (*e.g.*, 9/8/4).

Cyclical generation replacement, called takeover (TO), occurs every week (at 20°C). During this phase, the entire parental generation of zooids in a colony synchronously

ceases filtering and is resorbed while the asexually-derived generation of buds mature and replaced it. Primary buds become the new zooids, budlets become the new primary buds and a new budlet generation grows. The TO phase involves massive programmed cell death (PCD) of zooid organs via apoptosis followed by programmed removal of cell corpses by circulating phagocytes within approximately 24-36h (20°C) (Lauzon et al., 1992; Manni et al., 2007; Franchi et al., 2016). The blastogenetic cycle, *i.e.* the interval between the siphons opening of two following adult zooid generations. lasts 7 days (at 20°C). The lifespan of each individual in a colony, from its appearance as a bud primordium to the end of its filtering activity at TO, lasts about 3 weeks at 20°C (Manni et al., 2007). When colonies at different blastogenetic developmental phases fuse to create chimeras, the development of one partner will speed up in order to assure a rapid equalization of the phase differences (Watanabe, 1953, 1962).

In the following sections, we will review some of the aspects of blastogenesis. In particular, we will focus on experimental studies of bud removal and the consequent effects on zooid growth and lifespan, duration of the blastogenetic cycle, blastogenetic capabilities, left-right asymmetry and regenerative capabilities. These topics will be discussed in the context of the developmental and evolutionary biology of ascidians.

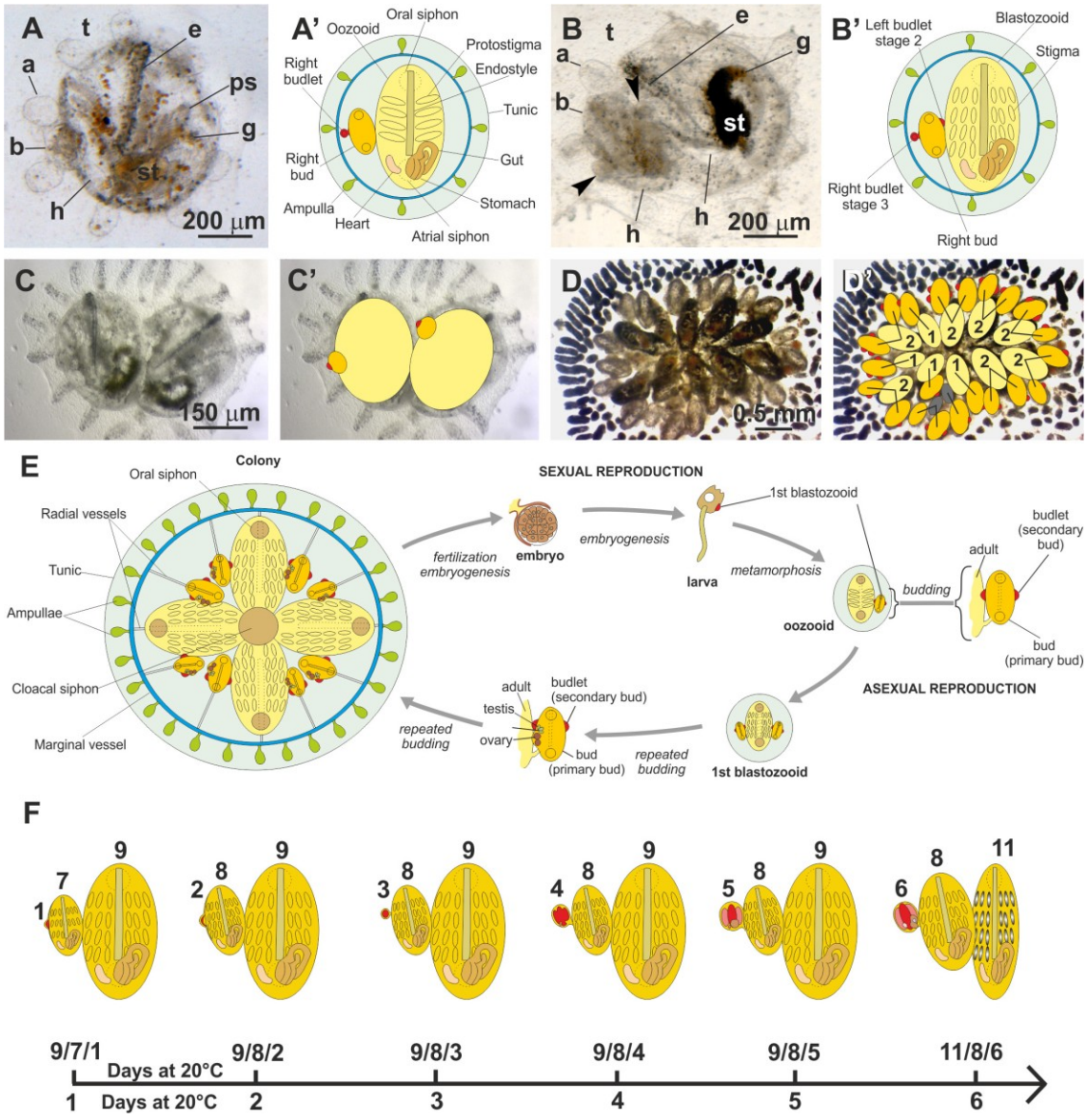

Fig. 2: Ventral view of an oozooid (**A**), an adult blastozooid of the first blastogenetic generation (**B**), a young (**C**) and old (**D**) colony. **A'-D'**: schematic drawings of **A-D;** zooids, buds and budlets are marked with different colors; in **C'-D'**, drawings are superimposed to images. Only the right bud (**b**) is present in **A** and **B**; the single budlets is poorly recognizable in **A**; budlets are present on both sides in **B** (**arrowheads**). Note that the young colony in **C** possesses fewer buds (only the right ones) than the older colony in **D**, where most of the zooids (marked with number 2) bear two buds and only a few (marked by number 1) bear only one bud. Black lines link each bud to its parent. Some buds bear three budlets. The two grey zooids are adult individuals in early TO; their buds are still developing and survive their parent. **a**: ampulla; **e**: endostyle; **g**: gut; **ps**: protostigma; **st**: stomach; **t**: tunic. **E**. Life cycle of *B. schlosseri* (modified by Gasparini et al., 2014).

3. Leaflets and flowers: morphological observations of palleal budding

Palleal budding is the phenomenon that astonished Spallanzani: how can leaflets (buds) in the zoophyte (zooid) double, while remaining similar to the old zoophyte? However, if the eminent researcher had followed the zoophyte's growth today, he would have discovered an oval zooid, being replaced by two buds that grew from its body wall. The primitive tools available to Spallanzani did not allow him to observe the appearance of budlets and follow their development.

The new budlet arises as a disc-shaped thickening (blastogenetic developmental stage 1) of the peribranchial epithelium of a bud at the blastogenetic developmental stage 7. The bud primordium, containing candidate pluripotent stem cells, arches perpendicularly to the bud wall that forms a hemisphere (stage 2) and then skews towards the anterior end of the parental bud. At this stage, the budlet anterior-posterior and dorsal-ventral axes are already established (Sabbadin et al., 1975; Manni et al., 2007). Body axis seems to be related to the vascularization of the budlet, as the entrance of the affluent vessel (coming from the bud) marks the posterior end of the budlet (Izzard, 1973; Sabbadin et al., 1975). A detailed description of budlet organogenesis can be found in Manni et al. (2007).

4. Genes associated with palleal budding

Current knowledge regarding genes and pathways associated with blastogenesis is limited. The majority of the available molecular data is descriptive and aims to verify gene expression patterns in buds *vs* adult zooids. For a minute number of genes, gene silencing experiments were performed, but the exact mechanism for their role in blastogenesis is still far from being understood. Here, we summarize the list of genes that were identified so far.

Laird et al. (2005b) identified Athena, a gene, unique to tunicates that is highly transcribed when a new budlet appears during the TO phase, when compared to other blastogenetic developmental phases. Genetic knockdown of *Athena* results in blastogenesis defects ranging from the delay of budlet development and growth impairment to altered organogenesis and developmental failure of the left buds (Laird et al., 2005b).

Another gene highly transcribed at TO is mortalin, a highly conserved chaperone member of the hsp70 family, involved in various functions ranging from stress responses to control of cell proliferation and inhibition of apoptosis (Londono et al., 2012). Its transcript is present in normal zooids and absent in zooids undergoing resorption. Allosteric inhibition of the protein leads to severe alteration of zooid morphology, in particular in the development of: digestive system, endostyle and gonads (Ben-Hamo et al., 2018). When compared to adult tissues, bud tissues express higher levels of the mortalin proteins (Ben-Hamo et al., 2018), PL10 and cadherin (Rosner et al., 2006, 2007).

Tissues of budlets and buds stained with antibodies raised against β-catenin, indicate a role of the Wnt pathway in blastogenesis, also supported by the interference of Wnt agonists and antagonists with normal bud development (Rosner et al., 2014; Di Maio et al., 2015).

The involvement of the TGFβ pathway is suggested by the immunopositivity of bud tissues to anti-TGFβ and the alteration in bud development induced by TGFβ agonists (Rosner et al., 2014).

Rosner et al. (2014) also found that the antibody for p-Mek1/2, an enzyme of the MAPK/ERK signal transduction pathway, stains bud tissues, whereas colony exposure to p-Mek1/2 inhibitors resulted in malformed buds (Rosner et al., 2014).

An orthologue of *ptx* is also transcribed in bud tissues: it is located in the gut epithelium, the oral siphon rudiment, and the developing neural complex (Tiozzo et al., 2005). The knock-down of this gene results in budding impairment and colony death (Tiozzo and De Tomaso, 2009).

The development of musculature during budding has been studied by *in situ* hybridization of muscular actin and troponin-T (Degasperi et al., 2009).

Furthermore, during blastogenesis, orthologues of vertebrate *Six1/2*, *Six3/6*, *Eya* and *FoxI*, associated with placode formation, are transcribed in the cells lining the forming branchial slits and siphons in the buds (Gasparini et al., 2013).

Internal tissues of the developing buds of the congeneric colonial species *B. primigenus* express nanos, a protein typically expressed by stem cells, repressing apoptosis and maintaining cell pluripotency (Sunanaga et al., 2008).

A new set of differentially transcribed genes in the epithelia of the bud primordia of *B. schlosseri* has been recently identified. It includes genes for transcription factors related

to stemness and development, telomere maintenance, tumor suppression, and signal transduction pathways (Ricci et al., 2016a,b).

Corey et al. (2016) studied the cellular and molecular framework underlying loss of tolerance to one partner within a natural *B. schlosseri* chimera. In this experiment, one chimeric partner is eliminated in a process of allogeneic resorption. A few days before the resorption of one chimeric partner, the development of the buds in the resorbing partner is halted (termed developmental arrest; Corey et al., 2016). Although this study was focused on the resorption event in a chimera, the comprehensive sequencing analysis described revealed upregulated expression of genes and pathways in normally developing budlets *vs* budlets with halted development (Corey et al., 2016). These upregulated genes and pathways are associated with embryogenesis and development. The top ranked genes differentially expressed in the budlets (secondary buds) of the resorption winner include: the transcription regulator *hist1h3b*, the anti-apoptotic gene *g2e3*, genes associated with embryonic development like *tbx1*, *six1* and *hmx1*, heart and stem cell proliferation *osr1*, and *neurog3* which is involved in neurogenesis and endocrine cell development (Corey et al., 2016).

Many of the genes known to be associated with development, regeneration and stem cells are expressed in the buds. Using next generation sequencing technologies to map in detail the genetic program of blastogenesis might shed light on the robust regeneration capacities of colonial tunicates.

5. Stem cells and palleal budding

Adult stem cells are multipotent, self-renewing progenitor cells uniquely capable of both reproducing themselves and differentiating into a diverse range of specialized cell types. Studies in vertebrates revealed that tissue specific stem cells persist throughout adult life and are essential for the repair and regeneration of specific organs such as skin, brain and blood (review in Weissman, 2015). Identification and isolation of tissue specific stem cells is challenging and demands the design of experiments that can demonstrate self-renewing ability and multidifferentiative potential.

In recent years, the interest in marine invertebrate stem cells has rapidly grown due to the potential of better understanding fundamental biological processes (*e.g.*, senescence, regeneration, cell reprogramming) (Ballarin et al., 2018).

In *B. schlosseri* chimeras, the buds and gametes of one or both chimeric partners become a blend of both genotypes or, in some cases, are completely replaced by the cells of one partner (Sabbadin and Zaniolo, 1979; Pancer et al., 1995; Stoner and Weissman, 1996; Stoner et al., 1999). This chimerism persists even when the blood vessels connecting the fused colonies are disconnected, and it follows genetically heritable hierarchies for germline "winners" and "losers" (Sabbadin and Zaniolo 1979; Stoner et al., 1999). The reproducibility and longevity of this phenomenon led to the hypothesis that chimerism is mediated by blood borne stem cells (Sabbadin and Zaniolo 1979; Rinkevich and Weissman 1987; Pancer et al., 1995; Stoner and Weissman 1996; *Stoner et al., 1999).*

By transplanting a single cell which had expressed a high enzymatic activity of aldehyde dehydrogenase and a set of serial engraftment assays, Laird et al. (2005a) revealed that adult stem cells are responsible for a stable long-term chimerism in *B. schlosseri.* Criteria for a candidate stem cell were both the induction of long-term, stable, multilineage chimerism and demonstrated self-renewal potential (Laird et al., 2005a).

In vivo cell labeling, cell engraftment, and time lapse imaging showed that the anterior ventral region of the subendostylar sinus (termed endostyle niche) in *B. schlosseri* zooids harbors and exports somatic stem cells, and that the cell islands which are located along the endostyle harbor germline stem cells (Voskoboynik et al., 2008; Rinkevich et al., 2013). The subendostylar sinus is a hemolymphatic sinus ventral to the endostyle, the long glandular groove in the ventral side of the branchial sac (Burighel and Brunetti, 1971). The endostyle has an iodine-concentrating activity and is considered a homolog of the vertebrate thyroid gland (Burighel and Cloney, 1997; Ogasawara et al., 1999). In *B. schlosseri*, *in-situ* hybridization and immunostaining of the endostyle in zooids and buds reveal unique expression patterns of site-specific factors that are linked to developmental regulation and stem cell activity including β-catenin, Piwi, Oct4, STAT, Raldh, RAR, pSmad2 and more supporting the key role of the endostyle as a niche for stem cells involved in bud development (Voskoboynik et al., 2008; Rinkevich et al., 2013).

The prospective isolation of germline and somatic stem cells in *B. schlosseri* (Laird et al., 2005a) and the identification of stem cell niches in this organism suggest that palleal budding in colonial ascidians is mediated by tissue specific stem cells that migrate

through the colony vasculature and seed developing buds. However, although studies done so far suggested that budding in *B. schlosseri* are stem cell mediated phenomena (Laird et al., 2005a; Voskoboynik et al., 2008; Rosental et al., 2018), we can not exclude the possibility of dedifferentiation. In the ascidian *Polyandrocarpa misakiensis,* budding has been suggested to depend on the transdifferentiation of the peribranchial epithelium, where cells acquire new differentiation markers (Kawamura and Fujiwara, 1994, 1995). Comprehensive lineage tracing of individual cells that use transgenic lines will be needed to prove transdifferentiation. Future studies that will investigate the cellular and molecular mechanisms underlying palleal budding in tunicates will advance our knowledge on stem cell mediated regeneration processes.

6. Interactions among coexisting generations: experiments of bud removal

To better understand the asexual development of a colony and the relationships between the zooids, buds and budlets, oozooids were settled on slides and their development was followed for 7 blastogenetic generations (49 days) (Sabbadin, 1955, 1958; Gasparini et al., 2015). Colonies were observed every day and the number and position of buds, zooid size and blastogenetic developmental phases were recorded (Fig. 3). Fourteen colonies were used as a control, and the others were used for experiments of bud removal (budectomy). These experiments, reviewed below, provided basic knowledge regarding homeostatic and regenerative capacities of budlets, asymmetric blastogenetic potential, colony growth rate, length of the blastogenetic cycle, and the interactions among coexisting generations.

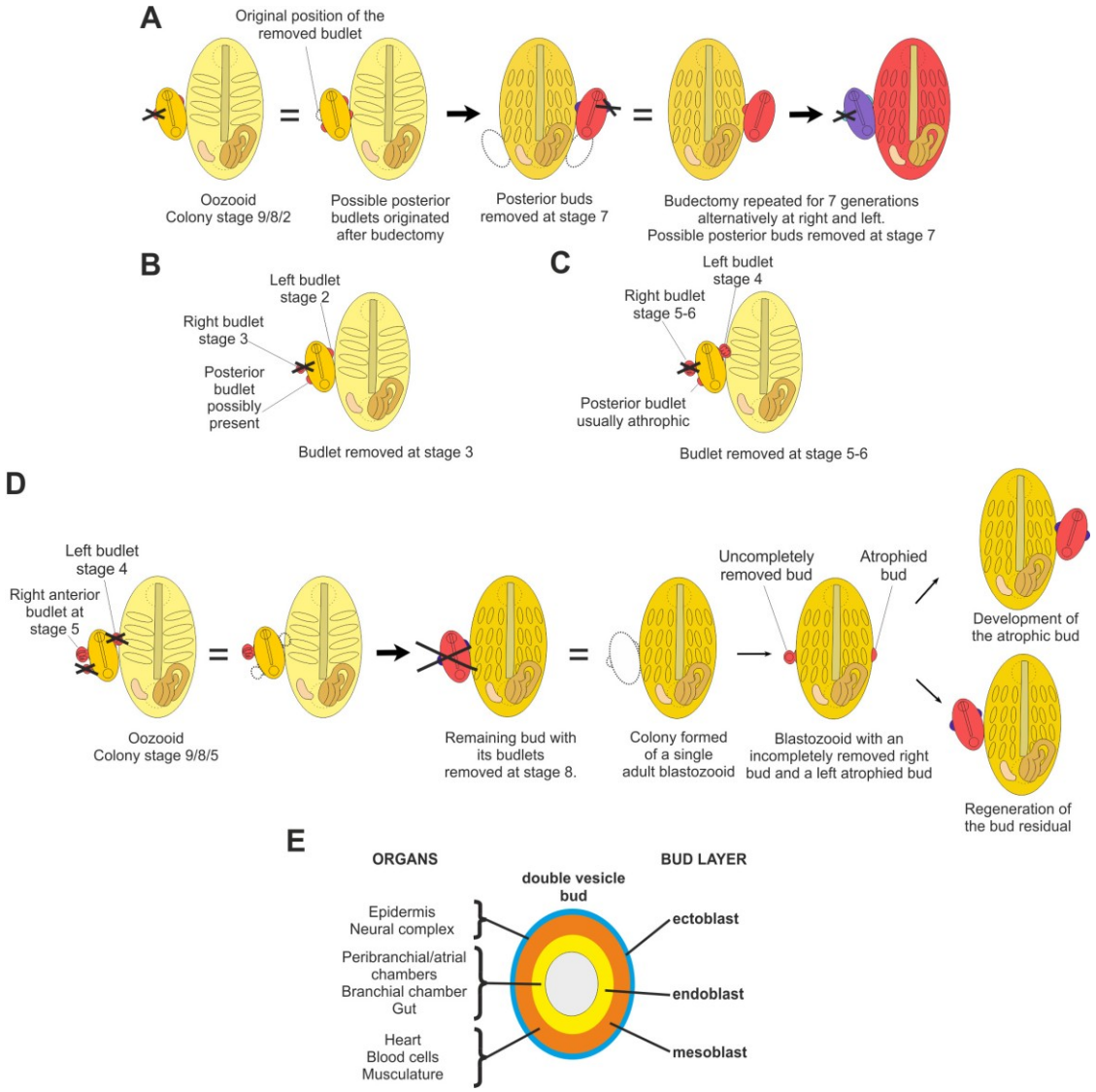

Fig. 3: Experimental plan of bud removal experiments performed by Sabbadin (1958). **A-C**. only one bud was left in buds; removal carried out at colonial phase 9/8/2 (**A**), 9/8/3 (**B**), and 9/8/5-6 (**C**). The same individual (as budlet, bud, or zooid) is marked by the same color over generations; the original position of removed zooids is indicated by dotted line; removals are indicated by crossed lines. **Arrow**: change of generation; = colony after removal. **D**. Removal of buds at stage 8 leads to colonies with adult zooid and its atrophied bud or bud remnants. The final effect is the development of the atrophied bud or the regeneration of the bud remain. **E**. Blastogenetic cycle of a colony. Each adult blastozooid filters for about one week at 18°C before being resorbed at the TO. Colonial phases are indicated by a combination of three numbers separated by slashes; developmental stages of adults, buds and budlets are indicated above the zooids (modified from Manni et al., 2014). **F.** Scheme of the double vesicle stage budlet showing organ derivation from bud layers (modified from Manni and Burighel, 2006).

6.1 Blastogenetic capabilities

The number of budlets produced by buds on zooids of the first blastogenetic generation is lower than that produced by buds of the following generations (generations 1-7; Fig. 4A, Suppl. Table 1). Under normal conditions, both sides of the bud can form bud primordia and each bud can originate up to four budlet primordia. Buds possess an asymmetrical blastogenetic potential, *i.e.*, they produce more budlets on the right side of the body than on the left (Fig. 4B, Suppl. Tables 2, 3). In addition, right anterior budlets are slightly advanced in development with respect to the left and posterior budlets (Sabbadin, 1958). On both sides, posterior budlets are preferentially resorbed with respect to the anterior ones (Fig. 4B,C; Suppl. Table 3) (Sabbadin, 1958; Watkins, 1958). Therefore, the right anterior budlets are more likely to develop into adult zooids. In order to study the asymmetric blastogenetic potential of buds, *i.e.* the different ability of the two sides to produce budlets, budectomy experiments were performed on young colonies (Fig. 3A-C). The aim of the experiment was to verify if budlet removal on a side resulted in a blastogenetic potential variation on the opposite side, *i.e*., if there is a competition between the two budding sites. Indeed, when all the budlets except one are removed, the blastogenetic potential of the colony is altered. Specifically, the remaining budlet, once bud, forms more budlets than usual, *i.e*. up to three budlet primordia on the right side and up to two on the left (Fig 5A). In addition, budectomy enhances budlet ability to complete their development: the number of budlets (right posterior, left anterior and posterior) going through developmental arrest is significantly reduced in surgically altered colonies in comparison to the controls (Suppl. Table 5). Conversely, the number of posterior bud primordia, and the number of left anterior budlets that resume normal development are significantly higher as compared to control. In addition, in experimental and control colonies, budlet productivity is lower in younger generations than in older ones (Fig. 5A, Suppl. Table 6).

In conclusion, these results show that while under normal conditions the right side produces a higher budlet number (up to 3) than the left. Following removal of the buds on the right side, the left side of the buds and its posterior locations can support normal development. They also demonstrate that budectomy increases the blastogenetic capabilities of colonies.

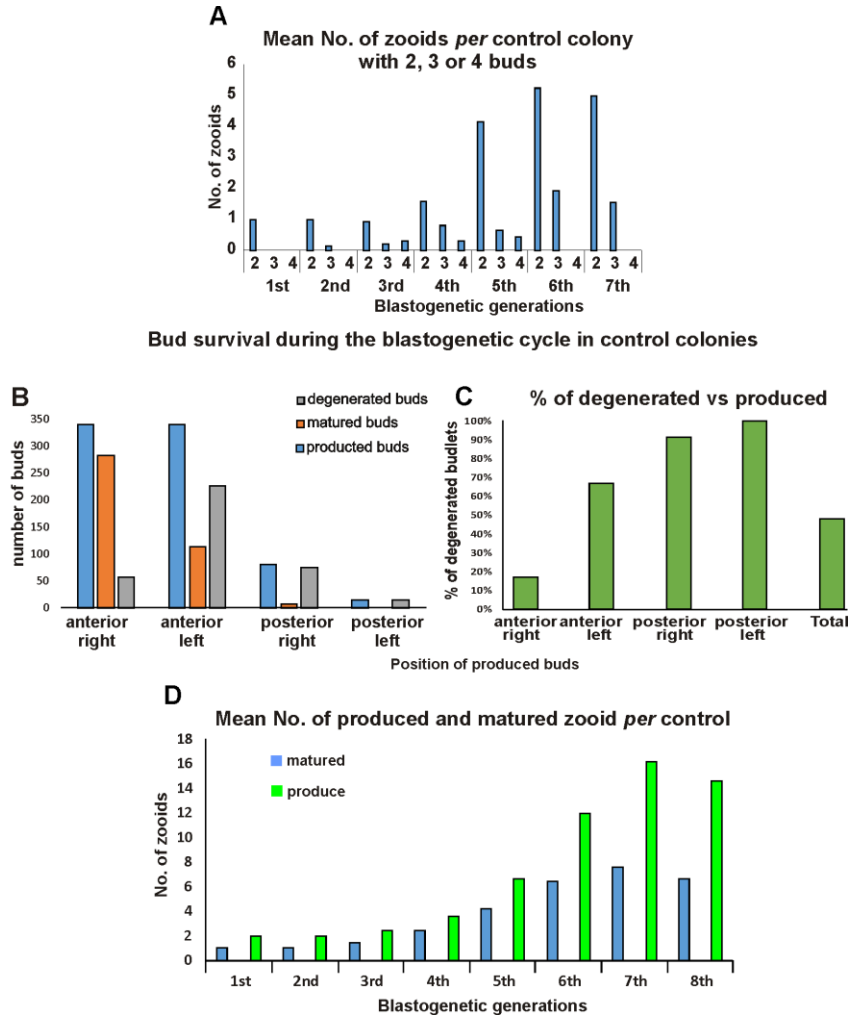

Fig. 4: **A**: Mean number of adult zooids per colony with 2, 3 or 4 buds in the first seven blastogenetic generations (data in Suppl. Table 1). **B**: number of budlets produced (light blue bars), matured to buds (orange bars) or undergone atrophied degeneration (grey) in the anterior right, posterior right, anterior left and posterior left sides of the buds of control colonies (data in Suppl. Table 3). **C**: percentage of degenerated budlets in the same locations (data in Suppl. 3). **D**: mean number of budlets produced *per* blastogenetic generation in a control colony (green bars) and mean number of them reaching the adult stage (light blue bars) (data in Suppl. Table 4).

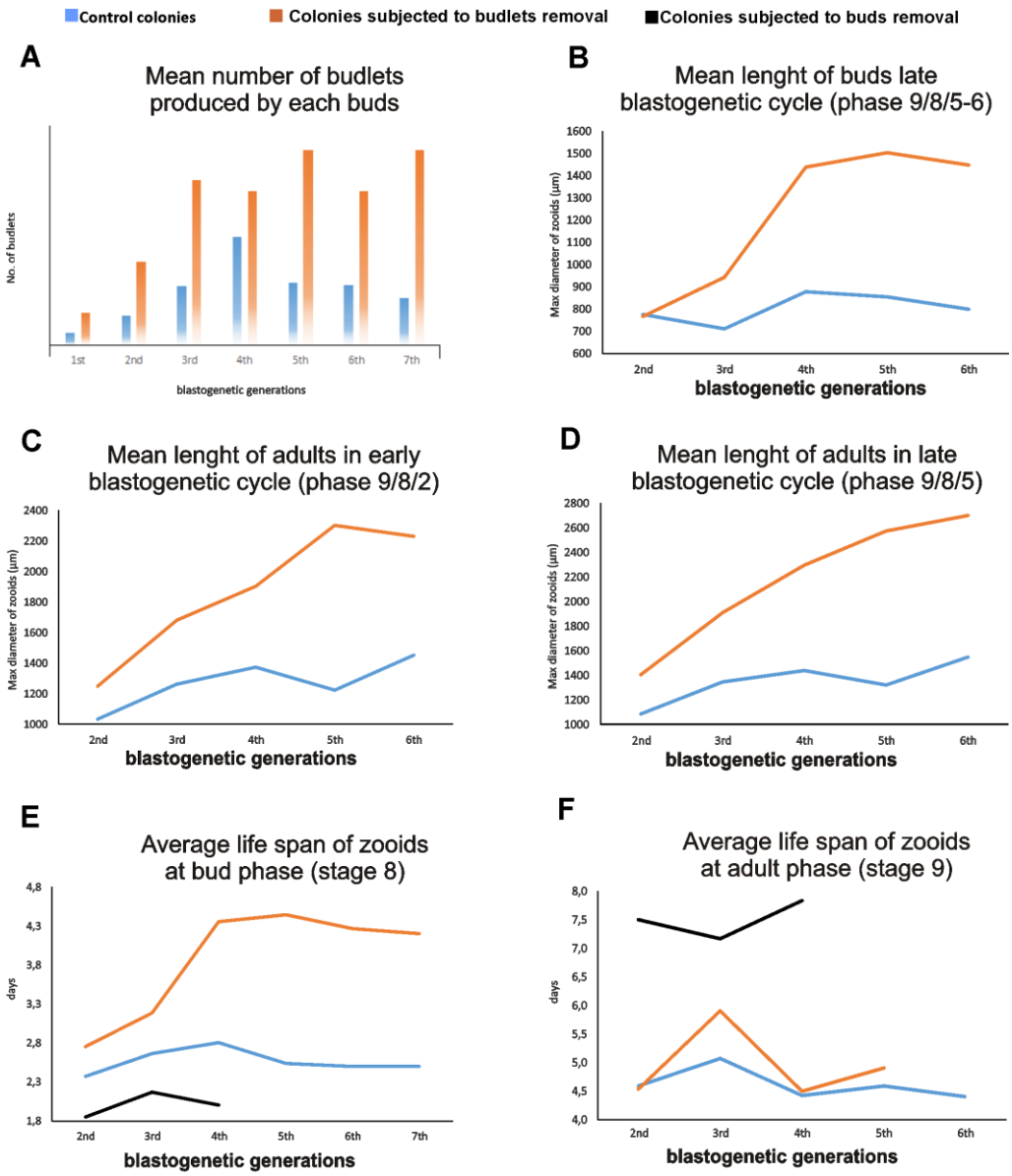

Fig. 5: **A**. mean number of budlets produced by control buds (light blue bars) and by single budlets, after the removal experiments, once become buds (orange bars), in the first seven blastogenetic generations. **B-D**: mean length of buds at blastogenetic developmental stage 8 (**B**) and of adults at developmental phase 9/8/2 (**C**) and 9/8/5 (**D**) in control colonies (light blue lines) and in colonies subjected to budlet removal (orange lines) (data in Suppl. Table 7 and 8). **E-F**: mean duration of blastogenetic developmental stage 8 (**E**) and 9 (**F**) in control colonies (light blue) and in colonies subjected to removal of budlets (orange lines) and of buds at stage 8 (black lines) (data in Suppl. Table 11).

6.2 Homeostatic and regenerative capability of budlets

Under normal conditions a high percentage (around 50%) of budlets undergo degeneration during development (Fig 4C,D; Suppl. Tables 3, 4). Most of these budlets are the posterior ones and those on the left side. They can persist as "atrophied" budlets (*i.e*., budlets unable to complete their blastogenetic development) on the bud/adult body wall.

A specific budectomy experiment was performed to verify the ability of atrophied budlets to resume development. As the budlets of the first blastozooid reached the blastogenetic developmental stage 5-6, all the budlets but the right anterior one were removed; once the remaining budlet developed into bud, it was itself removed, creating a colony of a single adult zooid (Fig. 3D). This two-step removal experiment was thought to guarantee colony survival, since the contemporary removal of all the budlets frequently caused colony death. In the single-zooid colonies, remnants of an incompletely removed budlets (or remnant of the anterior right bud) could regenerate new budlets that expedite their development and reach the double vesicle stage (stage 3) (Fig. 3D). Moreover, athropied budlets survived on the adult zooid body wall could resume development. The experiment revealed high regeneration capacities in budlets and demonstrated that the atrophied ones can develop into normal buds. In a few cases, even two budlets formed from an atrophied single budlet, suggesting that the atrophy state is not due to budlet inability to develop, but it is the result of competition between blastogenetic generations.

During budlet regeneration or atrophied budlet development, the achievement of the double vesicle stage represented the first sign of normal blastogenetic development recovery. The double vesicle stage is considered ''a triploblastic vesicle of the gastrula type'' (Brien, 1968), based on its organogenetic capacities: the outer vesicle is formed by the epidermis and will give rise to the zooid epidermis, whereas the inner vesicle and the mesenchyme will form all the internal tissues of the zooid (Fig. 3E) (Manni and Burighel, 2006; Manni et al., 2007; Ricci et al., 2016a).

It is important to note that the parental bud in colonies at advanced developmental phases do not develop new budlets (budlet-ectomy performed on or after stage 7). This suggests that the blastogenetic capabilities are inhibited in buds after the developmental stage 7, a stage where the budlets developed from a disc on the wall of the bud. These

experiments demonstrated that the blastogenetic competence is restricted in time and space. The factors that determine and restrict it are unknown.

6.3 Zooid growth during blastogenesis

The size of the zooid is dependent on its bud size: it changes over generations, with a general trend to increase (Berrill, 1941a,b; Sabbadin, 1958).

Budectomy experiments were used to analyze zooid growth and to investigate if it is influenced by competition between budlets developing on the same bud, and by competition among generations coexisting in the colony (Sabbadin, 1958; Lauzon et al., 2002).

The budectomy experiment showed that when all buds but one were removed from the zooids, the size of the following generation zooids was larger than the first ones (Fig. 5B-D; Suppl. Tables 7, 8). Possible explanations are: i) in experimental colonies, the single maturing bud per generation does not need to compete for nutrients with other buds, and it solely benefits from parental degeneration at TO; ii) once adult, this zooid supports the development of only one bud; iii) bud and adult generation time (*i.e.*, stages 8 and 9), in experimental individuals, last longer than in controls (see below), so that they can grow for a longer period of time.

Bud and/or adult zooid removal was also used to study the involvement of buds / zooids and the vascular system on regulating programmed cell death (PCD) and cell clearance during the TO phase (Lauzon et al., 2007). This study revealed: a bud-independent signal that activates PCD in old zooids and a bud-dependent, survival signal that acts in short-range fashion via the colonial vasculature and requires mature buds (Lauzon et al., 2007). The importance of the availability of an adequate quantity of nutrients for bud development is suggested by the requirement of appropriate phagocytosis for the onset of a new blastogenetic cycle, as indicated by the severe impairment of bud development when phagocyte activity is inhibited (Voskoboynik et al., 2004). Therefore, the same kinds of turn-over processes occurring in long-lived animals *(i.e.*, continual death and disposal of aged cells counterbalanced by regeneration from stem and progenitor cells) ensure the growth of the colony by cycles of death and regeneration of its constituent zooids (Lauzon et al., 2002).

6.4 Synchronization among generations and duration of the blastogenetic cycle

The blastogenetic cycle is characterized by synchronized development of all buds and budlets in the colony. Zooids degeneration during the TO phase is also synchronized. Budectomy can perturb the synchronization among generations and influence the duration of the blastogenetic cycle providing information on the relationships between adult zooids and their buds (Sabbadin, 1958; Lauzon et al., 2007). When colonies grow in unfavorable environmental conditions, the number of budlets and buds decreases, and adult zooids tend to be resorbed before they are fully developed. When this happens, primary buds mature to functional zooids earlier. Stress conditions also perturb synchronization in 34% of colonies observed (Sabbadin, 1958). Under extreme environmental conditions, colonies can survive with only two generations of individuals (zooids and primary buds), with reduced blastogenetic and growing capabilities. This occurs when the older generation is resorbed, and buds enter the adult stage before their budlets are capable of budding. (Suppl. Tables 9-11). Conversely, when budlets and buds are removed (Fig. 3D), adult zooids remain active for a longer time compared to the controls (Fig. 5F; Suppl. Table 11).

Furthermore, the incomplete removal of advanced right buds can induce the regeneration of new budlets from bud remnants when adults have already entered TO. The removal can also trigger the development of atrophied budlets on the opposite side (Fig. 3D). These buds are smaller than those developed from normal budlets, and the time they take to develop is significantly shorter (Fig. 5E, Suppl. Table 11), since they are forced to open their siphons and begin filtration as soon as possible for colony survival, with limited or no energy provisions for their growth from the parental zooids (Sabbadin, 1958).

The above observations indicate a close relationship between buds and adults: the growth of the former is dependent on the resorption of the latter at TO. Once buds are removed, zooids need more time to bud new generations that will replace them; conversely, as reported, precocious resorption of the adult zooids determines a faster development of buds to become adults.

More than three coexisting generations were observed in several zooids, where all but one of the buds were removed (see colony group C in Suppl. Table 9). In these experiments, the extension of the adult state beyond the normal period of blastogenesis

might explain this phenomena. Considering that a longer adult lifespan causes a longer bud lifespan (Fig. 5E-F; Suppl. Table 11), a new generation of primary buds appears before the generation change (Sabbadin, 1958). This new primary bud generation can give rise to budlets (fourth generation) that, once at the blastogenetic developmental stage 7, are able to bud a fifth blastogenetic generation of budlets before the adult zooids complete their resorption at TO. This anomalous phase can be indicated by the formula 11/9/8/7/1. Similar phenomena has been observed when a chemical treatment (BHT) prevented the resorption of the colony zooids (Voskoboynik et al., 2004) in *B. schlosseri* and also in *Symplegma reptans* (Sugino and Nakauchi, 1987), an ascidian belonging to the same family - Styelidae - as *Botryllus*.

7. Left-right axes determination in blastogenesis: the *situs inversus viscerum*

In ascidians, zooids have a marked bilateral asymmetry: the digestive tract is located on the left of the branchial basket, laterally to its posterior tract, and the heart is located ventrally, at the bottom of the branchial chamber, on the right side of the midline marked by the endostyle. Occasionally, the bilateral asymmetry of viscera appears reversed: the digestive tract extends to the right of the branchial chamber, and the heart is placed on the left of the midline. This condition, known as *situs inversus viscerum* (*SIV*) (Figs. 6-7), is rare (< 0.1%) in nature: only a single oozooid, out of 1,500 in *B. schlosseri* (Sabbadin, 1956) and few reversed blastozooids out of many thousands in *Metandrocarpa taylori* (Watanabe and Newberry, 1976) were found. These zooids are able to multiply regularly by budding and produce normal gametes.
As previously reported (Fig. 4A; Suppl. Table 1), in small colonies, *e.g*. those formed by the oozooid and its bud and budlets, or by zooids belonging to the first blastogenetic generations, usually only the right budlet can develop. In such small colonies (at the developmental phase 9/8/2), the removal of the single bud at the blastogenetic developmental stage 8 can result in: i) the resumption of development of the left budlet (most frequent event); ii) the recovery of development of a posterior bud, if present; iii) the regeneration of a new bud from an incompletely removed bud; iv) the death of the colony left without any bud (Fig. 4; Sabbadin, 1956, 1958). In most of the cases where colonies survive, buds having resumed their development maintain the parental *situs viscerum* (Table 1) (Fig. 6A). This is the rule in the case of regenerated buds after

incomplete removal. However, in 12% of the cases of development from an atrophied bud, especially when the adult zooids undergo a precocious TO before the formation of viscera in the budlet (stage 4), *SIV* appears (Table 2) (Fig. 6B, 7). The occurrence of *SIV* in incompletely removed buds that have regenerated, was reported in *S. reptans* (Sugino and Nakauchi, 1987) and can also be experimentally induced in *P. misakiensis* (Kawamura and Watanabe, 1982; Oda and Watanabe, 1981, 1982). The probability to obtain buds with *SIV* decreases in older blastogenetic generations. The highest frequency (17.64%) is observed in oozooids; it decreases to 13.38% in the 1st blastozooid and to 7.54% in colonies formed by the second blastozooids and their buds. However, when buds at developmental stage 8 are destroyed (tearing of the body wall and viscera removal) without affecting their budlets, and circulation between the adult zooid and the bud remains intact (Fig. 6C), the parental asymmetry is maintained and *SIV* never appears (Sabbadin, 1960). Repeated experiments indicate that, once present, *SIV* always originates in the buds, and is preserved in the subsequent blastogenetic generations (up to 20) as zooids with *SIV*. In this way, large colonies of hundreds of individuals can be obtained with *SIV* in all zooids (Sabbadin, 1956, 1960). However, the inverted asymmetry cannot be transmitted sexually as colonies with *SIV* undergoing sexual reproduction always originate colonies with normal *situs viscerum*. When genetically compatible colonies with normal asymmetry are left to fuse with colonies with *SIV*, zooids with opposite asymmetry coexist in the same chimeric colony and their buds maintain the asymmetry of their parent zooids (Fig. 8) even when adult SIV zooids are ablated to enhance the influence of normal zooids. This suggests that *SIV* is an epigenetic phenomenon, not controlled by factors diffusing from the common circulation, and indicates that the determination of bilateral asymmetry is very precocious, present in the budlets as early as developmental stage 3. Probably, the parental control occurred directly through the peribranchial epithelium, from which budlets derived and upon which they depend for their polarity (Sabbadin, 1966).

In normally asymmetric zooids of *B. schlosseri*, the blastogenetic potential is higher on the right side, whereas the ability to mature gonads is higher on the left side (Gasparini et al., 2015). Once a zooid develops an inverted bilateral asymmetry, its blastogenetic and gonadogenetic potentials are also reversed (Sabbadin, 1956, 1960; Gasparini et al., 2015). In colonies with normal asymmetry, 73% of buds emerge on the right side and 27% on the left one, whereas inverted colonies produce 25% of right buds and 75% of

left buds (Sabbadin, 1960). In gonadogenesis, gonads are usually observed on the left side in 68% of the observed control zooids, whereas, in *SIV* colonies, the right side produced more eggs in 76% of the zooids (Sabbadin, 1960).

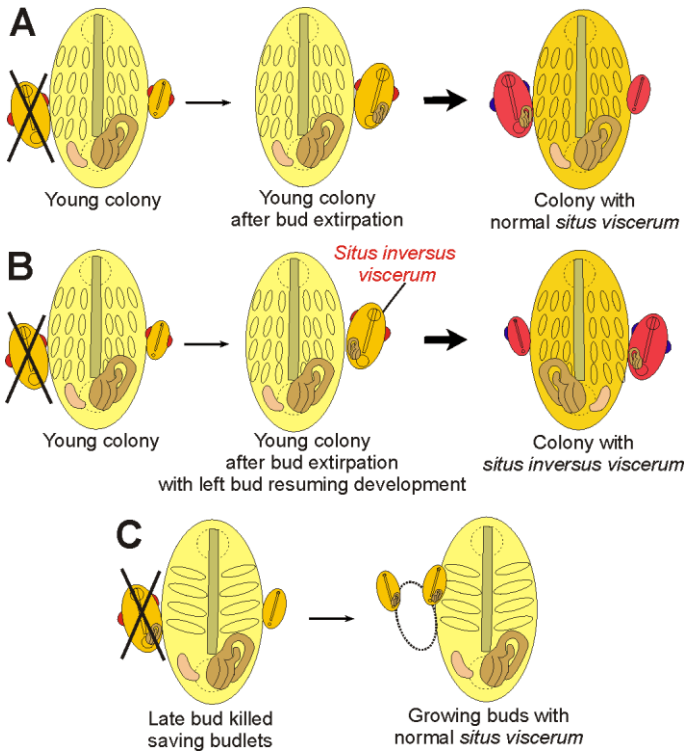

Fig. 6: Experiments of bud removal causing *SIV* appearance (Sabbadin, 1960). Color code and symbols as in Fig. 4. Ventral view. **A**: a high percentage of zooids derived from atrophied budlets resuming development after the removal of the right anterior bud having reached the blastogenetic developmental stage 8 maintain a normal *situs viscerum*, evidenced by the gut on the left side and the heart on the right side of the body. **B**: if buds removal occurs when colonies are approaching TO, *SIV* can develop (note that gut and heart have an opposite position with respect to endostyle, as compared with colonies with normal *situs viscerum*). **C.** In the case buds are killed without affecting their budlets, the parental asymmetry is maintained and *SIV* never appears.

Asymmetry of parental zooid	**Asymmetry of buds**					
	Normal			Reversed		
	Buds with normal growth	Restored buds	Buds with late development	Buds with normal growth	Restored buds	Buds with late development
Normal	21	4	21	5	–	9
Percentage	**77**			**23**		
Reversed	1	–	1	26	4	8
Percentage	**5**			**95**		

Table 1: Percentages of buds with normal or reversed bilateral asymmetry of viscera (*situs viscerum*) obtained in experiments of late bud extirpation from young colonies and comparison with bilateral asymmetry of the parental zooid.

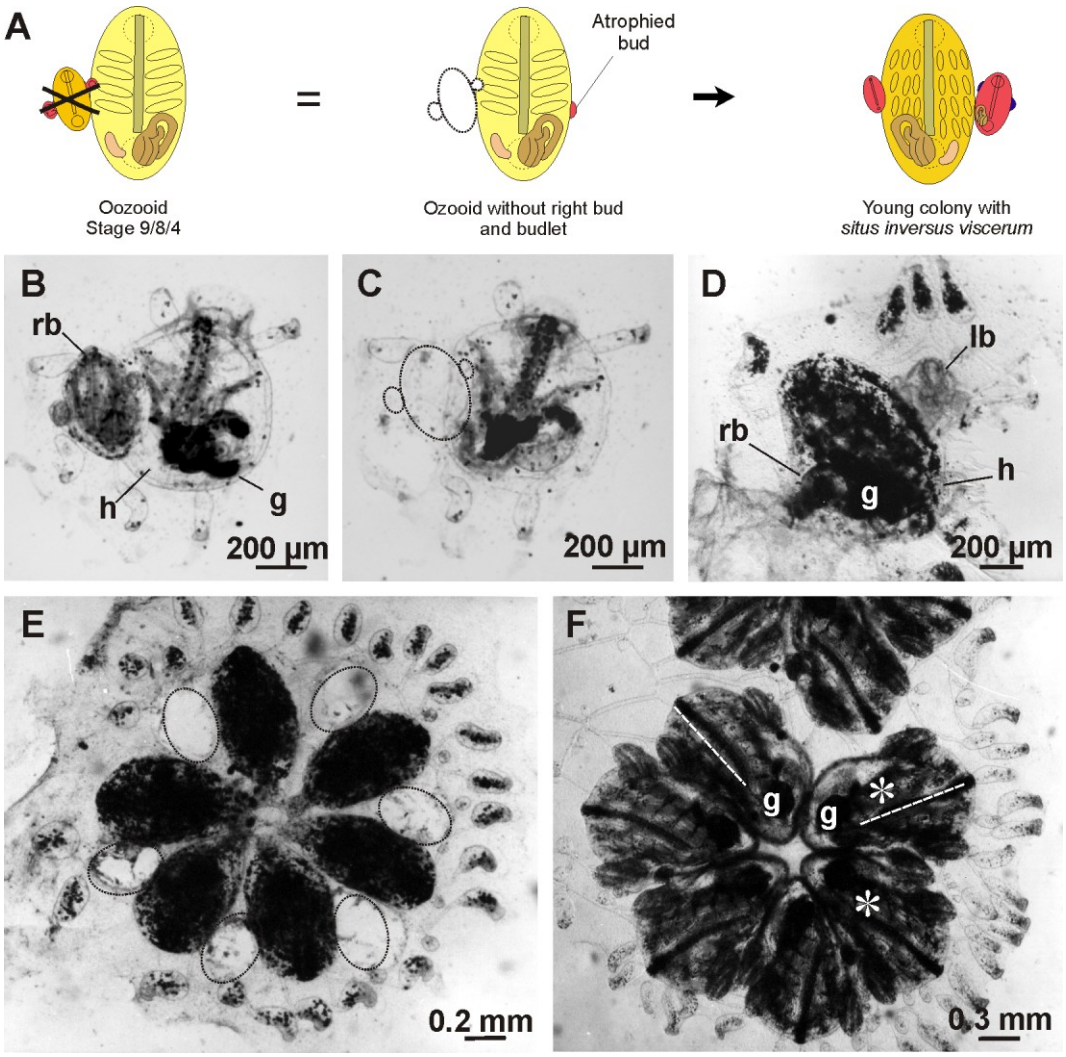

Fig. 7: **A**: SIV induction in the first blastozooid by removal of the oozooids right bud. **B**: control oozooids. **C**: oozooids deprived of its bud. **D**: blastozooid with SIV deriving from the recovery of the atrophied left budlets. **E**: colony with removed buds. The recovery of its atrophied budlets resulted in a colony (**F**) with two SIV zooids (**asterisks**). **g**: gut; **h**: heart; **lb**: left budlet; **rb**: right budlet; the endostyle is marked with a dotted line.

Asymmetry and functional condition of parental zooid	**Asymmetry of buds**	
	Normal	Reversed
Normal, filter-feeding	100	–
Reversed, filter-feeding	–	100
Normal, at TO	75	25
Reversed, at TO	100	100

Table 2: Percentages of buds with normal or reversed bilateral asymmetry of viscera (*situs viscerum*) in relation to the functional conditions of the parental zooid and its asymmetry at the moment of bud differentiation.

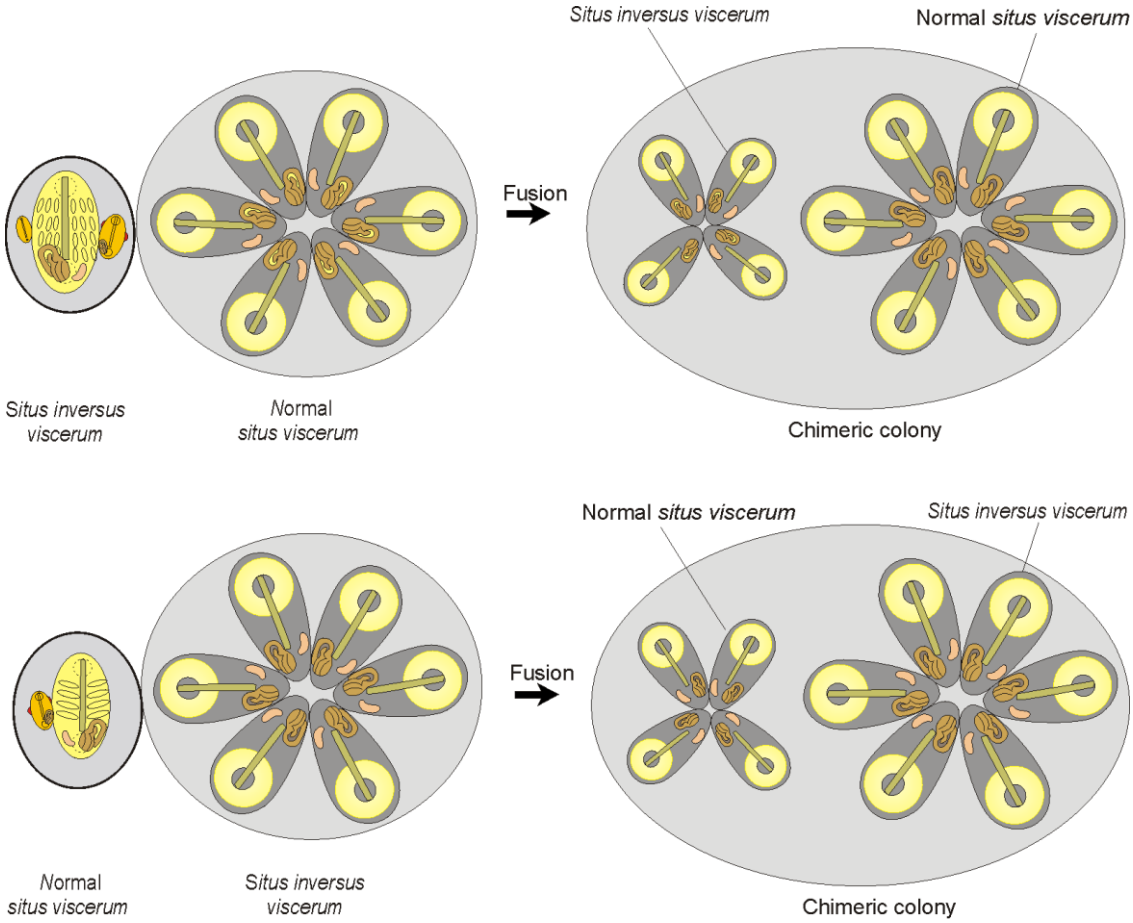

Fig. 8: Effect of colony size on bilateral asymmetry in parabiosis experiments. Young colony with *SIV* fused with a larger, genetically compatible colony with normal *situs viscerum* (top) and young colony with normal *situs viscerum* fused with a larger, genetically compatible colony with *SIV*. In both cases, the chimeric colony maintains the original bilateral asymmetry of the zooids over generations.

8. An alternative asexual reproduction: the vascular budding

Vascular budding (termed whole-body regeneration when induced experimentally; Rinkevich et al., 1995; Voskoboynik et al., 2007) was first described in botryllid ascidians more than two hundred years ago (Savigny, 1816) and observed again by Giard (1872). However, it was denied by Metschnikow (1869), who was convinced that buds originated only from the body walls (palleal budding). Bancroft (1903b) and Herdman (1925) again described the process. In species of the genus *Botrylloides*, vascular budding is generally associated with the process of aestivation or hibernation, during which colonies resorb their zooids to overcome the adverse periods. Zooids appear again, formed by tunic vessels, when environmental conditions turn mild

(Bancroft, 1903b; Oka and Watanabe, 1959; Burighel et al., 1976; Rinkevich et al., 1995; Rinkevich et al., 2007a, 2007b; Brown et al., 2009; Atsumi and Saito, 2011). Conversely, in *B. primigenus*, vascular budding is a physiological process that occurs continuously near the leading edge of the colony, contributing to the growth of the colony (Oka and Watanabe, 1957b). A physiological vascular budding has also been reported in the stolidobranch styelid *Symplegma brakenhielmi* (Gutierrez and Brown, 2017) and the phebobranch *Perophora viridis* (Freeman, 1964).

In *B. schlosseri*, vascular budding is usually repressed and occurs only after the removal of all the zooids and the buds from the colonial matrix (*i.e.*, the tunic and the common vasculature) in colonies approaching or undergoing TO (Fig. 9A-D; Milkman, 1967; Sabbadin et al., 1975; Voskoboynik et al., 2007; Kürn et al., 2011; Ricci et al., 2016a) and implies a sequence of morphological abnormal developmental steps (Voskoboynik et al., 2007). Vascular buds maintain the asymmetry of the parental colony (Table 3), suggesting that the colonial matrix has a role of in the transmission of the bilateral asymmetry to newly-formed vascular buds (Sabbadin et al., 1975). Unlike palleal buds, vascular buds are formed by the epidermis lining the vasculature and circulating cells (hemoblasts), featuring stem cell properties (Oka and Watanabe, 1957b; Rinkevich et al., 1995; Voskoboynik et al., 2007), able to originate both the soma and germ line (Sunanaga et al., 2006; Voskoboynik et al., 2007). A bud primordium appears as an aggregate of hemocytes, adhering to the vessel epithelium, that show the morphology of stem cells, such as small size and high nucleus-cytoplasm ratio (Freeman, 1964; Oka and Watanabe, 1957b; Voskoboynik et al., 2007; Rinkevich et al., 2007b, 2008). In botryllid ascidians, these cell aggregates appear at the bases of the ampullae (the blind endings of the tunic vessels) and, later, organize to form a double vesicle stage, critical for bud organogenesis and normal bud development (Oka and Watanabe, 1957b; Rinkevich et al., 1995). A heart-like organ is the first organ to develop in the vascular buds, supporting efficient blood flow to the regenerating area and essential to zooid development (Voskoboynik et al., 2007). Vascular budding is part of the normal life cycle of *Botrylloides leachii* (Rinkevich et al., 1995; Rinkevich et al., 2007a). In this species, the process occurs in five stages (Zondag et al., 2016; Blanchoud et al., 2017). In the first stage, lasting 15 h, wound healing takes place, then, a restructuring of the vessel architecture and of the ampullae occurs leading to the formation of small regeneration niches (stage 2), followed by the contraction of the tissues (stage 3) and the

homing of stem cells in the regeneration niches (stage 4). Finally, the competition among the various stem cell aggregates (stage 5) leads to the maturation of a single bud per experimental fragment (Rinkevich et al., 2007a, 2007b, 2008; Zondag et al., 2016; Blanchoud et al., 2017).

Buds	Asymmetry of the parental colony	Asymmetry of buds	
		Normal	Reversed
Palleal, isolated	Normal	100	–
	Reversed	–	100
Palleal, transplanted	Donor and recipient reversed	–	100
	Donor normal, recipient reversed	100	–
Vascular	Normal	97	3
	Reversed	–	100

Table 3: Percentages of palleal (isolated in place or transplanted) and vascular buds with normal or reversed bilateral asymmetry of viscera (*situs viscerum*) in relation to the bilateral asymmetry of the parental colony.

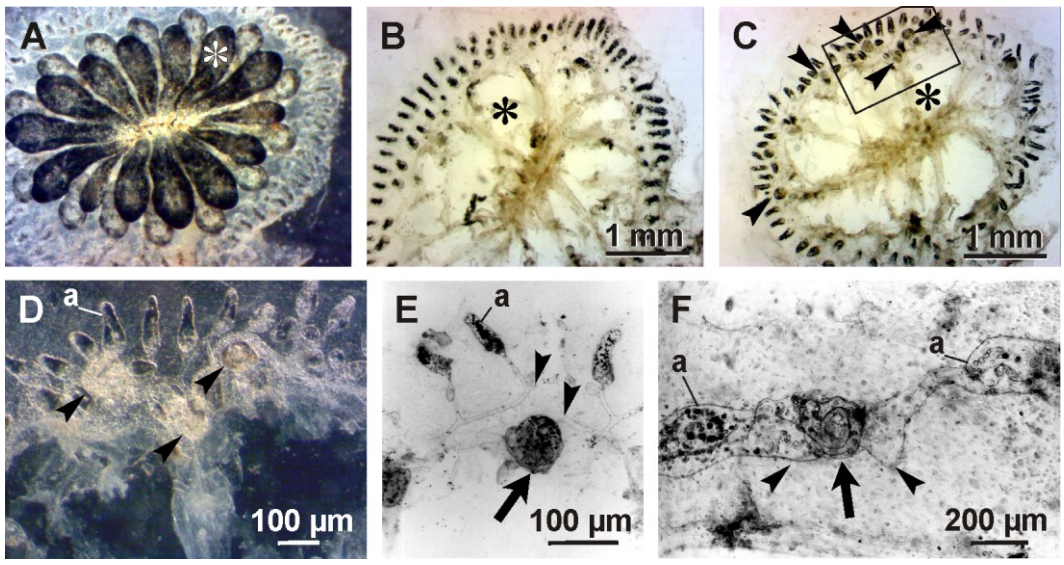

Fig. 9: A-D: vascular budding. **A**: colony before the removal of zooids and buds. **B**: remaining colonial matrix. **C-D**: vascular buds (**arrowheads**) in the colonial matrix. The asterisks mark the location of a reference zooid in the colonial matrix. The squared area in **C** is enlarged in **D**. **E**: isolated palleal bud (**arrow**). Note the truncated edges of the marginal vessel (**arrowheads**) **F**: isolated palleal bud (**arrow**) contacted by two ampullae (**arrowheads**). **a**: ampulla.

9. Genes associated with vascular budding

Recently, the expression pattern of a number of genes related to vascular budding have been studied in various botryllid species except *B. schlosseri*.

Vascular buds do not express *piwi* in *B. primigenus* (Sunanaga et al., 2010). However, a role of hemocytes lining the vessel epithelium, able to proliferate and expressing *piwi*, has been postulated in the formation of the bud primordia in *Botrylloides violaceus* (Brown et al., 2009) and *B. leachii* (Rinkevich et al., 2010). Analogous to palleal budding of colonial ascidians (Kawamura et al., 1993, 2013), vascular budding in *Botrylloides* requires the presence of retinoid acid (RA): RA inhibitors block the process, whereas RA agonists accelerate bud formation and increase the number of buds per experimental fragment (Rinkevich et al., 2007a). In addition, serine proteases are also required, as serine protease inhibitors alter the development of vascular buds in *Botrylloides* (Rinkevich et al., 2007b). This is probably in relation with the role of the enzyme in remodeling the extracellular matrix (Rinkevich et al., 2007b). This hypothesis agrees with the observation that the transcription of a trypsin-like serine protease increases upon RA treatment in the budding ascidian *P. misakiensis* (Ohashi et al., 1999). In botryllid ascidians, the transcripts for aldehyde dehydrogenase, an enzyme involved in RA synthesis, and a serine protease similar to the mammalian urokinase-type plasminogen activator, are mainly located in stem cell populations (Laird et al., 2005a) but are also present in other cells including circulating phagocytes (Rinkevich et al., 2007a, 2007b). The latter are deeply involved in innate immune responses of botryllid ascidians (Franchi and Ballarin, 2017). This suggests a key role of these cells in vascular budding, in addition to their ascertained role in palleal budding (Voskoboynik et al., 2004). The above results imply the involvement of innate immune responses in morphogenetic events of colonial ascidians. According to this, *B. leachii* vascular budding is associated with the differential transcription of various immune genes codifying for membrane and soluble proteins acting both as receptors or adhesion proteins (*e.g.*, lectins, integrins) and effectors (*e.g.*, complement factors, serine proteases) (Rinkevich et al., 2007b). An increased transcription of genes involved in cell signaling and for transcription factors has also been revealed by EST's derived from early stages of vascular buds (Rinkevich et al., 2008).

10. Strategies for survival in isolated or transplanted buds and blastogenetic regeneration

When all the adult zooids and budlets in a colony are removed, the remaining buds (at blastogenetic developmental stage 8) can reach adulthood even if all the left buds and about 40% of the right buds undergo resorption (Zaniolo et al., 1976). Once they become adults, only the right buds are able to develop to full functionality.

When buds are isolated from the common vasculature, vascularization is required for their survival as development does not progress without the connection to the tunic vessels (Zaniolo et al., 1976) (Fig. 9E-F). New branches sprout from the colonial marginal vessel attracted by the isolated buds: they join the buds always on the right side (or on the left side in case of buds with *SIV)*. In normal blastogenesis, the entrance of the affluent vessel marks the posterior end of the bud in both vascular and transplanted buds (Sabbadin et al., 1975; Zaniolo et al., 1976). Sometimes, isolated buds can form their own vascular system and are progressively resorbed without reaching adulthood, allowing the development of their right bud, which can form a functional adult. In this case, when a new adult is formed, its buds are at the blastogenetic developmental stage 4 or 5, so that, for a short period of time, the budlet generation is lacking and two, instead of three, generations are present (Zaniolo et al., 1976).

Palleal buds removed from the parental zooid at developmental stages 1-3, and transplanted in the colonial matrix of a genetically compatible colony, can grow if vascularized and maintain their bilateral asymmetry (Sabbadin et al., 1975). Once isolated, they can also be cultured *in vitro*, where they can survive up to 5 months (Rabinowitz and Rinkevich, 2003, 2004). If cultured in an artificial medium at later developmental stages (4-5), they form epithelial monolayers expressing cadherin, PL10, piwi and mortalin (Rabinowitz and Rinkevich, 2011; Ben-Hamo et al., 2018). However, cells stop dividing after 24-72 h, without producing any permanent cell line (Rabinowitz et al., 2009; Rabinowitz and Rinkevich, 2011). Collectively, the study of the development and senescence of these transient cell cultures from dissected buds evidences that, under *in vitro* conditions, the normal growth processes are replaced by different developmental pathways, but also that internal clocks programming cyclical death, are replaced by new biological mechanisms with different timetables (Rabinowitz and Rinkevich, 2004).

In the Japanese species *P. misakiensis* (Kawamura and Fujiwara; 1995) and *B. primigenus*, (Kawamura et al., 2006), the establishment of stable cell lines from bud tissues was reported. The results are still debated as a contamination by traustochytrids protists is suspected (Rinkevich, 1999).

The term **"**blastogenetic regeneration"**,** introduced by Sugino and Nakauchi (1987), indicates the regeneration of a colony from fragments of buds through the emission of buds from the bud remnants that, after healing of the cut surfaces, are progressively resorbed. The process was initially described in *B. schlosseri* (Majone, 1977), in young colonies (at the developmental phase 9/8/4), where both adults (stage 9) and budlets (stage 4) were removed as well as the posterior part of the buds (stage 8). The anterior fragments, containing the oral siphon, the neural complex, part of the branchial basket and of the endostyle remained connected to the tunic circulation via the radial vessel. In these fragments, the internal tissues lose their morphology and are progressively resorbed, and new vascular connections with the colonial marginal vessel replace the original radial vessel. Five to six days after the operation, new budlets sprout from the bud remnant: only one of them reaching adulthood. Up to 17% of the zooids obtained by blastogenetic regeneration, have inverted asymmetry (Majone, 1977). A similar regeneration process was described in *S. reptans* (Sugino and Nakauchi, 1987), together with a normal regeneration of bud fragments through a morphallactic process, also reported in *P. misakiensis* (Oda and Watanabe, 1982; Sugino and Nakauchi, 1987).

11. Future perspectives

Colonial ascidians are representative of tunicates, the sister group of vertebrates. They are the only chordates capable of asexual reproduction and vascular budding. Colonial ascidians are ideal models for the study of tissue regeneration and development, due to their diverse reproductive strategies, relatively short lifespan, simple morphological and genomic organization, and easy experimental use. The studies described above detail the varied strategies *B. schlosseri* colonies undertake to survive and propagate. These strategies include: variations in bud developmental potential, zooid growth potential, and duration of a generation cycle, and under certain conditions the number of coexisting generations and the number of coexisting genotypes (formation of chimeras). Old and young generations coexisting in the colony,

create a continuous balance between the energy provided by the adult zooids sustaining the colony and the energy required to support bud development. Today, new molecular and gene manipulation tools can be used to study these biological phenotypes. The anatomical and developmental ontology of *B. schlosseri* asexual development is now available, allowing the use of a controlled and shared vocabulary among different laboratories (Manni et al., 2014). The hypothesis of the close evolutionary relationship between tunicates and vertebrates (Delsuc et al., 2018; Kocot et al., 2018; Giribet, 2018) is also supported by analysis of hundreds of nuclear genes from 15 species, including the colonial tunicate *B. schlosseri* (Voskoboynik et al., 2013a) and outcomes of single gene/structure/pathway studies on *B. schlosseri* asexual reproduction (Degasperi et al., 2009; Gasparini et al., 2013, 2016). The genomes of *B. schlosseri* and *B. leachii* have been published (Voskoboynik et al., 2013a; Blanchoud et al., 2018), and transcriptomes covering different reproductive/regenerative traits are available (Voskoboynik et al., 2013a, 2013b; Campagna et al., 2016; Corey et al., 2016; Kowarsky et al., 2017; Rosental et al., 2018; Ricci et al., 2016b). Methods to label, sort and transplant specific cell populations, and assayed cell differentiation capacities have been developed (Laird et al., 2005a; Voskoboynik et al., 2008; Lauzon et al., 2013; Rinkevich et al., 2013; Corey et al., 2016; Rosental et al., 2018). In addition, powerful imaging systems allow the tracing of labeled cells *in vivo* via the transparent body of young colonies (Voskoboynik et al., 2008; Rinkevich et al., 2013; Rodriguez et al., 2017; Rosental et al., 2018), and methods to silence specific genes (Laird et al., 2005b; Rosner et al., 2006, 2007, 2013; Tiozzo and De Tomaso, 2009; Voskoboynik et al., 2013b; Ricci et al., 2016a) are available. Moreover, powerful statistical approaches take advantage of coloniality, in which each individual zooid is essentially a biological replicate and differences among individuals derive only from external perturbations (*e.g.*, experimental variations) (Gasparini et al., 2014; Manni et al., 2018).

Altogether, the knowledge gained through 60 years of experimental studies of *B. schlosseri,* and the methods and databases developed, render *B. schlosseri* an excellent model for the study of stem cell mediated regenerative processes, development, chimerism and senescence.

Acknowledgments

The authors thank Prof. F. Majone for the picture of isolated palleal bud (Fig. 9F), Karla Palmeri and Katherine Ishizuka for excellent edits. This work was supported by grants from the University of Padova - Progetti di Ricerca di Ateneo [Grant 2015 - CPDA153837] to LM and from COST (COST action 16203) to LB and NIH grants RO1GM100315 to A.V.

REFERENCES

- Atsumi MO., Saito Y. (2011). Studies on Japanese botryllid ascidians. V. A new species of the genus *Botrylloides* very similar to *Botrylloides simodensis* in morphology. Zool Sci 28: 532-542

- Ballarin L., Rinkevich B., Bartscherer K., Burzynski A., Cambier S., Cammarata M., Domart-Coulon I., Drobne D., Encinas J., Frank U., Geneviere A-M., Hobmayer B., Löhelaid H., Lyons D., Martinez P., Oliveri P., Peric L., Piraino S., Ramšak A., Rakers S., Rentzsch F., Rosner A., Da Silva TH., Somorjai I., Suleiman S., Coelho AV. (2018). Maristem — Stem cells of marine/aquatic invertebrates: from basic research to innovative applications. Sustainability 10(2): 526

- Bancroft FW. (1903a). Variation and fusion of colonies in compound ascidians. Proc California Acad Sci (Ser 3) 3: 137-186

- Bancroft FW. (1903b). Aestivation of *Botrylloides gascoi* Della Valle. Mark Anniversary Volume, 147-166

- Ben-Hamo O., Rosner A., Rabinowitz C., Oren M., Rinkevich B. (2018). Coupling astogenic aging in the colonial tunicate *Botryllus schlosseri* with the stress protein mortalin. Dev Biol 433: 33-46

- Berrill NJ. (1941a). The development of the bud in *Botryllus*. Biol Bull 80:169–184

- Berrill NJ. (1941b). Size and morphogenesis in the bud of *Botryllus*. Biol Bull 80:185–193

- Berrill NJ. (1951). Regeneration and budding in tunicates. Biol Rev 26:456–475

- Blanchoud S., Zondag L., Lamare MD., Wilson MJ.. (2017). Hematological analysis of the ascidian *Botrylloides leachii* (Savigny, 1816) during whole-body regeneration. Biol Bull 232: 143-157

- Blanchoud S., Rutherford K., Zondag L., Gemmell NJ., Wilson MJ. (2018). *De novo* draft assembly of the *Botrylloides leachii* genome provides further insight into tunicate evolution. Sci Rep 8: 5518

- Brien P. (1968). Blastogenesis and morphogenesis. Adv Morphogen 7: 151–203

- Brown FD., Keeling EL., Le AD., Swalla BJ. (2009). Whole body regeneration in a colonial ascidian, *Botrylloides violaceus*. J Exp Zool 312B: 885-900

- Bruguière JG. (1792). Encyclopédie méthodique. Histoire naturelle des vers. Tome premier. Panckoucke, Paris, 1-757

- Brunetti., Manni L., Mastrototaro F., Gissi C., Gasparini F. (2017). Fixation, description and DNA barcode of a neotype for *Botryllus schlosseri* (Pallas, 1766) (Tunicata, Ascidiacea). Zootaxa 4353: 29-50

- Burighel P., Brunetti R. (1971). The circulatory system in the blastozooid of the colonial ascidian *Botryllus schlosseri* (Pallas). Boll Zool 38: 273–289

- Burighel P., Cloney RA. (1997). Urochordata: Ascidiacea. In: Harrison FW, Ruppert EE, editors. Microscopic anatomy of invertebrates. Vol. 15. New York: Wiley-Liss, Inc. 221–347

- Burighel P., Brunetti R., Zaniolo G. (1976). Hibernation of the colonial ascidian *Botrylloides leachi* (Savigny): histological observations. Boll Zool 43: 293-301

- Burnet FM. (1971). Self recognition in colonial marine forms and flowering plants in relation to the evolution of immunity. Nature 232: 230–235

- Campagna D., Gasparini F., Franchi N., Vitulo N., Ballin F., Manni L., Valle G., Ballarin L. (2016). Transcriptome dynamics in the asexual cycle of the chordate *Botryllus schlosseri*. BMC Genomics 17: 275

- Corey DM., Rosental B., Kowarsky M., Sinha R., Ishizuka KJ., Palmeri KJ., Quake SR., Voskoboynik A., Weissman IL. (2016). Developmental cell death programs license cytotoxic cells to eliminate histocompatible partners. Proc Natl Acad Sci USA 113: 6520-6525

- Degasperi V., Gasparini F., Shimeld SM., Sinigaglia C., Burighel P., Manni L. (2009). Muscle differentiation in a colonial ascidian: organisation, gene expression and evolutionary considerations. BMC Dev Biol 9: 48

- Della Valle A. (1881). Nuove contribuzioni alla storia naturale delle ascidie composte del Golfo di Napoli. Atti Acc Naz Lincei Mem (ser. 3) 10: 431-498

- Delsuc F., Philippe H., Tsagkogeorga G., Simion P., Tilak MK., Turon X., López-Legentil S., Piette J., Lemaire P., Douzery EJP. (2018). A phylogenomic framework and timescale for comparative studies of tunicates. BMC Biol. 16(1):39

- Di Maio A., Setar L., Tiozzo S., De Tomaso AW. (2015). Wnt affects symmetry and morphogenesis during post-embryonic development in colonial chordates. Evodevo 6: 17

- Franchi N., Ballarin L. (2017). Immunity in protochordates: the tunicate perspective. Front Immunol 8, 674

- Franchi N., Ballin F., Manni L., Schiavon F., Basso G., Ballarin L. (2016). Recurrent phagocytosis-induced apoptosis in the cyclical generation change of the compound ascidian *Botryllus schlosseri*. Dev Comp Immunol 62: 8-16

- Freeman G. (1964). The role of blood cells in the process of asexual reproduction in the tunicate *Perophora viridis*. J Exp Zool 156: 157-184

- Ganin M. (1870). Neue Tatsachen aus der Entwicklungsgeschichte der Ascidien. Zeitschr wiss. Zool. 20: 512-518

- Gärtner J. (1774). Zoophyta, quaedam minuta. In: Pallas PS, Specilegia Zoologia. Lange, Berlin, fasc. 10: 24-41

- Gasparini F., Shimeld SM., Ruffoni E., Burighel P., Manni L. (2011). Expression of a *Musashi*-like gene in sexual and asexual development of the colonial chordate *Botryllus schlosseri* and phylogenetic analysis of the protein group. J Exp Zool 316B: 562-573

- Gasparini F., Degasperi V., Shimeld SM., Burighel P., Manni L. (2013). Evolutionary conservation of the placodal transcriptional network during sexual and asexual development in chordates. Dev Dyn 242:752–66

- Gasparini F., Caicci F., Rigon F., Zaniolo G., Manni L. (2014). Testing an unusual *in vivo* vessel network model: a method to study angiogenesis in the colonial tunicate *Botryllus schlosseri*. Sci Rep 4: 6460

- Gasparini F., Manni L., Cima F., Zaniolo G., Burighel P., Caicci F., Franchi N., Schiavon F., Rigon F., Campagna D., Ballarin L. (2015). Sexual and asexual reproduction in the colonial ascidian *Botryllus schlosseri*. Genesis 53: 105-120

- Gasparini F., Skobo T., Benato F., Gioacchini G., Voskoboynik A., Carnevali O., Manni L., Dalla Valle L. (2016). Characterization of Ambra1 in asexual cycle of a non-vertebrate chordate, the colonial tunicate *Botryllus schlosseri*, and phylogenetic analysis of the protein group in Bilateria. Mol Phylogenet Evol 95: 46-57

- Giard AM. (1872). Recherches sur les ascidies composée ou synascidies. Arch Zool Exp Gén 1: 501-687

- Gibin C. (1997). L'esplorazione del golfo di Venezia. I disegni del naturalista chioggiotto Stefano Chiereghin per Lazzaro Spallanzani. T&G Edizioni, Conselve

- Gibin C. (2013). Lettere di Stefano Andrea Renier (Chioggia 1759-Padova 1830) professore di Storia Naturale. Il Leggio Libreria Editrice, Sottomarina

- Giribet G. (2018). Phylogenomics resolves the evolutionary chronicle of our squirting closest relatives. BMC Biol 16(1):49

- Gutierrez S., Brown FD. (2017). Vascular budding in *Symplegma brakenhielmi* and the evolution of coloniality in styelid ascidians. Dev Biol 423: 152-169

- Haeckel E. (1899). Kunstformen der Natur. Verlag des Bibliograpischen Insitutts, Leipzig and Wien

- Herdman EC. (1925). *Botryllus*. Trans Liverpool Biol Soc Proc 39: 201-236

- Hjort J. (1893). Über den Entwicklungscyclus der zusammengesetzen Ascidien. Mitt Zool Stn Neapel 10: 584-617

- Izzard CS. (1973). Development of polarity and bilateral asymmetry in the palleal bud of *Botryllus schlosseri* (Pallas). J Morphol 139: 1-26

- Kawamura K., Fujiwara S. (1994). Transdifferentiation of pigmented multipotent epithelium during morphallactic development of budding tunicates. Int J Dev Biol 38:369-377

- Kawamura K., Fujiwara S. (1995). Establishment of cell lines from multipotent epithelial sheet in the budding tunicate, Polyandrocarpa misakiensis. Cell Struct Funct 20: 97–106

- Kawamura K., Watanabe H. (1982). Pattern development in palleal buds of the polystyelid ascidian, *Polyandrocarpa misakiensis*: bud grafting induces bilateral asymmetry conversion through polarity reversal. J Exp Zool 224: 145-156

- Kawamura K., Hara K., Fujiwara S. (1993). Developmental role of endogenous retinoids in the determination of morphallactic field in budding tunicates. Development 117: 835-845

- Kawamura K., Takeoka S., Takahashi S., Sunanaga T. (2006). *In vitro* culture of mesenchymal lineage cells established from the colonial tunicate *Botryllus primigenus*. Zool Sci 23: 245-254

- Kawamura K., Shiohara M., Kanda M., Fujiwara S. (2013). Retinoic X receptor-mediated transdifferentiation cascade in budding tunicates. Dev Biol 384: 343-355

- Kowarsky M., Hotta K., Manni L., Anselmi C., Neff NF., Ishizuka KJ., Palmeri KJ., Okamoto J., Quake SR., Weissman IL., Voskoboynik A. (2017). The molecular signatures of development in *Botryllus schlosseri*. 9th International Tunicate Meeting, New York, July 17-21, 111

- Kocot KM., Tassia MG., Halanych KM., Swalla BJ. (2018). Phylogenomics offers resolution of major tunicate relationships. Mol Phylogenet Evol 121:166-173

- Kürn U., Rendulic S., Tiozzo S., Lauzon RJ. (2011). Asexual propagation and regeneration in colonial ascidians. Biol Bull 221: 43-61

- Laird DJ., De Tomaso AW., Weissman IL. (2005a). Stem cells are units of natural selection in a colonial ascidian. Cell 123: 1351-1360

- Laird DJ., Chang W-T., Weissman IL., Lauzon RJ. (2005b). Identification of a novel gene involved in asexual organogenesis in the budding ascidian *Botryllus schlosseri*. Dev Dyn 234: 997-1005

- Lauzon RJ., Ishizuka KJ., Weissman IL. (1992). A cyclical, developmentally-regulated death phenomenon in a colonial urochordate. Dev Dyn 194: 71–83

- Lauzon RJ., Ishizuka KJ., Weissman IL. (2002). Cyclical generation and degeneration of organs in a colonial urochordate involves crosstalk between old and new: a model for development and regeneration. Dev Biol 249: 333–348

- Lauzon RJ., Kidder SJ., Long P. (2007). Suppression of programmed cell death regulates the cyclical degeneration of organs in a colonial urochordate. Dev Biol 301: 92-105

- Lauzon RJ., Brown C., Kerr L., Tiozzo S. (2013). Phagocyte dynamics in a highly regenerative urochordate: insights into development and host defense. Dev Biol 374(2):357-373

- Linnaeus C. (1767). Systema naturae per regna tria naturae, secundum classes, ordines, genera, species, cum characteribus, differentiis, synonymis, locis. 12th Edition. Salvius, Stockholm

- Londono C., Osorio C., Gama V., Alzate O. (2012). Mortalin, Apoptosis, and Neurodegeneration. Biomolecules 2(1):143-164

- Majone F. (1977). Regeneration of isolated bud fragments of *Botryllus schlosseri*. Acta Embryol Exp 1: 11-19

- Manni L., Burighel P. (2006). Common and divergent pathways in alternative developmental processes of ascidians. Bioessays 28: 902-912

- Manni L., Zaniolo G., Cima F., Burighel P., Ballarin L. (2007). *Botryllus schlosseri*: a model ascidian for the study of asexual reproduction. Dev Dyn 236: 335-352

- Manni L., Gasparini F., Hotta K., Ishizuka KJ., Ricci L., Tiozzo S., Voskoboynik A., Dauga D. (2014). Ontology for the asexual development and anatomy of the colonial chordate *Botryllus schlosseri*. PLoS One 9: e96434

- Manni L., Anselmi C., Burighel P., Martini M., Gasparini F. (2018), Differentiation and induced sensorial alteration of the coronal organ in the asexual life of a tunicate. Integr Comp Biol 58: 317-328

- Metschnikow E. (1869). Entwicklungsgeschichtliche Beiträge. VII. Über die Larven und Knospen von *Botryllus*. Bull Acad Imp Sc St Petersbourg 13: 291–293

- Milkman R. (1967). Genetic and developmental studies on *Botryllus schlosseri*. Biol Bull 132: 229-243

- Oda T., Watanabe H. (1981). Reversal of polarity and laterality in the polystyelid ascidian, *Polyandrocarpa misakiensis*. Proc Japan Acad 57B: 333-336

- Oda T., Watanabe H. (1982). Induction of malformed zooids and determination of polarity in palleal buds of the polystyelid ascidian, *Polyandrocarpa misakiensis*. J Exp Zool 220: 21-31

- Ogasawara M., Di Lauro R., Satoh N. (1999). Ascidian homologs of mammalian thyroid peroxidase genes are expressed in the thyroid-equivalent region of the endostyle. J Exp Zool 285: 158-169

- Ohashi M., Kawamura K., Fujii N., Yubisui T., Fujiwara S. (1999). A retinoic acid-inducible modular protease in budding ascidians. Dev Biol 214: 38-45

- Oka H., Watanabe H. (1957a). Colony-specificity in compound ascidians as tested by fusion experiments. A preliminary report. Proc Imp Acad Japan 33: 657-659

- Oka H., Watanabe H. (1957b). Vascular budding, a new type of budding in *Botryllus*. Biol Bull 112: 225-240

- Oka H., Watanabe H. (1959). Vascular budding in *Botrylloides*. Biol Bull 117: 340-346

- Oka H., Watanabe H. (1960). Problems of colony-specificity in compound ascidians. Bull Mar Stat Asamushi, Tohoku Univ 10: 153-155

- Olivi G. (1792). Zoologia Adriatica ossia catalogo ragionato degli animali del Golfo e delle Lagune di Venezia: preceduto da una dissertazione sulla storia fisica e naturale del Golfo e accompagnato da memorie, ed osservazioni di fisica storia naturale ed economia. Remondini, Bassano

- Pallas PS. (1766). Elenchus zoophytorum sistens generum adumbrationes generaliores et specierum cognitarum succinctas descriptiones cum selectis auctorum synonymis. van Cleef, The Hague

- Pancer Z., Gershon H., Rinkevich B. (1995). Coexistence and possible parasitism of somatic and germ cell lines in chimeras of the colonial urochordate *Botryllus schlosseri*. Biol Bull 189:106-112

- Pizon A. (1893). Histoire de la blastogénèse chez les Botryllides. Ann Sc Nat s 7, Zool 14: 1-386

- Rabinowitz C., Rinkevich B. (2003). Epithelial cell cultures from *Botryllus schlosseri* palleal buds: accomplishments and challenges. Methods Cell Sci 25: 137-148

- Rabinowitz C., Rinkevich B. (2004). In vitro delayed senescence of extirpated buds from zooids of the colonial tunicate *Botryllus schlosseri*. J Exp Biol 207: 1523-1532

- Rabinowitz C., Rinkevich B. (2011). *De novo* emerged stemness signatures in epithelial monolayers developed from extirpated palleal buds. In Vitro Cell Dev Biol Anim 47: 26-31

- Rabinowitz C., Alfassi G., Rinkevich B. (2009). Further portrayal of epithelial monolayers emergent *de novo* from extirpated ascidians palleal buds. In Vitro Cell Dev Biol Anim 45: 334-342

- Renier SA. (1793). Sopra il Botrillo piantanimale marino. Opuscoli scelti sulle scienze e sulle arti, Milano, 4 (16): 256-267

- Ricci L., Cabrera F., Lotito S., Tiozzo S. (2016a). Redeployment of germ layers related TFs shows regionalized expression during two non-embryonic developments. Dev Biol 416: 235-248

- Ricci L., Chaurasia A., Lapébie P., Dru P., Helm RR., Copley RR., Tiozzo S. (2016b). Identification of differentially expressed genes from multipotent epithelia at the onset of an asexual development. Sci Rep 6: 27-57

- Rinkevich B. (1993). Immunological resorption in *Botryllus schlosseri* (Tunicata) chimeras is characterized by multilevel hierarchical organization of histocompatibility alleles. A speculative endeavor. Biol Bull 184: 342-345

- Rinkevich B. (1999). Cell cultures form marine invertebrates: ostacles, new approaches and recent improvements. J Biotechnol 70: 133-153

- Rinkevich B., Weissman IL. (1987). A long-term study on fused subclones in the ascidian *Botryllus schlosseri*: the resorption phenomenon (Protochordata: Tunicata). J Zool 213: 717-733

- Rinkevich B., Saito Y., Weissman IL. (1993). A colonial invertebrate species that displays a hierarchy of allorecognition responses. Biol Bull 184: 79-86

- Rinkevich B., Shlemberg Z., Fishelson L. (1995). Whole-body protochordate regeneration from totipotent blood cells. Proc Natl Acad Sci USA 92: 7695-7699

- Rinkevich Y., Paz G., Rinkevich B., Reshef R. (2007a). Systemic bud induction and retinoic acid signaling underlie whole body regeneration in the urochordate *Botrylloides leachi*. PLoS Biol 5: 900-913

- Rinkevich Y., Douek J., Haber O., Rinkevich B., Reshef R. (2007b). Urochordate whole body regeneration inaugurates a diverse innate immune profile. Dev Biol 312: 131-146

- Rinkevich Y., Rinkevich B., Resheaf R. (2008). Cell signaling and transcription factor genes expressed during whole body regeneration in a colonial chordate. BMC Dev Biol 8: 100

- Rinkevich Y., Rosner A., Rabinowitz C., Lapidot Z., Moiseeva E., Rinkevich B. (2010). *Piwi* positive cells that line the vascular epithelium, underlie whole body regeneration in a basal chordate. Dev Biol 345: 94-104

- Rinkevich Y., Voskoboynik A., Rosner A., Rabinowitz C., Paz G., Oren M., Douek J., Alfassi G., Moiseeva E., Ishizuka KJ., Palmeri KJ., Weissman IL., Rinkevich B. (2013). Repeated, long-term cycling of putative stem cells between niches in a basal chordate. Dev Cell 24: 76-88

- Rodriguez D., Braden BP., Boyer SW., Taketa DA., Setar L., Calhoun C., Maio AD., Langenbacher A., Valentine MT., De Tomaso AW. (2017). *In vivo* manipulation of the extracellular matrix induces vascular regression in a basal chordate. Mol Biol Cell 28:1883-1893

- Rondelet G. (1555). Universae aquatilium historiae pars altera, cum veris ipsorum imaginibus. M Bonhomme, Lugduni

- Rosental B., Kowarsky M., Seita J., Corey DM., Ishizuka KJ., Palmeri KJ., Chen S-Y., Sinha R., Okamoto J., Mantalas G., Manni L., Raveh T., Clarke DN., Newman AM., Neff NF., Nolan GP., Quake SR., Weissman IL., Voskoboynik A. (2018). Evolutionary origin of the mammalian hematopoietic system found in a colonial chordate, BioRxiv https://doi.org/10.1101/206318

- Rosner A., Paz G., Rinkevich B. (2006). Divergent roles of the DEAD-box protein BS-PL10, the urochordate homologue of human DDX3 and DDX3Y proteins, in colony astogeny and ontogeny. Dev Dyn 235: 1508-1521

- Rosner A., Rabinowitz C., Moiseeva E., Voskoboynik A., Rinkevich B. (2007). BS-cadherin in the colonial urochordate *Botryllus schlosseri*: one protein, many functions. Dev Biol 304: 687-700

- Rosner A., Moiseeva E., Rabinowitz C,. Rinkevich B. (2013). Germ lineage properties in the urochordate *Botryllus schlosseri* - From markers to temporal niches. Dev Biol 384: 356-374

- Rosner A., Alfassi G., Moiseeva E., Paz G., Rabinowitz C., Lapidot Z., Douek J., Haim A., Rinkevich B. (2014). The involvement of three signal transduction pathways in botryllid ascidian astogeny, as revealed by expression patterns of representative genes. Int J Dev Biol 58: 677-692

- Sabbadin A. (1955). Osservazioni sullo sviluppo, l'accrescimento e la riproduzione di *Botryllus schlosseri* (Pallas) in condizioni di laboratorio. Boll Zool 22: 243-263

- Sabbadin A. (1956). *Situs inversus viscerum* provocato sperimentalmente in *Botryllus schlosseri* (Pallas) Ascidiacea. Rend Accad Naz Lincei (Cl Sci FF MM NN) 20: 659–666

- Sabbadin A. (1958). Analisi sperimentale dello sviluppo delle colonie di *Botryllus schlosseri* (Pallas) [Ascidiacea]. Arch It Anat Embr 58: 178-221

- Sabbadin A. (1960). Nuove ricerche sull'inversione sperimentale del "*situs viscerum*" in *Botryllus schlosseri* (Ascidiacea). Arch Ocean Limnol 12: 131-143

- Sabbadin A. (1962). Le basi genetiche della capacità di fusione fra colonie in *Botryllus schlosseri* (Ascidiacea). Rend Accad Naz Lincei (Cl Sci FF,MM,NN) 32: 1031-1035

- Sabbadin A. (1966). Aspetti e problemi della vita coloniale. Boll Zool 33: 23–28

- Sabbadin A., Zaniolo G. (1979). Sexual differentiation and germ cell transfer in the colonial ascidian *Botryllus schlosseri*. J Exp Zool 207: 289–304

- Sabbadin A., Zaniolo G., Majone F. (1975). Determination of polarity and bilateral asymmetry in palleal and vascular buds of the ascidian *Botryllus schlosseri*. Dev Biol 46: 79-87

- Savigny JC. (1816). Mémoires sur les animaux sans vertèbres, vol. 2. Doufour, Paris

- Schlosser JA., Ellis J. (1755-1756). An account of a curious, fleshy, coral-like substance; in a letter to Mr. Peter Collinson, F.R.S. from Dr. John Albert Schlosser, M.D.F.R.S. with some observations on it communicated to Mr. Collinson by Mr. John Ellis, F.R.S. Philos T Roy Soc 49: 449-452

- Scofield VL., Schlumpberger JM., West LA., Weissman IL. (1982). Protochordate allorecognition is controlled by a MHC-like gene system. Nature 295: 499-502

- Spallanzani L. (1784). Giornale di esperienze sulla fauna marina della laguna di Chioggia. Mss Regg B57

- Stoner DS., Weissman IL. (1996). Somatic and germ cell parasitism in a colonial ascidian: possible role for a highly polymorphic allorecognition system. Proc Natl Acad Sci USA 93: 15254-15259

- Stoner DS., Rinkevich B., Weissman IL. (1999). Heritable germ and somatic cell lineage competitions in chimeric colonial protochordates. Proc Natl Acad Sci USA 96:148-153

- Sugino YM., Nakauchi M. (1987). Budding, life pan, regeneration and colonial regulation in the ascidian, *Symplegma reptans*. J Exp Zool 244: 117-124

- Sunanaga T., Saito Y., Kawamura K. (2006). Postembryonic epigenesis of *Vasa*-positive germ cells from aggregated hemoblasts in the colonial ascidian, *Botryllus primigenus*. Develop Growth Differ 48: 87-100

- Sunanaga T., Satoh M., Kawamura K. (2008). The role of *Nanos* homolog in gametogenesis and blastogenesis with special reference to male germ cell formation in the colonial ascidian, *Botryllus primigenus*. Dev. Biol 324: 31–40

- Sunanaga T., Inubushi H., Kawamura K. (2010). Piwi-expressing hemoblasts serve as germline stem cells during postembryonic germ cell specification in colonial ascidian, *Botryllus primigenus*. Dev Growth Differ 52: 603-614

- Taneda Y., Watanabe H. (1982a). Studies on colony specificity in the compound ascidian, *Botryllus primigenus* Oka.I. Initiation of "nonfusion" reaction with special reference to blood cell infiltration. Dev Comp Immunol 6: 43-52

- Taneda Y., Watanabe H. (1982b). Effects of X-irradiation on colony specificity in the compound ascidian, *Botryllus primigenus* Oka. Dev Comp Immunol 6: 665-673

- Taneda Y., Saito Y., Watanabe H. (1985). Self- or non-self discrimination in ascidians. Zool Sci 2: 433-442

- Tiozzo S., De Tomaso AW. (2009). Functional analysis of Pitx during asexual regeneration in a basal chordate. Evol Dev 11: 152-162

- Tiozzo S., Christiaen L., Deyts C., Manni L., Joly JS., Burighel P. (2005). Embryonic versus blastogenetic development in the compound ascidian *Botryllus schlosseri*: insights from Pitx expression patterns. Dev Dyn 232: 468-478

- Voskoboynik A., Rinkevich B., Weiss A., Moiseeva E., Reznick AZ. (2004). Macrophage involvement for successful degeneration of apoptotic organs in the colonial urochordate *Botryllus schlosseri*. J Exp Biol 207: 2409–2416

- Voskoboynik A., Simon-Blecher N., Soen Y., Rinkevich B., De Tomaso AW., Ishizuka K., Weissman IL. (2007). Striving for normality: whole body regeneration through a series of abnormal generations. FASEB J 7: 1335-1344

- Voskoboynik A., Soen Y., Rinkevich Y., Rosner A., Ueno H., Reshef R., Ishizuka KJ., Palmeri KJ., Moiseeva E., Rinkevich B., Weissman IL. (2008). Identification of the endostyle as a stem cell niche in a colonial chordate. Cell Stem Cell 3: 456-464

- Voskoboynik A., Neff NF., Sahoo D., Newman AM., Pushkarev D., Koh W., Passarelli B., Fan HC., Mantalas GL., Palmeri KJ., Ishizuka KJ., Gissi C., Griggio F., Ben-Shlomo R., Corey DM., Penland L., White RA. 3rd, Weissman IL., Quake SR. (2013a). The genome sequence of the colonial chordate, *Botryllus schlosseri*. Elife 2: e00569

- Voskoboynik A., Newman AM., Corey DM., Sahoo D., Pushkarev D., Neff NF., Passarelli B., Koh W., Ishizuka KJ., Palmeri KJ., Dimov IK., Keasar C., Fan HC., Mantalas GL., Sinha R., Penland L., Quake SR., Weissman IL. (2013b). Identification of a colonial chordate histocompatibility gene. Science 341: 384-387

- Watanabe H. (1953). Studies on the regulation in fused colonies in *Botryllus primigenus* (Ascidiae Compositae). Sci Rep Tokyo Bun Daig 7B: 183-198

- Watanabe H. (1962). Further studies on the regulation in fused colonies in *Botryllus primigenus* (Ascidiae Compositae). Sci Rep Tokyo Kyo Daig 10B: 253-284

- Watanabe H., Newberry AT. (1976). Budding by oozooids in the polystyelid ascidian *Metandrocarpa taylori* Huntsman. J Morphol 148: 161-176

- Watkins MJ. (1958). Regeneration of buds in *Botryllus*. Biol Bull 115: 147-152

- Watterson RL. (1945). Asexual reproduction in the colonial tunicate, *Botryllus schlosseri* (Pallas) Savigny, with special reference to the developmental histoty of intersiphonal bands of pigment cells. Biol Bull 88: 71-103

- Weissman IL. (2015). Stem cells are units of natural selection for tissue formation, for germline development, and in cancer development. Proc Natl Acad Sci USA112: 8922-8928

- Zaniolo G., Sabbadin A., Resola C. (1976). Dynamics of the colonial cycle in the ascidian, *Botryllus schlosseri*. The fate of isolated buds. Acta Embryol Exper 2: 205-213

- Zondag LE., Rutherford K., Gemmell NJ,, Wilson MJ. (2016). Uncovering the pathways underlying whole body regeneration in a chordate model, *Botrylloides leachi* using *de novo* transcriptome analysis. BMC Genomics 17:114

Suppl. Table 1. Budding in control colonies. Number of individual that produced 2, 3 or 4 buds during each generation (modified from Sabbadin, 1958).

Colony	blastogenetic generations																				mean budlets *per* individual
	1st			2nd			3rd			4th			5th			6th			7th			
	2	**3**	**4**	**2**	**3**	**4**	**2**	**3**	**4**	**2**	**3**	**4**	**2**	**3**	**4**	**2**	**3**	**4**	**2**	**3**	**4**	
A	1	0	0	1	0	0	1	0	0	1	0	1	3	1	0	4	0	0	2	3	0	2.33
B	1	0	0	0	1	0	1	1	0	2	1	0	6	0	0	4	0	0	8	0	0	2.12
C	1	0	0	1	0	0	1	0	0	1	1	0	3	0	0	4	0	0	3	0	0	2.06
D	1	0	0	1	0	0	1	0	0	2	0	0	1	1	0	4	0	0	3	0	0	2.07
E	1	0	0	1	0	0	2	0	0	0	1	1	4	1	0	8	0	0	4	6	0	2.34
F	1	0	0	1	0	0	1	0	0	0	0	1	3	0	0	2	0	0	3	0	0	2.16
G	1	0	0	1	0	0	1	0	0	1	0	0	2	0	0	2	0	0	0	2	0	2.20
H	1	0	0	1	0	0	0	0	2	2	4	0	11	0	0	8	3	0	17	0	0	2.22
I	1	0	0	1	0	0	1	0	0	2	0	0	3	0	0	1	2	0	0	6	0	2.47
J	1	0	0	1	0	0	1	0	0	1	1	0	2	2	0	8	0	0	6	0	0	2.13
K	1	0	0	2	0	0	1	0	0	2	0	0	2	1	0	4	1	0	9	0	0	2.08
L	1	0	0	1	1	0	0	1	2	7	0	0	14	0	0	10	18	0		//		
M	1	0	0	1	0	0	2	0	0	0	1	1	4	3	0	9	1	0		//		
N	1	0	0	1	0	0	0	1	0	1	2	0	0	0	6		//			//		
mean budlets *per* individual	2			2.12			2.55			2.51			2.29			2.27			2.24			

Suppl. Table 2. Bud blastogenetic ability in control colonies in relation to their position on parental zooids. All budding budlets of blastogenetic generations 1st to 6th have been analyzed (modified from Sabbadin, 1958).

Position of the budding buds	Number of budding buds	Number of produced budlets	Average number of budlets for each bud
anterior right	196	463	2.36
anterior left	116	255	2.19
posterior right	11	23	2.09
posterior left	2	4	(2.00)

Suppl. Table 3. Produced, matured or degenerated budlets in the different developmental stages up to the 8th blastogenetic generation in control colonies (modified from Sabbadin, 1958).

	position of produced budlets				
	anterior right	anterior left	posterior right	posterior left	Total
N° of producted budlets	339	339	81	14	773
N° of matured budlets	282	112	7	//	401
N°of degenerated budlets	57	227	74	14	372
% of degenerated vs produced	16,81%	66,96%	91,35%	100%	48,12%
N° of degenerated budlets					
st. 1-3	53	153	58	3	267 71,77%
st. 4-6	//	10	5	7	22 5,91%
st. 7	//	38	3	1	42 11,29%
st. 8	4	26	8	3	41 11,02%

Suppl Table 4. Colony growth in control colonies. Number of the matured individuals in each blastogenetic generation (numerator) as compared with the total number of budlets (denominator) (modified from Sabbadin, 1958).

Colonies	Blastogenetic generations								Total	%
	1st	2nd	3rd	4th	5th	6th	7th	8th		
1st	1/2	1/2	1/2	1/2	2/6	3/9	4/8	4/13	17/44	38,63
2nd	1/2	1/2	2/3	3/5	4/7	4/12	5/8	5/16	25/55	45,45
3rd	1/2	1/2	1/2	1/2	2/5	3/6	3/8	3/6	15/33	45,45
4th	1/2	1/2	1/2	1/2	2/4	3/5	3/8	3/6	15/31	48,38
5th	1/2	1/2	1/2	2/4	4/7	8/11	10/16	9/26	36/70	51,42
6th	1/2	1/2	1/2	1/2	2/4	2/6	3/4	3/6	14/28	50
7th	1/2	1/2	1/2	1/2	1/2	2/4	2/4	2/6	11/24	45,83
8th	1/2	1/2	2/2	6/8	6/16	11/22	8/25	8/34	43/111	38,73
9th	1/2	1/2	1/2	2/2	3/4	3/6	6/8	12/18	29/44	65,9
10th	1/2	1/2	1/2	2/2	4/5	5/10	6/16	11/12	31/51	60,78
11th	1/2	1/2	1/4	2/2	3/4	5/7	7/11	13/18	35/50	66
12th	1/2	1/2	3/5	7/11	14/14	22/28	35/74	//	//	//
13th	1/2	1/2	2/2	2/4	6/7	6/17	7/21	//	//	//
14th	1/2	1/2	1/2	3/3	6/8	12/24	//	//	//	//
	14/28	14/28	19/34	34/51	59/93	89/167	99/211	73/161	401/773	
%	50.00	50.00	55.88	66.66	63.44	53.29	46.91	45.34	51.87	

Suppl Table 5. Posterior budlets in both control and experimental colonies (budlet extirpation at stage 2) (modified from Sabbadin, 1958).

Pools	total number of budlets	Total number of posterior budlets			% of posterior left budlets	Number of posterior degenerated budlets at stage 1-6		
		Right	Left	Total		Right	Left	Total
Control	323	48	9	57 17,64%	15,78	36	5	41 71,92%
Budlet extirpation at stage 2	188	42	26	68 36,17%	38,23	3	5	8 11,76%

Suppl Table 6. Budding in both control and experimental colonies (budlet extirpation at stage 2). Number of individuals that produced 2, 3, 4 or 5 budlets in the different blastogenetic generations (modified from Sabbadin, 1958).

Pools		Number of individuals that produced 2, 3, 4 or 5 budlets for each blastogenetic generation																									
		1st			2nd			3rd			4th				5th				6th				7th				
		2	3	4	2	3	4	2	3	4	2	3	4	5	2	3	4	5	2	3	4	5	2	3	4	5
Control																											
	N° of individuals	14			12	2		10	1	2	8	7	4		23	8	3		32	21			35	14			
	Average budlets *per* bud ± SE	2.0 ± 0.0			2.1 ± 0.1			2.4 ± 0.2			2.8 ± 0.2				2.4 ± 0.1				2.4 ± 0.1				2.3 ± 0.1			
Budlet extirpation at stage 2	N° of individual	10	2		6	5	1	3	3	6	3	4	5		1	4	7		3	4	5		1	3	6		
	Average budlets per bud ± SE	2.2 ± 0.1			2.6 ± 0.2			3.2 ± 0.2			3.2 ± 0.2				3.5 ± 0.2				3.2 ± 0.2				3.5 ± 0.2			

Suppl Table 7. Average size of buds at the beginning (phase 9/8/2) and at the end (phase 9/8/5) of the stage 8 in both the control and experimental colonies (budlet extirpation at stage 2)(modified from Sabbadin, 1958).

Pools		Initial stage 8					Final stage 8				
		2nd gen.	3rd gen.	4th gen	5th gen.	6th gen.	2nd gen.	3rd gen.	4th gen	5th gen.	6th gen.
Control											
	N° of individuals	3	14	20	29	46	6	13	19	28	29
	Average size ± SE	344.8 ± 35.0	376.3 ± 8.8	397.3 ± 15.8	453.3 ± 10.5	416.5 ± 8.8	775.3 ± 56.0	710.5 ± 49.0	876.8 ± 35.0	854.0 ± 28.0	799.8 ± 24.5
Budlet extirpation at stage 2											
	N° of individuals	9	10	7	8	3	7	11	9	5	3
	Average size ± SE	395.5 ± 14.0	435.8 ± 24.5	444.5 ± 26.3	491.8 ± 26.3	449.8 ± 61.3	768.3 ± 106.8	943.3 ± 84.0	1440.3 ± 140.0	1030.8 ± 196.0	1447.3 ± 308.0

Suppl Table 8. Average size of adult zooids during early blastogenetic cycle (phase 9/8/2) and late blastogenetic cycle (phase 9/8/5) in control and experimental colonies (budlet extirpation at stage 2) (modified from Sabbadin, 1958).

Pools		Adult at early blastogenetic cycle (phase 9/8/2)					Adult at late blastogenetic cycle (phase 9/8/5)				
		2nd gen.	3rd gen.	4th gen	5th gen.	6th gen.	2nd gen.	3rd gen.	4th gen	5th gen.	6th gen.
Control											
	N° of individuals	14	18	24	28	30	14	16	23	28	30
	Average size ± SE	1037.8 ± 59.5	1265.3 ± 54.3	1373.8 ± 42.0	1226.8 ± 35.0	1452.5 ± 54.3	1083.3 ± 71.8	1351.0 ± 63.0	1442.0 ± 50.8	1321.3 ± 42.0	1548.8 ± 70.0
Budlet extirpation at stage 2											
	N° of individuals	9	9	9	5	3	8	9	9	7	5
	Average size ± SE	1347.5 ± 96.3	1821.8 ± 94.5	1925.0 ± 133.0	1881.35 ± 250.3	1599.5 ± 248.5	1538.3 ± 112	2012.5 ± 112	2296.02 ± 92.8	2268.0 ± 94.5	2112.3 ± 98.0

Suppl. Table 9. Blastogenetic phases observed in control and experimental colonies when a blastogenetic generation is reaching (final stage 8) or has just reached (initial stage 9) the adult stage (functional maturity) (modified from Sabbadin, 1958).

final stage 8					initial stage 9				
		pool					pool		
	Colonial phase	*Control*	*Budlet extirpation at stage 2*	*Bud extirpation at stage 8*		Colonial phase	*Control*	*Budlet extirpation at stage 2*	*Bud extirpation at stage 8*
A	11-9/8/2	8	2	17	A	0-11/9/3	4	8	6
	11-9/8/3	28	10	9		0-11/9/4	16	4	10
	11/8/4	23	2	3		0/9/5-6	29	1	7
B	9/8/4-5	41	21	1	B	11/9/5-6	14	5	
	11/8/5-6	59	12			0-11/9/7/1	81	39	1
	11-9/8/7/1	12	16						
C	11-9/8/7/1+		11		C	0-11/9/8/2		11	
	11-9/8/8/2					0-11/9/8/3			
	11-9/8/8/3		3			0-11/9/8/4		3	
	9/8/8/4		1			9/9/8/5		1	
	11/9/8/5		1			11/11/9/7/1		1	
	11/9/8/7+					11/11/9/8/2			
Total		171	79	30	**Total**		144	73	24
A	%	34,50	17,72		A	%	34,03	17,81	
B	%	65,5	62,03		B	%	65,97	60,27	
C	%		20,25		C	%		21,92	

Suppl. Table 10. Average size (μm) of buds and adults in both the control and in experimental colonies deriving from budlets having resumed their development after the extirpation of the right anterior bud at stage 8 (modified from Sabbadin, 1958).

Pools		Initial stage 8		Final stage 8		Adult in early blastogenetic cycle (phase 9/8/2)		Adult in late blastogenetic cycle (phase 9/8/5)	
		2nd gen.	3rd gen.	2nd gen.	3rd gen.	2nd gen.	3rd gen.	2nd gen.	3rd gen.
Control									
	N° of individuals	3		6	13	14		14	16
	Average size ± SE	344.8 ± 35.0		775.3 ± 56.0	710.5 ± 49.0	1037.8,3 ± 59.5		1083.3 ± 71.8	1351.0 ± 63.0
Bud extirpation at stage 8									
	N° of individuals	7		7	5	5		4	4
	Average size ± SE	280.0 ± 14.0		435.8 ± 24.5	437.5 ± 47.3	770 ± 40.3		813.8 ± 35.0	927.5 ± 50.8

Suppl Table 11. Average life span (days) of the stage 8 and 9 in the different blastogenetic generations of both the control and the experimental pools of colonies (modified from Sabbadin, 1958).

Pool		Stage 8						Stage 9				
		2nd gen.	3rd gen.	4th gen.	5th gen.	6th gen.	7th gen.	2nd gen.	3rd gen.	4th gen.	5th gen.	6th gen.
Control												
	N° of individuals	8	12	15	14	14	11	15	14	14	14	11
	Average ± SE	2.4 ± 0.3	2.7 ± 0.2	2.8 ± 0.2	2.5 ± 0.1	2.5 ± 0.2	2.5 ± 0.2	4,6	5,1	4,4	4,6	4,4
Budlet extirpation at stage 2												
	N° of individuals	12	11	11	12	11	5	12	11	11	11	6
	Average ± SE	2,8	3,2	4,4	4,5	4,3	4,2	4,5	5,9	4,5	4,9	
Bud extirpation at stage 8												
	N° of individuals	10	3	3				8	3	3		
	Average ± SE	1.85 ± 0.2	2.2 ± 0.4	2.0 ± 0.0				7,5	7,2	7,8		

Chapter 2

Shared and divergent pathways of nervous system development in the synchronized sexual and asexual reproduction of the colonial chordate *Botryllus schlosseri*

Article in preparation

ABSTRACT

Ascidians are tunicates that share with chordates the development of the larval nervous system from a neural plate. This nervous system, similar to the vertebrate nervous system though smaller, degenerates during larval metamorphosis and is replaced in the sessile, filter-feeding oozooid, by a cerebral ganglion. The latter forms from a rudiment ultimately derived from the anterior neural plate. In colonial ascidians, such as *Botryllus schlosseri*, zooids are also produced by budding. In this species, adult individuals undergo cyclical regression and reabsorption and are replaced in physiological activities by their bud. Here, the cerebral ganglion does not originate from a neural plate, but from a dorsal multipotent area of the early bud. We used *B. schlosseri* to compare the nervous system formation in the two different developmental pathways, *i.e*. embryogenesis and blastogenesis. In mature colonies, embryos develop within adult individuals and larvae escape from the colony just before the phase of adult regression (the takeover). In order to account for this process, we developed a method for culturing embryos *in vitro* to study their development. Using a combination of *in vivo*, confocal, histological observations, and 3D reconstructions, we were able to describe the embryonic development and draft a timetable. We then compared the nervous system morphogenesis in embryos, with the better understood processes that occur in buds. We also sequenced transcriptomes of embryos and buds at several stages and analyzed them with attention to the nervous system. We found some genes specifically expressed during blastogenesis with others expressed during embryogenesis. However, most genes were expressed in both developmental pathways. Furthermore, our data show a strict temporal relationships between nervous system morphogenesis and gene expression during the formation of the larval brain and its degeneration at metamorphosis, the formation of the adult brain in embryos and the parallel process in buds, and the degeneration of the adult nervous system at takeover.

INTRODUCTION

Ascidians belong to the taxon Tunicata that is part of the phylum Chordata together with Cephalochordata and Vertebrata. Based on molecular features, the subphyla Tunicata and Vertebrata are considered sister groups and constitute the taxon Olfactores (Delsuc et al., 2018). They share several anatomical features. Some of them define the chordate body pattern, such as the notochord, a segmented musculature, gill slits, the dorsal hollow neural tube, and secondary mechanoreceptor cells (Fujiwara and Kawamura, 2003; Horie et al., 2018; Rigon et al., 2018). Others, such as neural crest-like cells and neurogenic placodes likely derived from embryonic proto-placodal areas, are specific to olfactores (Schlosser, 2006; Jeffery, 2007; Patthey et al., 2014; Manni and Pennati, 2016).

Reproductive strategies are diverse within tunicates and include both the sexual and the asexual methods. Solitary ascidians, such as *Ciona intestinalis* and *Halocynthia roretzi*, reproduce only sexually. They produce a free-swimming tadpole larva, which lives some hours before undergoing an extensive metamorphosis. This involves the formation or the completion of development of prospective juvenile organs and their 90° rotation within the body, whereas many larval tissues, including the larval tail and brain, undergo apoptosis and are reabsorbed (Chambon et al., 2002). The resulting juvenile is a sessile, filter-feeding animal.

The embryonic development of solitary ascidians, in particular species belonging to the *Ciona*, *Phallusia*, and *Oikopleura* genera, has been studied in great detail (Nishida, 2008; Rothbächer et al., 2007; Brozovic et al., 2017; Stach and Anselmi, 2015;). These species are oviparous and produce a large number of small and transparent eggs, which are ovulated and fertilized in seawater. Thanks to *in vitro* fertilization and embryo culture, these species became the preferred model of investigating cell lineage and determination, and morphogenesis. Anatomical and developmental ontologies are now available for several solitary ascidians, allowing for standardized studies (https://www.aniseed.cnrs.fr/). Ascidian embryogenesis is characterized by a stereotyped development that is based on invariant early cell lineages and a remarkably small cell number (Kumano and Nishida, 2007). These unique and highly derived features make it possible to study the chordate developmental process at cellular and subcellular resolutions.

A number of ascidian species also reproduce asexually by budding (or blastogenesis) producing zooids (called blastozooids) using pluripotent/multipotent stem cells (Voskoboynik et al., 2008; Manni et al., 2018). Blastozooids are organized in colonies and are clonal individuals, derived from cycles of blastogenesis from an individual (oozooid) originating from the metamorphosis of a single larva. Both solitary and colonial ascidians exhibit regenerative abilities (Kawamura et al., 2008).

Blastogenesis has been extensively studied in the ascidian *Botryllus schlosseri* (Fig. 1). In this species, a colony is characterized by synchronized waves of budding cycles accompanied by the regression and reabsorption of filtering adults, which are replaced by new zooids (Voskoboynik and Weissman 2014; Manni et al., 2014). Blastozooids are organized in star-shaped systems embedded in a common tunic; a colonial circulatory system of vessels joins all the blastozooids. *B. schlosseri* can be easily cultured on glass slides in laboratory conditions and many experimental tools, such as zooid extirpation, gene silencing, microinjection, imaging, and *in situ* hybridization, have been developed to study its biology (Sabbadin, 1955; Manni et al., 2007, 2018). Moreover, a distinct regenerative process, called whole body regeneration, is activated when buds and zooids are surgically removed in a colony, leaving only the vasculature and the tunic (Voskoboynik et al., 2007; Manni et al., 2018). The entire body can be regenerated even if no pre-existing zooids are present. This suggests that the pluripotent and/or multipotent stem and progenitor cells that initiate budding can migrate and that regions within the colony vasculature are suitable niches (Voskoboynik et al., 2007).

Sexual reproduction in colonial ascidians occurs cuncurreltly with asexual reproduction. Usually colonial species produce a few yolky eggs that are larger and more opaque than those produced by solitary ascidians. Both fertilization and embryogenesis occur within the parental zooids, with or without parental nutrient contribution to the embryonic development (Manni et al., 1993; Zaniolo et al., 1994;). This renders colonial ascidians unsuitable for extensive studies on embryo development. In *B. schlosseri*, attempts to fertilize isolated eggs with isolated sperm and to follow their development *in vitro* were done in the past (Milkman and Borgmann 1963; Milkman 1967) and late embryo development was described using histological sections (Scott, 1934; Grave, 1934; Grave and Woodbridge, 1924; Manni et al., 1999). However, cell lineage and a comprehensive description and timetable of complete embryo development is not yet available.

Yet the contemporary presence of different reproductive strategies (*i.e.* embryogenesis and blastogenesis) that generate similar individuals (oozooids from eggs and blastozooids from pluripotent somatic cells), renders colonial ascidians suitable to investigate how developmental events are integrated to generate the animal form. Thanks to their key phylogenetic position, these organisms can improve scientific understanding of the evolution of molecular mechanisms of morphogenesis in chordates (Manni and Burighel, 2006). In this context, the study of the nervous system (NS) is of particular interest as it involves the placodal territories and neural crest-like cells that are considered crucial for vertebrate evolution (Manni and Burighel, 2006; Schlosser 2006; Patthey et al., 2014).

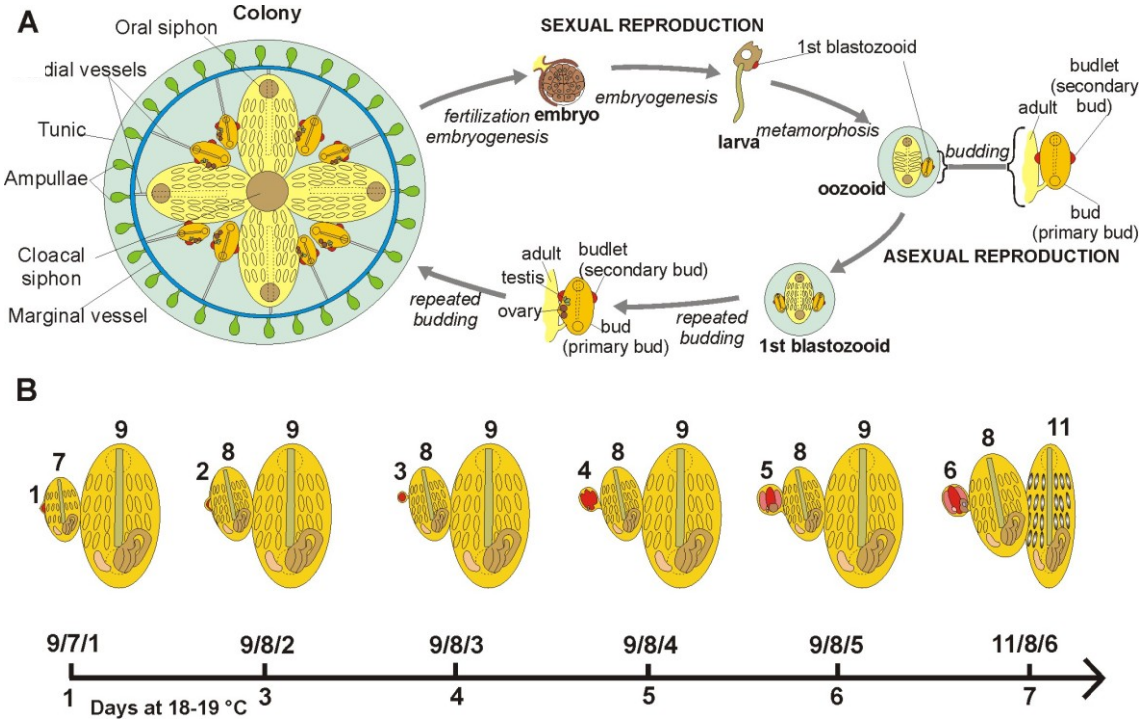

Fig. 1: *B. schlosseri* life cycle. **A:** *B. schlosseri* reproduces both through sexual and asexual (budding) pathways, giving rise to identical adult body plans. Upon settlement, the tadpole larva metamorphoses into a founder individual (oozooid), which generates a colony through asexual budding. **B:** The colony includes three overlapping generations: adult zooids, primary buds, and secondary buds. Each week buds grow, replacing the previous generation of zooids, which die through a massive apoptosis in the phase called takeover (11/8/6). (Modified from Manni et al., 2018 – Chapter 1 of the present thesis).

The neurogenesis, neuroanatomy, and neurophysiology of ascidian larvae have been the subject of numerous studies that have explored the evolution of the chordate nervous system (NS) (Holland and Holland, 1999; Satoh, 2003; Meinertzhagen et al., 2004; Manni and Pennati, 2016). From a morphological and functional perspective, the larval

central (C) NS consists of four regions extending anterior-posteriorly: the sensory vesicle (with the otolith, the ocellus, and the pressure organ), the neck, the visceral ganglion, and the tail nerve cord. These regions can be linked to vertebrate structures, based on morphology and gene expression, so that the larval CNS is a smaller model of that found within vertebrates (Lemaire, 2011). The sensory vesicle is thought to correspond to the vertebrate prosencephalon and mesencephalon; the neck to the vertebrate midhindbrain boundary; the visceral ganglion to the rhomboencephalon, and the anterior tail nerve cord to the spinal cord. Most studies on the CNS have been performed on the two solitary species *C. intestinalis* and *H. roretzi*. Although there are differences between larvae belonging to solitary and colonial species, especially regarding the degree of adult organ rudiment development, the basic anatomy of the CNS is considered similar (Manni and Pennati, 2015).

As is typical for chordate development, the ascidian larval CNS originates from the enrollment of the neural plate to form a neural tube (Nicol and Meinertzhagen, 1988a Lemaire et al., 2002). During gastrulation, the neural plate is formed by cells in their ninth mitotic generation and is organized in four rows of animal blastomeres and two rows of vegetal blastomeres. In addition, the adult NS, which will become functional during metamorphosis and will replace the degenerating larval NS, originates from larval components derived from the neural plate (Nicol and Meinerzthagen, 1988a). It is important to note that in adult individuals of colonial species an identical NS develops during budding, where a neural plate never forms, offering the opportunity to investigate how a new genetic program for brain development evolved.

The adult NS exhibits a typical invertebrate-like organization, as an ovoid brain, called cerebral ganglion, from which the peripheral nerves arise (Manni and Pennati, 2015). It is associated with a neural gland, a sac-like organ, which is opened by a ciliated duct and a funnel-shaped dorsal tubercle into the prebranchial region (*i.e.,* the region comprised between the base of the oral siphon and the first row of stigmata). In most ascidians, the neural gland continues posteriorly in a long dorsal strand reaching the viscera and associated with a dorsal strand plexus of neurons. In *B. schlosseri*, the dorsal strand is absent and a small, ovoid body called the dorsal organ is considered homologous to the dorsal strand (Burighel et al., 1998).

The development of the neural complex during embryo and larva development has been analyzed in some species and with different experimental approaches (Sasakura et al.,

2012). Classically, the neural complex was considered to originate from the neurohypophysial duct (or neurohypophysis). This is a duct deriving from the anterior left neural plate (Nicol and Meinertzhagen, 1988b). Observations using transmission electron microscopy showed that the wall of the neurohypophysial duct undergoes extensive mitosis to produce neuroblasts, which aggregate to form the cerebral ganglion (Manni et al. 1999, 2005.). In *C. intestinalis*, this process occurs during metamorphosis, when the neurohypophysial duct elongates to produce both the neural gland and its posterior dorsal strand (Manni et al., 2005). The contribution of non-neuronal ependymal cells and cholinergic neurons of the larval CNS to the cerebral ganglion formation has also been proposed (Dufour et al., 2006; Horie et al., 2011).

In *B. schlosseri*, buds develop the cerebral ganglion from neuroblasts that originate, as migratory cells, from a tubular structure known as the dorsal tube (Burighel et al., 1998). The dorsal tube originates as evagination of the bud's dorsal side. The tube directly differentiates the adult neural gland and serves as the cellular source for neurons. This process shows a number of similarities with the events that occur during embryogenesis and metamorphosis in *B. schlosseri* (Manni and Burighel, 2006).

In this study, we aim to compare the NS development in embryogenesis and blastogenesis in *B. schlosseri*, through a combination of morphological and molecular approaches. We succeeded in: culturing embryos *in vitro*; drafting an embryo development timetable; describing embryo development using *in vivo*, confocal and histological observations, and 3D reconstructions; sequencing transcriptomes for several stages of embryogenesis and blastogenesis; and comparing mechanisms of NS development in both reproductive strategies. Our data illustrate the strict temporal relationships between NS morphogenetic events and expression patterns of associated genes during the formation of the larval brain and its degeneration at metamorphosis, the formation of the adult brain in embryo and the parallel process in bud, and the degeneration of the adult NS at takeover.

RESULTS AND DISCUSSION

Embryo development in *Botryllus schlosseri*

B. schlosseri embryos can survive and develop outside the parental body

In order to carefully study in *B. schlosseri* the processes occurring during embryogenesis from a morphological and molecular perspective, we observed the development of embryos *in vitro*. In this species, embryos develop inside the parental peribranchial chamber attached to a placental cup (Zaniolo et al., 1987). As embryos in a colony develop at the same rate, we used several mature colonies to obtain embryos from different developmental stages to culture. The relationship between bud development and sexual reproduction (Scott, 1934; Manni et al., 2007) was used to indicate the embryo developmental period/stage.

We succeeded in culturing embryos outside the parental body and observed their development until the oozooid stage.

The percentage of embryos surviving in each stage is reported in Table 1, where "Starting stage" indicates the developmental stage at the time of embryo removal from a colony. "Total number of oozoids" and "% of oozoids" indicate the number and the percentage of embryos that survived the metamorphosis stage to become filter-feeding oozooids; some of them were normal (see "number of normal oozoids" and "% of normal oozoids" in Table 1), instead others showed abnormalities in the development. In general, embryos removed at early developmental stages (until the neurula period) had lower chances to pass through metamorphosis than those removed at later stages. For example, only 20% of embryos removed from the parental zooid during gastrulation developed completely and normally; conversely, in a batch of embryos removed during the wrap stage, 68% of removed embryos completed normal development. In a number of cases, the oozooids died soon after metamorphosis. Most often this occurred because of an anomalous development of their ampullae and their inability to adequately attach to the substrate. Indeed, the final number of normal oozooids was considerably lower than the total number of oozooids obtained from metamorphosed larvae.

We believe our success in culturing embryos to be very important as it provides for new perspectives and opportunities in the study of this species. Tools like *in vitro* embryo manipulation and transgenesis, which are so far inaccessible in the study of *B.*

schlosseri, could be modified in near future to allow for the advancement of comparative, developmental, and evolutionary studies.

Colony ID	Developmental Period/Stage	Number of removed embryos	Total number of oozooids	Number of normal oozooids	% of oozoids	% of normal oozoids
2.0	2 cell stage	16	5	3	31.25%	18.75%
2.1	2 cell stage	18	4	2	22.2%	11.1%
7	16 cell	25	20	2	80%	8%
3	After 16-cell until gastrulation	3	2	0	66.67%	0
6	Gastrula	10	4	2	40%	20%
9	Neurula	18	8	2	44.4%	11.1%
1	Neurula	11	7	2	63.6%	18.1%
4	1.5 wrap	25	10	3	40%	12%
5	1.5 wrap	25	20	17	80%	68%
12	1.5 wrap	20	10	3	50%	15%

Table 1: Number of cultured embryos per stage and percentage of embryos completing development. See text for details.

Timetable and description of B. schlosseri *development*

The ability to culture embryos outside the parental colony allowed us to draft a timetable for some developmental periods/stages encompassing development from the zygote to the oozooid (Table 2; Figs. 2-6).

Considering the invariant lineage of ascidian embryos, *B. schlosseri* embryo development was subdivided into metaperiods, periods, and stages according to the developmental ontology of *Ciona intestinalis* (available at https://www.aniseed.cnrs.fr/). Initial developmental periods/stages (until the tailbud stage) were identified using *in vivo* observations. Development prior to the 16-cell stage was easily identified. However, after this stage, we grouped together several stages of the cleavage period until gastrulation. Yolk within blastomeres made embryos opaque, rendering it challenging to follow each mitosis. Gastrulation was indicated by the presence of the blastopore.

Subsequent stages, prior to the hatching larva stage, were defined using a combination of *in vivo*, confocal and histological observations. For the tailbud period, the main parameter we used to define the stages is the length of the tail that grows below the chorion and encircles the trunk 1.5 times at its maximum extension (Manni et al., 1999). These stages do not correspond with those described for *C. intestinalis* development, because of the heterochrony existing between the two species during the development of larva and juvenile structures (Manni et al., 2004). In particular, we recognized

embryos at the following stages: “initial tailbud”; “¾ wrap”, for embryos with tail making a three-quarter turn around the trunk; “1 – 1.5 wrap”, for embryos with tail making between 1 and 1.5 turns around the trunk; and “1.5 wrap”, for embryos with tail making 1.5 turns around the trunk.

Post-larval stages were described by considering larval behaviour and shape.

Unfortunately, we were not able to identify the exact time of fertilization, which occurs inside the parental body just after siphon opening (Milkman, 1967). Such observations would be necessary to produce a precise timetable. Although our timetable could be improved and more precisely defined in the future, it represents a foundation for the elaboration of the developmental and anatomical ontology of the embryonic development in *B. schlosseri* that will complement the available ontology of the blastogenetic development (Manni et al., 2014).

Below we give the first description of the embryonic development of *B. schlosseri* (Table 2), using complementary information obtained from: 1) *in vivo* observations of developing embryos and movies, 2) confocal microscopy (virtual sections and 3D reconstructions), 3) histology based on serial sections of whole embryos cut according different planes, and 4) 3D reconstructions based on serial sections of two selected periods (adhesion and oozooid). We present the description of each stage/period accompanied by a series of general pictures.

Metaperiod	**Period**	**Stage**	**Hpf**
Pre-embryonic development			
	Pre-fertilization		
		Unfertilized egg	
Embryonic development, pre-metamorphosis			
	Zygote		0hr
	Cleavage		
		2 cells*	1hr
		4 cells*	2hr
		8 cells*	4hr
		16 cell*	6hr
		After 16-cell until gastrulation*	8hr
	Gastrula*		16hr-23hr
	Neurula*		25hr-29hr
	Tailbud		
		Initial tailbud*	31hr
		¾ wrap*	40hr
		1 - 1.5 wrap*	44hr
		1.5 wrap*	66hr
	Swimming larva		
		Hatching larva*	4 days
Metamorphosis			
	Adhesion*		5 days
	Body axes rotation*		6 days

Post-metamorphosis			
	Oozooid*		7 days

Table 2: Timetable of the development of *B. schlosseri* embryo at 23°C. Hpf: hours post fertilization.*: stages/periods sequenced for transcriptome analyses.

Pre-embryonic development

Period: Pre-fertilization

Stage: Unfertilized egg. The ovulated egg contains densely packed yolk globules and is about 250-300 μm in diameter (Manni et al., 1994). A continuous layer of inner follicular cells, which participate with the oviduct cells to form the placental cup (Zaniolo et al., 1987), covers it. Inner follicle cells lie on the acellular vitelline coat (or chorion). A number of test cells are in the perivitelline space.

Embryonic development

Period: pre-metamorphosis

Stage: Zygote (1 cell stage) (Fig. 2 A-A'). The zygote is a single fertilized cell. The stage extends from the fertilization up to the end of the first mitotic cycle and lasts about 0-1 hour.

Stage: 2 cell (1 hour after fertilization) (Fig. 2 B-B'). The first cleavage plane is vertical, along the animal-vegetal axis, and separates the left and right halves of the embryo.

Stage: 4 cell (2 hours after fertilization) (Fig. 2 C-C'). The second cleavage plane is vertical and perpendicular to the first one. It separates the anterior from the posterior halves of the embryo.

Stage: 8 cell (4 hours after fertilization) (Fig. 2 D-D'). The third cleavage plane is horizontal and separates the animal from the vegetal territories. At this stage, the four founder lineages are defined: A, anterior vegetal; B, posterior vegetal; a, anterior animal; b, posterior animal (Conklin, 1905).

Stage: 16 cell (6 hours after fertilization) (Fig. 2 E-E'). The embryo possesses groups of cells of different size and that are clearly recognizable. The animal and vegetal cells

have undergone the fourth cleavage and blastomeres show bilateral symmetry in their arrangements.
During these early stages, embryos are characterized by circular shape and pink color (brown under stereomicroscope).

Stage: after 32-cell until gastrulation (8 hours after fertilization) (Fig. 2 F-F'). Blastomeres are dividing, but the number of cell divisions is no longer detectable using *in vivo* observations under a stereomicroscope.

Period: Gastrula (16-23 hours after fertilization) (Fig. 2 G-G'). During gastrulation, the blastopore can be recognized as the site where cells enter into the embryo with a clear movement inside. The neural plate forms.

Period: Neurula (25-29 hours after fertilization) (Fig. 2 H'-H'). After the gastrula stage, the embryo is pear shaped. Its color is lighter than in previous stages but still pinkish. The anterior and lateral walls of the blastopore grow and cover the blastopore itself. The posterior portion of the neural tube starts to close. Cells are no longer easy to identify.

Period: Tailbud
Stage: Initial Tailbud (31-39 hours after fertilization) (Fig. 3 A-A''). The first separation between tail and trunk territories appears. Different embryonic tissues are recognizable at histological level, as determined by the shape, size, and arrangement of cells, and the spatial relation among tissues. Epithelia are recognizable as monolayers. Small epidermal cells cover the entire embryo. The NS is in the typical dorsal position. Its cells have regular shape and are smaller than the endodermal cells. The anterior neuropore is present. In the trunk, the NS is differentiated as mass of nerve cells: in the tail, it elongates in the nerve cord, from the dorsal to the notochord. Endodermal cells are very rich in yolk, they form the pharynx rudiment in the trunk and the endodermal strand in the tail which is ventral to the notochord. The pharynx has an oval lumen. Mesenchymal cells occupy spaces between the epidermal and endodermal leaflets in the ventral and lateral trunk. In the central position of the embryo tail, the notochord is oval with pyramidal cells rich in yolk.

Stage: ¾ wrap (40 hours after fertilization) (Fig. 3 B-B''). The three anterior papillae protrude anteriorly. In the trunk, the sensory vesicle with the photolith, the pigmented organ responding to both gravity and light (Sorrentino et al., 2000), the visceral ganglion, the neck, and the nerve cord are recognizable. The neuropore is closed. A small left ganglionic vesicle is in continuous with the neurohypophyseal duct. The latter is a small duct opening into the pharynx. It is involved in the delamination of neuroblasts to form the adult cerebral ganglion. The pharynx is larger than in the previous stage; it is depressed dorsally by sensory vesicle and on the left by the growing tail. It exhibits two lateral-dorsal wings embracing the visceral ganglion. The atrial chamber rudiment is present as dorsal ectodermal invagination. Its bottom, on the right and on the left, represents the rudiments of the peribranchial chambers. Blood lacunae are wider as epithelia are thinning for yolk consumption and organs are enlarging. The heart is in form of a compact mass of mesodermal cells. The notochord cells are located in a single line. Muscle cells in the tail are organized in three symmetric lines of cells flanking the notochord.

Stage: 1 wrap (44-66 hours after fertilization) (Fig. 3 C-C''). The embryo is still pinkish in color and the trunk maintains a relatively circular shape. The three papillae are in the form of ectodermal evagination, without a cavity and the interpapillary region is depressed. The larval tunic (inner cuticular layer and inner compartment) is visible. On the pharynx (branchial chamber) floor, the endostyle is recognizable and, posteriorly, the pharynx extends into the esophagus and stomach rudiments. The atrial chamber rudiment loses its original communication with outside. The two peribranchial chambers are inside the embryo and contact the branchial chamber through the protostigmata. The latter are in the form of increasingly thick peribranchial epithelia contacting the branchial epithelium. The heart begins to invaginate along the raphe. In histological sections, myofibrils are recognizable within the tail muscle cells.

Stage: *1.5 wrap* (66 hours after fertilization) (Fig. 3 D-D''). The three papillae increase their anterior protrusion and are covered by the tunic. The eight blood ampullae are recognizable. The branchial chamber is more deformed than in the previous stage. The stomach is a posterior-left elongation of the esophagus. Two-three protostigmata are perforated following an anterior-posterior pattern. The peribranchial chambers are

ventrally elongated and, on the left, the peribranchial chamber is close to the stomach. The oral siphon rudiment is present. It contacts the dorsal groove, a deep longitudinal depression filled with tunic (Scott, 1934; Manni et al., 1999). The sensory vesicle is on the right of the visceral ganglion. The neurohypophyseal duct parallels the dorsal groove and is separated from the left ganglionic vesicle.

Period: Swimming larva

Stage: Hatching larvae (4 days after fertilization) (Fig. 4 A-A''). The larva has a trunk 400 mm long and a tail 1 mm long (Manni et al., 2004). Its anterior region expands in the eight ampullae surrounding a central protruding area with the three papillae. Some endostyle bands are recognizable. Both the rudiments of the oral and atrial siphons face the dorsal groove. Some of the eight stomach folds are recognizable. The gut is completely enveloped by the preribranchial leaflet. The pyloric gland is visible. Both the left and right buds are recognizable as peribranchial epithelium thickenings. The pericardium and the myocardium are well separated. The larval brain is organized in a large sensory vesicle, the visceral ganglion, the neck, and the nerve cord. The left ganglionic vesicle does not contact with the neurohypophyseal duct (now differentiating into the neural gland). The adult neural complex is composed of the differentiating cerebral ganglion and neural gland. The yolk is almost disappeared.

Metamorphosis

Period: Adhesion (5 days after fertilization) (Fig.4 B-B'', 5). The larva adheres with its papillae to the substrate. They are depressed among the ampullae that thicken in their apical area, elongating forward. The tail is still complete, but it begins to regress. It is embedded in a tunic sheath, empty in the distal portion. The tail proximal epidermis begins to thicken. The larval NS begins to degenerate, whereas the neural complex is differentiating.

Period: Body axes rotation (6 days after fertilization) (Fig.4 C-C''). The tail is almost completely absorbed within the trunk. The ampullae expand on the substrate and become narrow proximally so that their peduncles are recognizable. Anatomical structures previously anterior are now ventral, whereas the posterior structures are dorsal. The endostyle is parallel to the substrate.

Post-metamorphosis

Period: Oozooid (7 days after fertilization) (Fig. 4 D-D'', 6). The tail remnant is no longer recognizable. The marginal vessel has an arch-shape and joins the ampullae. The branchial basket and the stigmata are enlarged. Both the oral and the atrial siphons are open and filtration begins. The cerebral ganglion, the neural gland with its ciliated aperture, and the dorsal organ, form the neural complex. The heart is beating. The right bud, at stage 5 (Manni et al., 2014), is developing.

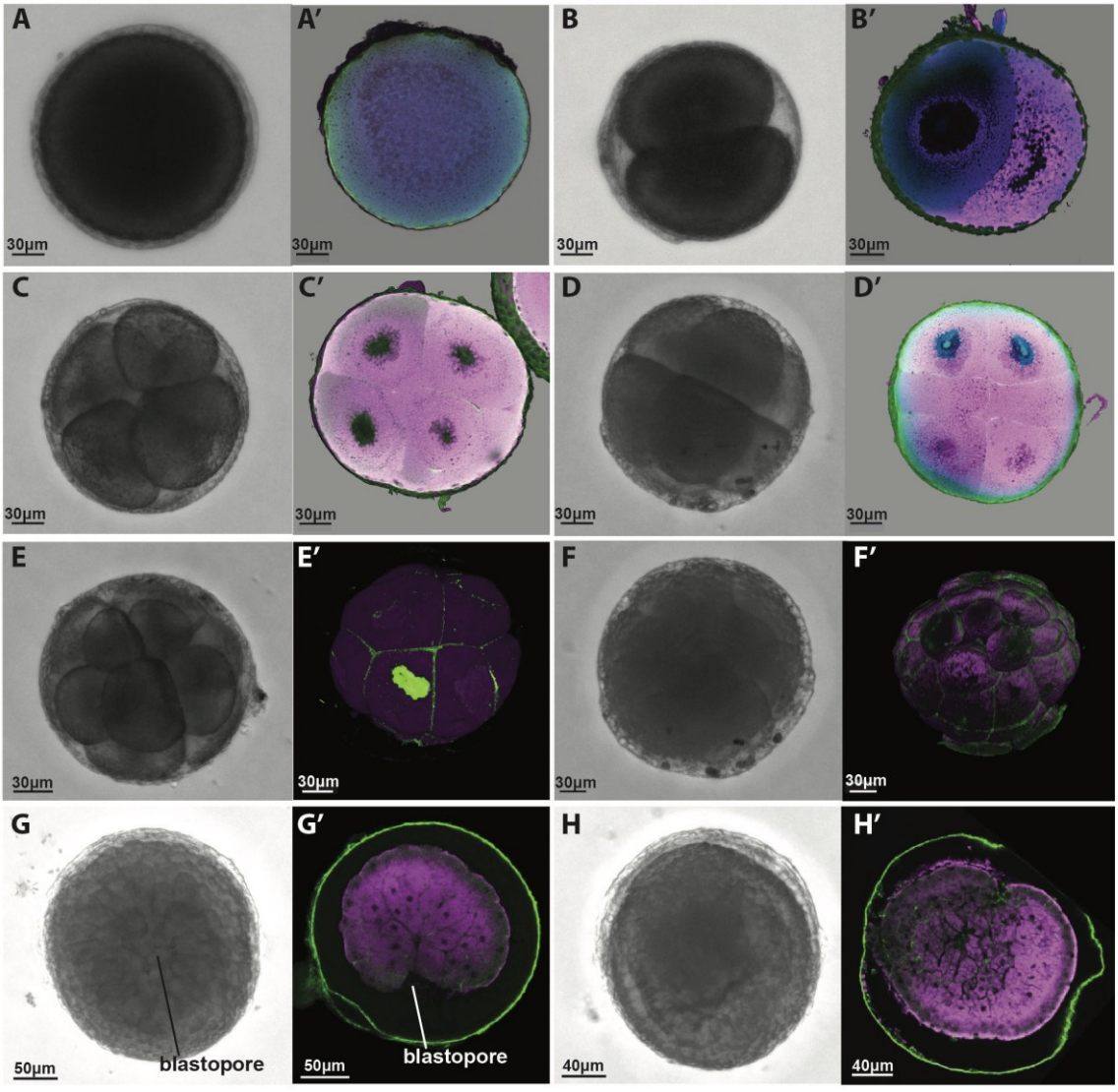

Fig. 2: Embryonic development, pre-metamorphosis in *B. schlosseri*. **A**: Unfertilized egg, **B**: 2 cell stage, **C:** 4 cell stage, **D:** 8 cell stage, **E:** 16 cell stage, **F:** after 16 cells until gastrulation, **G:** gastrula period, **H:** neurula period. A-H: *in vivo* pictures. A'-H': confocal images. Green: Alexa Phalloidin 546 for actin staining; pink: cell mask orange for cytoplasm staining; blue: DAPI for nucleus staining.

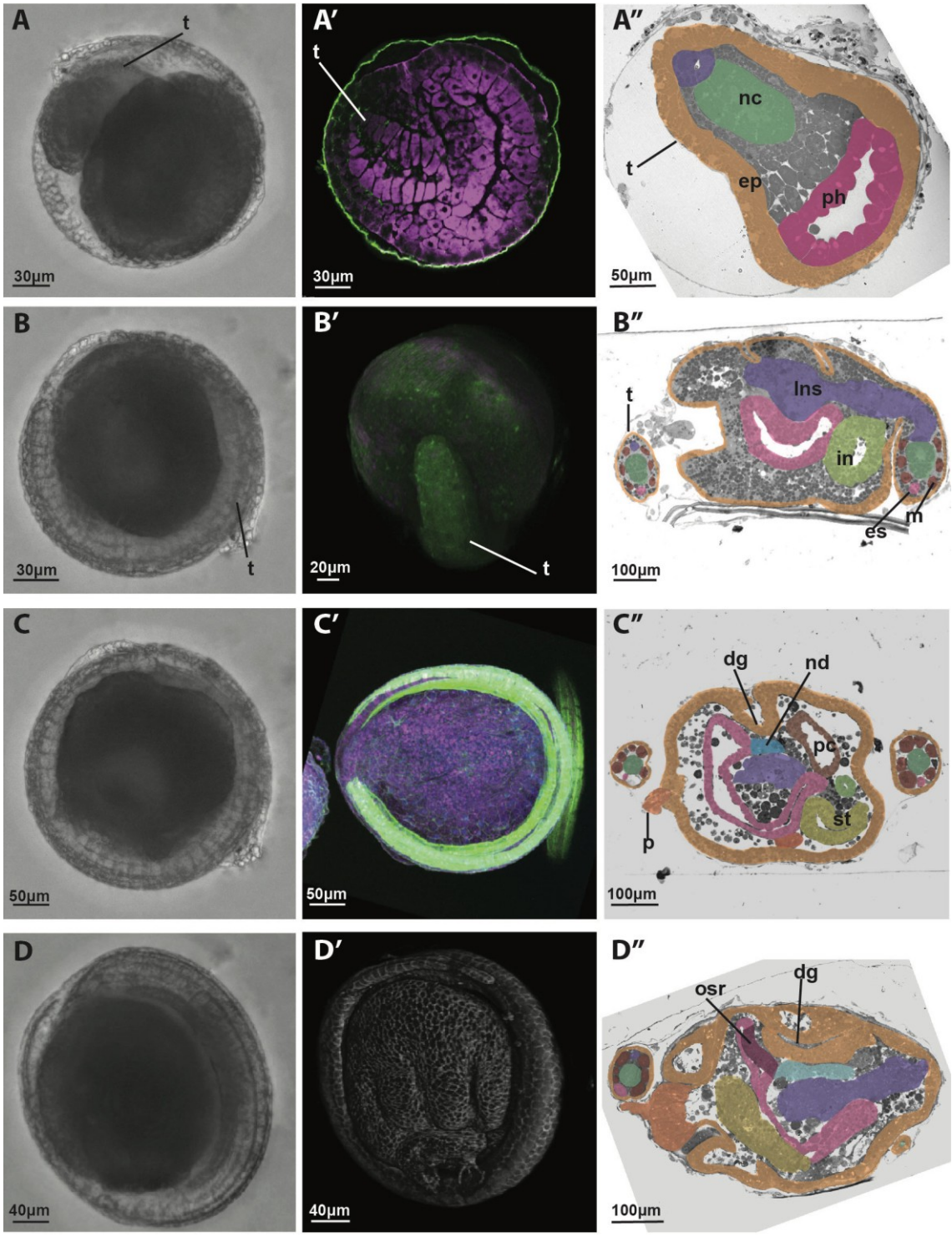

Fig. 3: Embryonic development, pre-metamorphosis in *B. schlosseri*. **A:** initial tail bud stage, **B:** ¾ wrap stage, **C:** 1-1.5 wrap stage, **D:** 1.5 wrap stage. A-D: *in vivo* pictures. A'-D': confocal images. Green: Alexa Phalloidin 546 for actin staining; pink: cell mask orange for cytoplasm staining; blue: DAPI for nucleus staining. **t**: tail. A'''-D''': histological sections, structures are color-coded; **dg**: dorsal groove, **ep**: epidermis, **es**: endodermal strand, **in**: intestine, **lns**: larval NS, **m**: muscle, **nc**: notochord, **nd**: neurohypophysial duct, **osr**: oral siphon rudiment, **p**: papillae, **pc**: peribranchial chamber, **ph**: pharynx, **st**: stomach.

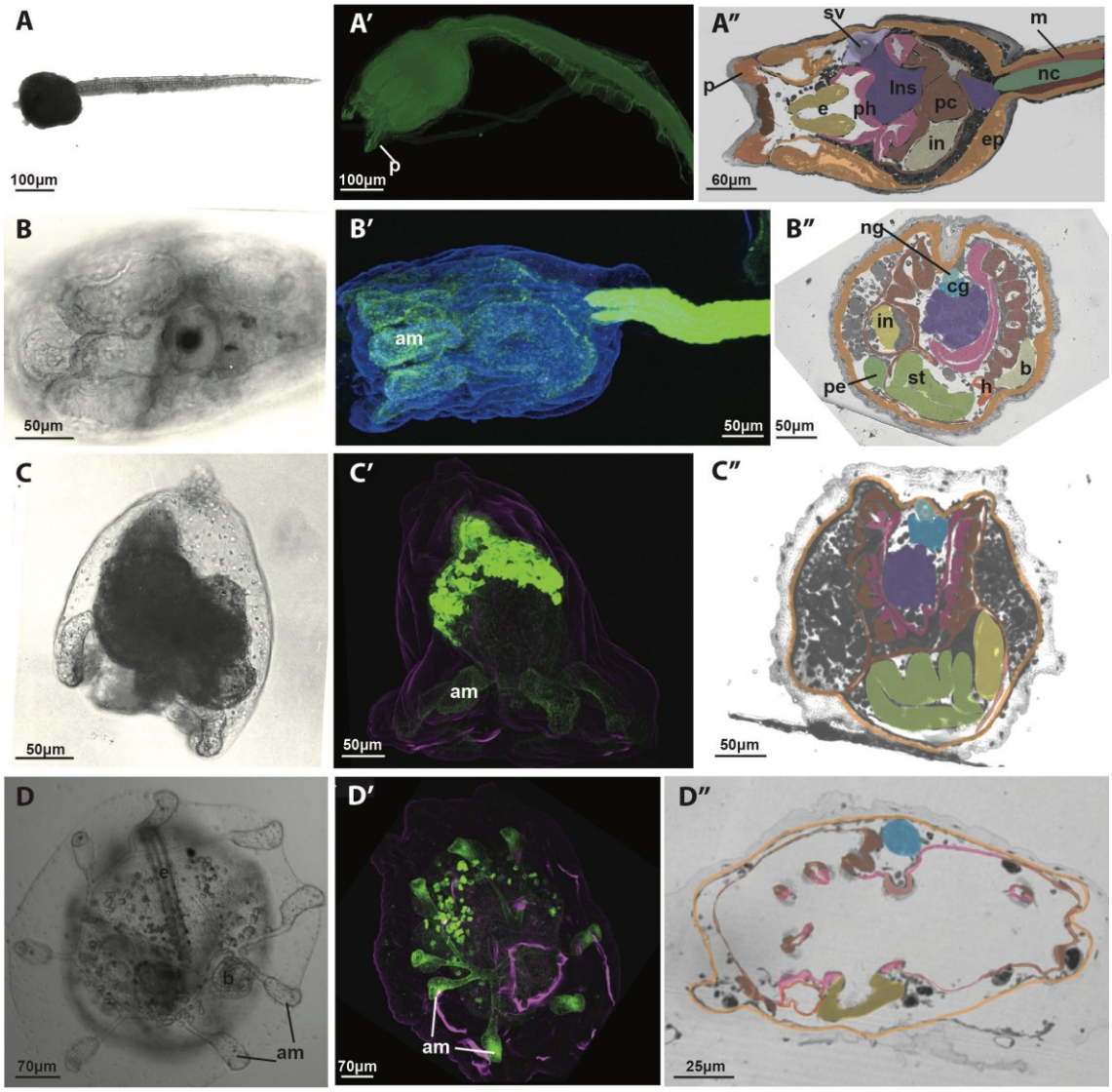

Fig. 4: Embryonic development, pre-metamorphosis, Metamorphosis, and Post-metamorphosis in *B. schlosseri*. **A:** hatching larvae stage, **B:** adhesion period, **C:** body axes rotation period, **D:** oozooid. A-D: *in vivo* pictures. A'-D': confocal images. Green: Alexa Phalloidin 546 for actin staining; pink: cell mask orange for cytoplasm staining; blue: DAPI for nucleus staining. **am**: ampullae; **p**: papillae. A'"-D'": histological sections, structures are color-coded; **cg**: cerebral ganglion, **b**: bud, **e**: endostyle, **ep**: epidermis, **h**: heart, **in**: intestine, **lns**: larval NS, **m**: musculature, **nc**: notochord, **ng**: neural gland, **p**: papillae, **pe**: peribranchial epithelium, **pc**: pyloric caecum, **ph**: pharynx, **st**: stomach, **sv**: sensory vesicle.

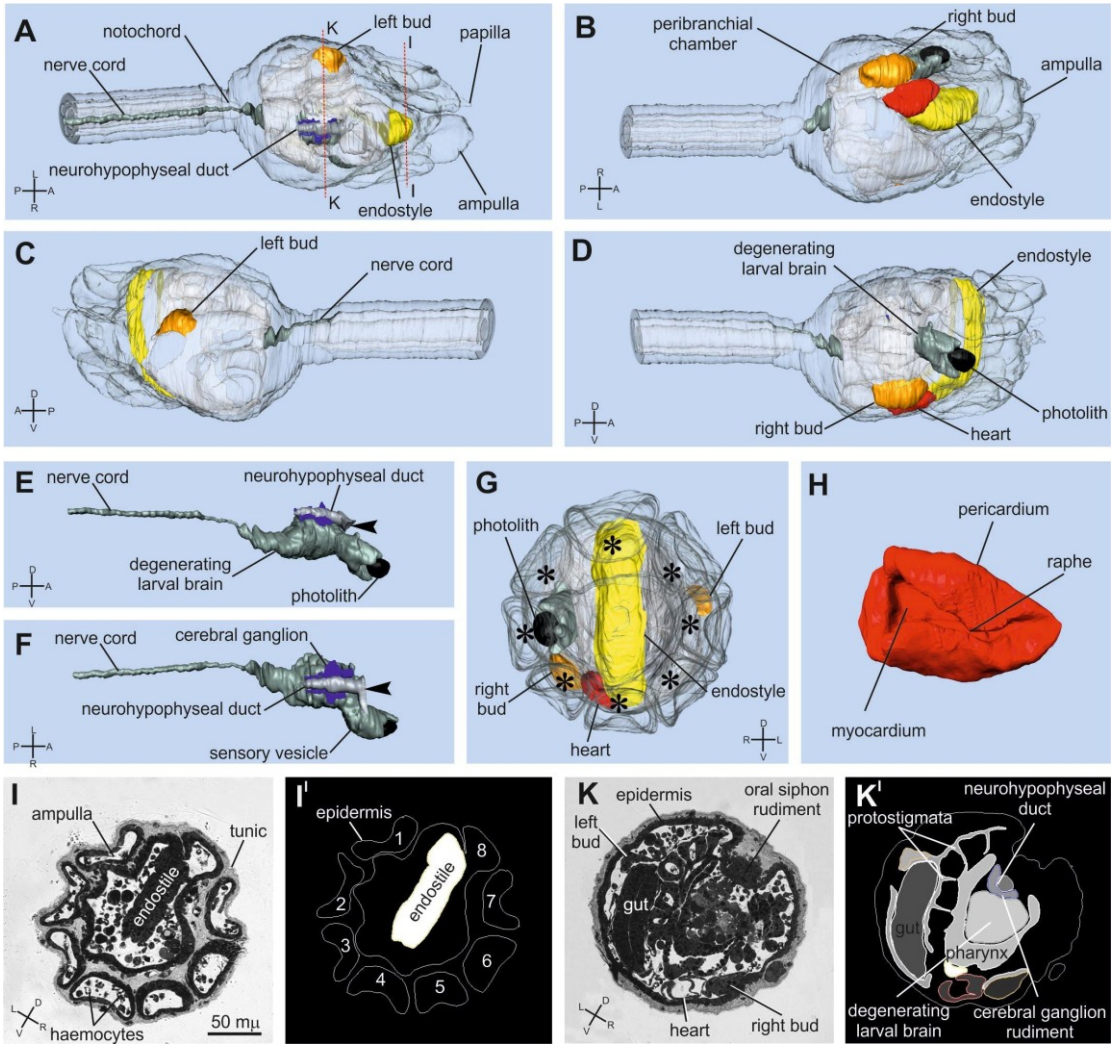

Fig. 5: A-H. 3D reconstruction of a larva in early metamorphosis (Adhesion Period) from transverse histological serial sections. Labeled larval structures are: budlets (orange), cerebral ganglion (violet), endostyle (yellow), heart (red), larval nervous system (dark grey), neurohypophyseal duct (light gray), photolith (black). Other structures are transparent. In A-D, the larva is viewed from the dorsal (A), ventral (B), left (C) and right (D) side. The red dotted lines in A represent the levels of sections in I and K. In E-F, right (E) and dorsal (F) views of the larval nervous system and the neural complex rudiment (neurohypophyseal duct and cerebral ganglion). Anterior at right. G. Anterior view of the larva. Note the eight ampullae (asterisks) for larval adhesion. H. Heart. For enlargements, refer to the histological sections in I and K. **I-K.** Histological sections of the larva at level of ampullae (I) and oral siphon rudiment (K). Toluidine blue. I^I and K^I show the larval structures segmented on sections I and K.

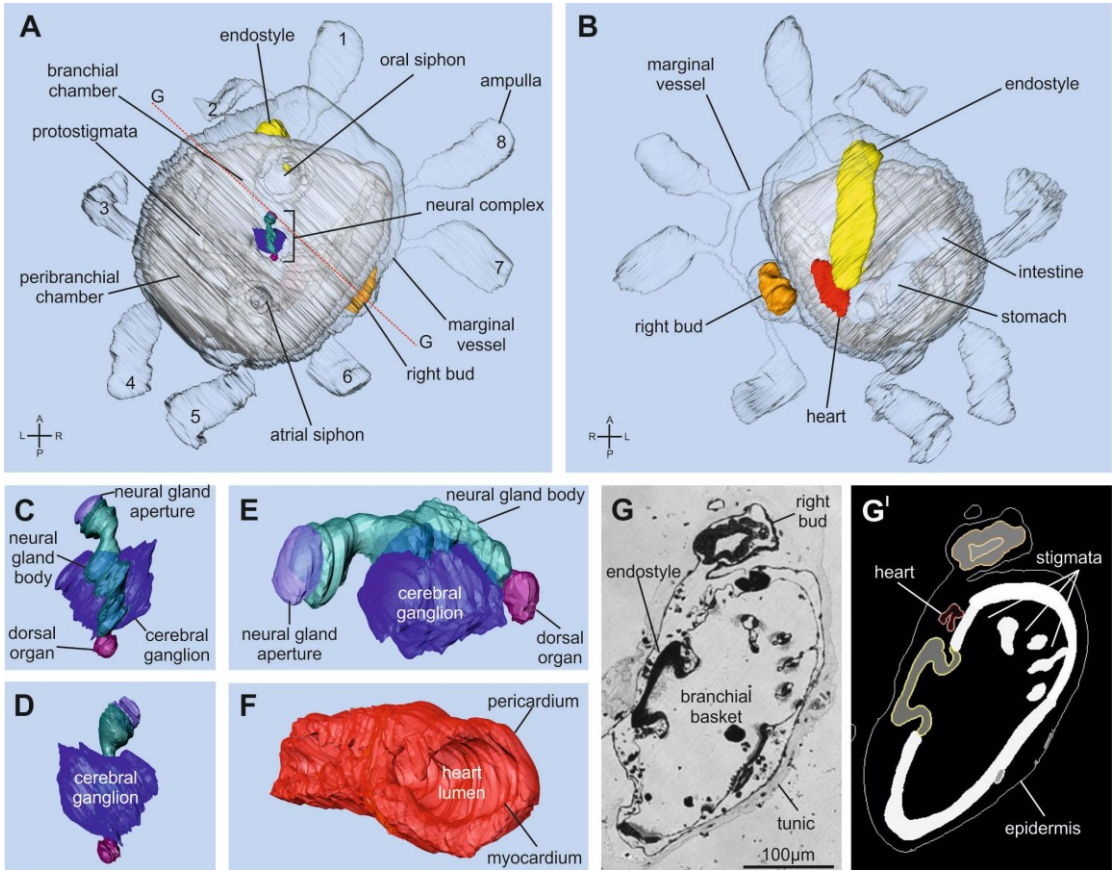

Fig. 6: A-F. 3D reconstruction of an oozooid (Oozooid Period) from oblique histological serial sections. Labeled larval structures are: right budlet (orange), cerebral ganglion (violet), dorsal organ (burgundy), endostyle (yellow), heart (red), neural gland (green), neural gland aperture (purple). Other structures are transparent. Note the eight ampullae (1-8) attaching the oozooid to substrate. A: dorsal view; B: ventral view. The red dotted line in A represents the level of section in G. C-E. Neural complex viewed from dorsal (C), ventral (D), and lateral E) side. Anterior at top in C-D, at right in E F. Heart. For enlargements, refer to the histological section in G. **G-G^{I}.** Histological section (G) and the correspondent segmented structures (G^{I}).

We highlight that our description of embryogenesis and the definition of the stages/periods is in agreement with the previous reports on *B. schlosseri* embryogenesis, though such studies referred to few stages and/or introduced development in summary (Grave and Woodbridge, 1924; Grave, 1934; Scott, 1934; Manni et al, 1999; Sorrentino et al., 2000).

Comparing the embryogenesis of *B. schlosseri* with that of other ascidians, some anatomical differences are evident. The atrial chamber in *B. schlosseri* originates from a single ectodermal mid-dorsal rudiment, whereas in *C. intestinalis* (and in all Enterogona species) the chamber originates from a pair of dorsal ectodermal invaginations (Willey,

1893; Katz, 1983). The *B. schlosseri* embryo possesses an ectodermal dorsal groove where both siphons open, whereas in *C. intestinalis* the oral siphon rudiment and the paired atrial siphon rudiments open independently on the embryo surface (Manni et al., 2004). A photolith characterizes the larval sensory vesicle of *B. schlosseri* (properly, of colonial Styelidae), whereas in most of ascidian larvae the sensory vesicles possess an otolith and an ocellus (Sorrentino et al., 2000). A left ganglionic vesicle, not described in *C. intestinalis*, is present and possesses a possible residuum of a primitive photoreceptor organ (Sorrentino et al., 2000). Eight ectodermal ampullae develop for the stable adhesion of the metamorphosing larva; in *C. intestinalis*, an anterior stalk represents the holdfast.

Heterochrony between the *B. schlosseri* development and that one occurring in solitary ascidians, namely *C. intestinalis* (Chiba et al., 2004), is revealed by the timetable (Table 2). The "Embryonic development, pre-metamorphosis" Metaperiod lasts four days in *B. schlosseri*, as compared to one day at 18°C in *C. intestinalis*. The Metamorphosis and Post-metamorphosis periods in *B. schlosseri* last 3 days, whereas in *C. instestinalis* they last a dozen days at 18°C. These differences in developmental timing reflect the anatomical differences between larvae in *B. schlosseri* and *C. intestinalis*. The larvae possess transitory structures for larval life, larval-juvenile organs, and prospective juvenile organs (Burighel and Cloney, 1997), and the last two classes of organs are particularly well developed in the mature larvae of *B. schlosseri*.

Although it is not associated with a precise timetable, our description is accurate and combines complementary information coming from different experimental approaches. It represents the first modern description of the embryogenesis of a colonial ascidian.

Bud development in *Botryllus schlosseri*

In a colony, three blastogenetic generations coexist: the filter-feeding adults, their buds (primary buds), and the budlets (secondary buds) produced by buds. Cyclically, adult individuals degenerate and are reabsorbed during a phase of change of generations, called takeover. At the same time, their buds become the new adults, whereas the budlets (now buds) are ready to produce a new generation of budlets.

The blastogenesis of *B. schosseri* has been extensively investigated since the second half of the past century. Detailed accounts of blastogenesis and a review of the main

papers describing the bud development *in vivo* and by light and transmission electron microscopy can be found in Manni et al., 2007 and 2014.

Here we add, to previously published data, observations by confocal microscope and a 3D reconstruction of a primary bud with its secondary bud (Figs. 7-9). The 3D reconstruction from histological serial sections, where specific organs are marked with different colors, allows their recognition and the comprehension of their relationships with adjacent structures. Our original data complement those already published and provides valuable information for researchers unfamiliar with the anatomy of individuals formed through a non-conventional reproductive pathway, such as asexual reproduction.

Briefly, bud development is subdivided into 11 recognizable stages *in vivo* (Sabbadin 1955; Manni et al., 2014).

Stages 1-6 define the development of the secondary bud and correspond to the following:

1. The secondary bud appears as a thickened disc of the lateral peribranchial epithelium of a bud (Figs. 7A-A'', 9).
2. The thickened epithelium, accompanied by the epidermis, arches in a hemisphere (Fig. 7B-B'').
3. The secondary bud forms a closed double-layered vesicle ("double vesicle" stage"): the internal layer originates from the closure of the disc, the external layer originates from the eversion of the parental epidermis (Fig. 7C-C'').
4. The inner vesicle begins to evaginate to form the branchial and peribranchial chambers (Fig. 7 D-D'').
5. The stomach becomes recognizable as posterior evagination of the branchial rudiment (Fig. 7-E-E'').
6. The heart becomes recognizable and the radial vessels are formed (Fig. 8 F-F'').

Stages 7-8 refer to the primary bud:

7. Stigmata rudiments begin to form and rudiments of new secondary buds appear on the lateral body wall (Figs. 7A-A''- 9).
8. The heart starts beating (Fig. 5B-B'').

Stages 9-11 define the development of the adult:

9. The adult begins its functional filtering activity, opening its siphons
10. This stage refers to the sexually mature zooid with differentiated gonads and gametes
11. Takeover phase (Fig. 8 B-B''). It is subdivided in four sub-stages:
    - 11^1 - siphon retraction and closure
    - 11^2 - general shrinkage of zooids
    - 11^3 - further contraction of zooids and branchial dissolution
    - 11^4 - heart beat stops.

The method chosen to express the coexistence of three contemporary zooid generations in a colony (*i.e*., the colony phase) is a formula of three numbers separated by slashes (*e.g*., 9/8/3) (Sabbadin, 1955). Each number uniquely defines the developmental stage of each blastogenetic generation: the first is refers to adult filtering zooids, the intermediate to primary buds, and the last to secondary buds.

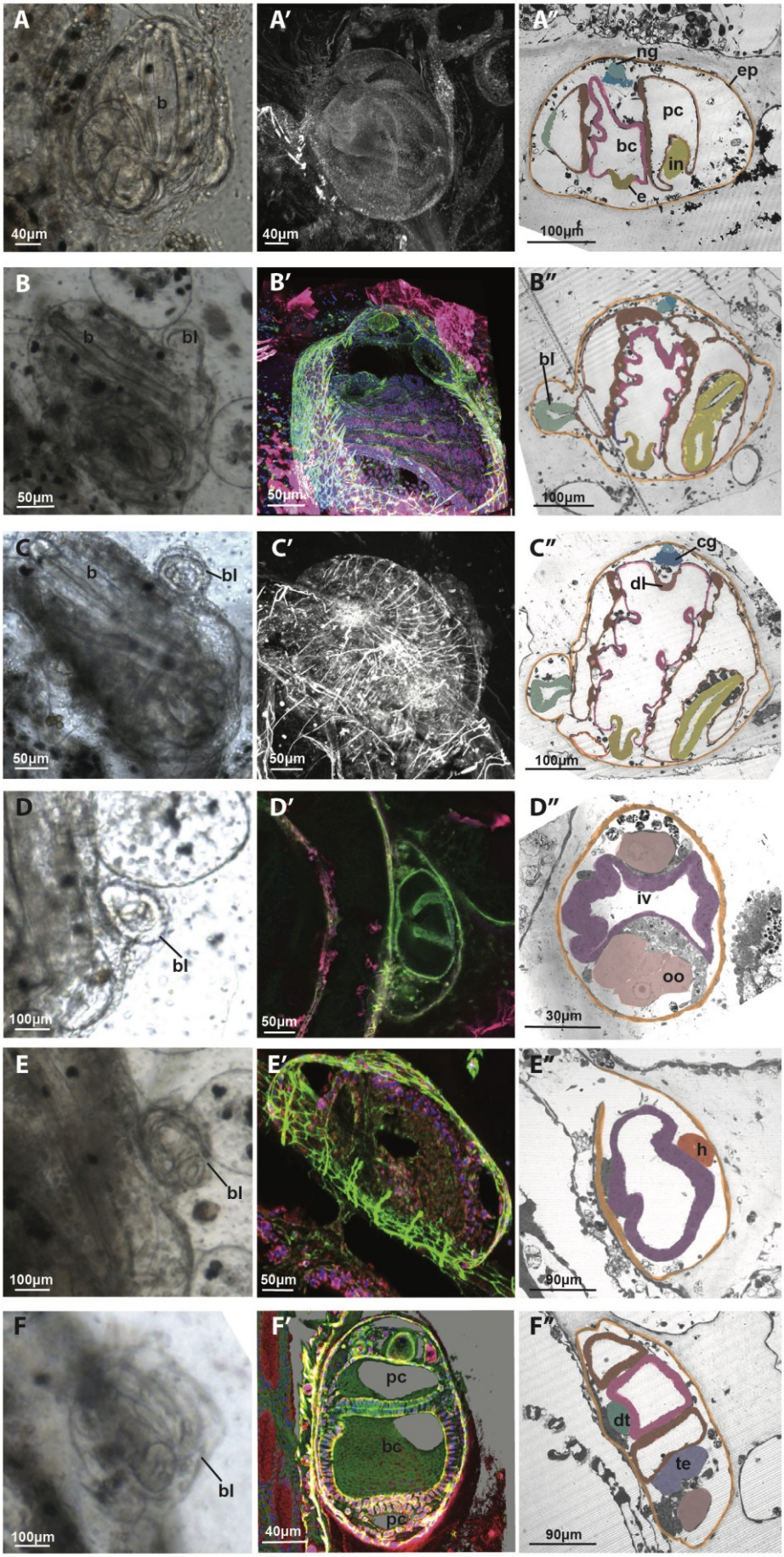
A
b
40µm
A′
40µm
A″
ng
ep
pc
bc
in
e
100µm
B
b
bl
50µm
B′
50µm
B″
bl
100µm
C
b
bl
50µm
C′
50µm
C″
cg
dl
100µm
D
bl
100µm
D′
50µm
D″
iv
oo
30µm
E
bl
100µm
E′
50µm
E″
h
90µm
F
bl
100µm
F′
pc
bc
pc
40µm
F″
dt
te
90µm

Fig: 7: Blastogenesis in *B. schlosseri*. **A**: 9/7/1; **B**: 9/8/2; **C**: 9/8/3; **D**: 9/8/4, **E**: 9/8/5; **F**: 9/8/6. The underlined number refers to the specific generation under consideration. A-F: *in vivo* pictures; b:bud (primary bud), bl: budlet (secondary bud). A'-F': confocal images. Green: Alexa Phalloidin 546 for actin staining; pink: cell mask orange for cytoplasm staining; blue: DAPI for nucleus staining. **b**: bud (primary bud), **bl**: budlet (secondary bud). A'''-F''': histological sections, structures are color-coded; **bc**: brachial chamber, **bl**: budlet, **cg**: cerebral ganglion, **dl**: dorsal lamina, **dt**: dorsal tube, **e**: endostyle, **ep**: epidermis **h**: heart, **in**: intestine, **iv**: inner vescicle, **ng**: neural gland, **oo**: oocyte, **pc**: peribranchial chamber, **te**: testis

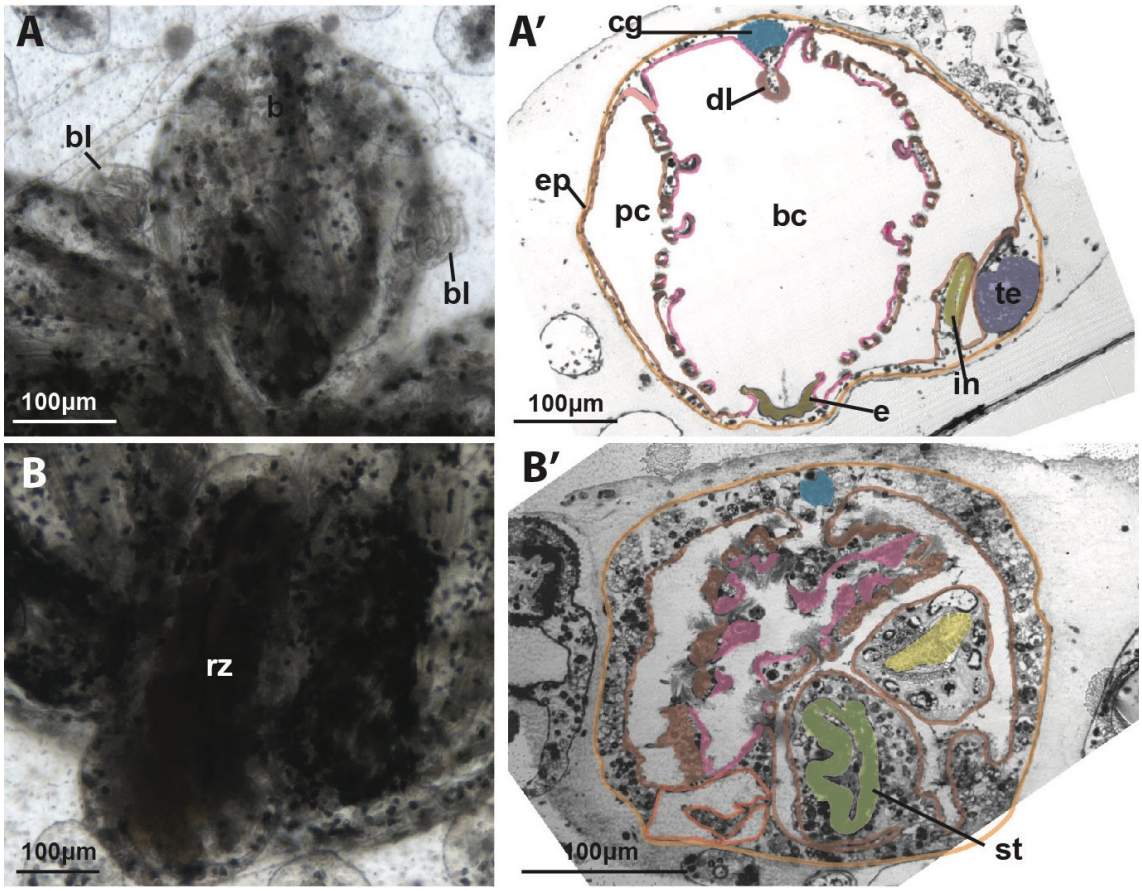

Fig. 8: Blastogenesis in *B. schlosseri*. **A**: 9/8/6; **B**: 11/8/6. A-B: *in vivo* pictures, **b**: bud (primary bud), **bl**: budlet (secondary bud), **rz**: regressive zooid. A''-B'': histological sections, structures are color-coded; **bc**: brachial chamber, **cg**: cerebral ganglion, **dl**: dorsal lamina, **e**: endostyle, **ep**: epidermis, **in**: intestine, **pc**: peribranchial chamber, **st**: stomach, **te**: testis.

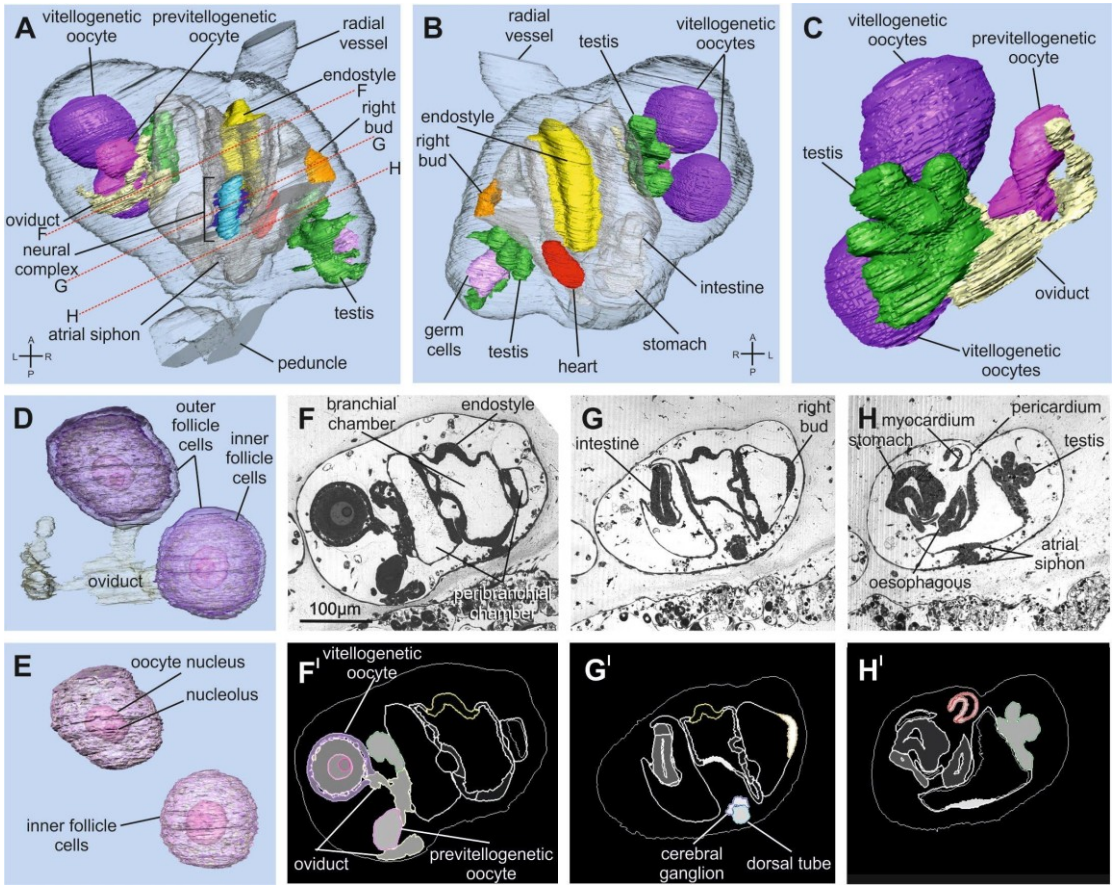

Fig. 9: A-E. 3D reconstruction of a bud at stage 7 with its budlet at stage 1 from oblique histological serial sections. Labeled larval structures are: budlets (orange), cerebral ganglion (violet), dorsal tube (light blue), endostyle (yellow), germ cells (light pink), heart (red), oviduct (pale yellow), previtellogenic oocyte (fuchsia), testis (green), vitellogenic oocytes (purple). Other structures are transparent. In A-B, the bud is viewed from dorsal (A) and ventral (B) sides. The red dotted lines in A represent the levels of sections in F-H. In C, detail of the male and female gonads. D-E. Female gonad. In D, outer follicle cells are transparent, to see inner follicle cells. In E, both oviduct and outer follicle cells were removed; inner follicle cells are transparent. For enlargements, refer to the histological sections in F-H. F-H^{I}. Histological sections of the bud at level of gonad (F), secondary bud (G), and atrial siphon rudiment (H). Toluidine blue. **F^{I}-H^{I}** show the bud structures segmented on sections F-H.

Relationship between embryo and bud development

In a mature colony, sexual and asexual cycles coincide and embryo development is closely related to the colonial blastogenetic phase. Ovulation occurs when the bud opens its siphon becoming an adult. Sperm coming from other colonies can therefore enter the zooids and fertilize the ovulated eggs, which are exposed to the seawater flow. The first accounts of the relationship between embryo and bud development were given in Milkman, 1967, and then in Manni et al., 2007. In the latter paper, the embryonic development was summarily subdivided into five stages: 1) ovulation, fertilization, and beginning of embryo development; 2) early tailbud embryo; 3) mid tailbud embryo; 4) late tailbud embryo, and 5) larval hatching. Now we can integrate our data of embryogenesis and blastogenesis into a more comprehensive picture, providing a precise definition of the temporal relationship that exists between the two reproductive pathways.

The first embryogenetic periods (zygote, cleavage, gastrula, neurula) occur rapidly during the first phase of blastogenesis (10/7/1) (Table 3). Embryos reach the Tailbud Period at the colony phase 10/8/2. The Period takes several days, depending on rearing temperature, ending at the colony phase 10/8/5. The hatching larva stage occurs just before the atrial siphon closure at takeover.

Colony phase	10/7/1	10/8/2	10/8/3	10/8/4-5	10/8/5
Period/stage of embryo development	Ovulation, fertilization, Zygote, Cleavage, Gastrula, and Neurula periods	Tailbud period: initial tailbud, tail ¾ stage	Tailbud period: 1-1.5 wrap stage	Tailbud period: 1,5 wrap	Swimming larva period: Hatching larva
Stage of bud development	Secondary bud evaginates from lateral wall of primary bud. Onset of a new cycle: oral and excurrent siphons of zooid open.	Skewing of secondary bud toward anterior hemisphere of parent zooid. Heartbeat begins in primary bud.	Secondary bud forms a closed double-layered vesicle.	Organogenesis begins in secondary bud. primary subdivisions are completed in secondary bud.	Takeover

Table 3: Relationship between main events of embryogenesis and colony phases.

These more detailed data concerning the relationship between the two developmental pathways will be helpful in future studies in which embryos are removed from colonies or analyzed within colonies.

Nervous system development in embryo: morphological events and transcriptome analyses

The development of the larval NS has not been described in *B. schlosseri.* Here, we report the first data on the gastrula and neurula periods, during which the neural plate forms and the neural tube rolls (Table 4). From our *in vivo* observations, we infer that the larval NS forms following the invariant cell lineage of ascidian embryos (Lemaire et al., 2002), although this could be confirmed using tracers. In *Halocynthia* and *Ciona*, the neural tissue derives from three lineages: the anterior vegetal A-line, and the animal a- and b-lines. During the tailbud period, the main nerve components (*i.e.*, the sensory vesicle with the photolith, the visceral ganglion, the neck, and the nerve cord) become recognizable. As reported above, in *B. schlosseri* a left ganglionic vesicle is present. This has been considered the antimere of the sensory vesicle (Pizon, 1893; Delage and Herouard, 1898, reviewed in Manni et al., 1999 and Sorrentino et al., 2000) and is in continuity with the neurohypophyseal duct. The left ganglionic vesicle disappears during metamorphosis.

Period/Stage	**16-cell**	**After 16-cell until gastrulation**	**Gastrula**	**Neurula**
Hpf	**6hr**	**8hr**	**16hr-23hr**	**25hr-29hr**
Larval NS	[1]a6.5 fate restricted at 32-cell stage; A7.4 fate restricted at the 44-cell stage; a7.9, a7.10, and a7.13 restricted at 64-cell	[1]A8.7, A8.8, A8.15, a.817, a8.18, a8.19, a820, a.825, b8.19 are fate restricted at 110-cell stage		Neural plate
Neural Complex				
Period/Stage	**Initial tailbud**	**¾ wrap**	**1 -1.5 wrap**	**1.5 wrap**
Hpf	**31hr**	**40hr**	**44hr**	**66hr**
Larval NS	Neural tube closure; rudiment of sensory vesicle present	Sensory vesicle, visceral ganglion, neck, and nerve cord recognizable; photolith in sensory vesicle; ganglionic vesicle communicating with the neurohypophyseal		
Neural Complex		Neurohypophyseal duct blinds at both extremities; pioneer nerve cell delamination	Neurohypophyseal duct separates from left ganglionic vesicle; fusion with anterior pharynx evagination	
Period/Stage	**Hatching larva**	**Adhesion**	**Body axis rotation**	**Oozooid**
Hpf	**4 days**	**5 days**	**6 days**	**7 days**
Larval NS		Larval NS in degeneration	Larval NS remnants recognizable	Larval NS remnants no more recognizable
Neural Complex	Cerebral ganglion, ciliated duct and neural gland body recognizable.		cerebral ganglion, ciliated duct, neural gland body and dorsal organ recognizable	

Table 4: Main events of larval NS and neural complex development during embryogenesis. Hpf: hours post fertilization. ([1] from Lemaire et al., 2002)

Our histological data confirm that the neural complex rudiment is represented by the ectodermal neurohypophysial duct, which forms from the left anterior end of the embryonal neural tube during the Neurula Period (Burighel and Cloney, 1997; Manni et al., 1999). The contribution of the larval NS to neural complex formation, as evidenced in *Ciona* (Horie et al., 2011), cannot be excluded in *B. schlosseri*.

It is important to note that the two brains, the larval brain and the emerging cerebral ganglion, coexist from the tailbud period until the completion of metamorphosis. Progressively, the first brain develops and then degenerates, whereas the second completes its development. In the oozooid, the first brain is no longer recognizable when the second is physiologically active. Therefore, in *B. schlosseri*, a coordinated series of events allows for contemporary brain degeneration and development.

In the oozooid, the ganglion exhibits an outer cortex of nerve cell bodies and an internal medulla. The latter consists of a neuropil of neuronal processes making classical synaptic contacts (Manni et al., 1999). The adult neural gland differentiates into a structure with a ciliated duct and the body of the gland. The posteriormost part of the neural gland differentiates into the dorsal organ, homologous to the dorsal strand (Manni and Pennati, 2016). The organization and temporal relationships between the larval NS and the neural complex during development are summarized in Figure 10.

Our *in vitro* embryo culture allowed us to collect embryos for the preparation of transcriptomes for 15 different developmental periods/stages (Table 2). Whole tissues were taken for RNA extraction and sequencing (n=44). We also sampled different tissues from adult individuals, including the neural complex (n=2), testes (n=8), endostyle (n=10), and ampullae (n=7), and sequenced their mRNA. On average 12 million 2x150 bp reads (Illumina Nextseq 500) were sequenced for each library.

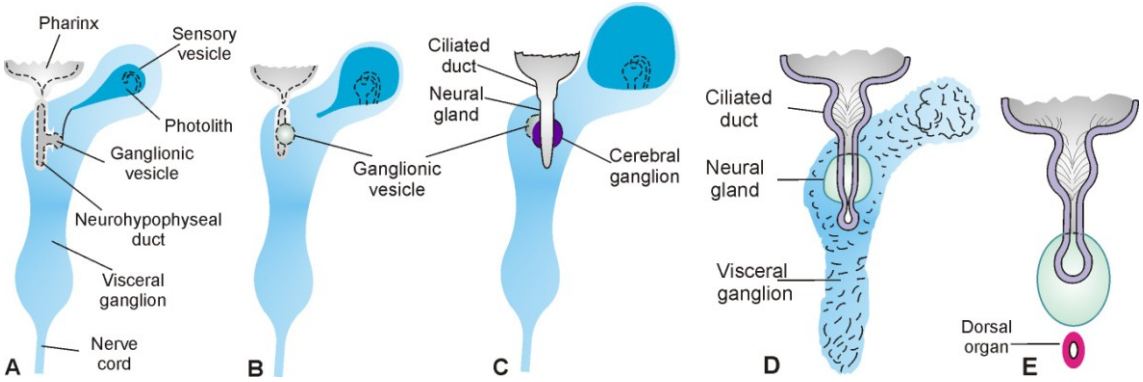

Fig. 10: Scheme of main developmental events during neural complex development in embryo. (Modified from Manni et al., 1999).

Following sequencing, reads were processed using a snakemake pipeline (Köster and Rahmann, 2012): trimmed to remove low quality bases and primers, merged if the reads from both ends overlapped and aligned to a database of *B. schlosseri* transcripts using bwa (mem algorithm), with likely PCR duplicates removed and before read counts were determined for each transcript - producing a count table. Samples were selected for all sets of contiguous times in embryogenesis and differentially expressed genes were found using edgeR. For each gene, statistically significant differences (FDR < 0.05) for all such comparisons were assessed and the optimal time signature for explaining the differentially expressed observations for each gene were identified. To further simplify the comparisons, time signatures were binarized, with 1 indicating "high" expression and 0 indicating "low" or zero expression, to produce a gene-time expression matrix for each gene along the developmental pathway. Tissue-associated transcripts were found by taking unions and intersections of pairwise differential expression analyses of the tissues. Brain associated genes were defined as those that are up-regulated in at least two of the comparisons with the testes, endostyle and ampullae. This resulted in 363 genes, 105 of which have putative human or mouse homologs.

With this library of tissue and development associated and gene expression, we then analyzed the genes related to the NS. Our main finding is the two stages of enrichment of NS associated genes (Fig. 11 A), the first between the 16 cell stage and the gastrula, the second between the ¾ and 1.5 wrap. They correspond with important developmental events (Table 2): the first corresponds to the time in *C. intestinalis* when neural progenitors are known to originate, the second during the period when the neural complex begins to differentiate from the neurohypophyseal duct. Additionally,

extending our analysis beyond the genes enriched in the brain transcriptome to consider genes with neuron development associated GO terms (namely, neuron differentiation, neuron development, and neurogenesis), we observed an enrichment of gene expression 1) after the gastrulation and 2) after the tailbud began developing (Fig. 11 B-D). This includes: the Wnt signalling pathway genes *Fzd10* and *Wnt6*; the homeobox transcription factor *EMX* (expressed in the dorsal telencephalon in developing mammals) and *MTPN*, which may be involved in the differentiation of cerebellar neurons in humans.

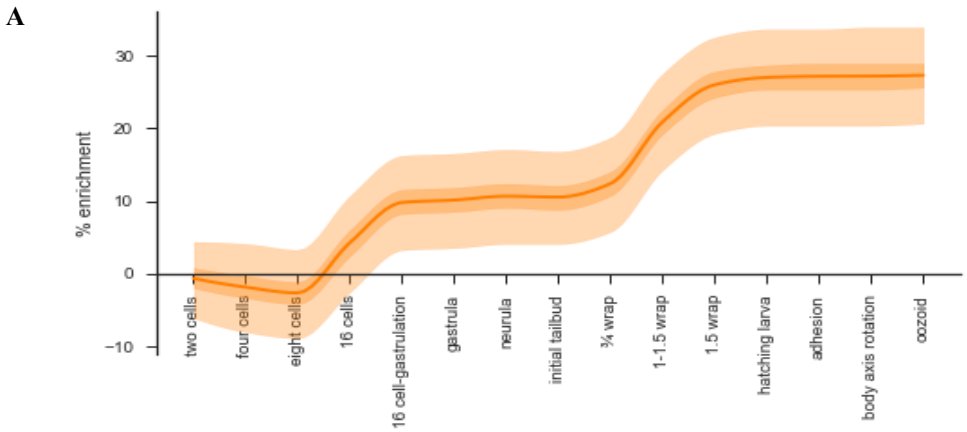

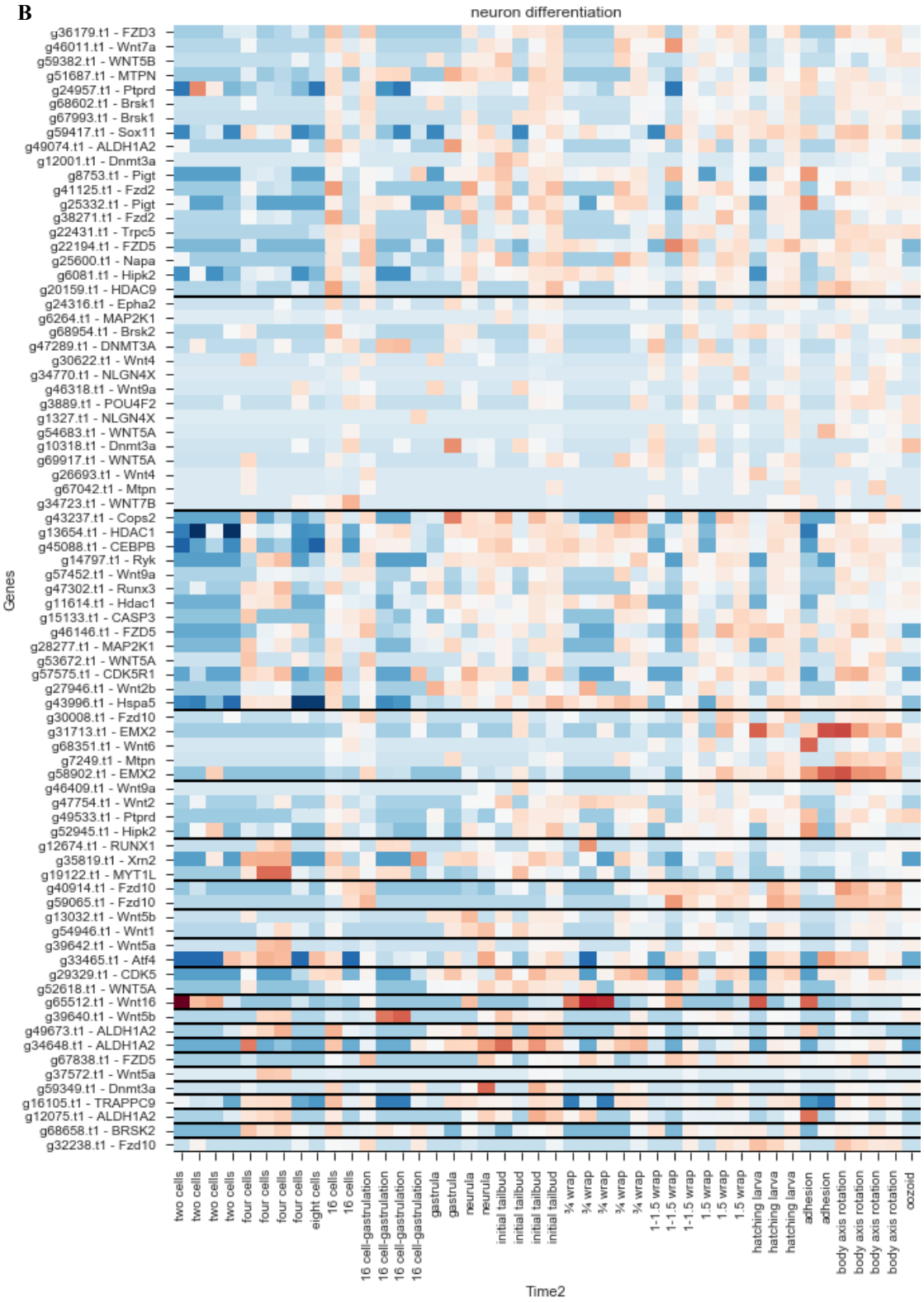
B
neuron differentiation
Genes
g36179.t1 - FZD3
g46011.t1 - Wnt7a
g59382.t1 - WNT5B
g51687.t1 - MTPN
g24957.t1 - Ptprd
g68602.t1 - Brsk1
g67993.t1 - Brsk1
g59417.t1 - Sox11
g49074.t1 - ALDH1A2
g12001.t1 - Dnmt3a
g8753.t1 - Pigt
g41125.t1 - Fzd2
g25332.t1 - Pigt
g38271.t1 - Fzd2
g22431.t1 - Trpc5
g22194.t1 - FZD5
g25600.t1 - Napa
g6081.t1 - Hipk2
g20159.t1 - HDAC9
g24316.t1 - Epha2
g6264.t1 - MAP2K1
g68954.t1 - Brsk2
g47289.t1 - DNMT3A
g30622.t1 - Wnt4
g34770.t1 - NLGN4X
g46318.t1 - Wnt9a
g3889.t1 - POU4F2
g1327.t1 - NLGN4X
g54683.t1 - WNT5A
g10318.t1 - Dnmt3a
g69917.t1 - WNT5A
g26693.t1 - Wnt4
g67042.t1 - Mtpn
g34723.t1 - WNT7B
g43237.t1 - Cops2
g13654.t1 - HDAC1
g45088.t1 - CEBPB
g14797.t1 - Ryk
g57452.t1 - Wnt9a
g47302.t1 - Runx3
g11614.t1 - Hdac1
g15133.t1 - CASP3
g46146.t1 - FZD5
g28277.t1 - MAP2K1
g53672.t1 - WNT5A
g57575.t1 - CDK5R1
g27946.t1 - Wnt2b
g43996.t1 - Hspa5
g30008.t1 - Fzd10
g31713.t1 - EMX2
g68351.t1 - Wnt6
g7249.t1 - Mtpn
g58902.t1 - EMX2
g46409.t1 - Wnt9a
g47754.t1 - Wnt2
g49533.t1 - Ptprd
g52945.t1 - Hipk2
g12674.t1 - RUNX1
g35819.t1 - Xrn2
g19122.t1 - MYT1L
g40914.t1 - Fzd10
g59065.t1 - Fzd10
g13032.t1 - Wnt5b
g54946.t1 - Wnt1
g39642.t1 - Wnt5a
g33465.t1 - Atf4
g29329.t1 - CDK5
g52618.t1 - WNT5A
g65512.t1 - Wnt16
g39640.t1 - Wnt5b
g49673.t1 - ALDH1A2
g34648.t1 - ALDH1A2
g67838.t1 - FZD5
g37572.t1 - Wnt5a
g59349.t1 - Dnmt3a
g16105.t1 - TRAPPC9
g12075.t1 - ALDH1A2
g68658.t1 - BRSK2
g32238.t1 - Fzd10
two cells
two cells
two cells
two cells
four cells
four cells
four cells
four cells
eight cells
16 cells
16 cells
16 cell-gastrulation
16 cell-gastrulation
16 cell-gastrulation
16 cell-gastrulation
gastrula
gastrula
neurula
neurula
initial tailbud
initial tailbud
initial tailbud
initial tailbud
¾ wrap
¾ wrap
¾ wrap
¾ wrap
¾ wrap
1-1.5 wrap
1-1.5 wrap
1-1.5 wrap
1.5 wrap
1.5 wrap
1.5 wrap
hatching larva
hatching larva
hatching larva
adhesion
adhesion
body axis rotation
body axis rotation
body axis rotation
body axis rotation
oozoid
Time2

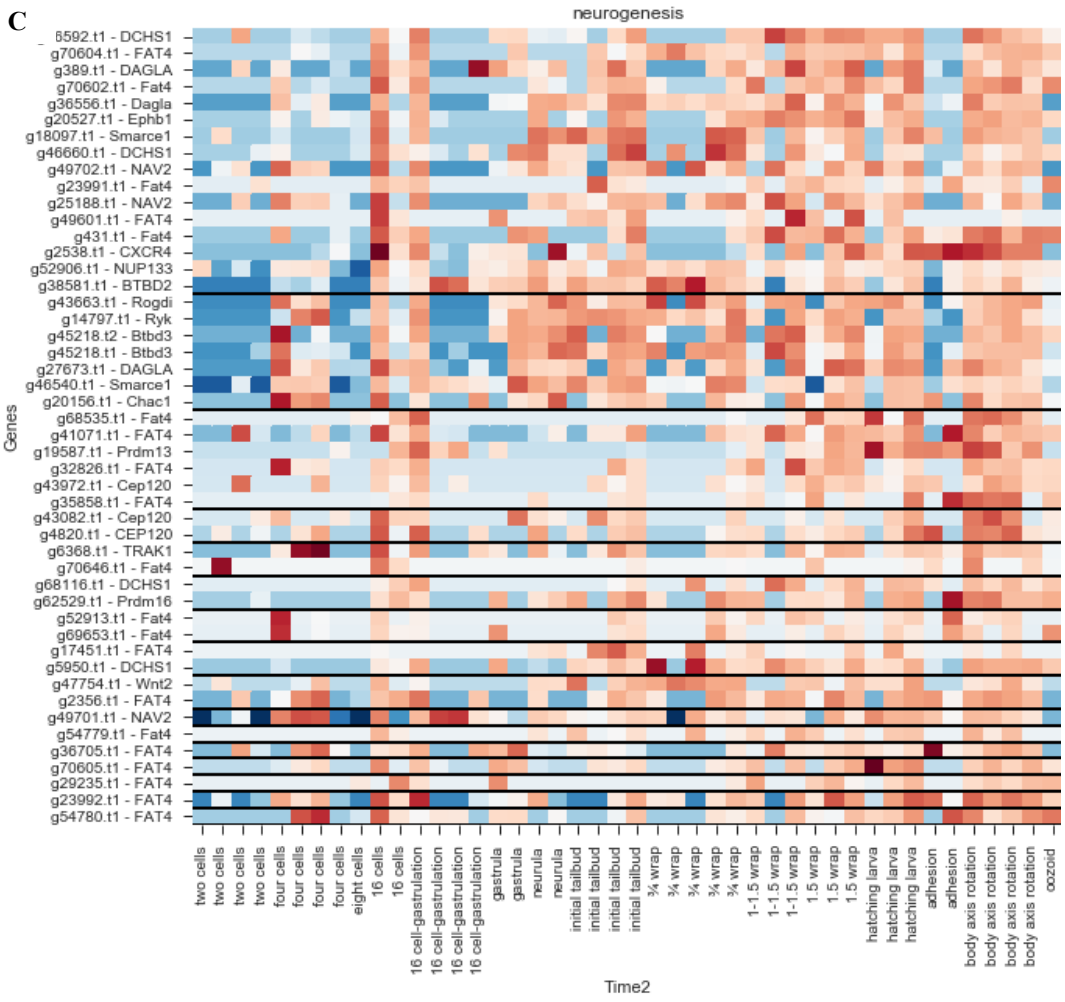
C
neurogenesis
Genes
6592.t1 - DCHS1
g70604.t1 - FAT4
g389.t1 - DAGLA
g70602.t1 - Fat4
g36556.t1 - Dagla
g20527.t1 - Ephb1
g18097.t1 - Smarce1
g46660.t1 - DCHS1
g49702.t1 - NAV2
g23991.t1 - Fat4
g25188.t1 - NAV2
g49601.t1 - FAT4
g431.t1 - Fat4
g2538.t1 - CXCR4
g52906.t1 - NUP133
g38581.t1 - BTBD2
g43663.t1 - Rogdi
g14797.t1 - Ryk
g45218.t2 - Btbd3
g45218.t1 - Btbd3
g27673.t1 - DAGLA
g46540.t1 - Smarce1
g20156.t1 - Chac1
g68535.t1 - Fat4
g41071.t1 - FAT4
g19587.t1 - Prdm13
g32826.t1 - FAT4
g43972.t1 - Cep120
g35858.t1 - FAT4
g43082.t1 - Cep120
g4820.t1 - CEP120
g6368.t1 - TRAK1
g70646.t1 - Fat4
g68116.t1 - DCHS1
g62529.t1 - Prdm16
g52913.t1 - Fat4
g69653.t1 - Fat4
g17451.t1 - FAT4
g5950.t1 - DCHS1
g47754.t1 - Wnt2
g2356.t1 - FAT4
g49701.t1 - NAV2
g54779.t1 - Fat4
g36705.t1 - FAT4
g70605.t1 - FAT4
g29235.t1 - FAT4
g23992.t1 - FAT4
g54780.t1 - FAT4
two cells
two cells
two cells
two cells
four cells
four cells
four cells
four cells
eight cells
16 cells
16 cells
16 cell-gastrulation
16 cell-gastrulation
16 cell-gastrulation
16 cell-gastrulation
gastrula
gastrula
neurula
neurula
initial tailbud
initial tailbud
initial tailbud
initial tailbud
¾ wrap
¾ wrap
¾ wrap
¾ wrap
¾ wrap
1-1.5 wrap
1-1.5 wrap
1-1.5 wrap
1.5 wrap
1.5 wrap
1.5 wrap
1.5 wrap
hatching larva
hatching larva
hatching larva
adhesion
adhesion
body axis rotation
body axis rotation
body axis rotation
body axis rotation
oozoid
Time2

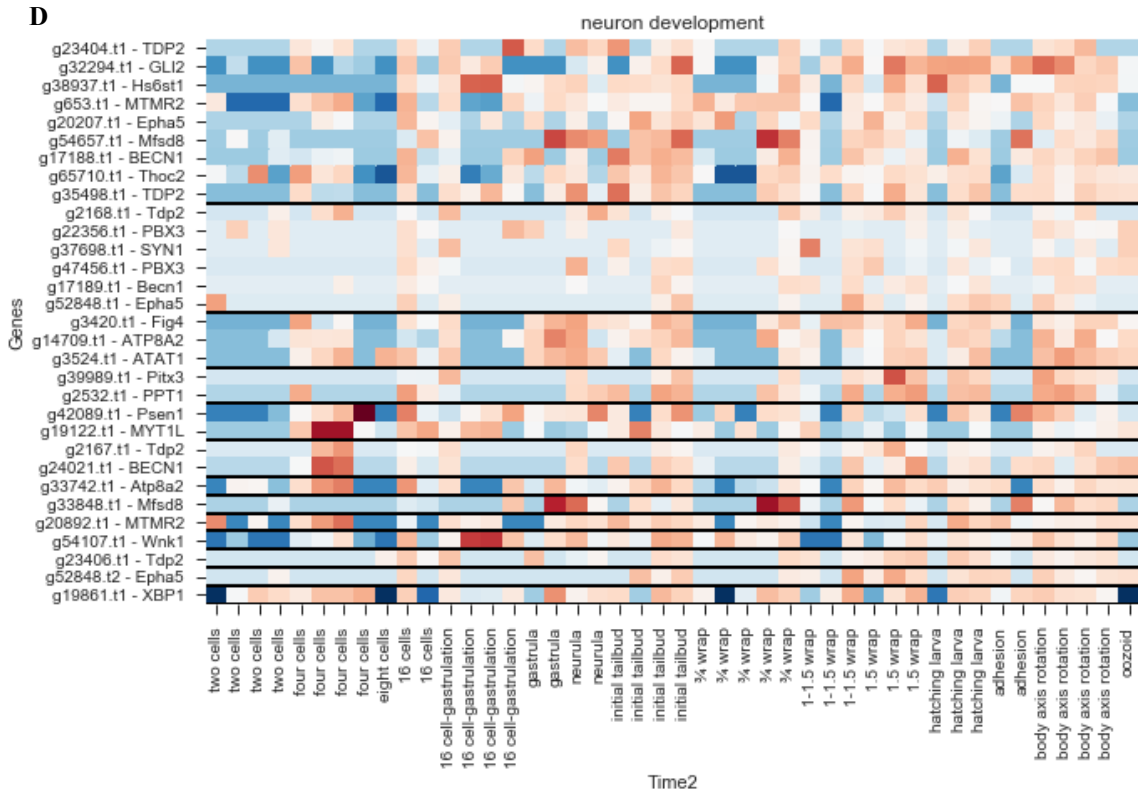

Fig. 11: Enrichment of brain genes during the development of the embryo. **A**. The solid line indicates the proportion of tissue-associated genes that are among those defined as active at each stage. Baseline (0%) is set under the null model of a random subset of genes. Light and dark shaded regions indicate the 50% and 99% confidence intervals under a hypergeometric model. **B-D.** Heatmaps of the expression of genes in the neuron differentiation, neuron development and neurogenesis GO terms with putative homology in *B. schlosseri* grouped by expression pattern. Expression values per gene are scaled to have a mean of zero. Red=high, blue=low.

Nervous system development in bud: morphological events and transcriptome analyses

The neural complex development during blastogenesis has been previously analysed at histological and ultrastructural level (Burighel et al., 1998). Here we confirm that the neural complex rudiment is recognizable in the secondary bud at stage 4 as a thickening of the bud dorsal area (Table 5, Fig. 12). In the following stages, this thickened area develops a tube (stage 5), the dorsal tube, which grows forward and then fuses with the pharyngeal wall (stage 6). During these stages, pioneer nerve cells delaminate from the dorsal tube and ultimately build up the cerebral ganglion. Meanwhile the dorsal tube, which loses its posterior connection with the forming atrial

chamber, differentiates into the neural gland. In adult blastozooids, the neural complex has the same organization of that of oozooids.

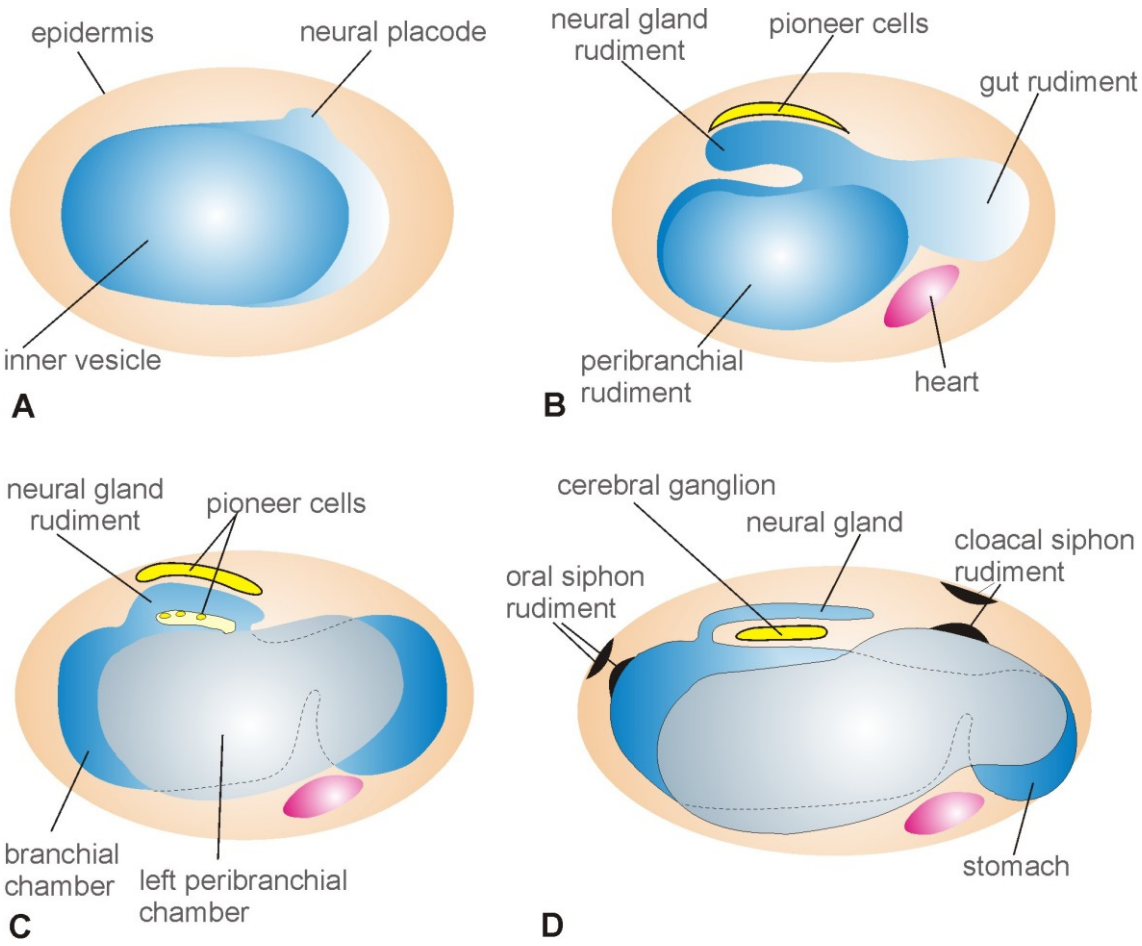

Fig. 12: Scheme of neural complex development during blastogenesis. A-D: lateral views of buds at stages 4-7, respectively. (Modified from Burighel et al., 1998).

1	2	3	4	5	6
			dorsal placode (thickening of the epithelium of the inner vesicle)	dorsoposterior evagination of the inner vesicle in form of blind tube; first delamination of neuroblasts from dorsal tube	tube opened anteriorly; posterior original aperture is closed
7/1	**8/2**	**8/3**	**8/4**	**8/5**	**8/6**
cerebral ganglion recognizable; first motor fibres from the ganglion: first appearance of motor nerves: pericoronal and subendostylar nerves; feeble gut and heart innervation	dorsal organ present; visceral nerve recognizable; transverse interstigmatic nerves present	Cortex and medulla in cerebral ganglion; cilia in ciliated duct of neural gland; nerves in gastric folds; longitudinal interstigmatic nerves present	Extended oral siphon innervation; nerve ring around each stigma	Dorsal organ entirely isolated from neural gland	[1]Nerve number reduction
9/7/1	**9/8/2**	**9/8/3**	**9/8/4**	**9/8/5**	**11/8/6**
Neural complex formed of cerebral ganglion, neural gland, and dorsal organ					Neural complex regression

Table 5: Main events of neural complex development during blastogenesis. ([1] From Zaniolo et al., 2002).

In our study, we selected and collected buds at several blastogenetic stages for the preparation of transcriptomes (Table 6). Secondary buds were isolated when they were enough large to be separated from their primary buds. In some cases, closed stages were grouped. Adult zooids at takeover were collected at the onset of the degenerating phase.

Stage	Zooids
9/7/1	Primary bud and secondary bud
9/8/2 - 9/8/3	Primary bud and secondary bud
9/8/4, 9/8/5	Secondary buds
11/8/6	Secondary buds
9/8/4 - 9/8/5	Primary buds
11/8/6	Primary buds
9/7/1	Adult
9/8/2 - 9/8/3	Adult
9/8/4 - 9/8/5	Adult
11/8/6	Adult in takeover

Table 6: Stages of blastogenesis used to prepare transcriptomes.

In total, we analysed 10 different developmental stages (n=29). Gonads were removed if visible. Libraries were made, sequenced, and the pipeline run identically to the methods described for embryogenesis (see previous paragraph). One difference in identifying the

time-dependent expression of genes in the cycle is that, due to the multigenerational nature of the colony, the best time signature was permitted to include zero, one or two "humps" to allow for cyclically expressed genes. Then, as above, brain associated genes were compared across the cycle (Fig. 13).

A

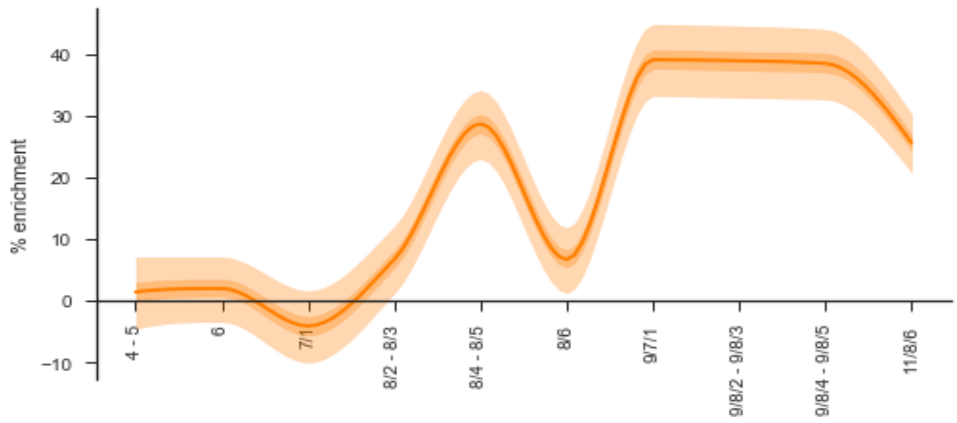

B

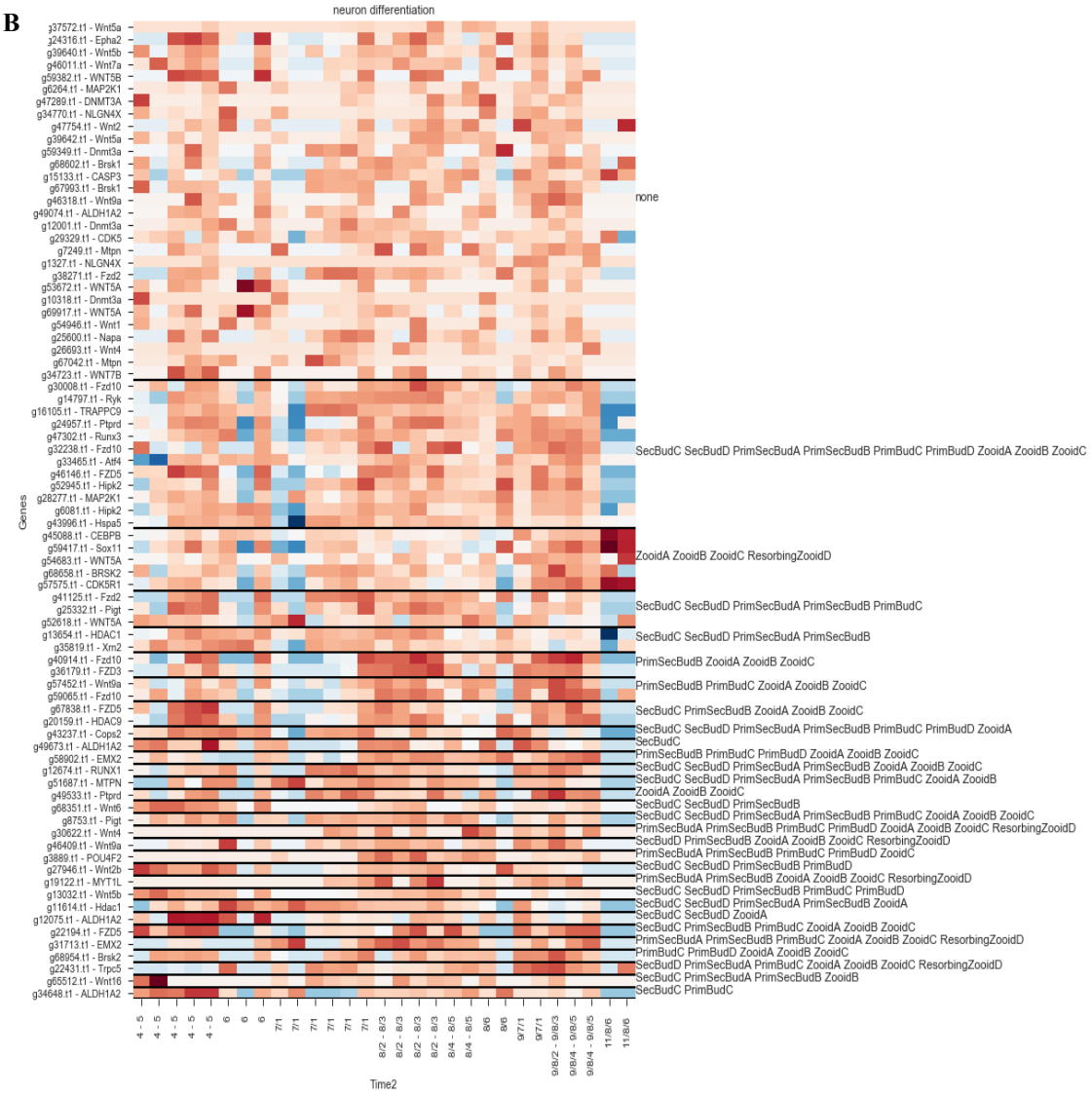
neuron differentiation
Genes
Time2
none
SecBudC SecBudD PrimSecBudA PrimSecBudB PrimBudC PrimBudD ZooidA ZooidB ZooidC
ZooidA ZooidB ZooidC ResorbingZooidD
SecBudC SecBudD PrimSecBudA PrimSecBudB PrimBudC
SecBudC SecBudD PrimSecBudA PrimSecBudB
PrimSecBudB ZooidA ZooidB ZooidC
PrimSecBudB PrimBudC ZooidA ZooidB ZooidC
SecBudC PrimSecBudB ZooidA ZooidB ZooidC
SecBudC SecBudD PrimSecBudA PrimSecBudB PrimBudC PrimBudD ZooidA
SecBudC
PrimSecBudB PrimBudC PrimBudD ZooidA ZooidB ZooidC
SecBudC SecBudD PrimSecBudA PrimSecBudB ZooidA ZooidB ZooidC
SecBudC SecBudD PrimSecBudA PrimSecBudB PrimBudC ZooidA ZooidB
ZooidA ZooidB ZooidC
SecBudC SecBudD PrimSecBudB
SecBudC SecBudD PrimSecBudA PrimSecBudB PrimBudC ZooidA ZooidB ZooidC
PrimSecBudA PrimSecBudB PrimBudC PrimBudD ZooidA ZooidB ZooidC ResorbingZooidD
SecBudD PrimSecBudB ZooidA ZooidB ZooidC ResorbingZooidD
PrimSecBudA PrimSecBudB PrimBudC PrimBudD ZooidC
SecBudC SecBudD PrimSecBudB PrimBudD
PrimSecBudA PrimSecBudB ZooidA ZooidB ZooidC ResorbingZooidD
SecBudC SecBudD PrimSecBudB PrimBudC PrimBudD
SecBudC SecBudD PrimSecBudA PrimSecBudB ZooidA
SecBudC SecBudD ZooidA
SecBudC PrimSecBudB PrimBudC ZooidA ZooidB ZooidC
PrimSecBudA PrimSecBudB PrimBudC ZooidA ZooidB ZooidC ResorbingZooidD
PrimBudC PrimBudD ZooidA ZooidB ZooidC
SecBudD PrimSecBudA PrimBudC ZooidA ZooidB ZooidC ResorbingZooidD
SecBudC PrimSecBudA PrimSecBudB ZooidB
SecBudC PrimBudC

C

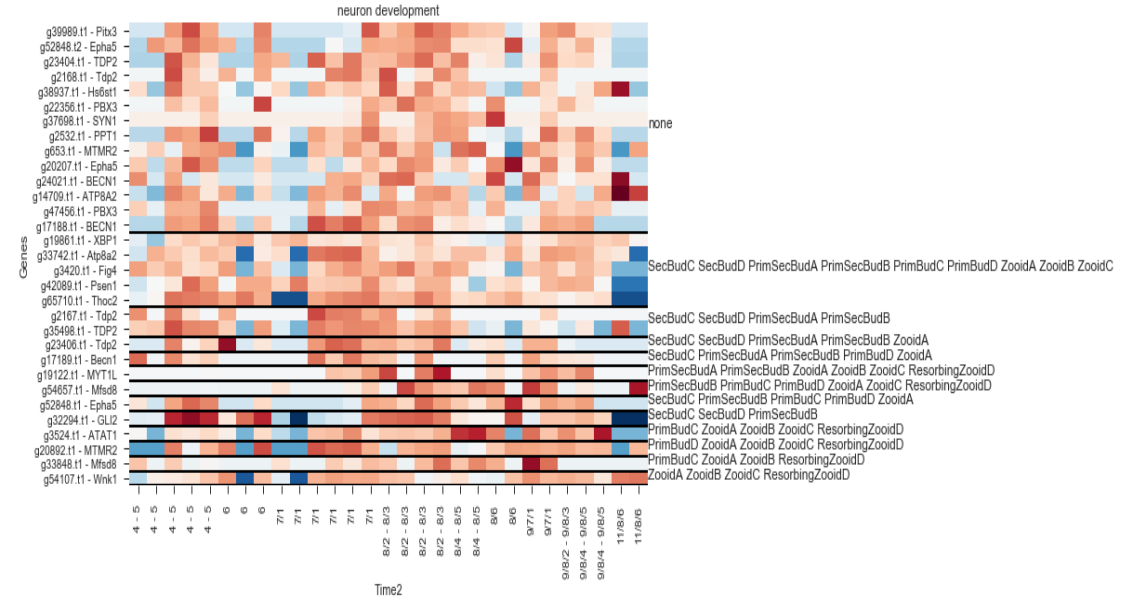
neuron development
Genes
Time2
none
SecBudC SecBudD PrimSecBudA PrimSecBudB PrimBudC PrimBudD ZooidA ZooidB ZooidC
SecBudC SecBudD PrimSecBudA PrimSecBudB
SecBudC SecBudD PrimSecBudA PrimSecBudB ZooidA
SecBudC PrimSecBudA PrimSecBudB PrimBudD ZooidA
PrimSecBudA PrimSecBudB ZooidA ZooidB ZooidC ResorbingZooidD
PrimSecBudB PrimBudC PrimBudD ZooidA ZooidC ResorbingZooidD
SecBudC PrimSecBudB PrimBudC PrimBudD ZooidA
SecBudC SecBudD PrimSecBudB
PrimBudC ZooidA ZooidB ZooidC ResorbingZooidD
PrimBudD ZooidA ZooidB ZooidC ResorbingZooidD
PrimBudC ZooidA ZooidB ResorbingZooidD
ZooidA ZooidB ZooidC ResorbingZooidD

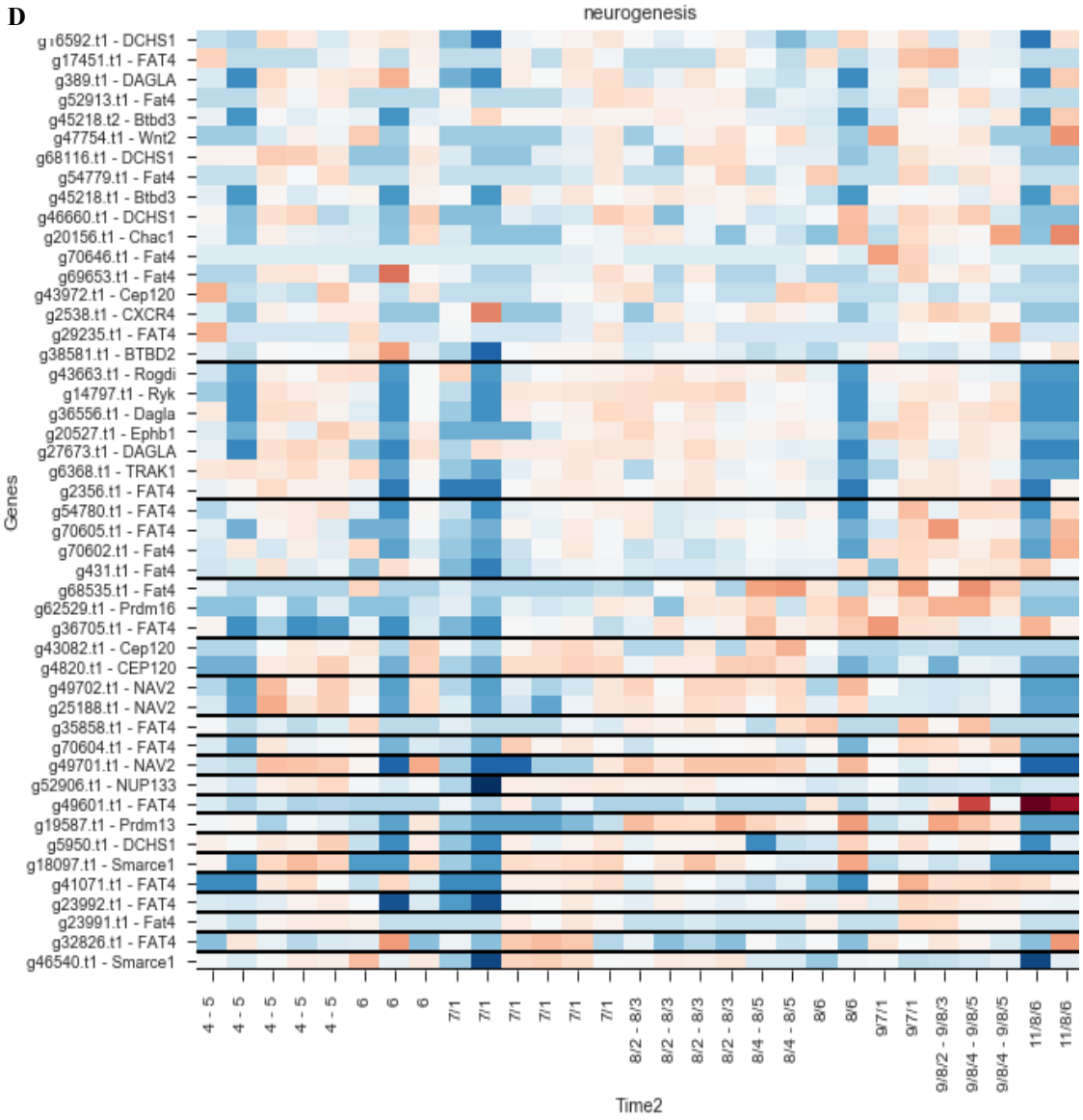

Figure 13: Enrichment of brain genes during blastogenetic development. **A**. The solid line indicates the proportion of tissue-associated genes that are among those defined as active at each stage. Baseline (0%) is set under the null model of a random subset of genes. Light and dark shaded regions indicate the 50% and 99% confidence intervals under a hypergeometric model. **B-D.** Heatmaps of the expression of genes in the neuron differentiation, neuron development and neurogenesis GO terms with putative homology in *B. schlosseri* grouped by expression pattern. Expression values per gene are scaled to have a mean of zero. Red=high, blue=low.

Embryogenesis *vs* blastogenesis: shared and divergent pathways in nervous system development

Our morphogenetic and molecular results allowed us to comparatively analyze the developmental processes occurring in embryos and buds.

From a morphological perspective, the two processes were compared in terms of topology, developmental mechanisms and terminology (Burighel and Manni, 2006; Gasparini et al., 2013). Although the initial stages of the two processes are different, several similarities were identified: the origin from tubular structures (the neurohypophysial duct in the embryo *vs* the dorsal tube in bud), similar anatomical relationships with adjacent organs, the secondary aperture of the tubular structures into the pharynx, the delamination of neuroblasts from their wall, and the common expression of some placodal genes (Pitx, Six1/2, Six3/6, Eya, and FoxI). The neural complex reaches the same final cytological organization in both cases.

Now, we can also directly compare the molecular profiles of NS associated genes during the two development processes. First, to determine whether different times in the cycles cluster together, the correlation of nervous genes active at each time were calculated (Fig. 14). Results indicate three clear stages in the development of the embryo: times prior to 16 cells, times between 16 cells and ¾ wrap, and times 1-15 wrap onwards. In the blastogenetic cycle, the strongest clustering is in the zooids (period 9) before takeover (phase 11/8/6).

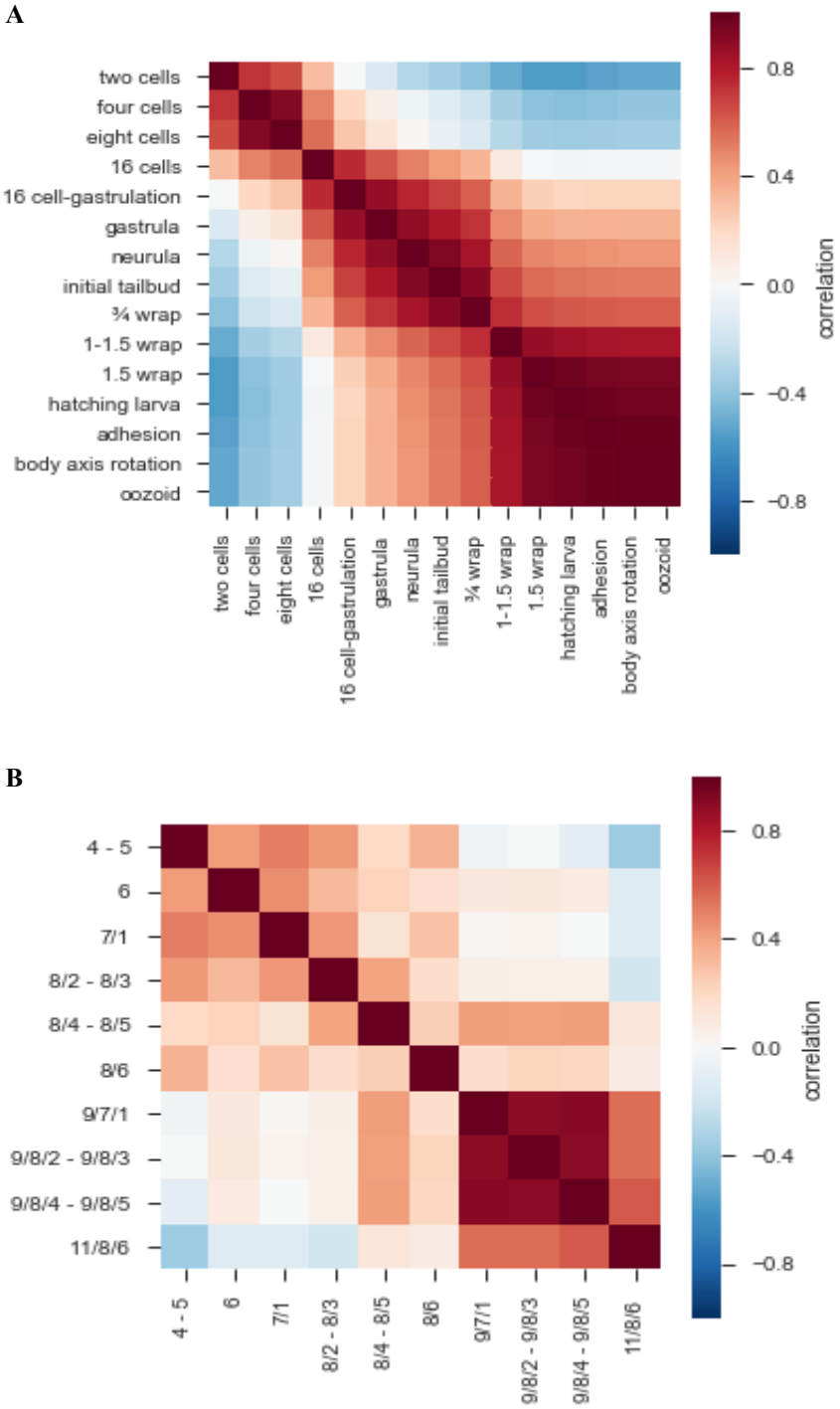

Fig. 14: Correlation of brain genes in the developmental pathways. At each time point, a binary vector of nervous genes active/inactive was correlated with all other times. **A**. Development of the embryo**. B.** Development in the bud.

Next, the two pathways were compared by computing the Jaccard distance (number of shared genes divided by the number of active genes) between times in each pathway (Fig. 15). This shows the strongest similarity is between the post 1-1.5 wrap and the 9th period (zooids). By focusing on genes either co-expressed or exclusively expressed in

one of the pathways, we began to identify different factors that may play a role in the different ways the brain can develop. There were 72 (16 with putative homology) embryo-exclusive brain-associated genes, 62 (17 with putative homology) blastogenetic-exclusive brain-associated genes including the transcription factor *Nr4a1* and the gene *SLC5A7*, associated with motor neurons and the spinal cord in humans. The list of co-expressed genes was the largest, with 129 in total (46 with putative homology), including the following NS associated genes: *Casq2*, *Neb*, *Npc1*, *RIPK3*, *SLC22A16*, *Sned1*, *Nebl*, *Pla2g4a*, *Gstt1, Mdga1* and TNR.

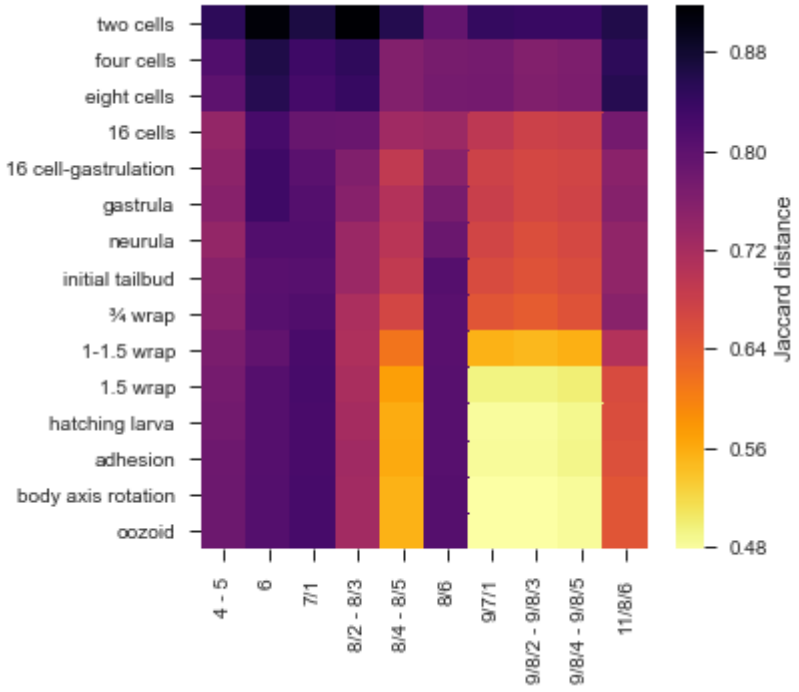

Fig. 15: Heatmap comparing expression of brain genes in embryogenesis (rows) and the blastogenetic cycle (columns).

CONCLUSIONS

In this work, we developed a number of products and techniques for the comparative analyses of the NS in embryogenesis and blastogenesis *of B. schlosseri*:

1. a method for culturing embryos in order to study *in vitro* their development.
2. a first description of the embryonic development and first draft of a timetable, thanks to the analyses of complementary information coming from different technical approaches.
3. first 3D reconstructions of selected developmental stages that give details of the anatomy at great resolution.
4. definition of the temporal relationships between sexual and asexual reproduction.
5. sequenced transcriptomes for several stages of embryogenesis and blastogenesis.
6. the molecular analyses well fit the NS morphogenetic events during both the developmental pathways.
7. the genes belonging to GO categories are associated to the NS and are expressed during both the developmental pathways.
8. comparison among differentially expressed genes in the two developmental pathways finding that some are specific, but most of the other are in common.

We believe these comparative analyses will significantly advance scientific understanding not only of the developmental aspects of tunicates, but also the evolution of the animal phenotype.

MATERIALS AND METHODS

Colonies for histological analysis and 3D reconstructions were collected on piers close to the Hydrobiological Station of the University of Padova (Chioggia, Italy) or during short trips aboard small vessels in the south part of Venetian Lagoon. Colonies can be found attached to various substrata including as hawsers, mollusc shells, aquatic plants (*e.g.*, *Zoostera marina*), and other ascidian species. Once collected, colonies were moved from their natural substratum and adhered to a glass slide according to Sabbadin's technique (1955). Colonies for *in vivo* observations, confocal imaging, and

molecular analysis were collected on piers in the harbor of Monterey (CA, USA), close to the Hopkins Marine Station of Stanford University. Colonies then were placed into an aquarium and tied to a glass slide as described in Rinkevich, 2005.

In vivo observations

For *in vivo* observation of embryo development, parental colonies were gently poked in order to extract their embryos. Embryos at different developmental stages were collected and then placed in Petri dishes containing filtered seawater. Embryos were reared at 23C° and carefully observed during their development using a BZ-9000 Keyence microscope.

Confocal Microscopy

Embryos and buds were fixed for 30 min at room temperature with 4% paraformaldehyde in MOPS buffer (0.1M 3-(N-Morpholino) propane sulfonic acid), adjusted to pH 7.5 and washed in PBT 2 times. Fixed samples were stained for 30 min in 1/1000 diluted cell mask orange for staining cytoplasm. After 3 washes with PBT, Alexa Phalloidin 546 was used for actin staining overnight at 4 C°.
Samples were made transparent by dehydrating them with a series of solutions of 2 – propanol in PBT and then with with BABB (benzyl alcohol (Sigma B-1042)/ benzyl benzoate (Sigma B-6630) 1:2 ratio). In case of nucleus staining, embryos were stained with DAPI (Vector Laboratories) instead of BABB and mounted in Vectashield mounting medium.
Stained samples were observed using confocal laser microscopy (Olympus fv1000) under x10 - x40 oil objective lens. 3D images were reconstructed from stack images (interval 1 to 3 μm) using Imaris software.

Histology

Embryos and buds were fixed for 2 hours in 1.5% glutaraldehyde in sodium cacodylated 0,2M and 1,6% NaCl buffer. After 3 washes in sodium cacodylated 0.2M

and 1.6% NaCl buffer, samples were post-fixed for $1^1/_2$ hour in 1% OsO_4 in cacodylate buffer 0.2M at 4°C.
Samples were dehydrated and then soaked in Epon and propylene solution. Before they were embedded in resin at 37°C, 45°C, 60°C, oriented and sectioned using a Leica ultramicrotome. Sections, 1µm thick, were stained with toluidine blue.

3D Reconstruction

A larva in adhesion, an oozooid and a bud were embedded in resin as previously described and serially transversely cut using a Diatome Histo Jumbo Knife (DITTA). Sections, 1µm thick, were arranged in chains of about 20 sections each and stained with toluidine blue. All the sections were then photographed. Images were aligned using Adobe Photoshop CS on a Windows 7 computer. Based on the resulting stack of images, 3D models of the anatomy of all organ systems were created in Amira 5.3.3 software (Mercury Computer Systems, Berlin).

Transcriptome preparation

We used the protocol described in Voskoboynik et al 2013 to extract RNA from whole colonies. Insulin syringes were used to dissect tissue samples which were flash frozen in liquid nitrogen to minimize RNA degradation and stored at -80 C. Using a mechanized Konte tissue grinder and pestle, samples were homogenized in the presence of lysis buffer (Qiagen RNAeasy Microkit #74004), and total RNA was extracted following the manufacturer's protocol. Resultant RNA was cleaned and concentrated (Zymo Research RNA Clean and Concentrator-5, R1015) and analyzed by an Agilent 2100 Bioanalyzer for quality analysis prior to library preparation. cDNA libraries were then prepared from high quality samples (RIN > 8) using Ovation RNA-seq v2(Nugen). Size selection was performed prior to barcoding using Zymo Research Select-a-Size DNA Clean and Concentrator Kit (D4080); Libraries were barcoded using NEBnext Ultra DNA Library Prep Kit Master for Illumina (New England Biolabs, E7370S) and NEBNext Multiplex Oligos for Illumina(New England Biolabs, E6609S) . Barcoded library samples were then sequenced on an Illumina NextSeq 500 (2x150bp, producing an average of 15 million reads/cell population).

Determination of gene counts was performed using a Snakemake pipeline. An outline of the steps is as follows: i) low quality bases and adapter sequences were removed using Trimmomatic (version 0.32) ii) overlapping paired end reads were merged using FLASH (version 1.2.11) iii) reads were aligned to the UniVec Core database using Bowtie2 (version 2.2.4) to remove biological vector and control sequences, iv) reads were aligned to the *Botryllus schlosseri* transcriptome with BWA ("mem" algorithm, version 0.7.12), v) aligned reads were sorted and indexed using SAMtools, PCR duplicates removed using PICARD ("MarkDuplicates" tool, version 1.128) and then transcript level counts directly counted from the BAM file.

Differential expression was performed using edgeR. In detail: the gene counts were compiled into a tabular format and loaded into R. Genes were retained with at least five counts per million in at least two samples. A simple model was used to compare the two sets of populations, with p-values adjusted using the Benjamini-Hochberg method to produce a false discovery rate (FDR). FDRs less than 0.05 were called as being differentially expressed. For the zooid cycle genes, all sets of contiguous times had samples selected and differentially expressed genes found in the above manner. For each gene, all such comparisons for which significant differences (FDR < 0.05) were collected and the best time signature that explains these DE observations for each gene was found. To further simplify the comparisons, these time signatures were binarized, with 1 indicating "high" expression and 0 indicating "low" or zero expression producing a gene-time expression matrix for each gene along the zooid's development cycle.

Enrichment plots were created by measuring the overlap of a gene set with the binary gene-time expression matrix. The baseline was calculated using a null model that assumed that the N genes of the geneset were taken randomly (without replacement) and using that to determine that expected proportion of "enriched" genes. A hypergeometric model was used to calculate the mean value as well as the 50% and 99% confidence intervals.

REFERENCES

- Brozovic M., Dantec C., Dardaillon J., Dauga D., Faure E., Gineste M., Louis A., , Naville M., Nitta K., Piette J., Reeves W., Scornavacca C., Simion P., Vincentelli R., Bellec M., Ben Aicha S., Fagotto M., Guéroult-Bellone M., Haeussler M., Jacox E., Lowe E., Mendez M., Roberge A., Stolfi A., Yokomori R., Brown T., Cambillau C., Christiaen L., Delsuc F., Douzery E., Dumollard R., Kusakabe T., Nakai K., Nishida H., Satou Y., Swalla B., Veeman M., Volff J. N., Lemaire P. (2018). ANISEED 2017: extending the integrated ascidian database to the

exploration and evolutionary comparison of genome-scale datasets. Nucleic Acids Research Volume 46, Issue D1: D718–D725

- Burighel P., Cloney R.A. (1997). Microscopic anatomy of invertebrates, Vol. 15. Hemichordata, Chaetognatha, and the invertebrate chordates.

- Burighel P., Lane N. J., Zaniolo G., Manni L. (1998). Neurogenic role of the neural gland in the development of the ascidian, *Botryllus schlosseri* (Tunicata, Urochordata). Journal of Comparative Neurology 394(2):230-241

- Chiba S., Sasaki A., Nakayama A., Takamura K., Satoh N. (2004). Development of *Ciona intestinalis juveniles* (through 2nd ascidian stage). Zoological science 21(3):285-298

- Delage Y., Herouard E. 1898. Traite de zoologie concrete, vol 8, Lesprocordes. Paris, Schleicher Freres

- Delsuc F., Philippe H., Tsagkogeorga G., Simion P., Tilak M. K., Turon X., Lopez-Legentil S., Piette J., Lemaire P., Douzery E. J. (2018). A phylogenomic framework and timescale for comparative studies of tunicates. BMC biology 16(1): 39

- Dufour H. D., Chettouh Z., Deyts C., De Rosa R., Goridis C., Joly J. S., Brunet J. F. (2006). Precraniate origin of cranial motoneurons. Proceedings of the National Academy of Sciences 103(23): 8727-8732

- Fujiwara S., Kawamura K. (2003). Acquisition of retinoic acid signaling pathway and innovation of the chordate body plan. Zoological science 20(7): 809-818

- Gasparini F., Degasperi V., Shimeld S. M., Burighel P., Manni, L. (2013). Evolutionary conservation of the placodal transcriptional network during sexual and asexual development in chordates. Developmental Dynamics 242(6):752-766

- Grave C. (1934).The Botryllus type of ascidian larva.

- Grave C., Woodbridge H. (1924). *Botryllus schlosseri* (Pallas): The behavior and morphology of the free swimming larva. Journal of Morphology 39(1):207-247

- Holland L. Z., Holland N. D. (1999). Chordate origins of the vertebrate central nervous system. Current opinion in neurobiology 9(5):596-602

- Horie R., Hazbun A., Chen K., Cao C., Levine M., Horie T. (2018). Shared evolutionary origin of vertebrate neural crest and cranial placodes. Nature 560(7717):228

- Horie T., Shinki R., Ogura Y., Kusakabe T. G., Satoh N., Sasakura, Y. (2011). Ependymal cells of chordate larvae are stem-like cells that form the adult nervous system. Nature 469(7331):52

- Chambon JP.,Soule J., Pomies P., Fort P., Sahuquet A., Alexandre D., Mangeat, B. PH.(2002). Tail regression in *Ciona intestinalis* (Prochordate) involves a Caspase-dependent apoptosis event associated with ERK activation. Development 129(13):3105-3114

- Jeffery W.R. (2007). Chordate ancestry of the neural crest: new insights from ascidians. In Seminars in cell & developmental biology (Vol. 18, No. 4:481-491). Academic Press

- Katz M. J. (1983). Comparative anatomy of the tunicate tadpole, *Ciona intestinalis*. The Biological Bulletin 164(1):1-27

- Kawamura K., Sugino Y., Sunanaga T., Fujiwara S. (2008). Multipotent epithelial cells in the process of regeneration and asexual reproduction in colonial tunicates. Development, growth & differentiation 50(1):1-11

- Köster J., Rahmann S. (2012). Snakemake—a scalable bioinformatics workflow engine. Bioinformatics 28(19):2520-2522

- Kumano G., Nishida H. (2007). Ascidian embryonic development: an emerging model system for the study of cell fate specification in chordates. Developmental dynamics: an official publication of the American Association of Anatomists 236(7):1732-1747

- Lemaire P. (2011). Evolutionary crossroads in developmental biology: the tunicates. Development 138(11):2143-2152

- Lemaire P., Bertrand V., Hudson C. (2002). Early steps in the formation of neural tissue in ascidian embryos. Developmental biology 252(2):151-169

- Manni L., Anselmi C., Cima F., Gasparini F., Voskoboynik A., Martini M., Peronato A., Burighel P., Zaniolo G., Ballarin L. (2018). Sixty years of experim studies on the blastogenesis of the colonial tunicate *Botryllus schlosseri*. Developmental biology. In press

- Manni L., Burighel, P. (2006). Common and divergent pathways in alternative developmental processes of ascidians. BioEssays 28(9):902-912

- Manni L., Pennati R. (2016). Tunicata. Structure and evolution of invertebrate nervous systems. Oxford University Press, Oxford: 699-718

- Manni L., Agnoletto A., Zaniolo G., Burighel P. (2005). Stomodeal and neurohypophysial placodes in *Ciona intestinalis*: insights into the origin of the pituitary gland. Journal of Experimental Zoology Part B: Molecular and Developmental Evolution 304(4):324-339

- Manni L., Gasparini F., Hotta K., Ishizuka K. J., Ricci, L., Tiozzo S., Voskoboynik A., Dauga, D. (2014). Ontology for the asexual development and anatomy of the colonial chordate *Botryllus schlosseri*. PloS one 9(5):e96434

- Manni L., Lane N. J., Joly J. S., Gasparini F., Tiozzo S., Caicci F., Zaniolo G., Burighel, P. (2004). Neurogenic and non neurogenic placodes in ascidians. Journal of Experimental Zoology Part B: Molecular and Developmental Evolution 302(5):483-504.

- Manni L., Lane N. J., Sorrentino M., Zaniolo G., Burighel P. (1999). Mechanism of neurogenesis during the embryonic development of a tunicate. Journal of Comparative Neurology 412(3):527-541

- Manni L., Zaniolo G., Burighel P. (1993). Egg envelope cytodifferentiation in the colonial ascidian *Botryllus schlosseri* (Tunicata). Acta Zoologica 74(2):103-113

- Manni L., Zaniolo G., Cima F., Burighel P., Ballarin L. (2007). Botryllus schlosseri: a model ascidian for the study of asexual reproduction. Developmental dynamics: an official publication of the American Association of Anatomists 236(2):335-352

- Meinertzhagen I.A., Lemaire P., Okamura Y. (2004). The neurobiology of the ascidian tadpole larva: recent developments in an ancient chordate. Annu. Rev. Neurosci.27:453-485

- Milkman R. (1967). Genetic and developmental studies on *Botryllus schlosseri*. The Biological Bulletin 132(2):229-243

- Milkman R., Borgmann M. (1963). External fertilization of *Botryllus schlosseri* eggs. In Biological Bulletin Vol. 125 No. 2: 385

- Nicol D., Meinertzhagen I.A. (1988a). Development of the central nervous system of the larva of the ascidian, *Ciona intestinalis* L: I. The early lineages of the neural plate. Developmental biology 130(2):721-736

- Nicol D., Meinertzhagen I.A. (1988b). Development of the central nervous system of the larva of the ascidian, *Ciona intestinalis* L: II. Neural plate morphogenesis and cell lineages during neurulation. Developmental biology 130(2):737-766

- Nishida H. (2008). Development of the appendicularian *Oikopleura dioica*: culture, genome, and cell lineages. Development, growth & differentiation 50: S239-S256

- Patthey C., Schlosser G., Shimeld S. M. (2014). The evolutionary history of vertebrate cranial placodes–I: cell type evolution. Developmental biology 389(1):82-97

- Pizon A. 1893. Histoire de la blastogenese chez les Botryllides. Ann Sci Natur Zool 14:1–386

- Rigon F., Gasparini F., Shimeld S.M., Candiani S., Manni L. (2018). Developmental signature, synaptic connectivity and neurotransmission are conserved between vertebrate hair cells and tunicate coronal cells. Journal of Comparative Neurology 526(6):957-971

- Rinkevich B. (2005). Conservation of coral reefs through active restoration measures: recent approaches and last decade progress. Environmental Science & Technology 39(12):4333-4342

- Rothbächer U., Bertrand V., Lamy C., Lemaire P. (2007). A combinatorial code of maternal GATA, Ets and β-catenin-TCF transcription factors specifies and patterns the early ascidian ectoderm. *Development* 134(22):4023-4032

- Sabbadin A. (1955). Osservazioni sullo sviluppo, l'accrescimento e la riproduzione di *Botryllus schlosseri* (Pallas), in condizioni di laboratorio. Italian Journal of Zoology 22(2): 243-263

- Sasakura Y., Mita K., Ogura Y., Horie T. (2012). Ascidians as excellent chordate models for studying the development of the nervous system during embryogenesis and metamorphosis. Development, growth & differentiation 54(3):420-437

- Satoh N. (2003). The ascidian tadpole larva: comparative molecular development and genomics. Nature Reviews Genetics 4(4):285

- Schlosser G. (2006). Induction and specification of cranial placodes. Developmental biology 294(2):303-351

- Scott F.M. (1934). Studies on the Later Embryonic Development of Tunicata: *Botryllus Schlosseri* and *Amaroecium Constellatum*. Ph.D. Thesis, Columbia University, New York

- Sorrentino M., Manni L., Lane N. J., Burighel P. (2000). Evolution of cerebral vesicles and their sensory organs in an ascidian larva. Acta Zoologica 81(3): 243-258

- Stach T., Anselmi C. (2015). High-precision morphology: bifocal 4D-microscopy enables the comparison of detailed cell lineages of two chordate species separated for more than 525 million years. BMC biology 13(1): 113

- Voskoboynik A., Weissman I.L. (2015). *Botryllus schlosseri*, an emerging model for the study of aging, stem cells, and mechanisms of regeneration. Invertebrate reproduction & development 59(sup1):33-38

- Voskoboynik A., Simon-Blecher N., Soen Y., Rinkevich B., De Tomaso A. W., Ishizuka K. J., Weissman I. L. (2007). Striving for normality: whole body regeneration through a series of abnormal generations. The FASEB Journal 21(7): 1335-1344

- Voskoskoboynik A., Soen Y., Rinkeivich Y., Rosner A., Uoneo H., Reshef R., Ishizuka K. J., Palmeri K. J., Moiseeva E., Rinkeivich B., Weissman I. L.(2008). Identification of the endostyle as a stem cell niche in a colonial chordate. Cell stem cell 3(4):456-464

- Willey A. (1893). Studies on the Protochordata. Quarterly journal of microscopical science 2(34):317-360

- Zaniolo G., Burighel P., Martinucci G. (1987). Ovulation and placentation in *Botryllus schlosseri* (Ascidiacea): an ultrastructural study. Canadian journal of zoology 65(5):1181-1190

- Zaniolo G., Lane N.J., Burighel P., Manni L. (2002). Development of the motor nervous system in ascidians. Journal of Comparative Neurology 443(2):124-135

- Zaniolo G., Manni L., Burighel P. (1994). Ovulation and embryo-parent relationships in *Botrylloides leachi* (Ascidiacea, Tunicata). Invertebrate reproduction & development 25(3): 215-225

Chapter 3

Cyclical neurogenesis and neurodegeneration in the colonial tunicate *Botryllus schlosseri*

Article in preparation

ABSTRACT

We studied the nervous system of the colonial ascidian *Botryllus schlosseri* during adult life. Ascidians are tunicates, the sister group of vertebrates, and are therefore very useful in elucidating processes occurring in more complex vertebrates. In *B. schlosseri* colonies, three generations of zooids coexist: the adult filter-feeding animals, their buds, and the budlets produced by buds. Every week, in laboratory conditions, adult zooids regress and are resorbed during a phase called takeover. At the same time their buds became the new adults, replacing the regressing parents in filtration. Simultaneously and cyclically, old brains that are in adult individuals are lost as new ones differentiate in buds and budlets. Our study compared several morphological, behavioural and molecular features in adult individuals belonging to different cyclical phases (early-, mid-, late-cycle, and takeover) and to colonies of different ages. We observed that the number of brain cells changes throughout adult zooid life, reaching its maximum in mid-cycle; then the cell number decreases until complete brain reabsorption during the takeover, suggesting that brain degeneration begins during the adult life, when zooids are still active. Transmission electron microscopy (TEM) and TUNEL assays used to examine adult brains showed that apoptosis is involved in neurodegeneration. Moreover, immunocytes contacting or infiltrating the brain increase in number during the adult life. Changes in brain cell number parallel changes in sensory cell number and the zooid's ability to respond to mechanical stimuli. The comparison between adult individuals belonging to young and old colonies showed that the latter are characterized by less brain cells and decrease behavioral responses. We analyzed differentially expressed genes in the brains of individuals belonging to young and old colonies. We found that the old colonies exhibit a pattern of differentially expressed genes associated with neurodegenerative diseases. Of those related to Alzheimer's disease, almost 400 genes expressed in the brain are differentially expressed between young and old colonies. In conclusion, our results indicate that *B. schlosseri* represents a useful model to study adult neurogenesis, neurodegeneration, and the effects of aging.

INTRODUCTION

Loss of brain function and neurodegeneration are common features of aging throughout diverse phyla. Research using model organisms such as the mouse, *Drosophila melanogaster*, *Caenorhabditis elegans* and zebrafish, has dramatically advanced our understanding of these processes over the past 50 years (Lopez-Otin et al., 2013; Reitz and Mayeux 2014; Kumar and Tsao 2018; Masters et al., 2018). Such studies often introduce known causative genetic mutations that are linked with human neurodegenerative diseases into animal models. However, many experiments do not fully recapitulate neuronal loss, supporting the hypothesis that neuronal death is caused by genetic factors combined to cellular and environmental factors.

Observations in some species suggest the existence of compensatory mechanisms protecting neurons from degeneration (Calne et al. 1991, Blesa et al. 2017,). Therefore, comparative studies of neurogenesis, neurodegeneration and aging, at the cellular and molecular level, can help advance our understanding of these complex phenomena. Here we propose to use the colonial tunicate *Botryllus schlosseri* as a model organism to understand basic principles of neurogenesis and neurodegeneration as well as the evolutionarily conserved molecular and cellular mechanisms that regulate them.

Tunicates are the sister group of vertebrates (Delsuc et al., 2006; Delsuc et al., 2018; Kocot et al., 2018), which enables them, from a phylogenetic perspective, to provide a phenotypic and genomic basis for modeling human neurogenesis, neurodegeneration, and aging. A large number of genes that are also involved in human neurodegenerative diseases (Gissi et al., 2006; Franchi et al., 2018; Virata and Zeller, 2010), display a high degree of conservation.

The colonial tunicate *B. schlosseri* is emerging model for the following reason: it is simple to obtain from nature and rearing in laboratory settings; it is easy to observe under a microscope; it can reproduce in captivity both sexually and by asexual budding, it has rapid development, and create genetically identical clones; it has an extraordinary regenerative ability; and it has a peculiar allorecognition system (Voskoboynik and Weissman 2014; Manni et al., 2018). Many modern molecular and cellular tools have been developed in the study of this species and diverse experimental approaches to induce regeneration can be performed (reviewed in Manni et al., 2018). Moreover, a sequenced genome with identified genes that can be selectively knocked-down with

morpholinos and the anatomical and developmental ontology are available (Voskoboynik et al., 2013; Manni et al., 2014).

In *B. schlosseri*, a colony is formed of several blastozooids, *i.e.* zooids derived from asexual reproduction by palleal budding (also called blastogenesis), that are grouped in star-shaped systems (Fig. 1A). In each system there is a central common cloacal siphon, whereas oral siphons open independently at its periphery (Manni et al., 2007). After fertilization, embryos develop into larvae within the parental zooids. The larvae, after a short swimming period, metamorphose into fully functional oozoids (the founders of new colonies) that generate a bud through asexual reproduction, which produces its own budlets. Three blastogenic generations coexist in the colony: the adult zooids, their buds, and the budlets (Fig. 1D). Their development is synchronized within the colony. The adult life lasts one week and can be divided in four main phases: the early-cycle (characterized by zooids which have just opened their siphons for filtering activity), the mid-cycle, the late-cycle, and a change of generation phase of the colon, called takeover (Fig. 1D). During the last phase in which the adult zooids are progressively reabsorbed, all the tissues (nervous system included) degenerate mainly through massive apoptosis. Simultaneously, buds mature into new adults and budlets become buds (Lauzon et al. 2002; Cima et al. 2003). The period between two takeovers represents a blastogenetic cycle, that is repeated throughout the colony life and lasts a week at ~20°C in laboratory conditions (Manni et al., 2018). Circulating immunocytes, including phagocytes and cytotoxic cells, concur to the takeover (Cima et al., 2016). Phagocytes contribute significantly to the clearance of apoptotic cells during the completion of the generation change and throughout the progression of bud development to adulthood (Ballarin et al., 2010; Cima et al., 2010; Voskoboynik et al., 2004). Cytotoxic cells, namely morula cells, are vacuolated cells containing the enzyme phenoloxidase involved in the cytotoxicity observed both *in vitro* and *in vivo* upon their activation (Franchi and Ballarin, 2016).

In *B. schlosseri*, the central nervous system (CNS) consists of a cerebral ganglion (or brain) (Fig 1 E-F). Together with the adjacent neural gland and dorsal organ, it forms the neural complex, which lies between the incurrent (oral) and excurrent (atrial) siphons and amply bathed by hemolymph (Fig 1 C) (Kano, 2010; Deyts et al., 2006; Manni and Pennati, 2016). The cerebral ganglion consists of a fibrous medulla of densely packed neuritis surrounded by a cortical ring of cell bodies. The neural gland,

likely involved in fluid regulation (Deyts et al., 2006; Ruppert, 1990), is dorsal to the cerebral ganglion and opens anteriorly into the branchial chamber through a ciliated duct and a dorsal tubercle (Burighel et al., 1998). The dorsal organ, whose function is unknown, is posterior to the gland. The sensory system is composed of several sensory cells, mostly mechanosensory cells that are spread throughout the body. They are principally located in the oral siphon wall, the region most sensitive to stimulation (Pennati et al., 2015). Sensory cells include both primary sensory cells (peripheral neurons) and secondary sensory cells. The latter are located on the oral tentacles and are considered homologous to vertebrate hair cells (Burighel et al., 2003; Rigon et al., 2018).

Here we show that in *B. schlosseri*, morphological, behavioral and molecular differences characterize the adult life during both the blastogenetic cycle and colony aging. This species, with its cyclical whole body degeneration associated with synchronised asexual reproduction, represents a useful model for understanding the evolutionary basis of human adult neurogenesis, neurodegeneration and aging.

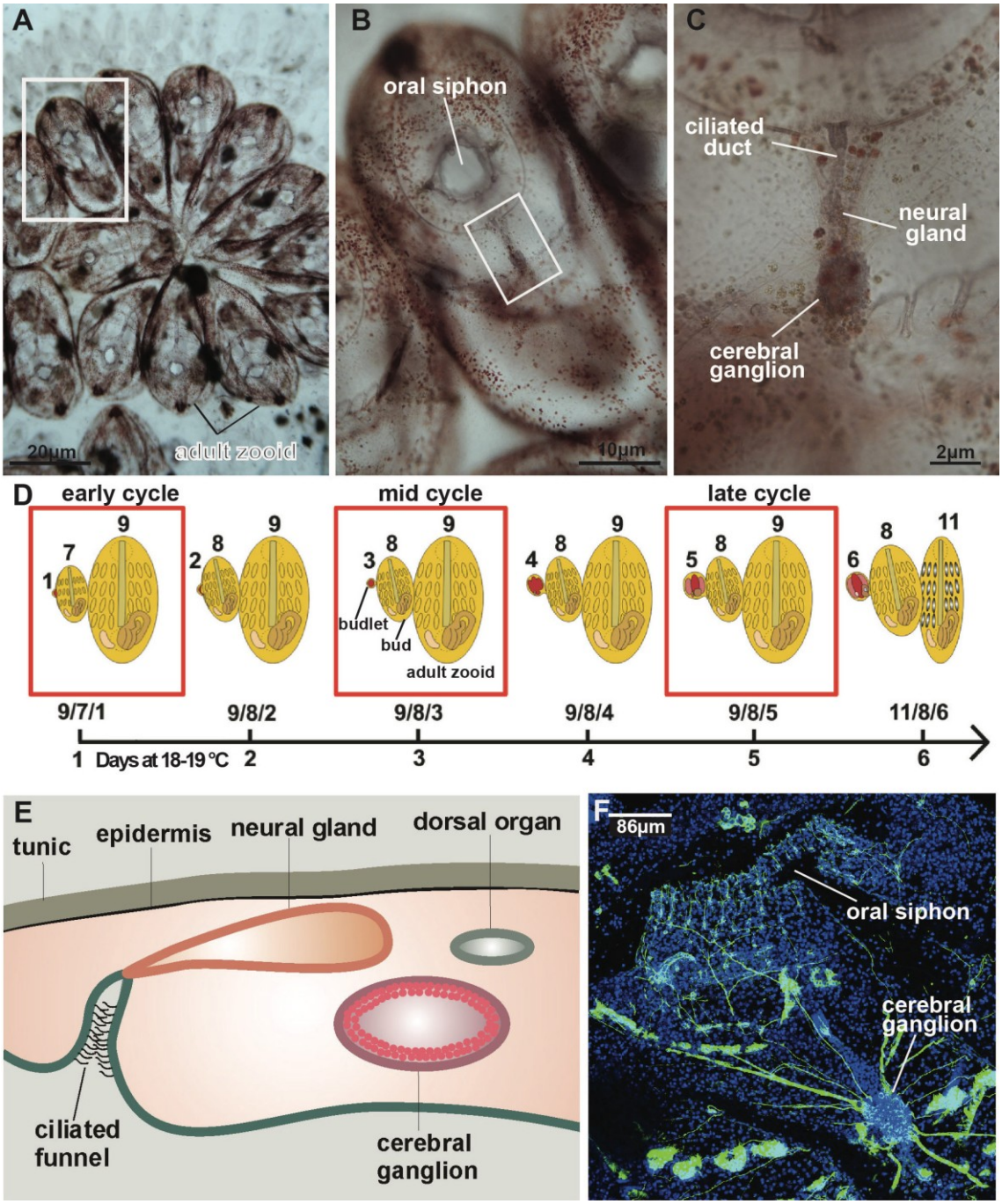

Figure 1: Colony of *B. schlosseri* and its nervous system. **A-C.** Each zooid in a colony has its own nervous system. The neural complex is located between the oral and cloacal siphon. Whole mounted colonies (see material and method section) **D**. The life of an adult lasts 1 week at constant temperature of 20°C and can be divided in three main phases: the early-cycle (9/7/1), the mid-cycle (9/8/3), and the late-cycle (9/8/5). (Modified from Manni et al., 2018). In the colony 3 different generation coexist: the adult, the bud and the budlet. **E**. Schematic representation of the neural complex of *B. schlosseri*. **F.** Whole mount labeling shows cerebral ganglion and peripheral nervous system (anti-alpha tubulin in green and DAPI in blue).

In this work we describe the *B. schlosseri* nervous system during the adult life and in zooids belonging to colonies with different ages from morphological, behavioral and molecular points of view.

RESULTS

NEUROGENESIS AND NEURODEGENERATION DISTINGUISH THE NEURAL COMPLEX DURING THE ADULT LIFE CYCLE

Previously, Burighel et al. (1998) and Manni et al. (1999) described the developmental dynamics of the neural complex during both blastogenesis and embryogenesis. With respect to blastogenesis, the previous studies were limited to the progression of the bud before reaching the adult stage. We here focus our attention on qualitative and quantitative morphodynamical changes of the neural complex during the adult life cycle of the blastozooids.

Neuron numbers evidence a two phases cycle in the adult CNS

In order to quantitatively characterize the CNS of *B. schlosseri* during the zooid's adult life, the number of cells in the ganglion was quantified.
An immunofluorescence approach, employing an anti-alpha tubulin antibody and a nuclear marker (i.e., DAPI), was used in conjunction with confocal microscopy to locate the neurites and the nuclei in the ganglion and to count the number of brain cells in each stage of the zooid adult life cycle. We found that the brain cell number is not stable, but rather follows a trend (Fig. 2 and Supplementary Material 1.1). Adult individuals showed an initial progressive increase in brain cell number (to about 930) until mid-cycle, followed by a progressive decrease before the complete ganglion reabsorption at the end of take-over. Results showed statistically significant differences between subsequent stages (Fig. 2B). These data provide evidence of the presence of two processes that partition adult zooid life: a constitutive adult neurogenesis in the first phases, followed by an outclassing neurodegeneration in later phases. The ability to produce new neurons in ascidians subject to brain extirpation is known in some species (Mackie et al., 2006; Dahlberg et al., 2009; Jeffery, 2015;). However, here we show that

neurogenesis also plays a in absence of traumatic events such as brain removal. In the congeneric species *Botryllus primigenus*, Kawamura and collaborators (2008) showed that adult zooids in early-cycle maintain a proliferative capability in some of their tissues (as pharyngeal inner longitudinal vessel and the posterior of the endostyle). This capability is lost during their life cycle. In *Diplosoma listerianum,* Skold and collaborators showed that the cerebral ganglion of adults have little or no proliferation and indicated that the ganglion is composed of mitotic cells.

Our results also demonstrate that brain degeneration begins during the adult life, when zooids are involved in filtering activity needed for colony survival, and is not limited to the takeover. Neurodegeneration then continues until the complete ganglion reabsorption at takeover, when all adult zooids of the colony are in regression (Ballarin et al., 2010; Cima et al., 2010). These dynamic changes in brain neuron number occur cyclically every week at 20°C, rendering this species a useful study organism to examine the balance between adult neurogenesis and neurodegeneration.

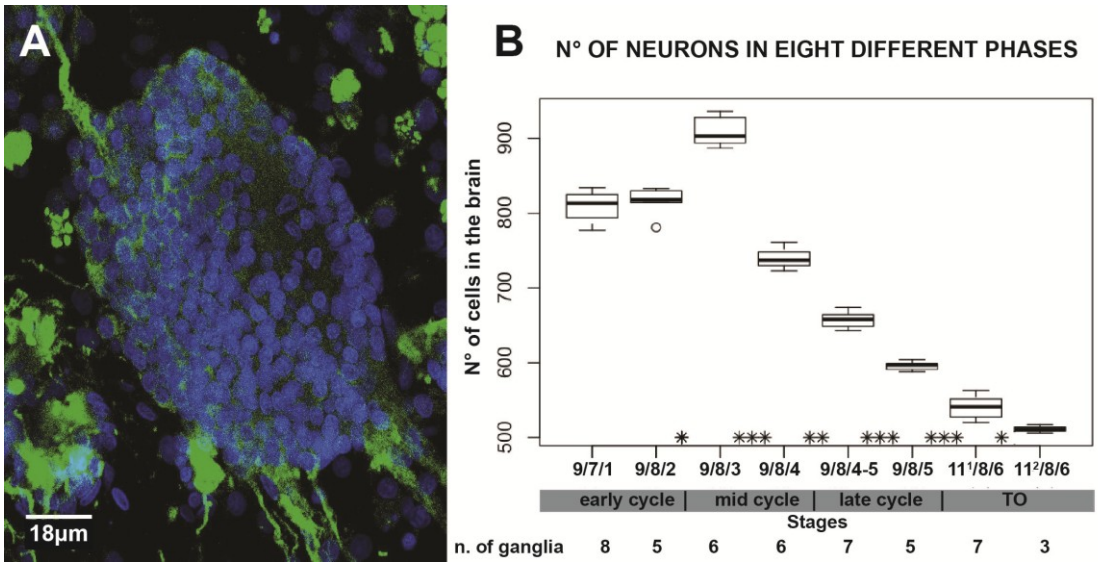

Figure 2. A: cerebral ganglion of *B. schlosseri* labelled with anti-alpha tubulin (green) and DAPI (blue). **B:** number of brain cells present in the adult brain during the blastogenetic stages (early-, mid-, late-cycle, and takeover). n. of ganglia indicates the number of studied samples. P-value < 0.05 (*); p-value < 0.01 (**); p-value < 0.001 (***).

Brain cell cytological features vary during the blastogenetic cycle

The previous results prompted us to use transmission electron microscopy (TEM) to analyze the ultrastructure of the cerebral ganglion in early-, mid-, late-cycle, and takeover in order to investigate if cytological features of brain cells change during the adult life (Fig. 3). Our TEM images of ganglions at early-cycle confirmed previously published data (Zaniolo et al., 2002, Burighel et al., 2001): the brain is composed of an external cortex made by two-three layers of neuronal somata having uniform shape and dimension, and an inner medulla of packed neuritis (Fig. 3A). The comparison among sections of ganglions in early- and late-cycle showed that the number of sectioned brain cells was considerably lower in late-cycle. Moreover, ganglions at late-cycle and takeover (Fig. 3C-D) generally showed a high number of brain cells with irregular shape and polymorphic nuclei with condensed chromatin, all cytological features clearly indicative of degenerative processes. In fact, cells with similar features were described in degenerating tissues of *B. schlosseri* both during takeover and larval metamorphosis, where apoptosis represents the main process of cell death (Shiaffino et al., 1974; Burighel and Schiavinato, 1984). To quantitatively investigate if these cytological features (typical of degenerative processes) change in the adult life cycle, we counted the brain cells with irregular nuclei with respect to the total number of brain cells, finding a significantly higher number of cells with irregular shape in late-cycle as compared to the early-cycle (Fig. 3E-F and Supplementary Material 1.2). Therefore, these TEM observations indicate that an increasing trend of degenerative processes involve brain cells, justifying the decrease in brain cell number described previously.

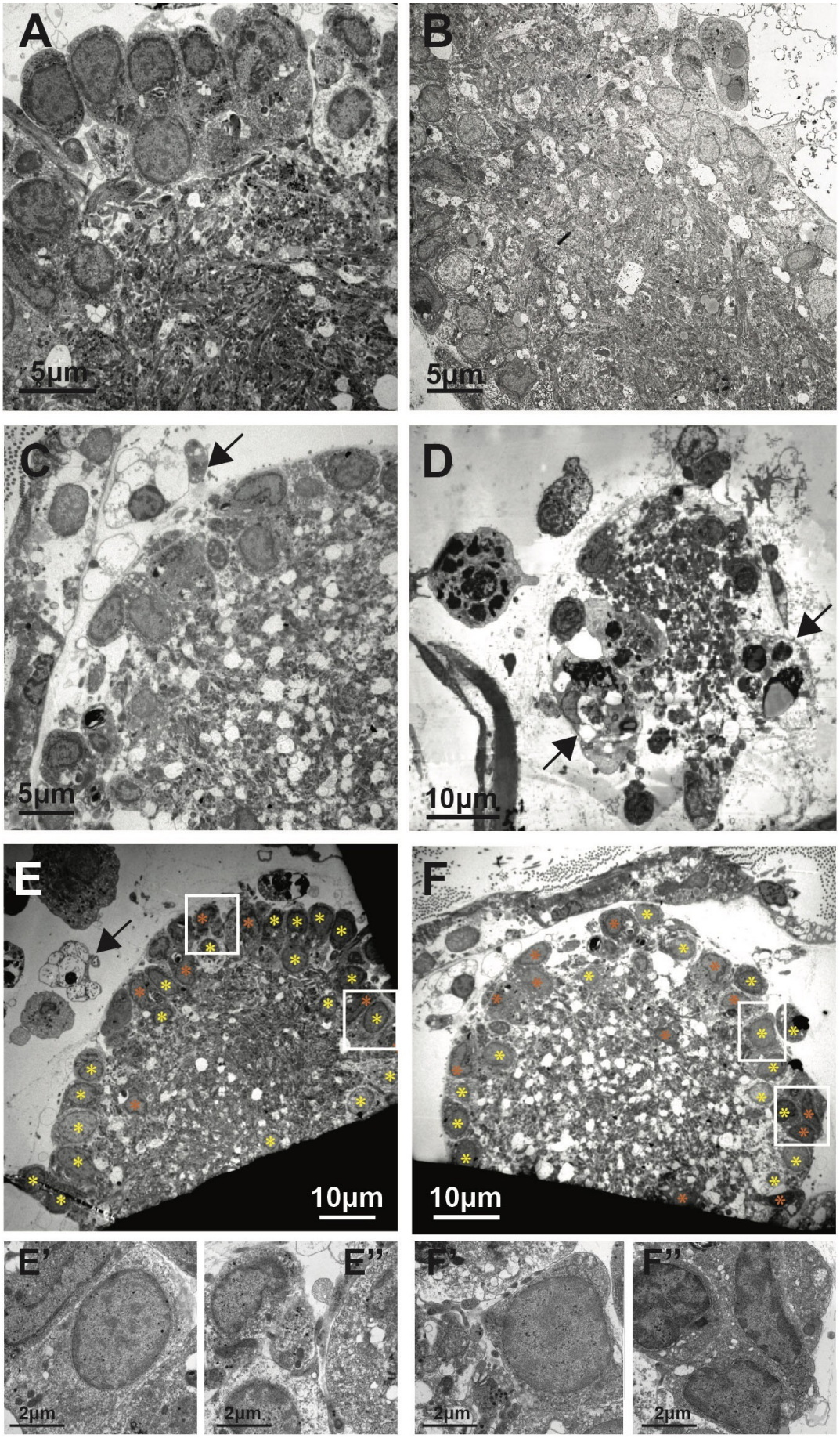
A
5μm
B
5μm
C
5μm
D
10μm
E
10μm
F
10μm
E'
2μm
E''
2μm
F'
2μm
F''
2μm

Figure 3: Cerebral ganglions at TEM of adult zooids in different blastogenetic phases **A.** Early-cycle. **B.** Mid-cycle. **C**. Late-cycle **D.** Takeover. **E-F** Yellow asterisks mark nuclei with regular shape, whereas orange asterisks mark nuclei with irregular shape. E: early-cycle; F: late cycle. The arrowhead indicates: a degranulated (C) and granulated (E) morula cell; phagocyte (D). The squared areas in E and F are enlarged in E',E" and F', F''. Nuclei with regular (**E'-F'**) and irregular (**E''-F''**) shape.

Neural complex components exhibit dynamic relationships during the cycle

We also carefully analyzed the relationship among the neural complex components (cerebral ganglion, neural gland, and dorsal organ) (Fig. 4A-E) during the adult zooid life using histological serial sections and 3D reconstructions. During blastogenesis, brain cells are produced by delamination of pioneer nerve cells from the rudiment of the neural complex in the dorsal tube of the budlet from the late-cycle phase of the colony (Burighel el al., 1998). The budlet's dorsal tube, while differentiating into the neural gland and the dorsal organ, produces nerve cells, which migrate and coalesce to build up the ganglion. The delamination of pioneer nerve cells is also identifiable in the final stages of bud development. We analyzed different though genetically homogeneous zooids belonging to the same colony in five blastogenetic stages (late bud before takeover, adults in early-, mid-, and late-cycle, and in takeover) (Fig. 4F-L). 3D reconstructions showed that the interactions and spatial relationships among the neural gland, dorsal organ and brain change. The three components of the neural complex of the adult zooids in the early-cycle, like the zooids in the previous stage (late bud before takeover), contact one another, resulting in a ganglion connecting both the neural gland and the dorsal organ in a several defined dorsal areas, where some cells and features of undifferentiated cells (large nuclear/cytoplasmic ratio, absence of vesicles or granules in cytoplasm) are recognizable (Fig. 5). The fibrous acellular lamina surrounding the ganglion is in continuity with the neural gland/dorsal organ basal lamina, indicating that they represent a morphological unit. Undifferentiated cells strongly resemble the pioneer nerve cells responsible of brain formation during blastogenesis (Burighel et al., 1998), suggesting that the neural gland and the dorsal organ maintain their neurogenic role during first phases of adult life cycle. The strict relation of the neural gland and dorsal organ with the ganglion changes during the mid-cycle: the organs are no longer in contact and the putative delaminating pioneer cells are no longer recognizable.

During the blastogenetic cycle, the dorsal organ changes shape and size: it is an ovoidal structure, with a simple epithelium in the bud. In comparison in the adult it is infiltrated by immunocytes (mainly morula cells), losing its ovoid shape. In the adult in late-cycle phase the dorsal organ is no longer recognizable. Furthermore, during takeover the spatial arrangement of the neural complex is perturbed, probably on account of the general shrinkage of degenerating zooids (Burighel and Shiavinato, 1984; Ballarin et al., 2010). We also analyzed the relationships between neural complex components in a number of individuals of whole mounted colonies at the same blastogenetic phases, confirming their dynamic relationships during the cycle (Fig. 1A-C). We hypothesize that the neurogenic role of both the neural gland and the dorsal organ is no longer present in mid-cycle and in the following stages. Although we cannot exclude the possibility that circulating stem cells can contribute to adult neurogenesis, as described during oral siphon regeneration in the ascidian genus *Ciona* (Jeffery, 2018), we suggest that both the neural gland and the dorsal organ play a role in increasing the number of brain cells in the first phases of the adult life in *B. schlosseri.*

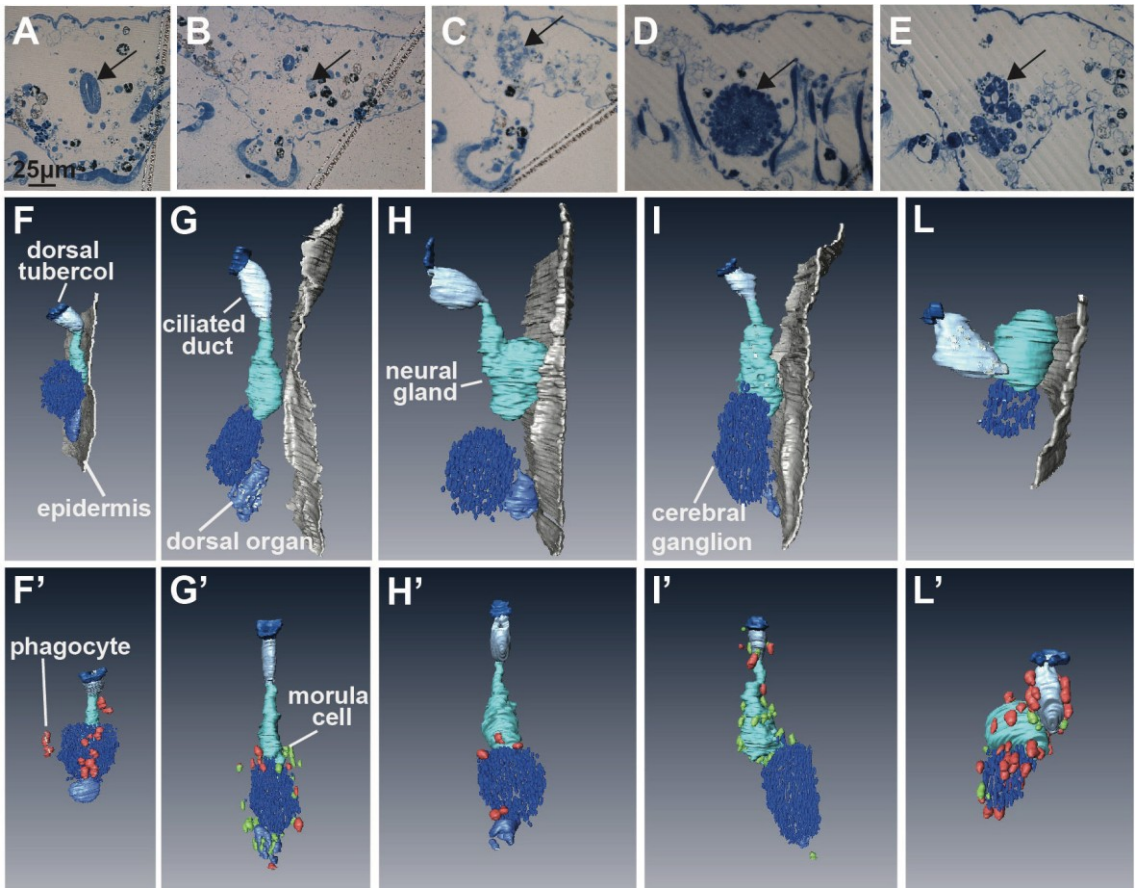

Figure 4: A-E: Transversal sections of an adult zooid in early cycle from anterior (A) to posterior (E). The arrows indicate the different tissue composing the neural complex. A: ciliated duct, B-C: neural gland duct and body, D: cerebral ganglion, E: dorsal organ. Toluidine blue. **F-L**: 3D reconstructions of the neural complex of a late bud (F) and an adult zooid in early-cycle (G), mid-cycle (H), late-cycle (I), and takeover (L). **F'-L':** morula cells (green) and phagocytes (red) contacting and within the ganglion (stages as in F-L). For enlargements of 3D reconstructions, refer to the histological sections in A-E.

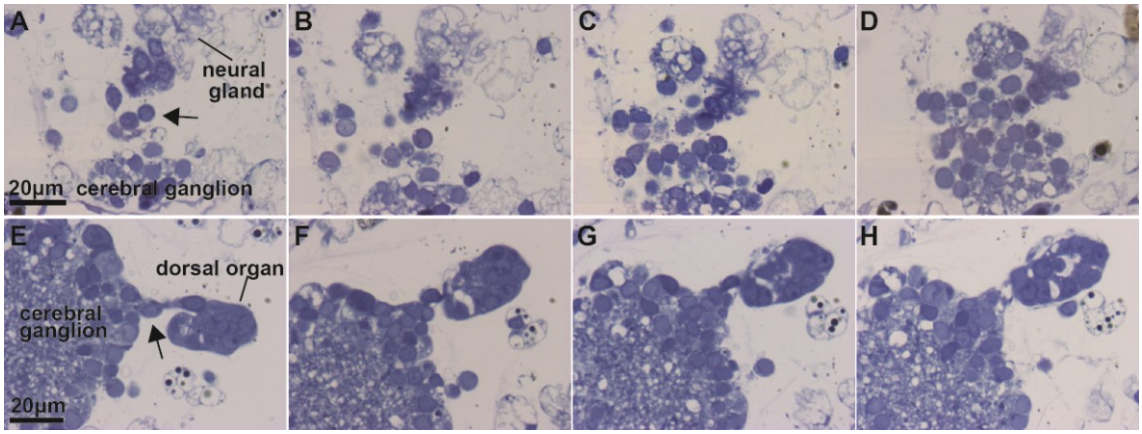

Figure 5: Cross histological serial sections (from anterior to posterior) showing the relationship between the cerebral ganglion and both the neural gland (**A-D**) and the dorsal organ (**E-H**). Some cells (arrows) are in continuity between the ganglion and both the dorsal organ and neural gland. Toluidine blue; the magnification is the same in all the sections.

Molecular signature of neurogenesis and neurodegeneration is present

Two complementary approaches were used to identify molecular signatures of neurogenesis and neurodegeneration. The first compared the expression of *B. schlosseri* brain transcriptome associated transcripts across the blastogenetic cycle; the second used the expression of homologues of neuron development and neuron differentiation associated genes.

Transcriptomes from the brain (n=2, ages of the colonies: 88 and 168 days, respectively) underwent high-throughput sequencing (Illumina Nextseq 500) and were compared to other tissues (testis, n=6, endostyle, n=6) taken from colonies in the early cycle. Genes that were differentially up-regulated (FDR < 0.05) when compared to both the other tissues were selected, n=208 (57 with putative human homologs). These genes were then compared with genes identified as being active at different times in the cycle from whole adult zooids (see methods). Additionally, the expression of genes that possessed some time-dependence were investigated. Most of these genes are not differentially expressed between the different stages, however there is a trend towards diminished expression during takeover. Indeed, 37 brain-associated genes are significantly down-regulated during this stage. This trend can be seen in Fig. 6A which shows a mild and flat enrichment of brain-associated genes until the takeover stage.

In a similar way, genes associated with the GO terms neuron development (GO:0048666) and neuron differentiation (GO:0030182) that had putative homology in

B. schlosseri were selected and their expression was measured at different times (Supplementary Material 2.1). Those that were differentially expressed between any time interval were selected and used to produce a heatmap (Fig. 6B). It should be noted that the vast majority of these genes are expressed in the brain at a level above 5 counts/million in at least one of the brain transcriptomes. The majority of genes are highly expressed at most stages before the takeover, however *Mfsd8* is restricted to the early cycle, and other genes with putative homologies to genes such as *Fzd10* and *XBP1* show trends towards being more highly expressed in the mid- and late- cycle. In humans, *Fzd10* is associated with Alzheimer's disease, cerebral palsy, and neural tube defects. *XBP1* is associated with Alzheimer's disease (Mendiola-Precoma et al., 2016), amyotrophic lateral sclerosis, and myotonic dystrophy (Ikezoe et al., 2007). Thus, higher expression of these genes during the degeneration of the brain (mid-late cycle) would be expected.

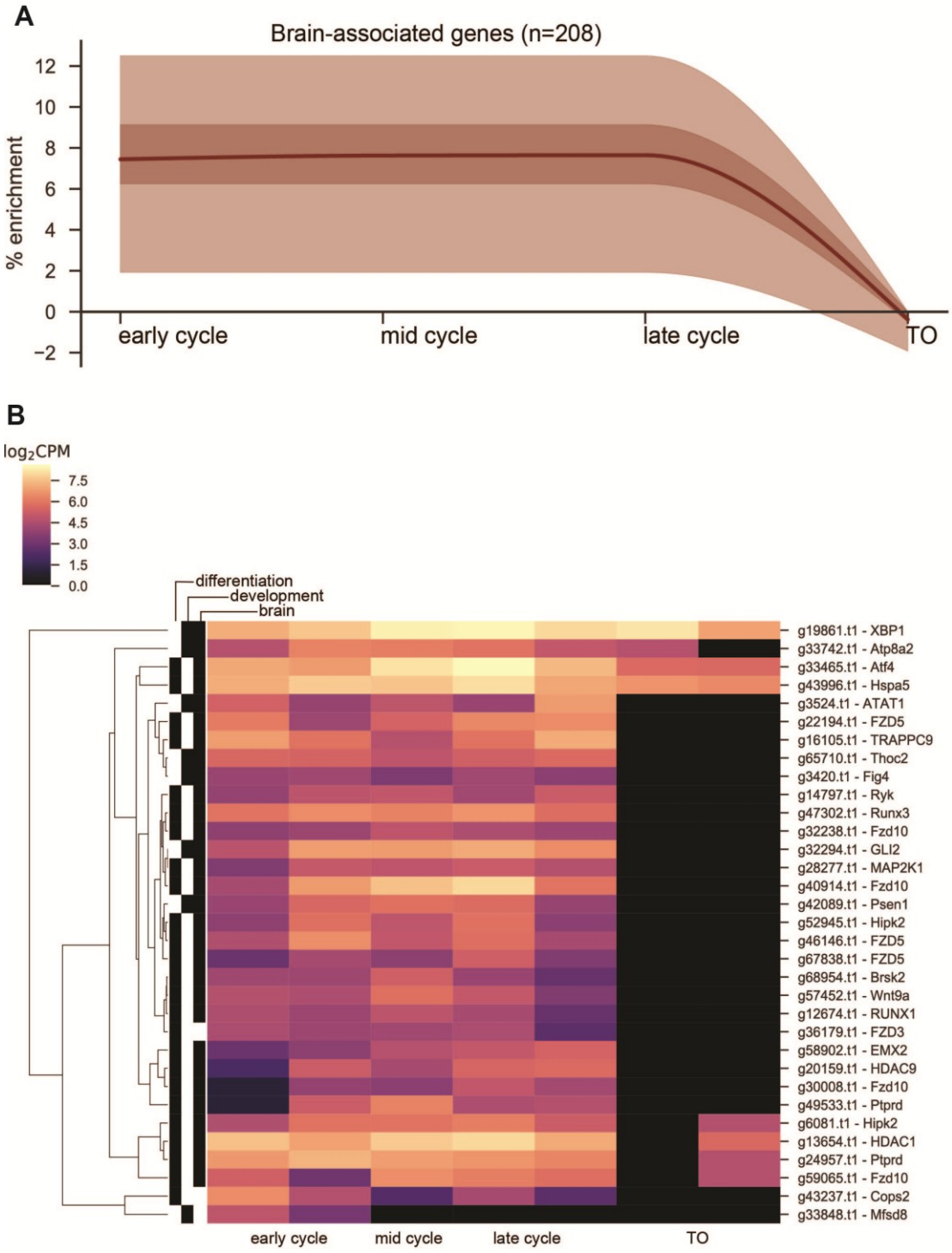

Figure 6: Molecular signatures of neurons. **A**. Enrichment plot showing the increase in proportion of genes active at different times in the blastogenetic cycle. The solid line is the proportion of active selected genes with the expected mean subtracted. Light and dark bands correspond to 50% and 99% confidence intervals, respectively. **B**. Heatmap of neuron differentiation and development associated genes that are differentially expressed throughout the blastogenetic cycle. Black regions on the left indicate whether the gene was in the neuron differentiation or neuron development gene pathway and indicates whether the gene was expressed in the brain transcriptome.

Immunocytes are recruited during neurodegeneration

Our TEM and histological results also revealed that brains during late-cycle and takeover were surrounded and/or infiltrated by a number of haemocytes, namely morula cells and phagocytes (Fig. 3C-E). Both are immunocytes involved in cell removal: morula cells contain, in their granules, molecules with cytotoxic actions against non-self corps. Phagocytes can actively move toward target cells and ingest them (Cima et al., 2010; Ballarin et al., 2010; Corey et al., 2016; Rosental et al., 2018). We quantified phagocytes by confocal microscopy in three colonial phases of different colonies (early-, mid- and late-cycle; n=8, n=10 and n=10, respectively), labeling them with an anti-RBL antibody, a rhamnose binding lectin specifically present on phagocyte cell membrane (Ballarin et al., 2010). Morula cells were identified according to the autofluorescence of their vacuoles. We counted the immunocytes both contacting and within the CNS, analyzing the data in aggregate (contacting and within the CNS) and separately (only contacting or only within the CNS). We found that the number of immunocytes significantly increased from early- to mid-cycle and from mid- to late-cycle in each analysis (Supplementary Material 1.3). The different function of the two immunocyte types prompted us to investigate which one the increase could be ascribed to. Our analyses indicated that each type had an increasing in number between early- and late-cycles. Yet intriguingly, while phagocytes were found permanently absent in the mid-cycle and significantly increased from the mid- to the late-cycle, morular cells increased continuously and significantly between subsequent colonial phases, with a larger significance between early- and mid-cycle. Previous work (Rosental et al., 2018) studying the hematopoietic system of *B. schlosseri* has identified a population of cytotoxic morula cells and determined a gene expression signature for them. The activity of these genes, differentially expressed in whole adult zooids during the blastogenetic cycle, is presented in Figure 7. Although the strongest contrast is between the takeover and the other stages, the majority of genes express at a somewhat higher level in the mid- or late- cycle as compared to the early cycle. This supports the idea that the increased cytotoxic activity of morula cells occurs later in the cycle.

TEM observations showed that both intact and degranulated morula cells were close to ganglions (previous Fig. 3C-D), suggesting that morula cells can release cytotoxic molecules inducing brain cell degeneration. TEM showed phagocytes containing neuron

debris in their phagocytic vacuoles (Fig. 3D), suggesting they are involved in brain cell removal.

We hypothesize that an interaction between morula cells and phagocytes is associated with neuron decrease during the last stages of zooid life. In *B. schlosseri*, such interatctions have been described in inflammatory reactions (Franchi and Ballarin, 2017). Through analyses of 3D reconstructions in adult clonal individuals at different stages, we also noted that the distribution of morula cells and phagocytes changes around the neural complex (Fig. 4A'-E'). In particular, we segmented both the morula cells and the phagocytes in direct contact with cells of the neural complex or within its components. We saw that, in early-cycle, phagocytes are mainly concentrated around and within the cerebral ganglion and the dorsal organ, whereas they are placed around neural gland in late-cycle. The entire neural complex is then contacted and infiltrated by immunocytes at takeover. These results are indicative of the dynamic role of morula cells and phagocytes and suggest that mechanisms resembling inflammation can be involved during the programmed neurodegeneration of *B. schlosseri*.

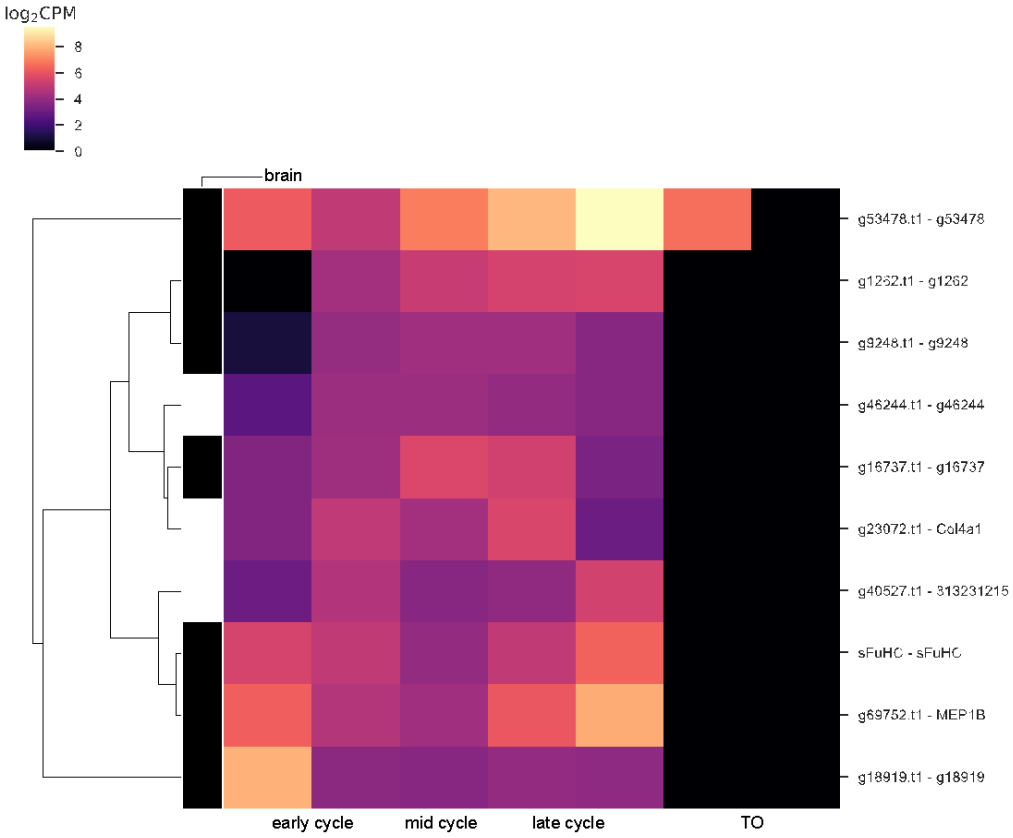

Figure 7: Heatmap of morula cell associated genes

Apoptosis is involved in the neurons' death

Brain cell degenerative features identified by TEM compelled to us to verify if apoptosis involves brain cells during the filter-feeding life of adult individuals. At takeover it represents the main mechanism of cell death (Ballarin et al., 2008; Cima et al., 2010). We tested 10 colonies (3 in early-cycle, 3 in mid-cycle, and 4 in last-cycle) for TUNEL reaction, where surprisingly few nuclei were found labeled in cerebral ganglions (Fig. 8). Statistical analysis was used to investigate whether significant differences were present in the percentage of apoptotic cells among each blastogenetic stage. The results from ANOVA and post-hoc tests indicated no significant difference among stages (Fig. 8B and Supplementary Material 1.4). Although we cannot exclude the existence of other mechanisms of brain cell death, such as necrosis, our data revealed that apoptosis plays a role in brain cell death during the entire blastogenetic cycle, not only during the takeover. Previous data on apoptosis in *B. schlosseri*, while representing a detailed account of apoptotic events during blastogenesis, failed to recognize apoptosis in adult individuals (Tiozzo et al., 2006). However, it is important to note that dying cells are rapidly cleared by circulating phagocytes (Ballarin at al., 2010), rendering apoptosis recognition difficult when few cells are involved. Considering that apoptosis in brain is present throughout adult life, a balance between this mechanism of cell death and neurogenesis occurring before the mid-cycle could be responsible for the specific trend in brain cell number above described. Once neurogenesis stops or strongly decreases at mid-cycle, the continuous effects of apoptosis would lead to the brain cell reduction.

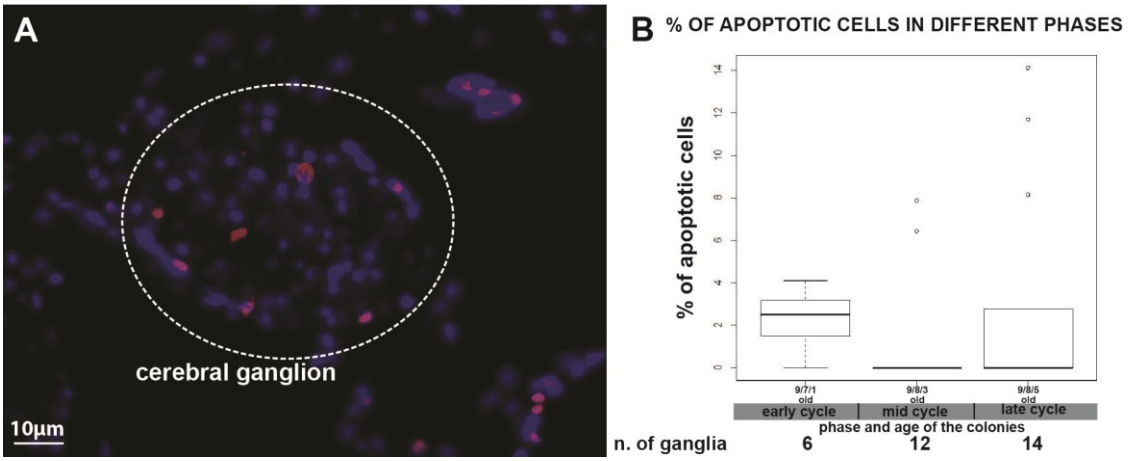

Figure 8: Apoptosis in cerebral ganglion. **A**: Histological section of an adult ganglion (dotted line) treated with Tunel Assay in late-cycle. Note a few apoptotic cells marked in red; blue: nuclei labelled with DAPI. **B**: Percentage of apoptotic cells in ganglion during early-, mid-, and late-cycle. P-value < 0.05 (*); p-value < 0.01 (**); p-value < 0.001 (***). The colonies were 6 months old.

Adult zooid behavioral performances change during the cycle

In order to investigate if the number of brain neurons is related to differential animal behavioral performance, we assessed the response of adult individuals to mechanical stimulations involving two different sensory and effector systems (Fig. 9). In the first experiment, we used a siphon stimulation test (SST) to examine the behavioral response of adult zooids to seawater flow jets directed towards the oral siphon (Fig. 9E). The oral siphon is rich in epidermal receptors, that are primary sensory cells (*i.e.*, peripheral neurons) located around the oral siphon (Mackie et al., 2006). They have been described in some solitary ascidians as single or paired neurons, located in the epidermis lining both the inner and the outer siphon wall. They possess a cilium extending in the tunic covering the epidermis, and an axon directed to the cerebral ganglion (Fig. 9D-10E). They are sensitive to vibrations and, once stimulated, they evoke the contraction of the oral siphon sphincter muscle, leading to siphon closure (Fig. 9E). In our experiments we tested a number of zooids belonging to different colonies (Table 1-2), stimulating them with seawater jets of increasing pressure, and recording the minimum pressure needed to evoke the oral siphon contraction in order to estimate animal sensitivity. We found that during the blastogenetic cycle zooids were sensitive to different pressure values (Fig. 9G and Supplementary Material 1.5). Individuals in mid-cycle were more sensitive than individuals in ealy and late phases, and that zooids in late-cycle were less sensitive than those in early-cycle.

A similar test (the tentacle stimulation test (TST)) was applied by directing jets of seawater towards the tentacles where the mechanoreceptors of the coronal organ are located (Fig. 9B-C). In contrast with the oral siphon epidermal receptors, coronal cells are secondary sensory cells, *i.e.* dedicated receptors without axons, contacted at their base by neuritis coming from the brain (Burighel et al., 2011) (Fig. 9D). These cells are considered homologous to vertebrate hair cells (Rigon et al., 2018; Manni et al., 2018). Their stimulation evokes the contraction of the atrial siphon (Mackie et al., 2006) (Fig. 9F). When stimulated, they elicit the squirting reaction (the contraction of both body

and atrial siphon muscle) and the ciliary arrest (Mackie et al., 2006). These responses cause the expulsion of seawater from the oral siphon (Fig. 9F). The aim of the TST was to obtain data on the minimum pressure value to which zooids responded by contracting their atrial siphon. Results showed significant differences among the blastogenetic phases (Fig 9H and Supplementary Material 1.6.1). Individuals in mid-cycle were more sensitive compared with the one in early and mid phase.

Therefore, both the SST and TST showed a cyclical performance of individuals during the blastogenetic cycle, suggesting a possible correlation between behavioral responses and the number of neurons in the brain. In particular, results indicated a relationship between the increase of neurons and responsiveness before the mid-cycle, and also their decrease after the mid-cycle.

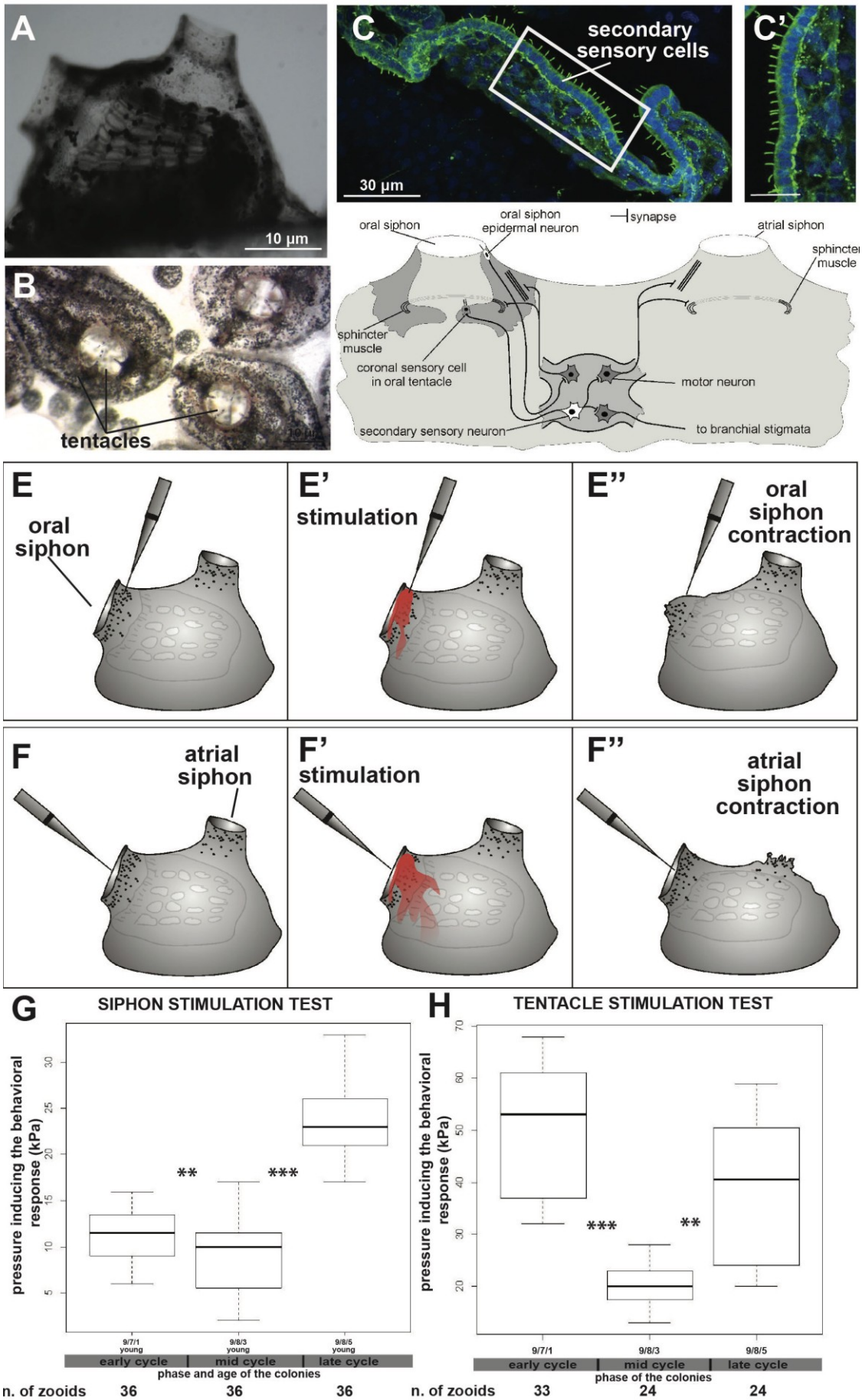
A
10 µm
B
tentacles
C
secondary sensory cells
30 µm
C'
oral siphon
oral siphon epidermal neuron
synapse
atrial siphon
sphincter muscle
sphincter muscle
coronal sensory cell in oral tentacle
motor neuron
secondary sensory neuron
to branchial stigmata
E
oral siphon
E'
stimulation
E''
oral siphon contraction
F
atrial siphon
F'
stimulation
F''
atrial siphon contraction
G
SIPHON STIMULATION TEST
pressure inducing the behavioral response (kPa)
**
***
9/7/1 young
9/8/3 young
9/8/5 young
early cycle
mid cycle
late cycle
phase and age of the colonies
n. of zooids 36 36 36
H
TENTACLE STIMULATION TEST
pressure inducing the behavioral response (kPa)
***
**
9/7/1
9/8/3
9/8/5
early cycle
mid cycle
late cycle
phase of the colonies
n. of zooids 33 24 24

Figure 9: A: Lateral view of a young zooid where the oral and atrial siphons are clearly visible. **B**: in vivo pictures of zooids with open oral siphons where tentacles are identifiable. **C**: tentacle at confocal microscope labelled with anti alpha tubulin (green) and DAPI (blue). The squared area in C is enlarged in C'. C': row of secondary sensory cells located along the tentacle provided by a kinocilium. **D**: schematic circuit diagram showing the general pathway of the innervation. **E-F:** experimental design of siphon stimulation test (SST) (E) and tentacle stimulation test (TST) (F). In red, jet of seawater used to stimulate the oral siphon epidermal receptors (E) and coronal organ (F). **G**: statistical analysis of STS performed on zooid during the three main phases of adult age. 3 weeks old. **H**: statistical analysis of TTS performed in zooid during the three main phases of adult age. The tested zooids belong to colonies with different ages.

Neurodegeneration involves also sensory cells

After considering the behavioral results reported above, we decided to investigate if the differences in zooid performance could also be related to the degeneration of sensory cells during the blastogenetic cycle. We marked the samples with anti-alpha tubulin and Hoechst (Fig. 10A-B), and we counted the number of oral siphon epidermal receptors around the internal oral siphon layer, in 15µm deep z-stacks starting from siphon apex. We analyzed 6 samples for each phase (early-, mid-, and late-cycle) and found that the number of oral siphon epidermal receptors was not constant. They tripled in number from early- to mid-cycle before decreasing in late-cycle. Statistical analyses indicate significant differences among stages (Fig. 10C and Supplementary Material 1.7.1). The resulting trend was similar to that of brain cells: the largest number of primary sensory cells was measured in mid-cycle. This is in agreement with the SST: when the number of primary sensory cells was higher zooids reacted to more moderate stimuli. We conclude that decreases in zooid behavioral performances can be related to the decrease of both neuron and sensory cells during adult life.

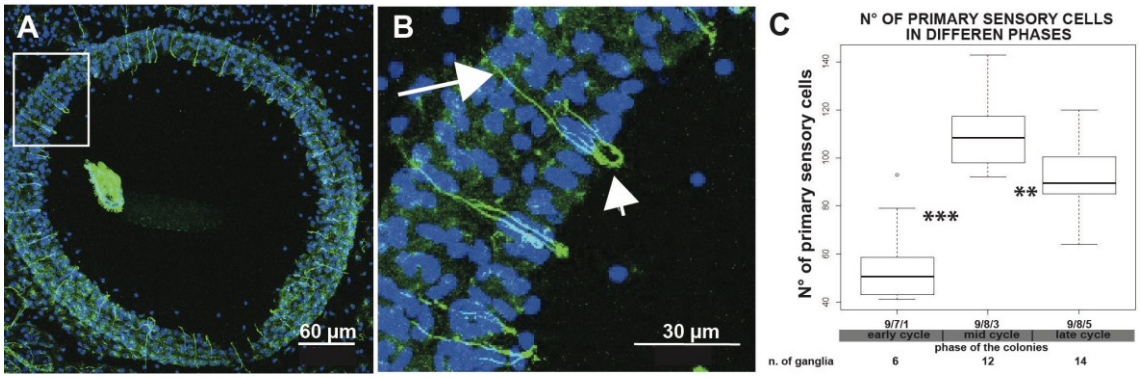

Figure 10: oral siphon epidermal receptors. **A**: Dorsal view of the oral siphon belonging to an adult individual stained with anti-alpha tubulin (green) and Hoechst (blue). The squared area in A is enlarged in B. **B**: Note some receptor cells provided of both a cilium (arrowheads) and axon (arrows). **C**: Number of receptors in adult individuals during the blastogenetic cycle. P-value < 0.05 (*); p-value < 0.01 (**); p-value < 0.001 (***). Tested zooids belonged to colonies of different ages.

Although we do not know why animals exhibit this trend during the blastogenetic cycle, we can hypothesize that it is related to spawning. Adult individuals are involved in continuous filtering activity during their life. When they open their siphon, mature eggs are ovulated in the peribranchial chamber and fertilized by sperm coming from other colonies (Manni et al., 2007). Embryos develop within the chamber and, before takeover, larvae leave the colony passing through the atrial siphon. There is no documented parental nutritional contribution to embryo development (Zaniolo et al., 1987). Sperm release occurs in mid-cycle. Apparently, this is the last physiological event occurring in adult zooids. We can postulate that, after sperm release, zooids have concluded their role, neurogenesis stops, and they undergo a slow degeneration while embryos conclude their development. Thus, the atrial siphon closure, which marks the beginning of takeover, would represent an intermediate step of a longer degenerative phase that begins after sperm release.

AGING INFLUENCES BOTH NERVOUS SYSTEM MORPHOLOGY AND BEHAVIOUR

In *B. schlosseri*, the life of an adult zooid (from the aperture of its siphons to its resorption) lasts one week in laboratory condition at ~20°C; however, the life of a colony spans many months and often years (Cima et al., 2015). To determine if colony

age can influence both zooid nervous system and behaviour, we compared some parameters in young colonies (3 weeks old) and old colonies (6 months old).

Adult zooids of young colonies possess more brain cells than those of old colonies

Using the method described above, we counted the number of brain cells in adult zooids in early-, mid-, and late-cycle belonging to colonies of different ages (Table 3) (Fig. 11 and Supplementary Material 1.8). This data indicated differences in brain cell number among the different phases, with similar trends in colonies of different ages (Fig. 11A). In young zooids in early-cycle the brain cells number resulted between 650 and 700. In mid-cycle, the number was higher, between 950 and 1050. Finally, in late-cycle, the number decreased, resulting between 860 and 960. In old colonies, the number of brain cells was significantly lower in all the three phases with respect to the young colonies (Fig. 11A). When comparing the number of neurons in young and old adults, independent from the phase of the colonies, our analysis indicated a significantly lower number of neurons in older zooids (fig. 11B).

Intriguingly, the brain cell number of zooids in late-cycle in young colonies was not statistically different to the maximum number of brain cells that adults reached in old colonies, in the mid-cycle. On the other hand, in young colonies the early-cycle had adult zooids with a significantly lower brain cell number in comparison with the other two phases. This indicates that buds in young colonies reached the adult early-cycle strongly far away from the potential maximum brain cell number. Altogether, taking into consideration that neuron cell death continuously occurs during the adult life cycle, and hypothesizing that neurogenesis stops (or strongly decreases) after mid-cycle, the data suggest that adults of young and old colonies have a different balance of neurogenesis/neurodegeneration.

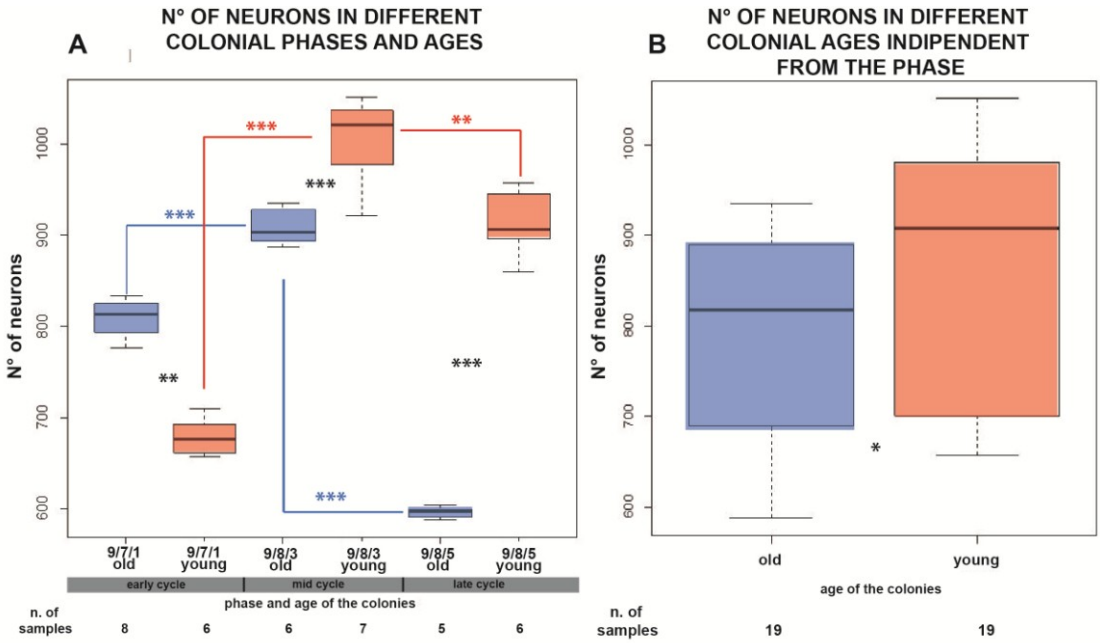

Figure 11: A. Number of brain cells in zooids in early-, mid-, and late cycle, in young (red) and old (blue) colonies. **B.** Number of brain cells in zooids belonging to old and young colonies. The blue asterisks indicate significant differences between groups of old colonies. The red asterisks indicate significant differences between young colonies. The black asterisks indicate significant differences between groups with different ages. P-value < 0.05 (*); p-value < 0.01 (**); p-value < 0.001 (***).

Zooids of young colonies have more sensory receptors than those of old colonies

We also compared the number of oral siphon epidermal receptors of adult individuals belonging to the three phases in both young and old colonies. In young colonies, our analysis showed significant differences between early- and mid-cycle (Fig. 12 and Supplementary Material 1.7.2-3). In old colonies, significant differences were evident among the three phases (early-cycle *vs* mid-cycle, mid-cycle *vs* late-cycle, and early-cycle *vs* late-cycle). Moreover, only for zooids belonging to the late-cycle was there a significant difference between the young and old colonies. As such, aging influences the number of these sensory cells at the end of the blastogenetic cycle if not before or after.

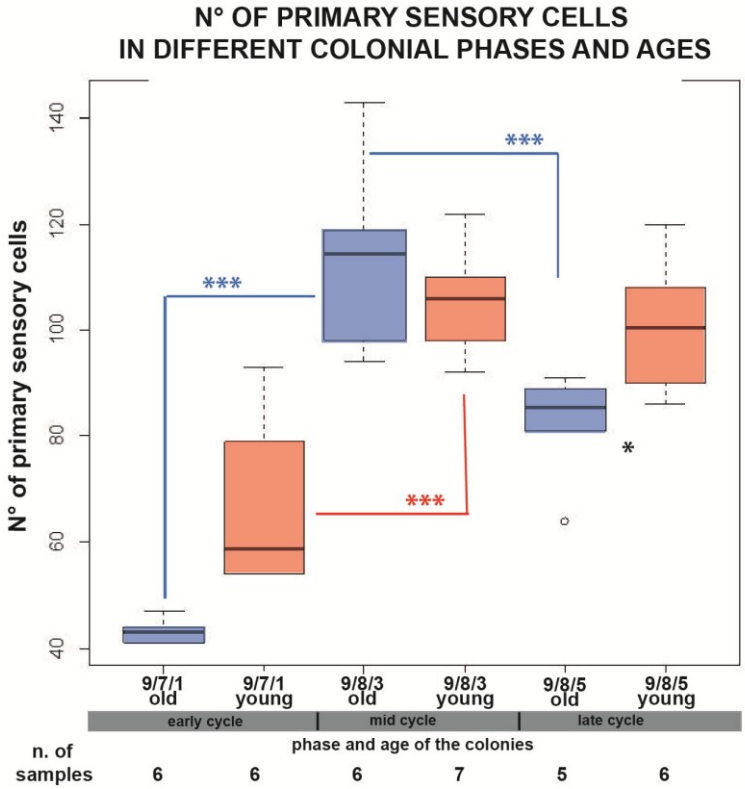

Figure 12: Number of oral siphon epidermal receptors in young (red) and old (blue) colonies. A significant difference is found in late cycle (black asterisk). Note the similar trend in young and old colonies. The red asterisks indicate significant differences between young colonies. The black asterisks indicate significant differences between groups with different ages. P-value < 0.05 (*); p-value < 0.01 (**); p-value < 0.001 (***).

Individuals of old colonies are less responsive than those of young colonies

We performed the TST on adult zooids belonging to the three blastogenetic phases and compared results from young and old colonies. Results showed significant differences among the blastogenetic phases, confirming previous behavioral analyses, but also between young and old colonies, independent of colonial phase (Fig. 13 and Supplementary Material 1.6.2-3). In both young and old colonies, individuals in mid-cycle were the most sensitive, and those in late-cycle were found to be less sensitive than those in mid-cycle. Statistical analysis showed that the differences between young and old colonies were significant, with old colonies less sensitive for each phase (Fig. 13A). Moreover, considering only the colony age (i.e. young vs old colonies) a significant difference was found between the two groups of colonies (Fig. 13B). These data indicate that aging also influences animal behavior, and the decrease in sensitivity to TST with the colonial age advancement is a general feature (Fig. 13B) throughout the adult life cycle.

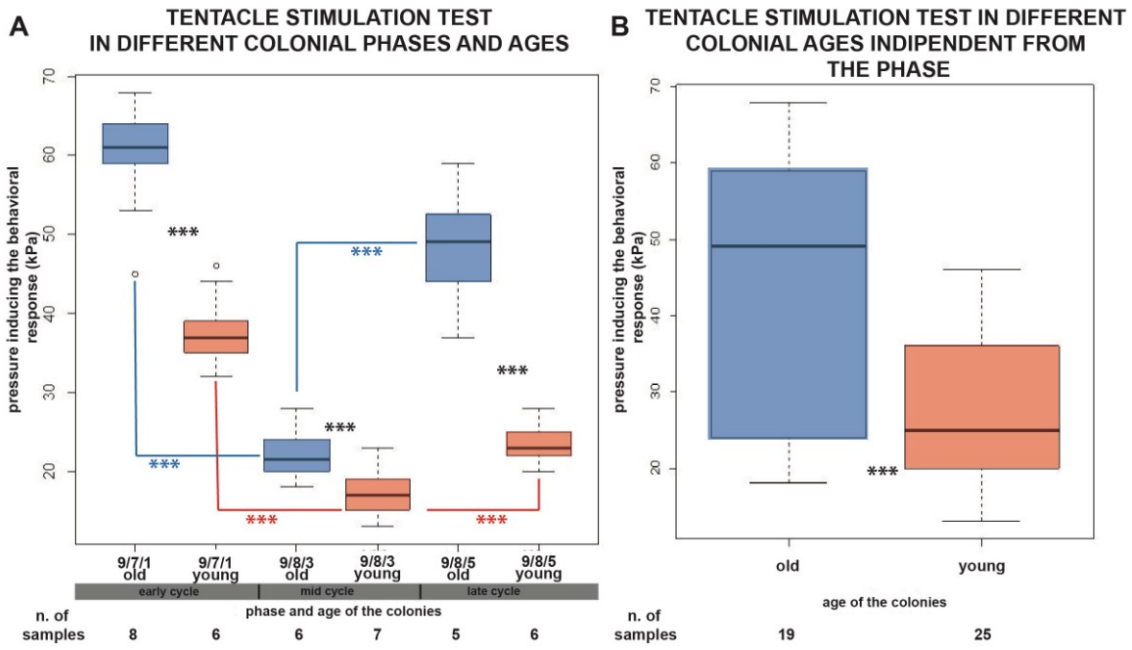

Figure 12: A. TST in young and old colonies in the three blastogenetic phases. Animal performance shows significant differences during the cycle and related with the colony age. **B.** Comparison between old and young colonies. The red asterisks indicate significant differences between young colonies. The black asterisks indicate significant differences between groups with different ages. P-value < 0.05 (*); p-value < 0.01 (**); p-value < 0.001 (***).

Molecular profile of old and young colonies revealed genes whose differential expression is associated with human neurodegenerative diseases

We studied the expression of neurodegenerative disease associated genes in colonies of different ages. In particular we compared young colonies (< 3 months) with old ones (> 8 years).

We found clear patterns of differentially expressed genes associated with 20 human neurodegenerative diseases in young and old colonies (Supplementary 2.2).

These neurodegenerative diseases include: Parkinson disease, muscular dystrophy, medulloblastoma, grn-related frontotemporal dementia, autosomal recessive non-syndromic sensorineural deafness, Emery-Dreifuss muscular dystrophy, Charcot-Marie-Tooth disease, Ewing sarcoma, Joubert syndrome, myotonic dystrophy, dilated cardiomyopathy, myotonic dystrophy, schizophrenia, microcephaly, hereditary spastic paraplegia, neural tube defects, amyotrophic lateral sclerosis, Huntington disease, Alzheimer disease, and neuroblastoma.

In particular, molecular profiles of old and young colonies revealed 393 genes whose differential expression correlates with Alzheimer's disease gene profile patterns. Among them, genes associated with amyloid β peptide plaque formation (*APP, PSEN1 and PSEN2)*, whose mutations are linked to the early onset of Alzheimer's and genetic markers (APOE and SORT1) that correlate with an increase of the risk of Alzheimer's (Kumar and Tsao, 2018). However, the cause for most Alzheimer's cases, which appear at ages over 65, is still largely unknown (Masters et al., 2018).

To identify potential genes and pathways that characterize neurodegeneration in *B. schlosseri*, we compared the expression profiles of 20 samples taken from organisms of different ages (old zooids in early-cycle (>8 years old) and young zooids in early-cycle (<3 months old)) with genes that are expressed in the *B. schlosseri* brain and are known to be associated with neurodegenerative diseases. There is a clear and pronounced distinction in the expression of these genes between the young and old colonies, indicating the potential of this model organism to be used in studies of neurodegeneration (Fig. 14). Within genes differentially expressed between young and old colonies, we found strong evidence for: (i) respiratory electron transport, ATP synthesis by chemiosmotic coupling, and heat production by protein pathway

uncoupling, (ii) plaque formation and APP metabolism pathway, (iii) A-beta signaling pathway, (iv) presenilin-mediated signaling pathway, (v) Alzheimer's disease pathway, (vi) apoptosis and survival caspase cascade, and (vii) circadian entrainment pathway, suggesting that this model organism is relevant to mammalian neurodegeneration and aging studies.

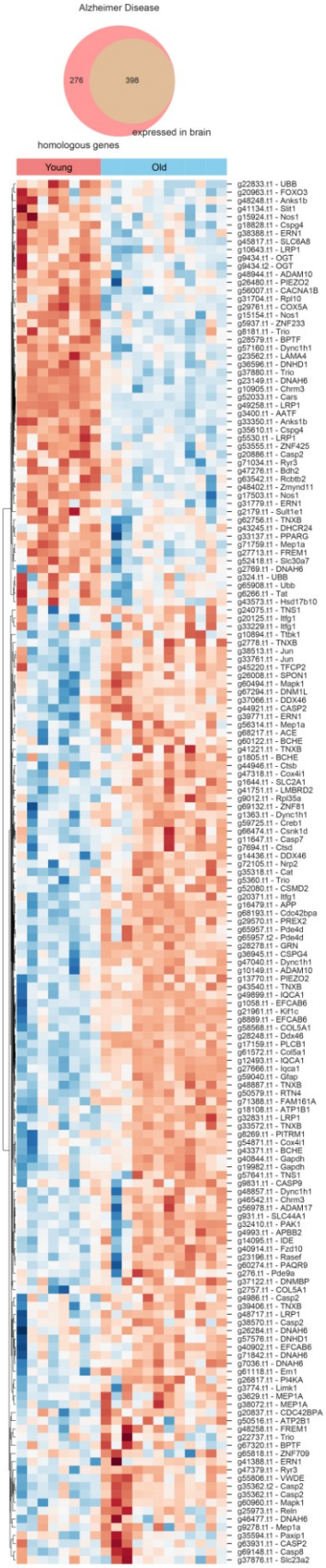
Alzheimer Disease
276
398
expressed in brain
homologous genes
Young
Old
g22833.t1 - UBB
g20963.t1 - FOXO3
g48248.t1 - Anks1b
g41134.t1 - Slit1
g15924.t1 - Nos1
g18828.t1 - Cspg4
g38388.t1 - ERN1
g45817.t1 - SLC6A8
g10643.t1 - LRP1
g9434.t1 - OGT
g9434.t2 - OGT
g48944.t1 - ADAM10
g26480.t1 - PIEZO2
g56007.t1 - CACNA1B
g31704.t1 - Rpl10
g29761.t1 - COX5A
g15154.t1 - Nos1
g5937.t1 - ZNF233
g8181.t1 - Trio
g28579.t1 - BPTF
g57160.t1 - Dync1h1
g23562.t1 - LAMA4
g36596.t1 - DNHD1
g37880.t1 - Trio
g23149.t1 - DNAH6
g10905.t1 - Chrm3
g52033.t1 - Cars
g49258.t1 - LRP1
g3400.t1 - AATF
g33350.t1 - Anks1b
g35610.t1 - Cspg4
g5530.t1 - LRP1
g53555.t1 - ZNF425
g20886.t1 - Casp2
g71034.t1 - Ryr3
g47276.t1 - Bdh2
g63542.t1 - Rcbtb2
g48402.t1 - Zmynd11
g17503.t1 - Nos1
g31779.t1 - ERN1
g2179.t1 - Sult1e1
g62756.t1 - TNXB
g43245.t1 - DHCR24
g33137.t1 - PPARG
g71759.t1 - Mep1a
g27713.t1 - FREM1
g52418.t1 - Slc30a7
g2769.t1 - DNAH6
g324.t1 - UBB
g65908.t1 - Ubb
g6266.t1 - Tat
g43573.t1 - Hsd17b10
g24075.t1 - TNS1
g20125.t1 - Ifitg1
g33229.t1 - Ifitg1
g10894.t1 - Tbk1
g2778.t1 - TNXB
g38513.t1 - Jun
g33761.t1 - Jun
g45220.t1 - TFCP2
g26008.t1 - SPON1
g60494.t1 - Mapk1
g67294.t1 - DNM1L
g37066.t1 - DDX46
g44921.t1 - CASP2
g39771.t1 - ERN1
g56314.t1 - Mep1a
g68217.t1 - ACE
g60122.t1 - BCHE
g41221.t1 - TNXB
g1805.t1 - BCHE
g44948.t1 - Ctsb
g47318.t1 - Cox4i1
g1644.t1 - SLC2A1
g41751.t1 - LMBRD2
g9012.t1 - Rpl35a
g69132.t1 - ZNF81
g1363.t1 - Dync1h1
g59725.t1 - Creb1
g66474.t1 - Csnk1d
g11647.t1 - Casp7
g7694.t1 - Ctsd
g14436.t1 - DDX46
g72105.t1 - Nrp2
g35318.t1 - Cat
g5360.t1 - Trio
g52080.t1 - CSMD2
g20371.t1 - Ifitg1
g18479.t1 - APP
g68193.t1 - Cdc42bpa
g29670.t1 - PREX2
g65957.t1 - Pde4d
g65957.t2 - Pde4d
g28278.t1 - GRN
g36945.t1 - CSPG4
g47040.t1 - Dync1h1
g10149.t1 - ADAM10
g13770.t1 - PIEZO2
g43540.t1 - TNXB
g49899.t1 - IQCA1
g1058.t1 - EFCAB6
g21961.t1 - Kif1c
g8889.t1 - EFCAB6
g58568.t1 - COL5A1
g28248.t1 - Ddx46
g17159.t1 - PLCB1
g61572.t1 - Col9a1
g12493.t1 - IQCA1
g27666.t1 - Iqca1
g59040.t1 - Gfap
g48887.t1 - TNXB
g50579.t1 - RTN4
g71388.t1 - FAM161A
g18108.t1 - ATP1B1
g32831.t1 - LRP1
g33572.t1 - TNXB
g8269.t1 - PITRM1
g54871.t1 - Cox4i1
g43371.t1 - BCHE
g40844.t1 - Gapdh
g19982.t1 - Gapdh
g57641.t1 - TNS1
g9831.t1 - CASP9
g48857.t1 - Dync1h1
g46542.t1 - Chrm3
g56978.t1 - ADAM17
g931.t1 - SLC44A1
g32410.t1 - PAK1
g4993.t1 - APBB2
g14095.t1 - IDE
g40914.t1 - Fzd10
g23196.t1 - Rasef
g60274.t1 - PAQR9
g276.t1 - Pde9a
g37122.t1 - DNMBP
g2757.t1 - COL5A1
g4986.t1 - Casp2
g39406.t1 - TNXB
g48717.t1 - LRP1
g38570.t1 - Casp2
g26284.t1 - DNAH6
g57576.t1 - DNHD1
g40902.t1 - EFCAB6
g71842.t1 - DNAH6
g70036.t1 - DNAH6
g61118.t1 - Eml1
g26817.t1 - Pi4KA
g3774.t1 - Limk1
g3629.t1 - MEP1A
g38072.t1 - MEP1A
g20837.t1 - CDC42BPA
g50516.t1 - ATP2B1
g48258.t1 - FREM1
g22737.t1 - Trio
g67320.t1 - BPTF
g65818.t1 - ZNF709
g41388.t1 - ERN1
g47379.t1 - Ryr3
g55806.t1 - VWDE
g35362.t2 - Casp2
g35362.t1 - Casp2
g60960.t1 - Mapk1
g25973.t1 - Reln
g46477.t1 - DNAH6
g9278.t1 - Mep1a
g35594.t1 - Pixip1
g63931.t1 - CASP2
g69148.t1 - Casp8
g37876.t1 - Slc23a2

Figure 14: Neurodegenerative gene expression in aging colonies. Upper: Venn diagrams showing the number of genes associated with Alzheimer's disease with putative homologies in *B. schlosseri* and how many of those genes are expressed in the brain. Lower: Heatmaps of these brain expressed genes that are differentially expressed between young and old colonies. Counts are log-transformed and normalized (mean=0, standard deviation=1). Red = high, blue = low.

CONCLUSION

This work shows that in *B. schlosseri*, the CNS, some sensory systems and associated behavioral responses change dynamically during adult zooid life. We found that the brain is not stable in cell number, which increases during the first phases of the cycle and then decreases before the brain is totally resorbed at takeover. Thes finding raises new questions about the processes of adult neurogenesis and neurodegeneration. The relationship between the brain and the others components of the neural complex (dorsal organ and neural gland) changes accordingly. Therefore, we suggest that these organs have an active role in adult neurogenesis.

Apoptosis involves the brain, suggesting that this cell death mechanism also plays a role tissue modelling during adult life, not only in takeover and development (Ballarin et al., 2010, Burighel et al., Cima et al. 2010, Tiozzo et al., 2006). Therefore, a balance between brain cell death and neurogenesis could be responsible for the specific trend in brain cell number. We also investigated immunocytes (morula cells and phagocytes) around and within the cerebral ganglion, finding that their number increases significantly during the cycle. This increase parallels an increase in expression of genes associated with a kind of immunocyte, the morula cells. Immunocytes could play an important role during neurodegeneration, that may be ascribed to their known roles of cytotoxicity (morula cells) and clearance activity (phagocytes) (Franchi and Ballarin, 2017).

The documented trend in brain neuron number correlates with that of the oral siphon epidermal receptors. In both cases, the highest number of cells is found in mid-cycle. These trends affect animal performance. The behavioral tests (SST and TST) that we developed, showed that the mechanical stimulation of oral siphon epidermal receptors and coronal cells vary during the cycle. The phase with the highest number of neurons and sensory cells (mid-cycle) represents the highest animal sensitivity, whereas the phase with the lowest number of neurons and sensory cells represents the lowest sensitivity.

We also demonstrated that this species is a useful model for analyzing aging. This process is similar and relevant to the mammalian aging on account of the extensive number of CNS genes homologous to human and mouse (present data; Voskoboynik et al. 2013) genes associated with neurodegenerative diseases. We found a differential expression of these genes between young and old colonies that is associated with the hallmarks of aging described in mammalian studies (Lopez-Otin et al., 2013; Masters et al. 2018). Specifically, clear patterns of differentially expressed genes associated with 20 human neurodegenerative diseases were found in young and old colonies. For Alzheimer's disease in particular, the differential expression of 393 genes correlated in old colonies. Age-related phenotypes, namely a lower brain cell number, a lower sensory cell number, and worse behavioral performances with respect to young colonies, were clearly evident in old colonies.

In conclusion, we believe that *B. schlosseri*, because of its cyclical blastogenesis, represents a robust, assayable and repeatable model to study mechanisms of neurodegeneration, neurogenesis, and how balance between the two varies with aging.

MATERIAL AND METHODS

Animals

Specimens of *Botryllus schlosseri* (family Botryllidae, order Stolidobranchiata) used in this study were collected from Venice lagoon. They were reared adhering to glass according to Sabbadin's (1955) technique at a constant temperature of 18°C. Thanks to the transparency of colonies, the daily development of buds was followed *in vivo* under the stereomicroscope in order to select the appropriate stages. The stages of colony life cycle were defined according to Sabbadin (1955) (Manni et al., 2014). Young colonies (few weeks old) were observed during the larval period and the metamorphoses period in order to assign them the exact age.

Behavioral Experiments

Based on previous work (Mackie et al., 2006), we performed two behavioral

tests: the siphon stimulation test (SST) and the tentacle stimulation test (TTS). The first test involved the stimulation of the oral siphon epidermal receptors, *i.e*. primary sensory cells located in the oral siphon wall, whereas the TTS involved the stimulation of the coronal cells, *i.e*. the secondary sensory cells of the oral tentacles. The tests consisted of a mechanical stimulation of the outer siphons wall of the tentacles with a solution jet generated by a microinjector. More specifically, we used a glass needle prepared with a Narishige PD-5 horizontal capillary puller, mounted on a Singer Mk1 micromanipulator. The water-jet used to stimulate the zooids was a solution of 0.5% red phenol in filtered seawater. Tests were performed in thermostatic chamber at constant temperature.

Each water jet (impulse) was produced after an interval of approximately 1 minute from the previous jet to allow the zooid to return to a relaxed condition. In this way, each impulse could be considered as "single", avoiding problems of habituation or sensitization. The jet pressure was gradually increased: starting from a minimum value of 001 kPa, at which no behavioral response was observed, the pressure was increased 001 kPa each time. Impulses were repeated until the pressure was sufficient to cause an oral siphon contraction (in case of the SST) or a squirting reaction (in case of the TST) at which point the pressure value was recorded.

The expected reaction of zooids to the SST was the closure of the oral siphon, while a typical squirting behavior consisted of a sudden atrial siphon closure and vigorous body contraction. The response to the tests was verified in adult zooids in early-, mid-, and late-cycle (Table 1-2). Both the experiments were carried out on three zooids belonging to three different systems for each colony. Both young and old colonies were used.

Blatstogenetic stage	**N° of zooids**	**N° of systems**	**Age of colony**
Early cycle	36	4	6 months old
	33	4	2 weeks old
Mid cycle	36	4	6 months old
	24	4	2 weeks old
Late cycle	26	4	6 months old
	24	4	2 weeks old

Table 1: Samples used in the tentacle stimulation test (TST)

Blatstogenetic stage	N° of zooids	N° of systems	Age of colony
Early cycle	36	4	2 weeks old
Mid cycle	36	4	2 weeks old
Late cycle	36	4	2 weeks old

Table 2: Samples used in the siphon stimulation test (STS)

Confocal Microscopy

Colonies at selected phases (Tab. 3-4) were anaesthetized with MS222 (tricaine methanesulfonate, Sigma, A5040-25) and fixed in 4% PFA in MOPS (0,1 M MOPS; 0,5 M NaCl; 1mM $MgSO_4$; 2mM EGTA) overnight at 4°C. Samples were washed 3 times in PBS (10 min each). In order to facilitate the permeabilization, samples were treated with 0,5% TritonX-100 at room temperature for 10 min and with Trypsin 0.1% + $CaCl_2$ 0.01% in PBS 1X for 10 minutes. In order to convert the natural green autofluorescence to far red, samples were colored with *blue evans* (Sigma, cat. n. E-2129) 0.02% in PBS for 15 minutes). They were blocked for 4h at room temperature in BSA (bovine serum albumin) 1% + sheep serum 2% in PBT (PBS + Tween-20, 0.05%). Specimens were incubated overnight at 4°C in 1:5000 primary antibody (monoclonal anti-alpha-tubulin; Sigma Aldrich, cat n. T5168) diluted in BSA 1% + sheep serum 2% in PBT. Following 3 washes in PBT, they were incubated for 2 h in secondary antibody (anti-mouse fluorescein conjugated, Calbiochem cat n. 401234) 1:100 in BSA 1% + sheep serum 2% in PBT. The labeled samples were washed 3 times in PBT (10 min each) and incubated with DAPI (Sigma, cat. N. D9542) (5µg/ml) for 5 minutes. Samples were washed 3 times in PBS and then placed in increasing concentrations of glycerol in PBS 1X (33% - 50% - 75%), 15 minutes each. Observations were carried out as soon as possible to avoid fluorescence decadence. Samples were mounted and examined using 63X oil-immersion objective lenses of *Leica SP5*. Series of Z-axes optical section of the ganglion were collected simultaneously every 0.5 µm visualizing both nuclei and tubulin. Z-stack series were visualized using an interactive graphic display (Wacom, DTU-2231).

The quantification of primary cells inside the oral siphon and nuclei, belonging to the cerebral ganglion, was performed utilizing Fiji software. With respect to the oral siphon epidermal receptors, cells possessing both a cilium and an axon were counted. Regarding the cerebral ganglion, nuclei in the different layers of the z-stacks were counted.

To detect the macrophages we used antibody anti RBL (Ballarin et al., 2013; Franchi et al. 2011, Gasparini et al., 2008; Franchi et al., 2010) previously used by Ballarin and colleagues following the above protocol. We analyzed 8 ganglia for early cycle, 10 for mid cycle and 10 for late cycle. The colonies were of mixed ages.

Blastogenetic stage	**N° of colonies**	**N° of ganglia**	**Age**
9/7/1	4	8	6 months old
	3	6	3 weeks old
9/8/2	4	6	6 months old
9/8/3	3	6	6 months old
	3	7	3 weeks old
9/8/4	3	6	6 months old
9/8/4-5	4	7	6 months old
9/8/5	3	5	6 months old
	3	6	3 weeks old
11^{1}/8/6	5	7	6 months old
11^{2}/8/6	3	3	6 months old

Table 3: Number of cerebral ganglion used for the brain cells quantification.

Blastogenetic stage	**N° of colonies**	**N° of siphons**	**Age**
9/7/1 (early cycle)	3	6	3 weeks old
	3	6	6 months old
9/8/3 (mid cycle)	3	6	3 weeks old
	3	6	6 months old
9/8/5 (late cycle)	3	6	3 weeks old
	3	6	6 months old

Table 4: Number of siphons used to quantify the primary sensory cell

Electron microscopy

Colonies were anesthetized with MS222 for 5–10 minutes; then, selected fragments of colonies, cut with a small blade, were fixed in 1.5% glutaraldehyde buffered with 0.2M sodium cacodylate, pH 7.4, plus 1.6% NaCl. After washing in buffer and post-fixation in 1% OsO4 in 0.2 Mcacodylate buffer, specimens were dehydrated and embedded in Araldite. Sections were stained with 1% toluidine blue in borax. Thin sections (60 nm thick) were provided contrast by staining with uranyl acetate and lead citrate. Photomicrographs were taken with Micrographs were taken with a FEI Tecnai G12 electron microscope operating at 75 kV.
Regarding the quantification of the brain's cell with or without regular shape, we analyzed 6 samples both in early and late cycle. We counted the percentage of cells with regular nuclei in relation to the total number of nuclei present in the section.

3D reconstruction

Five samples belonging to the same colony, fixed at four different colony phases (late bud stage, early-cycle, mid-cycle, late-cycle, and TO), were embedded in resin as previously described and serially cut using a Histo Jumbo Knife (Diatome).
Chains of sections, 1μm thick, were arranged in chains of about 20 sections each and stained with toluidine blue. The neural complex was serially photographed and Amira software was used to create 3D reconstructions.

Whole-mount preparations

Colonies adhering to glass slides were anesthetized with MS 222, fixed in Bouin's fluid, washed in PBS, and stained with Mayer's hemalum (Sigma-Aldrich, MHS32). After washing in distilled water, they were dehydrated in ethanol, cleared in Xylene, and mounted with Technovit 8100, EMS cat. n. 14654. We analyzed one colony for early cycle (27 blastozooids), three in mid cycle (60 blastozooids), one in late cycle (16 blastozooids) and three in TO (32 blastozooids).

Apoptosis detection

Colonies at selected phases (Table 5) were anesthetized with MS222 (Sigma, A5040-25), fixed for at least 2h in Karnowsky's solution (paraformaldehyde 4%, glutaraldehyde 0.1%, sodium cacodylate 0.4 M; pH 7.4), dehydrated in ethanol and embedded in Paraplast (Sherwood Medical). Sections (7 mm thick) were obtained with a Leitz 1212 microtome and stained with haematoxylin-eosin or used to detect apoptosis with the TUNEL reaction. Sections were permeabilized in a permeabilization solution (0,1% Triton X-100 in 0,1% sodium citrate, freshly prepared). Sections were then treated with the TUNEL reaction mixture according to the protocol (*In situ* Cell Death detection Kit, TMR red; Roche) and incubated for 1 h at 37°C in the dark. After 4 washes in phosphate buffer saline (PBS: NaCl0.13 M, KCl 2.7 mM, Na2 PO4 10 mM, KH2 PO4 1.7 mM; pH7.4), they were stained in 1µg/ml Hoechst (Hoechst 33342, trihydrochloride, tryhydrate) in PBS for 10 minutes, mounted with Vectashield (Vector Laboratories) and observed under a fluorescence microscopy (Olympus CX31). The number of labelled nuclei and the total number of nuclei in cerebral ganglions were counted. In the negative control, slices were incubated in Label Solution (without terminal transferase) instead of TUNEL reaction mixture.

Blastogenetic stage	N° of systems	N° of cerebral ganglia
Early cycle	3	6
Mid cycle	3	12
Late cycle	3	14

Table 5. Number of colonies used for the experiments and number of ganglia analyzed for the apoptosis quantification.

Statistics

Statistical analyses were performed using R software Environment version 3.5.1 (R Core Team, 2018).

Box and whisker plots were used to visualize data. For each dataset, the following methods were applied. 1) The Shapiro test was used to determinate wherever each

sample was normally distributed, then the Fligner-Killen test or the Bartlett test was used to verify the homogeneity of variance among samples in each dataset. The comparison of means was also performed with non-parametric Wilcoxon rank-sum test and /or the parametric t-test. 2) The Shapiro test, the Barlett or Fligner-Killen test were used. Then, the non-parametric one-way ANOVA equivalent, the Kruskal Wallis rank sum test, was used to verify the null hypothesis of equality of medians among samples. Subsequently, the post hoc Conover's test with Bonferroni value adjustment and corrected quartiles for ties (Pohlert, 2018) was used in case of rejection of the null hypothesis to calculate the pairwise multiple comparisons between samples.
For these statistics, differences were considered significant when p-values were <0.05.

Transcriptomes and gene analysis

We used the protocol described in Voskoboynik et al 2013 to extract RNA from whole colonies. Insulin syringes were used to dissect tissue samples which were flash frozen in liquid nitrogen to minimize RNA degradation and stored at -80 C. Using a mechanized Konte tissue grinder and pestle, samples were homogenized in the presence of lysis buffer (Qiagen RNAeasy Microkit #74004), and total RNA was extracted following the manufacturer's protocol. Resultant RNA was cleaned and concentrated (Zymo Research RNA Clean and Concentrator-5, R1015) and analyzed by an Agilent 2100 Bioanalyzer for quality analysis prior to library preparation. cDNA libraries were then prepared from high quality samples (RIN > 8) using Ovation RNA-seq v2(Nugen). Size selection was performed prior to barcoding using Zymo Research Select-a-Size DNA Clean and Concentrator Kit (D4080); Libraries were barcoded using NEBnext Ultra DNA Library Prep Kit Master for Illumina (New England Biolabs, E7370S) and NEBNext Multiplex Oligos for Illumina (New England Biolabs, E6609S). Barcoded library samples were then sequenced on an Illumina NextSeq 500 (2x150bp, producing an average of 15 million reads/cell population).
Determination of gene counts was performed using a Snakemake (Köster and Rahmann 2012) pipeline. An outline of the steps is as follows: i) low quality bases and adapter sequences were removed using Trimmomatic (Bolger et al., 2014) (version 0.32) ii) overlapping paired end reads were merged using FLASH (Magoč and Salzberg 2011) (version 1.2.11) iii) reads were aligned to the UniVec Core database using Bowtie2

(Langmead and Salzberg 2012) (version 2.2.4) to remove biological vector and control sequences, iv) reads were aligned to the *Botryllus schlosseri* transcriptome with BWA (Li and Durbin 2010) ("mem" algorithm, version 0.7.12), v) aligned reads were sorted and indexed using SAMtools, PCR duplicates removed using PICARD ("MarkDuplicates" tool, version 1.128) and then transcript level counts directly counted from the BAM file. Gene homology was determined based on the genome annotation (Voskoboynik et al., 2013). Briefly, the protein sequences were compared (blastp, evalue < 1e-10) to human and mouse proteomes (UniProtKB/Swiss-Prot) and to (blastx, evalue < 1e-10) the NCBI non-redundant protein database (nr). For each gene two annotations were produced: the best hit in nr and the best hit from mouse/human proteome (if present).

Differential expression was performed using edgeR (Robinson et al., 2010). In detail: the gene counts were compiled in a tabular format and loaded into R. Genes were retained with at least five counts per million in at least two samples. A simple model was used to compare the two sets of populations, with p-values adjusted using the Benjamini-Hochberg method to produce a false discovery rate (FDR). FDRs less than 0.05 were called as being differentially expressed. For the zooid cycle genes, all sets of contiguous times had samples selected and differentially expressed genes found in the above manner. For each gene, all such comparisons for which significant differences (FDR < 0.05) were collected and the best time signature that explains these DE observations for each gene was found. To further simplify the comparisons, these time signatures were binarized, with 1 indicating "high" expression and 0 indicating "low" or zero expression producing a gene-time expression matrix for each gene along the zooid's development cycle.

Enrichment plots were created by measuring the overlap of a gene set with the binary gene-time expression matrix. The baseline was calculated using a null model that assumed that N genes of the gene set were taken randomly (without replacement) and using that to determine that expected proportion of "enriched" genes. A hypergeometric model was used to calculate the main value as well as the 50% and 99% confidence intervals.

REFERENCES

- Ballarin L., Cammarata M., Franchi N., Parrinello N. (2013). Routes in innate immunity evolution: galectins and rhamnose-binding lectins in ascidians. In Marine Proteins and Peptides: Biological activities and applications:185-205

- Ballarin L., Schiavon F., Manni L. (2010). Natural Apoptosis During the Blastogenetic Cycle of the Colonial Ascidian *Botryllus schlosseri*: A Morphological Analysis. Zoological Science, 27(2): 96-102

- Ballarin L. (2008). Immunobiology of compound ascidians, with particular reference to *Botryllus schlosseri*: state of art. Inv. Surv. J 5: 54-74

- Blesa J., Trigo-Damas I., Dileone M., Del Rey N. L. G., Hernandez L. F., Obeso J. A. (2017). Compensatory mechanisms in Parkinson's disease: Circuits adaptations and role in disease modification. Experimental neurology 298:148-161

- Bolger A. M., Lohse M., & Usadel B. (2014). Trimmomatic: a flexible trimmer for Illumina sequence data. Bioinformatics 30(15): 2114-2120

- Burighel P. and Schiavinato A. (1984). Degenerative regression of the digestive tract in the colonial ascidian *Botryllus schlossen* (Pallas).Cell and tissue research, 235(2): 309-318

- Burighel P., Lane NJ., Gasparini F., Tiozzo S., Zaniolo G., Carnevali MDC., Manni L. (2003). Novel, secondary sensory cell organ in ascidians: in search of the ancestor of the vertebrate lateral line. Journal of Comparative Neurology 461: 236-249

- Burighel P., Lane NJ., Zaniolo G., Manni L. (1998). Neurogenic role of the neural gland in the development of the ascidian, *Botryllus schlosseri* (Tunicata, Urochordata). Journal of Comparative Neurology 394: 230-241

- Burighel P., Sorrentino M., Zaniolo G., Thorndike M C., Manni L. (2001). The Peripheral Nervous System of an Ascidian, *Botryllus schlosseri*, as Revealed by Cholinesterase Activity. Invertebrate Biology 120(2): 185-198

- Burighel P., Caicci F. & Manni L. (2011). Hair cells in non-vertebrate models: lower chordates and molluscs. Hearing research 273(1-2): 14-24

- Calne DB., Zigmond MJ. (1991). Compensatory mechanisms in degenerative neurologic diseases insights from Parkinsonism. Arch Neurol. 48(4):361–363

- Cima F., Ballarin L., Caicci F., Franchi N., Gasparini F., Rigon F., Schiavon F., Manni L. (2015). Life history and ecological genetics of the colonial ascidian *Botryllus schlosseri*. Zoologischer Anzeiger 257: 54-70

- Cima F., Manni L., Basso G., Fortunato E., Accordi B., Schiavon F., Ballarin L. (2010). Hovering between death and life: natural apoptosis and phagocytes in the blastogenetic cycle of the colonial ascidian *Botryllus schlosseri*. Developmental & Comparative Immunology 34(3): 272-285

- Cima F., Basso G. & Ballarin L. (2003). Apoptosis and phosphatidylserine-mediated recognition during the take-over phase of the colonial life-cycle in the ascidian *Botryllus schlosseri*. Cell and tissue research 312(3): 369-376

- Cima F., Franchi N. & Ballarin L. (2016). Origin and Functions of Tunicate Hemocytes. In The Evolution of the Immune System :29-49

- Corey DM., Rosental B., Kowarsky M., Sinha R.,Ishizuka KJ., Palmeri KJ., Quake SR., Voskoboynik A., Weissman IL. (2016). Developmental cell death programs license cytotoxic cells to eliminate histocompatible partners. Proceedings of the National Academy of Sciences 113(23): 6520-6525

- Dahlberg C., Auger H., Dupont S., Sasakura Y., Thorndyke M. & Joly J. S. (2009). Refining the *Ciona intestinalis* model of central nervous system regeneration. PloS one 4(2):e4458

- Delsuc F., Brinkmann H., Chourrout D., Philippe H. (2006). Tunicates and not cephalochordate are the closest living relatives of vertebrates. Nature 439: 965-968

- Delsuc F., Philippe H., Tsagkogeorga G., Simion P., Tilak MK., Turon X., Lopez-Legentil S., Piette J., Lemaire P., Douzery EJP. (2018). A phylogenomic framework and timescale for comparative studies of tunicates. BCM Biology 16(1): 39

- Deyts C., Casane D., Vernier P., Bourrat F., Joly JS. (2006). Morphological and gene expression similarities suggest that the ascidian neural gland may be osmoregulatory and homologous to vertebrate peri-ventricular organs. European Journal of Neuroscience 24(8): 299-308

- Franchi N., Ballarin L., Peronato A., Cima F., Grimaldi A., Girardello R., De Eguileor M. (2018). Functional amyloidogenesis in immunocytes from the colonial ascidian *Botryllus schlosseri*: Evolutionary perspective. Developmental & Comparative Immunology. In press

- Franchi N., Schiavon F., Carletto M., Gasparini F., Bertoloni G., Tosatto SC., Ballarin L. (2011). Immune roles of a rhamnose-binding lectin in the colonial ascidian *Botryllus schlosseri*. Immunobiology 216(6):725-736

- Franchi N., Ballarin L. (2016). Cytotoxic cells of compound ascidians. In Lessons in Immunity: 193-203

- Franchi N. & Ballarin L. (2017). Immunity in protochordates: the tunicate perspective. Frontiers in immunology 8: 674

- Gasparini F., Franchi N., Spolaore B., Ballarin L. (2008). Novel rhamnose-binding lectins from the colonial ascidian *Botryllus schlosseri*. Developmental & Comparative Immunology 32(10): 1177-1191

- Gissi C., Pesole G., Cattane E., Tartari M. (2006). Huntingtin gene evolution in Chordata and its peculiar features in the ascidian Ciona genus. BMC genomics 7(1): 288

- Ikezoe K., Nakamori M., Furuya H. Arahata H., Kanemoto S., Kimura T., Imaizumi K., Takahashi M., Sakoda S., Fujii N., Kira J. (2007). Endoplasmatic reticulum stress in myotonic dystrophy type 1 muscle. Acta Neuropathol. 114(5): 527-535

- Jeffery WR. (2018). Regeneration and Aging in the Tunicate Ciona intestinalis. In Conn's Handbook of Models for Human Aging (Second Edition): 521-531

- Kano S. (2010). Genomics and Developmental Approaches to an Ascidian Adenohypophysis Primordium. Integrative and Comparative Biology 50(1): 35-52

- Kawamura K., Tachibana M., Sunanaga T. (2008). Cell proliferation dynamics of somatic and germline tissues during zooidal life span in the colonial tunicate *Botryllus prymigenus*. Developmental Dynamics 237: 1812-1825

- Kocot KM., Tassia MG., Halanych KM., Swalla BJ. (2018). Phylogenomics offers resolution of major tunicate relationship. Molecular Phylogenetics and Evolution 121: 166-173

- Köster J. & Rahmann S. (2012). Snakemake—a scalable bioinformatics workflow engine. Bioinformatics 28(19),:2520-2522

- Kumar A., Tsao JW. (2018). Alzheimer Disease. StatPearls. Treasure Island (FL)

- Laird DJ., De Tomaso AW., Weissman IL. (2005). Stem cells are units of natural selection in a colonial ascidian. Cell 123(7):1351-60.

- Langmead B. & Salzberg S. L. (2012). Fast gapped-read alignment with Bowtie 2. Nature methods 9(4): 357

- Lauzon RJ., Ishizuka KJ., Weissman IL. (2002). Cyclical generation and degeneration of organs in a colonial urochordate involves crosstalk between old and new: a model for development and regeneration. Dev Biol 249(2):333-48

- Lauzon RJ., Ishizuka KJ. & Weissman IL. (1992). A cyclical, developmentally regulated death phenomenon in a colonial urochordate. Developmental dynamics 194(1):71-83

- Lauzon RJ., Patton CW. & Weissman IL. (1993). A morphological and immunohistochemical study of programmed cell death in *Botryllus schlosseri* (Tunicata, Ascidiacea).Cell and tissue research 272(1): 115-127

- Li H., Durbin R. (2010). Fast and accurate long-read alignment with Burrows–Wheeler transform. Bioinformatics 26(5): 589-595

- Lopez-Otin ., Blasco MA., Partridge L., Serrano M., Kroemer G. (2013). The hallmarks of aging. Cell 153(6):1194-217

- Mackie GO., Burighel P., Caicci F., Manni L. (2006). Innervation of ascidian siphons and their responses to stimulation. Canadian Journal of Zoology 84: 1146-1162

- Magoč, T. & Salzberg SL. (2011). FLASH: fast length adjustment of short reads to improve genome assemblies. Bioinformatics 27(21): 2957-2963

- Manni L., Anselmi C., Cima F., Gasparini F., Voskoboynik A., Martini M., Peronato A., Burighel P., Zaniolo G., Ballarin L. (2018). Sixty years of experimental studies on the blastogenesis of the colonial tunicate *Botryllus schlosseri*. Developmental Biology. In press.

- Manni L., Gasparini F., Hotta K., Ishizuka KJ., Ricci S., Tiozzo S., Voskoboynik A., Dauga D. (2014). Ontology for the asexual development and anatomy of the colonial chordate *Botryllus schosseri*. Plos One 9(5): e96434

- Manni L., Lane N., Sorrentino M., Zaniolo G., Burighel P. (1999). Mechanism of neurogenesis during the embryonic development of a tunicate. Journal of Comparative Neurology 412: 527-541

- Manni L., Zaniolo G., Cima F., Burighel P., Ballarin L. (2007). *Bortyllus schlosseri*: A model for the study of asexual reproduction. Developmental Dynamics 236: 335-352

- Manni L. & Pennati R. (2016). Tunicata. Structure and evolution of invertebrate nervous systems. Oxford University Press, Oxford :699-718

- Masters CL., Gu B., Laws S., Lim YY., Roberts B., Villemagn VL. & Beyreuther K. (2018). Alzheimer's Disease: Toward a Quantitative Biological Approach in Describing its Natural History and Underlying Mechanisms. In The Molecular and Cellular Basis of Neurodegenerative Diseases :57-79

- Mendiola-Precoma J., Berumen L.C., Padilla K., Garcia-Alcocer G. (2016). Therapies for prevention and treatment of Alzheimer's disease. BioMed research international. Vol 2016, article ID 2589276

- Pennati R., Ficetola GF., Brunetti R., Caicci F., Gasparini F., Griggio F., Sato A., Stach T., Kaul-Strehlow S., Gissi C., Manni L. (2015). Morphological differences between larvae of the *Ciona intestinalis* species complex: Hints for a valid taxonomic definition of distinct species. Plos One 10(5): e0122879

- Pohlert T. (2018). PMCMRplus: Calculate Pairwise Multiple Comparisons of Mean Rank Sums Extended. R package version 1.4.0

- Reitz C. and Mayeux R. (2014). Alzheimer disease: epidemiology, diagnostic criteria, risk factors and biomarkers. Biochemical pharmacology 88(4):640-651

- Rigon F., Gasparini F., Shimeld S. M., Candiani S., Manni L. (2018). Developmental signature, synaptic connectivity and neurotransmission are conserved between vertebrate hair cells and tunicate coronal cells. Journal of Comparative Neurology 526(6): 957-971

- Rosental B., Kowarsky M., Seita J., Corey DM., Ishizuka KJ., Palmeri KJ., Chen S-Y., Sinha R., Okamoto J., Mantalas G., Manni L., Raveh T., Clarke DN., Newman AM., Neff NF., Nolan GP., Quake SR., Weissman IL., Voskoboynik A. (2018). Evolutionary origin of the mammalian hematopoietic system found in a colonial chordate. BioRxiv https://doi.org/10.1101/206318

- Ruppert EE. (1990). Structure, ultrastructure and function of the neural gland complex of Ascidia interrupta (Chordata, Ascidiacea): clarification of hypotheses regarding the evolution of the vertebrate anterior pituitary. Acta Zoologica 71(3): 135-149

- Sabbadin A. (1955). Osservazioni sullo sviluppo, l'accrescimento e la riproduzione di *Botryllus schlosseri* (Pallas), in condizioni di laboratorio. Italian Journal of Zoology 22(2): 243-263

- Schiaffino S., Reggiani C. (1994). Myosin isoforms in mammalian skeletal muscle. Journal of Applied Physiology 77(2): 493-501

- Skold H. N., Stach T., Bishop J. D., Herbst E., Thorndyke M. C. (2011). Pattern of cell proliferation during budding in the colonial ascidian *Diplosoma listerianum*. The Biological Bulletin 221(1): 126-136

- Tiozzo S., Ballarin L., Burighel P., Zaniolo G. (2006). Programmed cell death in vegetative development: apoptosis during the colonial life cycle of the ascidian *Botryllus schlosseri*. Tissue and Cell 38: 193-201

- Virata M., Zeller R.W. (2010). Ascidians: an invertebrate chordate model to study Alzheimer's disease pathogenesis. Disease Models & Mechanisms 3: 377-385

- Voskoboynik A., Neff N.F., Sahoo D., Newman A.M., Pushkarev D., Koh W., Passarelli B., Fan H.C., Mantalas G.L., Palmeri K.J., Ishizuka K.J., Gissi C., Griggio F., Ben-Shlomo R., Corey D.M., Penland L., White R.A., Weissman I.L, Quake S.R. The genome sequence of the colonial chordate *Botryllus schlosseri*. (2013) Elife 2:e00569

- Voskoboynik A., Rinkevich B., Weiss A., Moiseeva E., Reznick A.Z. (2004). Macrophage involvement for successful degeneration of apoptotic organs in the colonial urochordate *Botryllus schlosseri*. Journal of experimental biology 207(14): 2409-2416

- Voskoboynik A., Weissman I. L. (2015). *Botryllus schlosseri*, an emerging model for the study of aging, stem cells, and mechanisms of regeneration. Invertebrate reproduction & development 59(sup1): 33-38

- Zaniolo G., Lane NJ., Burighel P., Manni L. (2002). Development of the motor nervous system in ascidians. J Comp Neurol.443(2):124-35

- Zaniolo G., Burighel P., Martinucci G. (1987). Ovulation and placentation in *Botryllus schlosseri* (Ascidiacea): an ultrastructural study. Canadian journal of zoology 65(5):1181-1190

SUPPLEMENTARY MATERIALS 1
datasets and analyses performed in R

- Command lines are in red.
- Descriptions and results are in black.
- "Young colonies" are up to three weeks old, "colonies" are about six months old.
- Asterisks denote significance in the comparisons between samples as follow:
*** < 0.001, ** < 0.01, * < 0.05

1.1 # Dataset and analysis of the quantification of neurons in the cerebral ganglion in adult zooids belonging to old colonies in eight different blastogenetic phases

```
## DATASET

### Number of neurons in adult zooids belonging to old colonies in the early
      blastogenetic phase (9/7/1)

        Bs971old_neur_random<- scan()
        0819 0786 0802 0810 0817 0834 0777 0831

### Number of neurons in adult zooids belonging to old colonies in the early
      blastogenetic phase (9/8/2)

        Bs982old_neur_random<- scan()
        0833 0822 0781 0814 0830 0814

### Number of neurons in adult zooids belonging to old colonies in the mid blastogenetic
      phase (9/8/3)

        Bs983old_neur_random<- scan()
        0936 0928 0910 0894 0887 0896

### Number of neurons in adult zooids belonging to old colonies in the mid blastogenetic
      phase (9/8/4)

        Bs984old_neur_random<- scan()
        0736 0730 0738 0748 0761 0723

### Number of neurons in adult zooids belonging to old colonies in the mid blastogenetic
      phase (9/8/4-5)

        Bs984to5old_neur_random<- scan()
        0674 0660 0649 0643 0658 0648 0669

### Number of neurons in adult zooids belonging to old colonies in the mid blastogenetic
      phase (9/8/5)

        Bs985old_neur_random<- scan()
        0604 0591 0597 0599 0588

### Number of neurons in adult zooids belonging to old colonies in the late
      blastogenetic phase (11¹/8/6)

        Bs11one86old_neur_random<- scan()
        0556 0522 0541 0547 0520 0533 0563

### Number of neurons in adult zooids belonging to old colonies in the late
      blastogenetic phase (11²/8/6)

        Bs11two86old_neur_random<- scan()
        0506 0511 0517


## ANALYSIS

### procedure for testing the normality distribution of samples
```

```
shapiro.test(Bs971old_neur_random)            # RESULT p-value = 0.6535
shapiro.test(Bs982old_neur_random)            # RESULT p-value = 0.1609
shapiro.test(Bs983old_neur_random)            # RESULT p-value = 0.4285
shapiro.test(Bs984old_neur_random)            # RESULT p-value = 0.8606
shapiro.test(Bs984to5old_neur_random) # RESULT p-value = 0.6986
shapiro.test(Bs985old_neur_random)            # RESULT p-value = 0.8739
shapiro.test(Bs11one86old_neur_random)        # RESULT p-value = 0.7273
shapiro.test(Bs11two86old_neur_random)        # RESULT p-value = 0.8999
```

```
### procedure for testing the homogeneity of variances among groups

bartlett.test

        # RESULT        Bartlett's K-squared = 8.8306, df = 7, p-value = 0.265
```

```
### ANOVA and post-hoc tests

kruskalTest

        # RESULT
        # Kruskal-Wallis test, chi-squared = 45.34, df = 7, p-value = 1.175e-07
               (***)

           # Warning message:
           # Ties are present. Quantiles were corrected for ties.

kwAllPairsConoverTest

        # RESULT
        #        Pairwise comparisons using Conover's all-pairs test

        #   a       b       c       d       e       f       g
        # b 1.00000 -       -       -       -       -       -
        # c 9.4e-07 3.9e-05 -       -       -       -       -
        # d 7.7e-06 2.8e-06 1.5e-13 -       -       -       -
        # e 5.0e-12 5.3e-12 < 2e-16 0.00556 -       -       -
        # f 4.5e-15 6.0e-15 < 2e-16 2.5e-07 0.02480 -       -
        # g < 2e-16 < 2e-16 < 2e-16 5.4e-13 3.3e-08 0.02480 -
        # h < 2e-16 < 2e-16 < 2e-16 5.5e-13 3.1e-09 0.00013 0.42137

           # P value adjustment method: bonferroni
           # Warning message:
           #   Ties are present. Quantiles were corrected for ties.
```

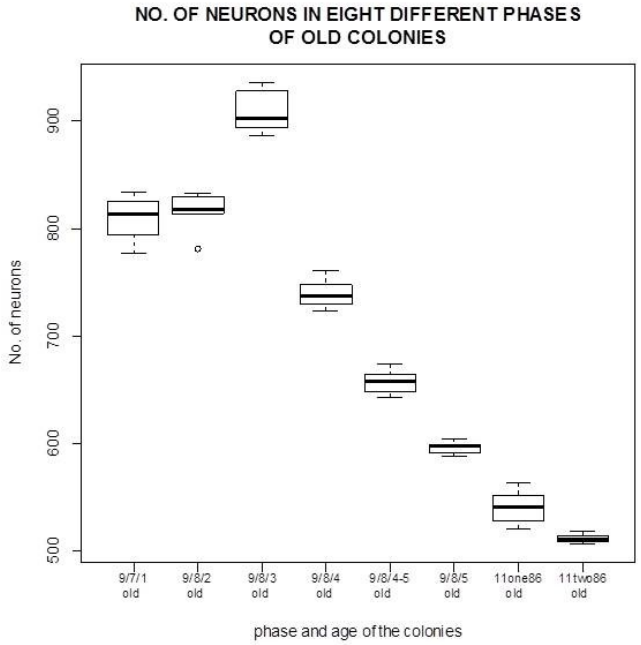

1.2 # Dataset and analysis of the rate of CNS neurons with irregular nucleus in adult zooids belonging to colonies of unknown age (blastogenetic phases 9/7/1 and 9/8/5)

```
## DATASET

### rate of CNS neurons with irregular nucleus in adult zooids in the early
      blastogenetic phase (9/7/1)

       Bs971_Ad_IrrNucCNS <- scan()
       0.24 0.15 0.38 0.42 0.5 0.10

### rate of CNS neurons with irregular nucleus in adult zooids in the late blastogenetic
      phase (9/8/5)

       Bs985_Ad_IrrNucCNS <- scan()
       0.42 0.54 0.66 0.42 0.76 0.39


## ANALYSIS

       shapiro.test(Bs971_Ad_IrrNucCNS )     # RESULT p-value = 0.6584
       shapiro.test(Bs985_Ad_IrrNucCNS )     # RESULT p-value = 0.2582


#### procedure for testing the homogeneity of variances among groups

       bartlett.test

              # RESULT       Bartlett's K-squared = 0.013706, df = 1, p-value = 0.9068


#### procedure to compare the mean of the two samples

       wilcox.test

              # RESULT
              # Wilcoxon rank sum test with continuity correction

              # W = 5, p-value = 0.04383
```

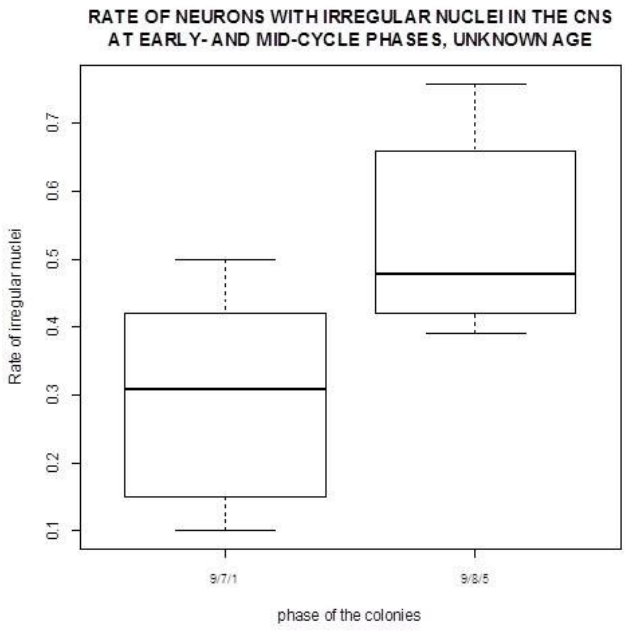

1.3 # Dataset and analysis of the quantification of immunocytes within and/or contacting the cerebral ganglion in adult zooids belonging to colonies of unknown age (blastogenetic phases 9/7/1, 9/8/3 and 9/8/5)

```
## 1) dataset and analysis of immunocytes (morula cells plus phagocytes).

### a) immunocytes (morula cells plus phagocytes) within the CNS.

#### DATASET

##### % of apoptotic cells in adult zooids in the early blastogenetic phase (9/7/1)

       Bs971_Ad_ImmIntCNS <- scan()
       0 0 2 2 2 2 4 4

##### % of apoptotic cells in adult zooids in the mid blastogenetic phase (9/8/3)

       Bs983_Ad_ImmIntCNS <- scan()
       1 8 6 2 6 5 4 3 13 5

##### % of apoptotic cells in adult zooids in the late blastogenetic phase (9/8/5)

       Bs985_Ad_ImmIntCNS <- scan()
       14 3 13 8 11 11 12 10 13 15


### ANALYSIS

       shapiro.test(Bs971_Ad_ImmIntCNS)      # RESULT p-value = 0.09288 (*)
       shapiro.test(Bs983_Ad_ImmIntCNS)      # RESULT p-value = 0.2995
       shapiro.test(Bs985_Ad_ImmIntCNS)      # RESULT p-value = 0.1565 (**)


#### procedure for testing the homogeneity of variances among groups

       bartlett.test

              # RESULT       Bartlett's K-squared = 4.8271, df = 2, p-value = 0.0895


#### ANOVA and post-hoc tests

       kruskalTest

              # RESULT
              # Kruskal-Wallis test, chi-squared = 16.168, df = 2, p-value = 0.0003085
                     (***)

                 # Warning message:
                 # Ties are present. Quantiles were corrected for ties.

       kwAllPairsConoverTest

              # RESULT
              #         Pairwise comparisons using Conover's all-pairs test
              #
              #   a       b
              # b 0.0274  -
              # c 7.2e-06 0.0061
              #
              # P value adjustment method: bonferroni
              # Warning message:
              #  Ties are present. Quantiles were corrected for ties.
```

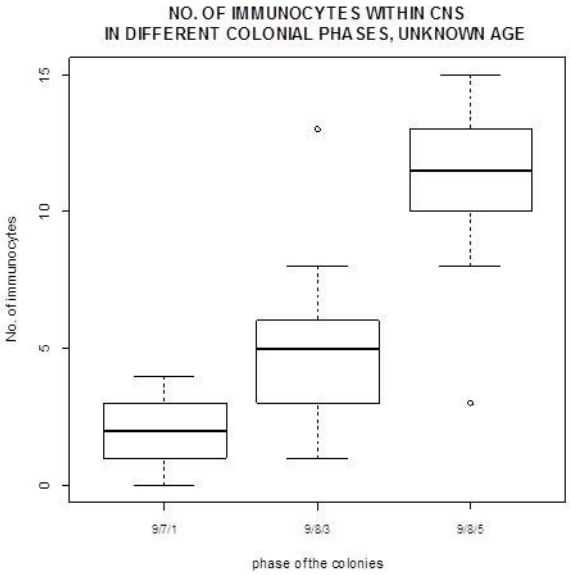


```
### b) immunocytes (morula cells plus phagocytes) contacting the CNS.

#### DATASET

##### % of apoptotic cells in adult zooids in the early blastogenetic phase (9/7/1)

        Bs971_Ad_ImmContCNS <- scan()
        0 0 3 2 4 3 4 6

##### % of apoptotic cells in adult zooids in the mid blastogenetic phase (9/8/3)

        Bs983_Ad_ImmContCNS <- scan()
        7 11 13 15 9 9 5 12 13 9

##### % of apoptotic cells in adult zooids in the late blastogenetic phase (9/8/5)

        Bs985_Ad_ImmContCNS <- scan()
        18 14 17 14 19 18 12 16 18 21


### ANALYSIS

        shapiro.test(Bs971_Ad_ImmContCNS)     # RESULT p-value = 0.5421
        shapiro.test(Bs983_Ad_ImmContCNS)     # RESULT p-value = 0.8593
        shapiro.test(Bs985_Ad_ImmContCNS)     # RESULT p-value = 0.7452


#### procedure for testing the homogeneity of variances among groups

        bartlett.test

                # RESULT        Bartlett's K-squared = 1.1217, df = 2, p-value = 0.5707


#### ANOVA and post-hoc tests

        kruskalTest

                # RESULT
                # Kruskal-Wallis test, chi-squared = 22.211, df = 2, p-value = 1.503e-05
                        (***)

                   # Warning message:
                   # Ties are present. Quantiles were corrected for ties.

        kwAllPairsConoverTest

                # RESULT
                #         Pairwise comparisons using Conover's all-pairs test
```

```
#
#   a       b
# b 3.3e-05 -
# c 2.2e-10 2.4e-05
#
# P value adjustment method: bonferroni
# Warning message:
#  Ties are present. Quantiles were corrected for ties.
```

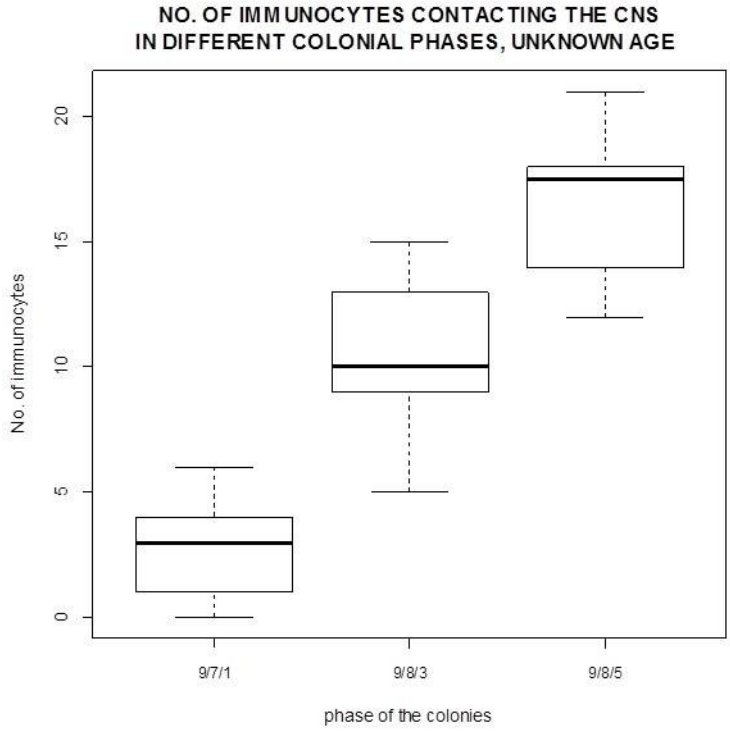

c) immunocytes (morula cells plus phagocytes) within and contacting the CNS.

DATASET

% of apoptotic cells in adult zooids in the early blastogenetic phase (9/7/1)

```
Bs971_Ad_ImmTotCNS <- scan()
0 0 5 4 6 5 8 10
```

% of apoptotic cells in adult zooids in the mid blastogenetic phase (9/8/3)

```
Bs983_Ad_ImmTotCNS <- scan()
8 19 19 17 15 14 9 15 26 14
```

% of apoptotic cells in adult zooids in the late blastogenetic phase (9/8/5)

```
Bs985_Ad_ImmTotCNS <- scan()
32 17 30 22 30 29 24 26 31 36
```

ANALYSIS

```
shapiro.test(Bs971_Ad_ImmTotCNS)      # RESULT p-value = 0.5433
shapiro.test(Bs983_Ad_ImmTotCNS)      # RESULT p-value = 0.5872
shapiro.test(Bs985_Ad_ImmTotCNS)      # RESULT p-value = 0.7866
```

procedure for testing the homogeneity of variances among groups

```
bartlett.test
```

```
# RESULT        Bartlett's K-squared = 1.5377, df = 2, p-value = 0.4636
```

ANOVA and post-hoc tests

```
kruskalTest
```

```
# RESULT
# Kruskal-Wallis test, chi-squared = 21.639, df = 2, p-value = 2.001e-05
        (***)

   # Warning message:
   # Ties are present. Quantiles were corrected for ties.
```

```
kwAllPairsConoverTest
```

```
# RESULT
#         Pairwise comparisons using Conover's all-pairs test
#
#   a       b
# b 0.00011 -
# c 9.2e-10 4.9e-05
#
# P value adjustment method: bonferroni
# Warning message:
#  Ties are present. Quantiles were corrected for ties.
```

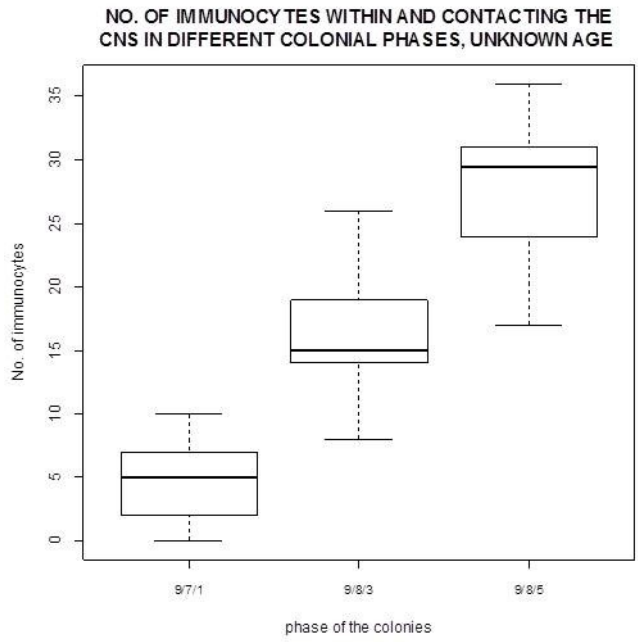

---

2) dataset and analysis of morular cells.

a) morular cells within the CNS.

DATASET

% of apoptotic cells in adult zooids in the early blastogenetic phase (9/7/1)

```
Bs971_Ad_MorIntCNS <- scan()
0 0 1 1 2 1 3 3
```

% of apoptotic cells in adult zooids in the mid blastogenetic phase (9/8/3)

```
Bs983_Ad_MorIntCNS <- scan()
1 8 6 2 6 5 4 3 12 5
```

```
##### % of apoptotic cells in adult zooids in the late blastogenetic phase (9/8/5)

        Bs985_Ad_MorIntCNS <- scan()
        12 3 10 5 9 10 12 8 11 12


#### ANALYSIS

##### procedure for testing the normality distribution of samples

        shapiro.test(Bs971_Ad_MorIntCNS)      # RESULT p-value = 0.1679
        shapiro.test(Bs983_Ad_MorIntCNS)      # RESULT p-value = 0.5438
        shapiro.test(Bs985_Ad_MorIntCNS)      # RESULT p-value = 0.07196


##### procedure for testing the homogeneity of variances among groups

        bartlett.test

                # RESULT        Bartlett's K-squared = 6.3397, df = 2, p-value = 0.04201
                        (*)


##### ANOVA and post-hoc tests

        kruskalTest

                # RESULT
                # Kruskal-Wallis test, chi-squared = 16.631, df = 2, p-value = 0.0002447
                        (***)

                   # Warning message:
                   # Ties are present. Quantiles were corrected for ties.

        kwAllPairsConoverTest

                # RESULT
                #         Pairwise comparisons using Conover's all-pairs test

                #   a       b
                # b 0.004   -
                # c 3.8e-06 0.024

                # P value adjustment method: bonferroni
                # Warning message:
                #  Ties are present. Quantiles were corrected for ties.
```

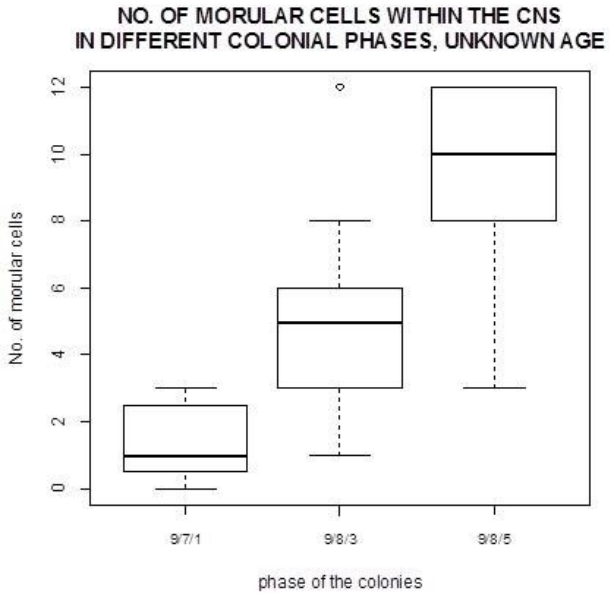

```
### b) morular cells contacting the CNS.

#### DATASET

##### % of apoptotic cells in adult zooids in the early blastogenetic phase (9/7/1)

       Bs971_Ad_MorContCNS <- scan()
       0 0 2 2 3 3 3 3

##### % of apoptotic cells in adult zooids in the mid blastogenetic phase (9/8/3)

       Bs983_Ad_MorContCNS <- scan()
       6 11 12 14 9 9 5 12 13 9

##### % of apoptotic cells in adult zooids in the late blastogenetic phase (9/8/5)

       Bs985_Ad_MorContCNS <- scan()
       13 11 13 10 13 16 11 12 15 17


#### ANALYSIS

##### procedure for testing the normality distribution of samples

       shapiro.test(Bs971_Ad_MorContCNS)     # RESULT p-value = 0.007732 (***)
       shapiro.test(Bs983_Ad_MorContCNS)     # RESULT p-value = 0.5411
       shapiro.test(Bs985_Ad_MorContCNS)     # RESULT p-value = 0.5572


##### procedure for testing the homogeneity of variances among groups

       fligner.test

              # RESULT       Fligner-Killeen:med chi-squared = 4.9093, df = 2, p-value
                     = 0.08589


##### ANOVA and post-hoc tests

       kruskalTest

              # RESULT
              # Kruskal-Wallis test, chi-squared = 19.13, df = 2, p-value = 7.012e-05
                     (***)

                 # Warning message:
                 # Ties are present. Quantiles were corrected for ties.

       kwAllPairsConoverTest

              # RESULT
              #         Pairwise comparisons using Conover's all-pairs test
              #
              #   a       b
              # b 8.3e-05 -
              # c 1.3e-07 0.031
              #
              # P value adjustment method: bonferroni
              # Warning message:
              #  Ties are present. Quantiles were corrected for ties.
```

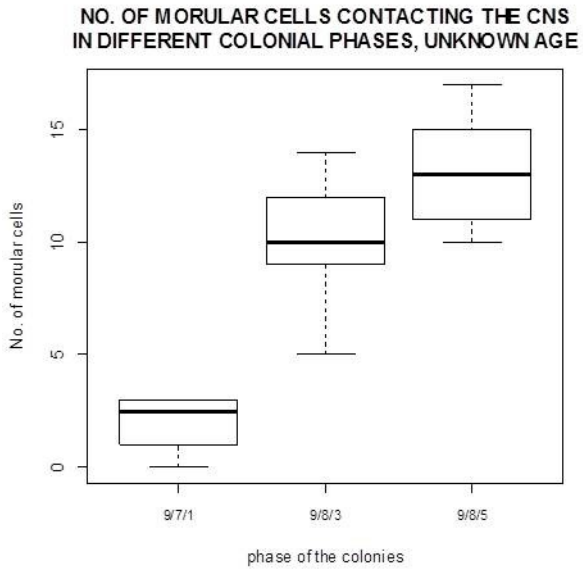

c) morula cells within and contacting the CNS.

DATASET

% of apoptotic cells in adult zooids in the early blastogenetic phase (9/7/1)

```
Bs971_Ad_MorTotCNS <- scan()
0 0 3 3 5 4 6 6
```

% of apoptotic cells in adult zooids in the mid blastogenetic phase (9/8/3)

```
Bs983_Ad_MorTotCNS <- scan()
7 19 18 16 15 14 9 15 25 14
```

% of apoptotic cells in adult zooids in the late blastogenetic phase (9/8/5)

```
Bs985_Ad_MorTotCNS <- scan()
25 14 23 15 22 26 23 20 26 29
```

ANALYSIS

procedure for testing the normality distribution of samples

```
shapiro.test(Bs971_Ad_MorTotCNS)      # RESULT p-value = 0.2026
shapiro.test(Bs983_Ad_MorTotCNS)      # RESULT p-value = 0.6917
shapiro.test(Bs985_Ad_MorTotCNS)      # RESULT p-value = 0.4063
```

procedure for testing the homogeneity of variances among groups

```
bartlett.test

        # RESULT        Bartlett's K-squared = 3.9101, df = 2, p-value = 0.1416
```

ANOVA and post-hoc tests

```
kruskalTest

        # RESULT
        # Kruskal-Wallis test, chi-squared = 19.945, df = 2, p-value = 4.666e-05
                (***)

           # Warning message:
           # Ties are present. Quantiles were corrected for ties.
```

```
kwAllPairsConoverTest

# RESULT
#         Pairwise comparisons using Conover's all-pairs test
#
#   a       b
# b 7.6e-05 -
# c 3.0e-08 0.0062
#
# P value adjustment method: bonferroni
# Warning message:
#  Ties are present. Quantiles were corrected for ties.
```

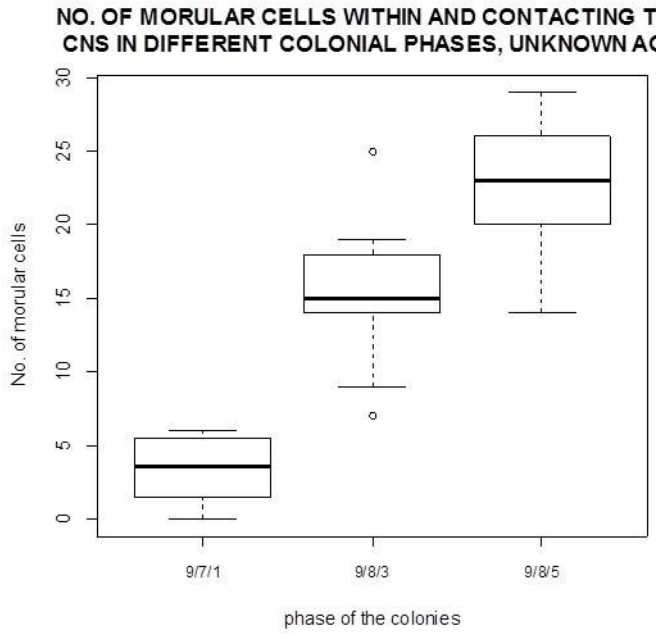

3) Dataset and analysis of phagocytes.

a) phagocytes within the CNS.

DATASET

```
##### % of apoptotic cells in adult zooids in the early blastogenetic phase (9/7/1)

Bs971_Ad_PhaIntCNS <- scan()
0 0 1 1 0 1 1 1

##### % of apoptotic cells in adult zooids in the mid blastogenetic phase (9/8/3)

Bs983_Ad_PhaIntCNS <- scan()
0 0 0 0 0 0 0 0 1 0

##### % of apoptotic cells in adult zooids in the late blastogenetic phase (9/8/5)

Bs985_Ad_PhaIntCNS <- scan()
2 0 3 3 2 1 0 2 2 3
```

ANALYSIS

```
##### procedure for testing the normality distribution of samples

shapiro.test(Bs971_Ad_PhaIntCNS)      # RESULT p-value = 0.0004791 (***)
shapiro.test(Bs983_Ad_PhaIntCNS)      # RESULT p-value = 1.004e-07 (***)
shapiro.test(Bs985_Ad_PhaIntCNS)      # RESULT p-value = 0.0553
```

```
##### procedure for testing the homogeneity of variances among groups

        fligner.test

                # RESULT        Fligner-Killeen:med chi-squared = 6.1599, df = 2, p-value
                        = 0.04596 (*)


##### ANOVA and post-hoc tests

        kruskalTest

                # RESULT
                # Kruskal-Wallis test, chi-squared = 12.986, df = 2, p-value = 0.001514
                        (**)

                   # Warning message:
                   # Ties are present. Quantiles were corrected for ties.

        kwAllPairsConoverTest

                # RESULT
                #          Pairwise comparisons using Conover's all-pairs test
                #
                #   a       b
                # b 0.15644 -
                # c 0.05905 0.00018
                #
                # P value adjustment method: bonferroni
                # Warning message:
                #  Ties are present. Quantiles were corrected for ties.
```

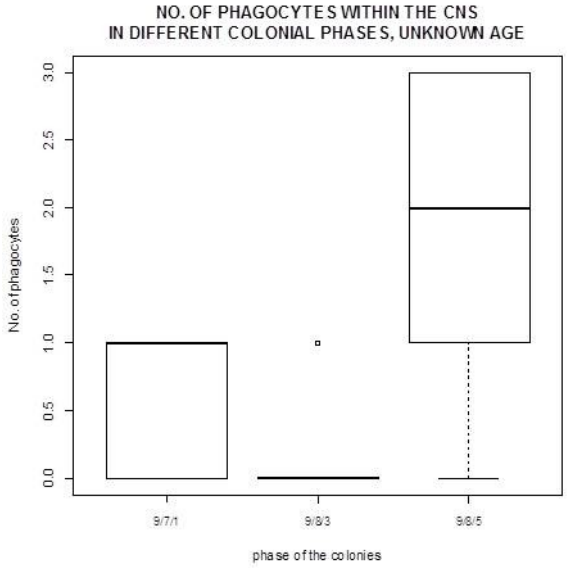


```
### b) phagocytes contacting the CNS.

#### DATASET

##### % of apoptotic cells in adult zooids in the early blastogenetic phase (9/7/1)

        Bs971_Ad_PhaContCNS <- scan()
        0 0 1 0 1 0 1 3

##### % of apoptotic cells in adult zooids in the mid blastogenetic phase (9/8/3)

        Bs983_Ad_PhaContCNS <- scan()
        1 0 1 1 0 0 0 0 0 0

##### % of apoptotic cells in adult zooids in the late blastogenetic phase (9/8/5)
```

```
Bs985_Ad_PhaContCNS <- scan()
5 3 4 4 6 2 1 4 3 4
```

ANALYSIS

```
##### procedure for testing the normality distribution of samples

shapiro.test(Bs971_Ad_PhaContCNS)     # RESULT p-value = 0.007109 (**)
shapiro.test(Bs983_Ad_PhaContCNS)     # RESULT p-value = 4.713e-05 (***)
shapiro.test(Bs985_Ad_PhaContCNS)     # RESULT p-value = 0.7316


##### procedure for testing the homogeneity of variances among groups

fligner.test

        # RESULT        Fligner-Killeen:med chi-squared = 3.5984, df = 2, p-value
                = 0.1654


##### ANOVA and post-hoc tests

kruskalTest

        # RESULT
        # Kruskal-Wallis test, chi-squared = 18.083, df = 2, p-value = 0.0001184
                (***)

           # Warning message:
           # Ties are present. Quantiles were corrected for ties.

kwAllPairsConoverTest

        # RESULT
        #          Pairwise comparisons using Conover's all-pairs test
        #
        #   a       b
        # b 0.79    -
        # c 6.5e-05 1.4e-06
        #
        # P value adjustment method: bonferroni
        # Warning message:
        #  Ties are present. Quantiles were corrected for ties.
```

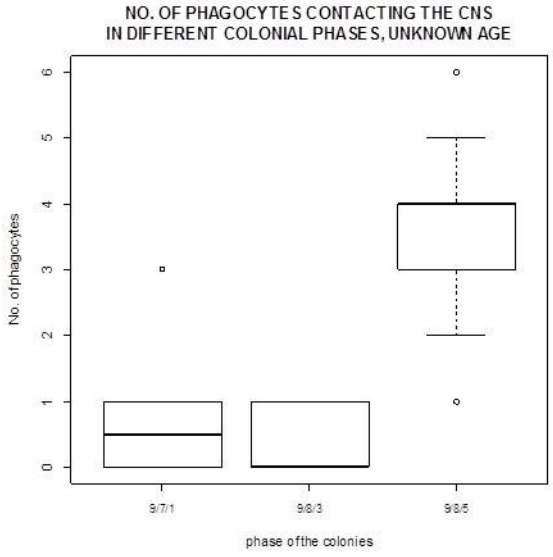


```
### c) phagocytes within and contacting the CNS.
```

```
#### DATASET

##### % of apoptotic cells in adult zooids in the early blastogenetic phase (9/7/1)

       Bs971_Ad_PhaTotCNS <- scan()
       0 0 2 1 1 1 2 4

##### % of apoptotic cells in adult zooids in the mid blastogenetic phase (9/8/3)

       Bs983_Ad_PhaTotCNS <- scan()
       1 0 1 1 0 0 0 0 1 0

##### % of apoptotic cells in adult zooids in the late blastogenetic phase (9/8/5)

       Bs985_Ad_PhaTotCNS <- scan()
       7 3 7 7 8 3 1 6 5 7


#### ANALYSIS

##### procedure for testing the normality distribution of samples

       shapiro.test(Bs971_Ad_PhaTotCNS)      # RESULT p-value = 0.178
       shapiro.test(Bs983_Ad_PhaTotCNS)      # RESULT p-value = 0.0001687 (***)
       shapiro.test(Bs985_Ad_PhaTotCNS)      # RESULT p-value = 0.09029


##### procedure for testing the homogeneity of variances among groups

       fligner.test

              # RESULT       Fligner-Killeen:med chi-squared = 6.1582, df = 2, p-value
                     = 0.046


##### ANOVA and post-hoc tests

       kruskalTest

              # RESULT
              # Kruskal-Wallis test, chi-squared = 17.866, df = 2, p-value = 0.0001319
                     (***)

                 # Warning message:
                 # Ties are present. Quantiles were corrected for ties.

       kwAllPairsConoverTest


              # RESULT
              #         Pairwise comparisons using Conover's all-pairs test
              #
              #   a       b
              # b 0.10643 -
              # c 0.00073 9.5e-07
              #
              # P value adjustment method: bonferroni
              # Warning message:
              #  Ties are present. Quantiles were corrected for ties.
```

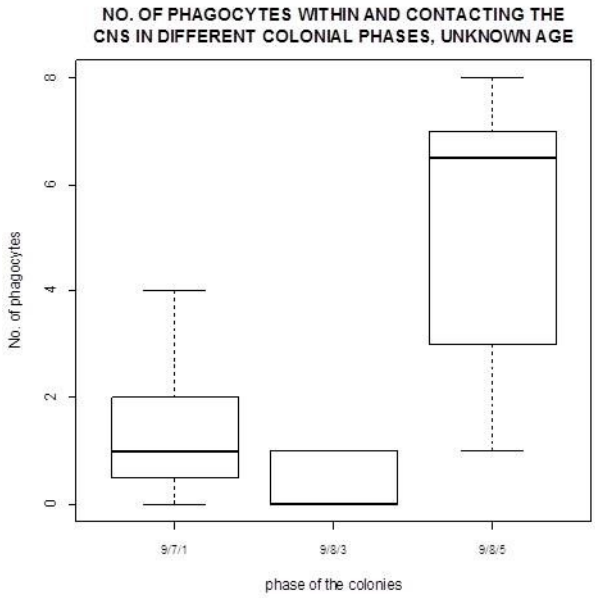

1.4 # Dataset and analysis of the quantification of apoptotic cells in the cerebral ganglion in adult zooids belonging to old colonies (blastogenetic phases 9/7/1, 9/8/3 and 9/8/5)

DATASET

```
### % of apoptotic cells in adult zooids in the early blastogenetic phase (9/7/1)

       Bs971_apopt <- scan()
       0 4.081632653 1.515151515 3.157894737 3.076923077 1.9230769230

### % of apoptotic cells in adult zooids in the mid blastogenetic phase (9/8/3)

       Bs983_apopt <- scan()
       0 7.865168539 0 0 0 0 6.422018349 0 0 0 0 0

### % of apoptotic cells in adult zooids in the late blastogenetic phase (9/8/5)

       Bs985_apopt <- scan()
       11.70212766 14.13043478 1.086956522 1.834862385 0 8.139534884 0 0 2.777777778 0 0
              0 0 0
```

ANALYSIS

```
### procedure for testing the normality distribution of samples

       shapiro.test(Bs971_apopt)      # RESULT p-value = 0.8343
       shapiro.test(Bs983_apopt)      # RESULT p-value = 1.305e-05 (***)
       shapiro.test(Bs985_apopt)      # RESULT p-value = 0.0001395 (***)


### procedure for testing the homogeneity of variances among groups

       fligner.test

              # RESULT       Fligner-Killeen:med chi-squared = 3.3306, df = 2, p-value
                     = 0.1891


### ANOVA and post-hoc tests
```

```
kruskalTest

        # RESULT
        # Kruskal-Wallis test, chi-squared = 18.828, df = 2, p-value = 8.156e-05
               (***)

           # Warning message:
           # Ties are present. Quantiles were corrected for ties.

kwAllPairsConoverTest

        # RESULT
        #         Pairwise comparisons using Conover's all-pairs test

        #   a     b
        # b 0.098 -
        # c 0.642 0.637

        # P value adjustment method: bonferroni
        # Warning message:
        #  Ties are present. Quantiles were corrected for ties.
```

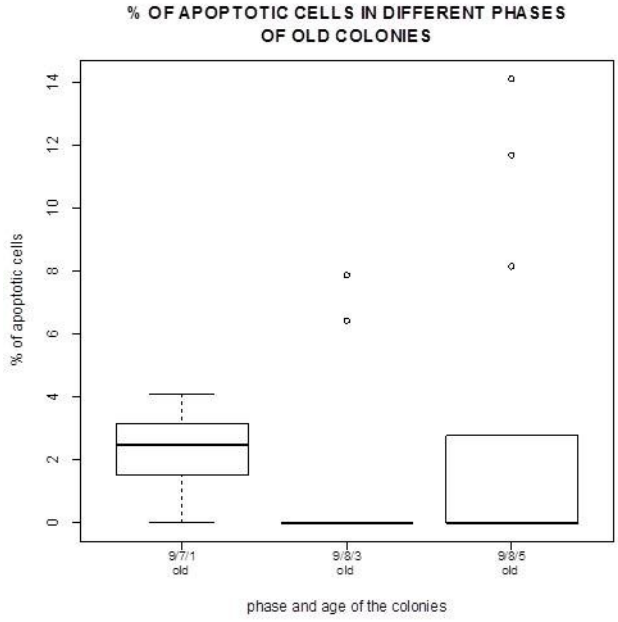

1.5 # Dataset and analysis of the jet pressure values (kpa) to the external wall of the oral siphon that induced the contraction in adult zooids of young colonies (blastogenetic phases 9/7/1, 9/8/3 and 9/8/5)

DATASET

```
### Adult zooids belonging to young colonies in the early blastogenetic phase (9/7/1)

        Bs971young_kPa_Sif_random<- scan()
        014 009 014 012 012 008 015 012 016
        008 011 009 012 006 009 008 010 009
        014 012 011 008 011 009 012 014 013
        014 011 009 016 012 010 013 014 011
```

```
### Adult zooids belonging to young colonies in the mid blastogenetic phase (9/8/3)

       Bs983young_kPa_Sif_random<- scan()
       002 005 005 003 003 004 004 006 002
       007 008 010 009 009 011 004 007 010
       012 017 009 010 014 011 012 011 014
       014 010 011 009 011 014 012 010 014

### Adult zooids belonging to young colonies in the late blastogenetic phase (9/8/5)

       Bs985young_kPa_Sif_random<- scan()
       020 025 023 029 030 027 028 021 024
       025 029 025 026 023 022 024 028 023
       021 024 019 023 026 019 029 020 022
       022 019 017 022 033 020 023 019 021


## ANALYSIS

### procedure for testing the normality distribution of samples

       shapiro.test(Bs971young_kPa_Sif_random)       # RESULT p-value = 0.2594
       shapiro.test(Bs983young_kPa_Sif_random)       # RESULT p-value = 0.1389
       shapiro.test(Bs985young_kPa_Sif_random)       # RESULT p-value = 0.3105


### procedure for testing the homogeneity of variances among groups

       bartlett.test

              # RESULT       Bartlett's K-squared = 7.5107, df = 2, p-value = 0.02339
                     (*)


### ANOVA and post-hoc tests

       kruskalTest

              # RESULT
              # Kruskal-Wallis test, chi-squared = 74.388, df = 2, p-value < 2.2e-16
                     (***)

                 # Warning message:
                 # Ties are present. Quantiles were corrected for ties.

       kwAllPairsConoverTest

              # RESULT
              #            Pairwise comparisons using Conover's all-pairs test

              #   a      b
              # b 0.0099 -
              # c <2e-16<2e-16

              # P value adjustment method: bonferroni
              # Warning message:
              #   Ties are present. Quantiles were corrected for ties
```

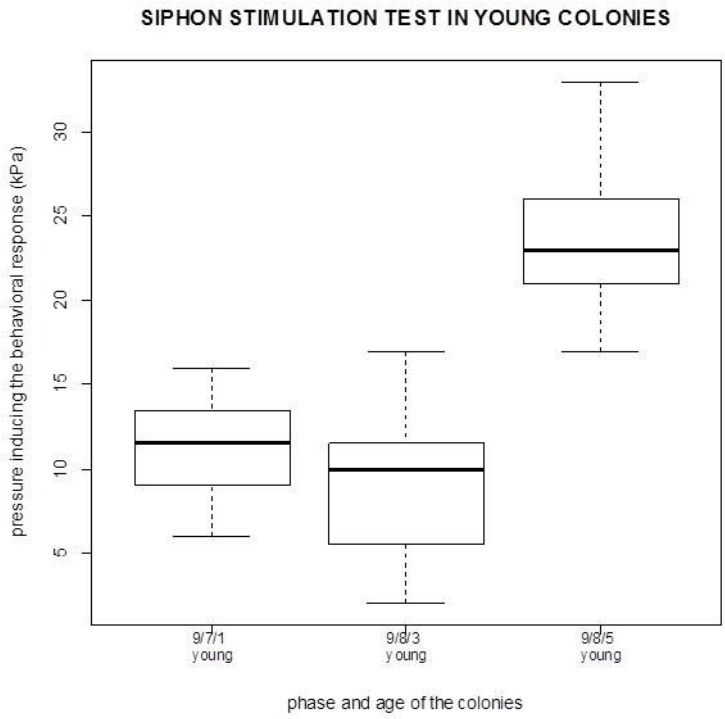

1.6 # Datasets and analyses of the jet pressure values (kPa) to the coronal organ that induced the squirting reaction in adult zooids phases of both young and old colonies (blastogenetic phases 9/7/1, 9/8/3 and 9/8/5).

1) Dataset and analysis depending on phase, but independent from the age.

DATASET

Adult zooids belonging to the early blastogenetic phase (9/7/1)

```
Bs971_kPa_OrgCor_random<- scan()
064 066 065 065 068 067 045 064 060
059 063 061 055 061 060 066 061 062
062 055 053 058 062 066 055 062 064
059 058 062 061 060 059 060 063 058
044 037 042 035 039 044 046 037 040
034 037 036 039 040 042 040 033 037
036 034 039 034 038 036 032 035 036
037 034 036 035 033 038
```

Adult zooids belonging to the mid blastogenetic phase (9/8/3)

```
Bs983_kPa_OrgCor_random<- scan()
024 025 020 021 024 019 019 018 020
020 024 021 023 021 020 020 023 021
023 021 025 019 022 020 021 024 023
023 025 027 024 018 021 025 024 028
016 017 023 022 019 021 014 020 019
014 016 017 015 019 017 020 017 014
015 017 013 019 017 014
```

```
#### Adult zooids belonging to the late blastogenetic phase (9/8/5)

       Bs985_kPa_OrgCor_random<- scan()
       046 053 057 056 057 055 055 059 056
       040 044 041 038 044 039 037 046 039
       049 052 050 045 051 046 044 052 049
       040 049 048 052 049 051 054 052 050
       023 021 022 023 021 024 025 022 025
       021 024 023 025 025 027 022 020 023
       020 027 024 028 023 025


### ANALYSIS

#### procedure for testing the normality distribution of samples

       shapiro.test(Bs971_kPa_OrgCor_random) # RESULT p-value =8.202e-07 (***)
       shapiro.test(Bs983_kPa_OrgCor_random) # RESULT p-value = 0.3042
       shapiro.test(Bs985_kPa_OrgCor_random) # RESULT p-value = 1.306e-05 (***)


#### procedure for testing the homogeneity of variances among groups

       fligner.test

              # RESULT       Fligner-Killeen:med chi-squared = 68.146, df = 2, p-value
                     = 1.594e-15 (***)


#### ANOVA and post-hoc tests

       kruskalTest

              # RESULT
              # Kruskal-Wallis test, chi-squared = 114.94, df = 2, p-value < 2.2e-16
                     (***)

                 # Warning message:
                 # Ties are present. Quantiles were corrected for ties.


       kwAllPairsConoverTest

              # RESULT
              #         Pairwise comparisons using Conover's all-pairs test

              # a       b
              # b < 2e-16 -
              # c 3.6e-07 < 2e-16
              #
              # P value adjustment method: bonferroni
              # Warning message:
              #  Ties are present. Quantiles were corrected for ties.
```

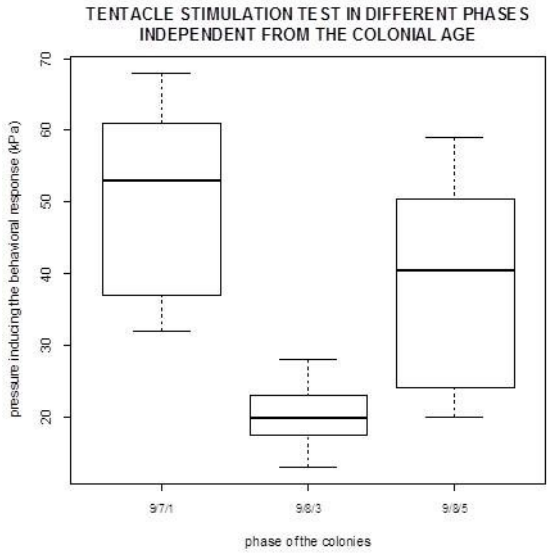

2) Dataset and analysis depending on age and phase.

DATASET

Adult zooids belonging to old colonies in the early blastogenetic phase (9/7/1)

```
Bs971old_kPa_OrgCor_random<- scan()
064 066 065 065 068 067 045 064 060
059 063 061 055 061 060 066 061 062
062 055 053 058 062 066 055 062 064
059 058 062 061 060 059 060 063 058
```

Adult zooids belonging to young colonies in the early blastogenetic phase (9/7/1)

```
Bs971young_kPa_OrgCor_random<- scan()
044 037 042 035 039 044 046 037 040
034 037 036 039 040 042 040 033 037
036 034 039 034 038 036 032 035 036
037 034 036 035 033 038
```

Adult zooids belonging to old colonies in the mid blastogenetic phase (9/8/3)

```
Bs983old_kPa_OrgCor_random<- scan()
024 025 020 021 024 019 019 018 020
020 024 021 023 021 020 020 023 021
023 021 025 019 022 020 021 024 023
023 025 027 024 018 021 025 024 028
```

Adult zooids belonging to young colonies in the mid blastogenetic phase (9/8/3)

```
Bs983young_kPa_OrgCor_random<- scan()
016 017 023 022 019 021 014 020 019
014 016 017 015 019 017 020 017 014
015 017 013 019 017 014
```

Adult zooids belonging to old colonies in the late blastogenetic phase (9/8/5)

```
Bs985old_kPa_OrgCor_random<- scan()
046 053 057 056 057 055 055 059 056
040 044 041 038 044 039 037 046 039
049 052 050 045 051 046 044 052 049
040 049 048 052 049 051 054 052 050
```

Adult zooids belonging to young colonies in the late blastogenetic phase (9/8/5)

```
Bs985young_kPa_OrgCor_random<- scan()
023 021 022 023 021 024 025 022 025
```

```
021 024 023 025 025 027 022 020 023
020 027 024 028 023 025
```

ANALYSIS

```
#### procedure for testing the normality distribution of samples

shapiro.test(Bs971old_kPa_OrgCor_random)            # RESULT p-value = 0.01099
       (**)
shapiro.test(Bs971young_kPa_OrgCor_random)   # RESULT p-value = 0.1017
shapiro.test(Bs983old_kPa_OrgCor_random)            # RESULT p-value = 0.1433
shapiro.test(Bs983young_kPa_OrgCor_random)   # RESULT p-value = 0.3154
shapiro.test(Bs985old_kPa_OrgCor_random)            # RESULT p-value = 0.2125
shapiro.test(Bs985young_kPa_OrgCor_random)   # RESULT p-value = 0.3985


#### procedure for testing the homogeneity of variances among groups

fligner.test

       # RESULT       Fligner-Killeen:med chi-squared = 30.564, df = 5, p-value
              = 1.142e-05 (***)


#### ANOVA and post-hoc tests

kruskalTest

       # RESULT
       # Kruskal-Wallis test, chi-squared = 172.98, df = 5, p-value < 2.2e-16
              (***)

          # Warning message:
          # Ties are present. Quantiles were corrected for ties.

kwAllPairsConoverTest

       # RESULT
       #        Pairwise comparisons using Conover's all-pairs test

       #   a       b       c       d       e
       # b < 2e-16 -       -       -       -
       # c < 2e-16 < 2e-16 -       -       -
       # d < 2e-16 < 2e-16 2.1e-11 -       -
       # e 2.6e-16 1.6e-13 < 2e-16 < 2e-16 -
       # f < 2e-16 < 2e-16 0.14    4.7e-16 < 2e-16

       # P value adjustment method: bonferroni
       # Warning message:
       #  Ties are present. Quantiles were corrected for ties.
```

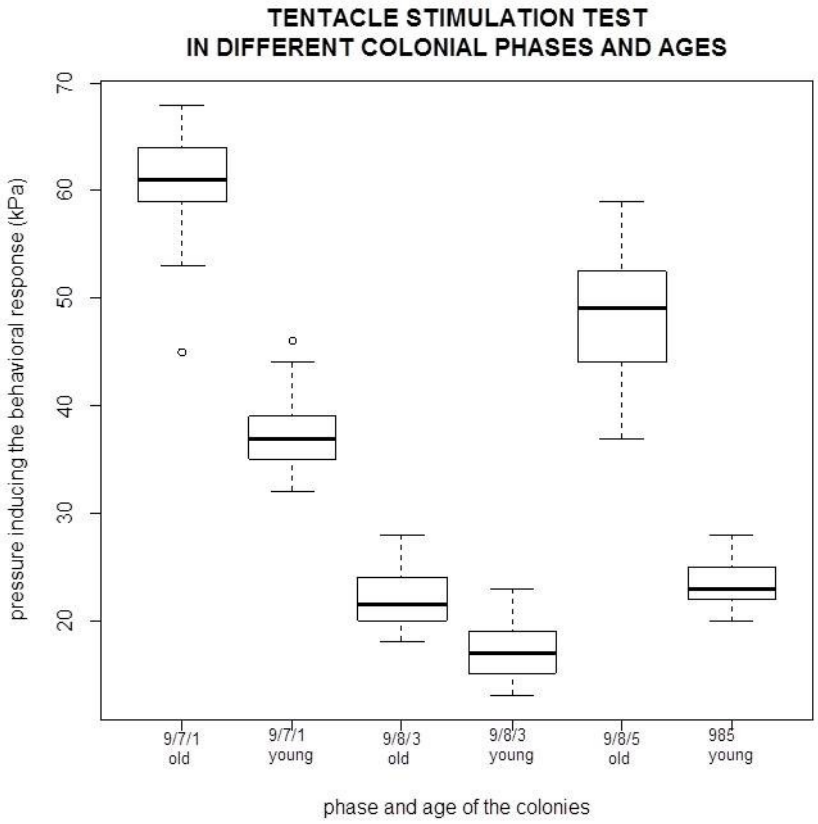

3) Dataset and analysis depending on age, but independent from the phase.

DATASET

Adult zooids belonging to old colonies

```
Bs_old_kPa_OrgCor_random<- scan()
064 066 065 065 068 067 045 064 060
059 063 061 055 061 060 066 061 062
062 055 053 058 062 066 055 062 064
059 058 062 061 060 059 060 063 058
024 025 020 021 024 019 019 018 020
020 024 021 023 021 020 020 023 021
023 021 025 019 022 020 021 024 023
023 025 027 024 018 021 025 024 028
046 053 057 056 057 055 055 059 056
040 044 041 038 044 039 037 046 039
049 052 050 045 051 046 044 052 049
040 049 048 052 049 051 054 052 050
```

Adult zooids belonging to young colonies

```
Bs_young_kPa_OrgCor_random<- scan()
044 037 042 035 039 044 046 037 040
034 037 036 039 040 042 040 033 037
036 034 039 034 038 036 032 035 036
037 034 036 035 033 038 016 017 023
022 019 021 014 020 019 014 016 017
015 019 017 020 017 014 015 017 013
019 017 014 023 021 022 023 021 024
025 022 025 021 024 023 025 025 027
022 020 023 020 027 024 028 023 025
```

ANALYSIS

procedure for testing the normality distribution of samples

```
shapiro.test(Bs_old_kPa_OrgCor_random)        # RESULT p-value = 3.384e-08 (***)
shapiro.test(Bs_young_kPa_OrgCor_random)      # RESULT p-value = 0.0002065 (***)
```

procedure for testing the homogeneity of variances among groups

```
fligner.test

        # RESULT        Fligner-Killeen:med chi-squared = 24.657, df = 1, p-value
                = 6.849e-07 (***)
```

test to compare the mean of the two samples

```
wilcox.test

        # RESULT
        #     Wilcoxon rank sum test with continuity correction

        #     W = 6833.5, p-value = 3.822e-11 (***)
```

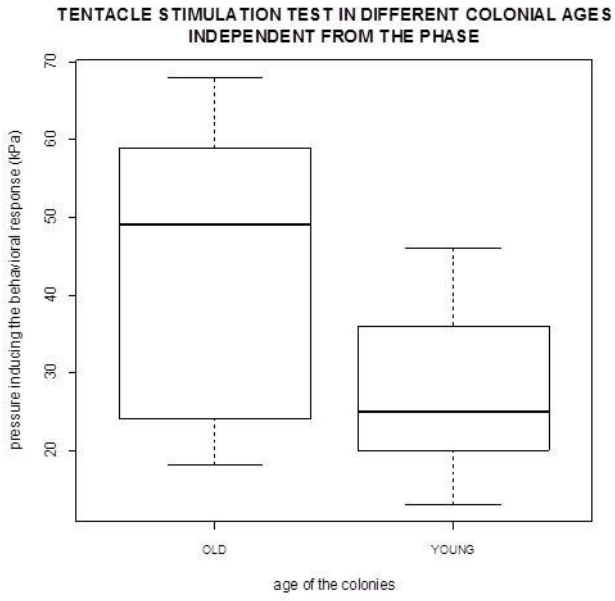

1.7 # Datasets and analyses of the quantification of primary sensory cells in the internal layer of the oral siphon in adult zooids belonging to both young and old colonies (blastogenetic phases 9/7/1, 9/8/3 and 9/8/5)

1) Dataset and analysis depending on phase, but independent from age

DATASET

Adult zooids belonging to the early blastogenetic phase (9/7/1)

```
Bs971youngold_prsen_sif_random<- scan()
054 079 060 093 054 057
041 044 043 043 047 041
```

```
#### Adult zooids belonging to the mid blastogenetic phase (9/8/3)

       Bs983youngold_prsen_sif_random<- scan()
       092 107 105 122 098 110
       098 094 143 119 116 113

#### Adult zooids belonging to the late blastogenetic phase (9/8/5)

       Bs985youngold_prsen_sif_random<- scan()
       120 108 102 090 086 099
       064 084 081 087 091 089

### ANALYSIS

#### procedure for testing the normality distribution of samples

       shapiro.test(Bs971youngold_prsen_sif_random) # RESULT p-value = 0.01081 (**)
       shapiro.test(Bs983youngold_prsen_sif_random) # RESULT p-value = 0.3795
       shapiro.test(Bs985youngold_prsen_sif_random) # RESULT p-value = 0.8019


#### procedure for testing the homogeneity of variances among groups

       fligner.test

              # RESULT       Fligner-Killeen:med chi-squared = 0.41412, df = 2, p-value
                     = 0.813


#### ANOVA and post-hoc tests

       kruskalTest

              # RESULT
              # Kruskal-Wallis test, chi-squared = 24.293, df = 2, p-value = 5.306e-06
                     (***)

                 # Warning message:
                 # Ties are present. Quantiles were corrected for ties.

       kwAllPairsConoverTest

              # RESULT
              #         Pairwise comparisons using Conover's all-pairs test

              #   a       b
              # b 1.8e-09 -
              # c 4.5e-05 0.0037

              # P value adjustment method: bonferroni
              #  Warning message:
              #   Ties are present. Quantiles were corrected for ties.
```

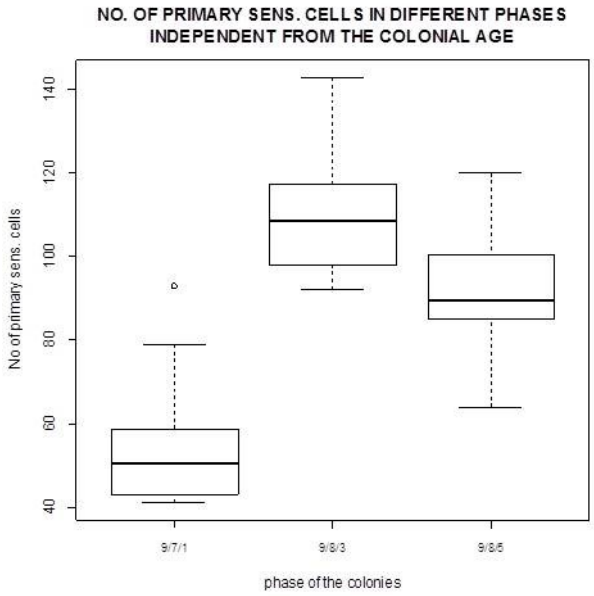

2) Dataset and analysis depending on age and phase.

DATASET

Adult zooids belonging to old colonies in the early blastogenetic phase (9/7/1)

```
Bs971old_prsen_sif_random<- scan()
041 044 043 043 047 041
```

Adult zooids belonging to young colonies in the early blastogenetic phase (9/7/1)

```
Bs971young_prsen_sif_random<- scan()
054 079 060 093 054 057
```

Adult zooids belonging to old colonies in the mid blastogenetic phase (9/8/3)

```
Bs983old_prsen_sif_random<- scan()
098 094 143 119 116 113
```

Adult zooids belonging to young colonies in the mid blastogenetic phase (9/8/3)

```
Bs983young_prsen_sif_random<- scan()
092 107 105 122 098 110
```

Adult zooids belonging to old colonies in the late blastogenetic phase (9/8/5)

```
Bs985old_prsen_sif_random<- scan()
064 084 081 087 091 089
```

Adult zooids belonging to young colonies in the late blastogenetic phase (9/8/5)

```
Bs985young_prsen_sif_random<- scan()
120 108 102 090 086 099
```

ANALYSIS

procedure for testing the normality distribution of samples

```
shapiro.test(Bs971old_prsen_sif_random)       # RESULT p-value = 0.3157
shapiro.test(Bs971young_prsen_sif_random)     # RESULT p-value = 0.06342
shapiro.test(Bs983old_prsen_sif_random)       # RESULT p-value = 0.5736
shapiro.test(Bs983young_prsen_sif_random)     # RESULT p-value = 0.9392
shapiro.test(Bs985old_prsen_sif_random)       # RESULT p-value = 0.0888
shapiro.test(Bs985young_prsen_sif_random)     # RESULT p-value = 0.8983
```

```
#### procedure for testing the homogeneity of variances among groups

        bartlett.test

                # RESULT        Bartlett's K-squared = 14.315, df = 5, p-value = 0.01373
                        (*)


#### ANOVA and post-hoc tests

        kruskalTest

                # RESULT
                # Kruskal-Wallis test, chi-squared = 28.47, df = 5, p-value = 2.945e-05
                        (***)

                   # Warning message:
                   # Ties are present. Quantiles were corrected for ties.

        kwAllPairsConoverTest

                # RESULT
                #         Pairwise comparisons using Conover's all-pairs test

                #   a       b       c       d       e
                # b 0.16833 -       -       -       -
                # c 4.7e-09 5.3e-06 -       -       -
                # d 3.6e-08 5.3e-05 1.00000 -       -
                # e 0.00494 1.00000 0.00024 0.00238 -
                # f 4.5e-07 0.00082 1.00000 1.00000 0.03303

                # P value adjustment method: bonferroni
                # Warning message:
                #  Ties are present. Quantiles were corrected for ties.
```

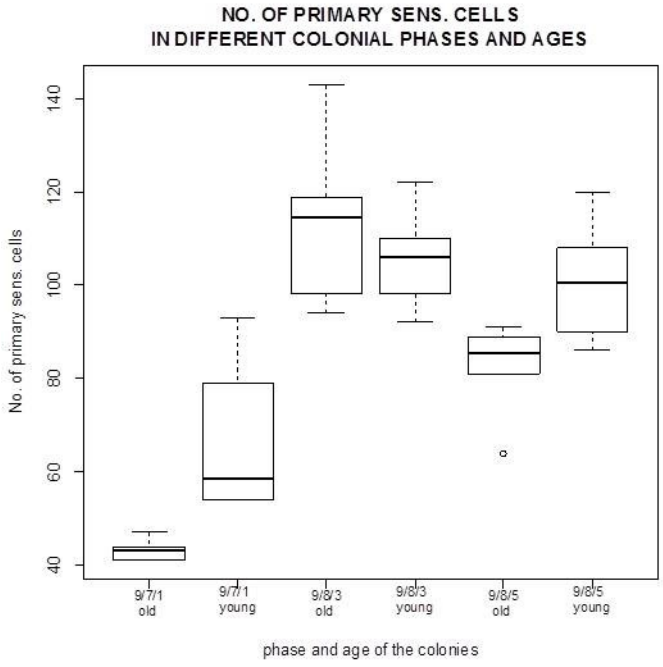

3) Dataset and analysis depending on age, but independent from the phase.

DATASET

Adult zooids belonging to young colonies

```
Bs_young_prsen_sif_random<- scan()
054 079 060 093 054 057
092 107 105 122 098 110
120 108 102 090 086 099
```

Adult zooids belonging to old colonies

```
Bs_old_prsen_sif_random<- scan()
041 044 043 043 047 041
098 094 143 119 116 113
064 084 081 087 091 089
```

ANALYSIS

procedure for testing the normality distribution of samples

```
shapiro.test(Bs_young_prsen_sif_random)      # RESULT p-value = 0.07799
shapiro.test(Bs_old_prsen_sif_random) # RESULT p-value = 0.9928
```

procedure for testing the homogeneity of variances among groups

```
bartlett.test

        # RESULT       Bartlett's K-squared = 2.199, df = 1, p-value = 0.1381
```

procedure to compare the mean of the two samples

```
wilcox.test

        # RESULT
        # Wilcoxon rank sum test with continuity correction

        # W = 206.5, p-value = 0.1638
```

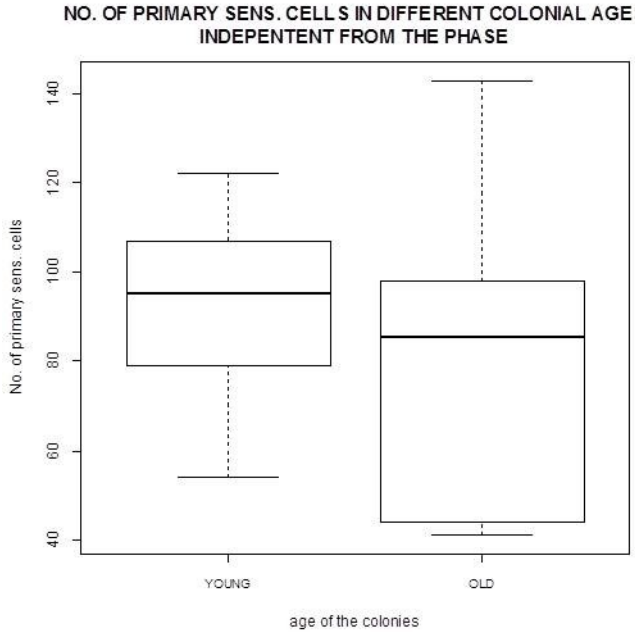

1.8 # Datasets and analyses of the quantification of neurons in the cerebral ganglion in adult zooids belonging to both young colonies and old colonies (blastogenetic phases 9/7/1, 9/8/3 and 9/8/5).

1) dataset and analysis depending on age and phase.

DATASET

Number of neurons in adult zooids belonging to old colonies in the early blastogenetic phase (9/7/1)

```
Bs971old_neur_random<- scan()
0819 0786 0802 0810 0817 0834 0777 0831
```

Number of neurons in adult zooids belonging to young colonies in the early blastogenetic phase (9/7/1)

```
Bs971young_neur_random<- scan()
0658 0710 0681 0674 0662 0693
```

Number of neurons in adult zooids belonging to old colonies in the mid blastogenetic phase (9/8/3)

```
Bs983old_neur_random<- scan()
0936 0928 0910 0894 0887 0896
```

Number of neurons in adult zooids belonging to young colonies in the mid blastogenetic phase (9/8/3)

```
Bs983young_neur_random<- scan()
1029 1021 1046 1052 1004 0921 0952
```

Number of neurons in adult zooids belonging to old colonies in the late blastogenetic phase (9/8/5)

```
Bs985old_neur_random<- scan()
0604 0591 0597 0599 0588
```

Number of neurons in adult zooids belonging to young colonies in the late blastogenetic phase (9/8/5)

```
Bs985young_neur_random<- scan()
0896 0946 0958 0907 0860 0906
```

ANALYSIS

procedure for testing the normality distribution of samples

```
shapiro.test(Bs971old_neur_random)            # RESULT p-value = 0.6535
shapiro.test(Bs971young_neur_random)  # RESULT p-value = 0.7834
shapiro.test(Bs983old_neur_random)            # RESULT p-value = 0.4285
shapiro.test(Bs983young_neur_random)  # RESULT p-value = 0.255
shapiro.test(Bs985old_neur_random)            # RESULT p-value = 0.8739
shapiro.test(Bs985young_neur_random)  # RESULT p-value = 0.7037
```

procedure for testing the homogeneity of variances among groups

```
bartlett.test

        # RESULT        Bartlett's K-squared = 16.284, df = 5, p-value = 0.006079
                (***)
```

ANOVA and post-hoc tests

```
kruskalTest

        # RESULT
```

```
# Kruskal-Wallis test, chi-squared = 34.357, df = 5, p-value = 2.021e-06
       (***)

   # Warning message:
   # Ties are present. Quantiles were corrected for ties.
```

```
kwAllPairsConoverTest
```

```
# RESULT
#        Pairwise comparisons using Conover's all-pairs test

#   a       b       c       d       e
# b 0.00445 -       -       -       -
# c 3.4e-05 2.7e-09 -       -       -
# d 1.4e-11 1.9e-14 0.00031 -       -
# e 1.4e-06 0.11546 8.1e-12 3.3e-16 -
# f 6.3e-06 6.8e-10 1.00000 0.00155 2.6e-12

# P value adjustment method: bonferroni
# Warning message:
#  Ties are present. Quantiles were corrected for ties.
```

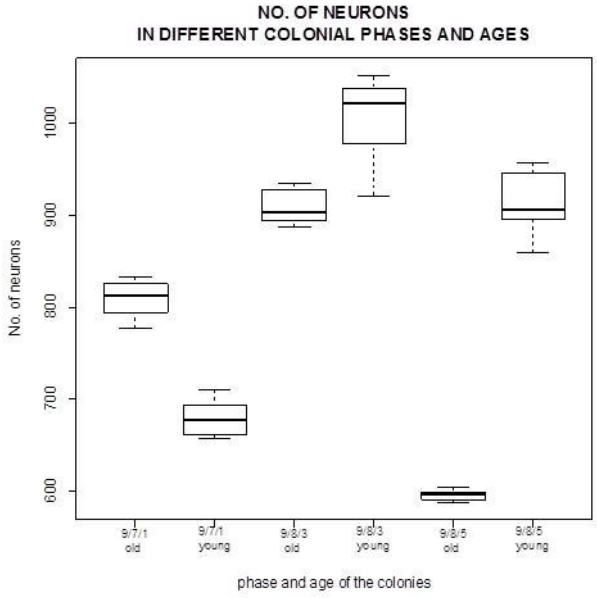

2) Dataset and analysis depending on phase, but independently from the age.

DATASET

Number of neurons in adult zooids in the early blastogenetic phase (9/7/1)

```
Bs971_neur_random<- scan()
0819 0786 0802 0810 0817 0834 0777 0831
0658 0710 0681 0674 0662 0693
```

Number of neurons in adult zooids in the mid blastogenetic phase (9/8/3)

```
Bs983_neur_random<- scan()
0936 0928 0910 0894 0887 0896
1029 1021 1046 1052 1004 0921 0952
```

Number of neurons in adult zooids in the late blastogenetic phase (9/8/5)

```
Bs985_neur_random<- scan()
0604 0591 0597 0599 0588
0896 0946 0958 0907 0860 0906
```

ANALYSIS

procedure for testing the normality distribution of samples

```
shapiro.test(Bs971_neur_random)        # RESULT p-value = 0.0196 (*)
shapiro.test(Bs983_neur_random)        # RESULT p-value = 0.06708
shapiro.test(Bs985_neur_random)        # RESULT p-value = 0.002418 (**)
```

procedure for testing the homogeneity of variances among groups

```
fligner.test

        # RESULT        Fligner-Killeen:med chi-squared = 6.6161, df = 2, p-value
                = 0.03659 (*)
```

ANOVA and post-hoc tests

```
kruskalTest

        # RESULT
        # Kruskal-Wallis test, chi-squared = 18.828, df = 2, p-value = 8.156e-05
                (***)

           # Warning message:
           # Ties are present. Quantiles were corrected for ties.

kwAllPairsConoverTest

        # RESULT
        #         Pairwise comparisons using Conover's all-pairs test

        #   a       b
        # b 5.2e-06 -
        # c 0.95200 0.00029

        # P value adjustment method: bonferroni
        # Warning message:
        # Ties are present. Quantiles were corrected for ties.
```

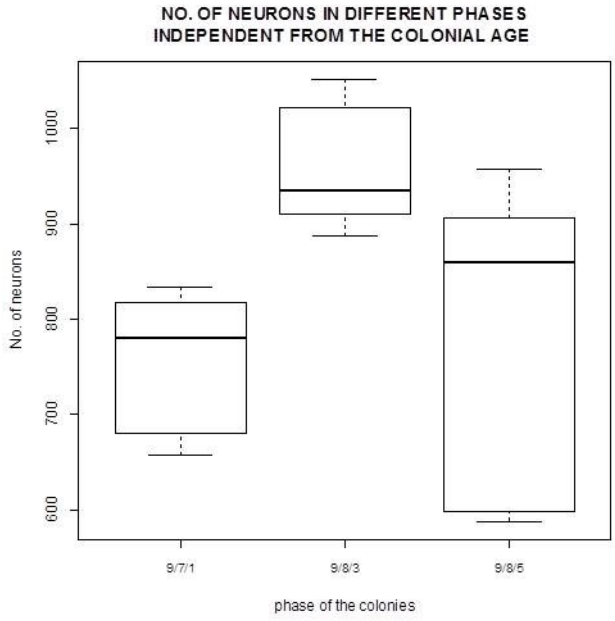

3) dataset and analysis depending on age, but independently from the phase.

DATASET

Number of neurons in adult zooids belonging to old colonies

```
Bs_old_neur_random<- scan()
0819 0786 0802 0810 0817 0834 0777 0831
```

```
0936 0928 0910 0894 0887 0896
0604 0591 0597 0599 0588
```

Number of neurons in adult zooids belonging to young colonies

```
Bs_young_neur_random<- scan()
0658 0710 0681 0674 0662 0693
1029 1021 1046 1052 1004 0921 0952
0896 0946 0958 0907 0860 0906
```

ANALYSIS

procedure for testing the normality distribution of samples

```
shapiro.test(Bs_old_neur_random)      # RESULT p-value = 0.004833 (**)
shapiro.test(Bs_young_neur_random)    # RESULT p-value = 0.01066 (**)
```

procedure for testing the homogeneity of variances among groups

```
fligner.test

        # RESULT       Fligner-Killeen:med chi-squared = 1.0885, df = 1, p-value
                = 0.2968
```

procedure to compare the mean of the two samples

```
wilcox.test

        # RESULT
        Wilcoxon rank sum test with continuity correction,
        W = 101.5, p-value = 0.02191 (*)
```

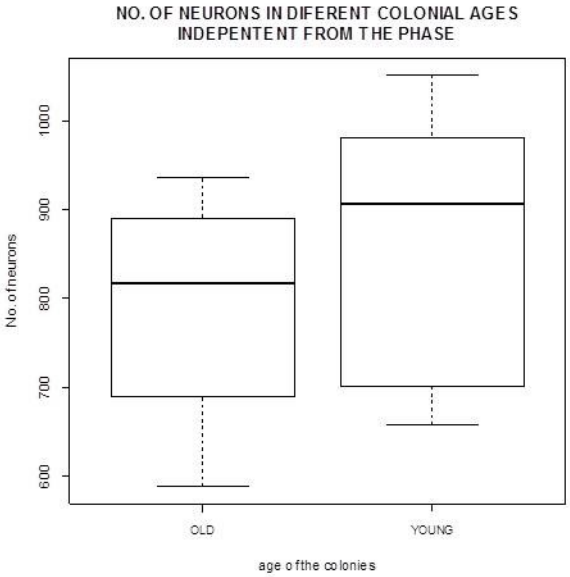

SUPPLEMENTARY MATERIAL 2.1

Supplementary Material 2.1: Molecular signatures of neurogenesis. A. Enrichment plot showing the increase in proportion of genes associated with the neuron development GO term that are active at different times in the blastogenetic cycle. Solid line is the proportion of active selected genes with the expected mean subtracted. Light and dark bands correspond to 50% and 99% confidence intervals, respectively. Red are the genes with putative homology in *B. schlosseri*. Blue are the genes expressed in the brain. B. Heatmap of neuron development associated genes that are differentially expressed throughout the blastogenetic cycle clustered by the gene expression pattern. Labels on the left are the *B. schlosseri* geneIDs and their homology, on the right are times at which the genes were found to be up regulated. Values plotted are the log-transformed counts/million, normalized to have a mean of zero (red = high, white = average, blue = low). **C-D**: as above, but for neuron differentiation.

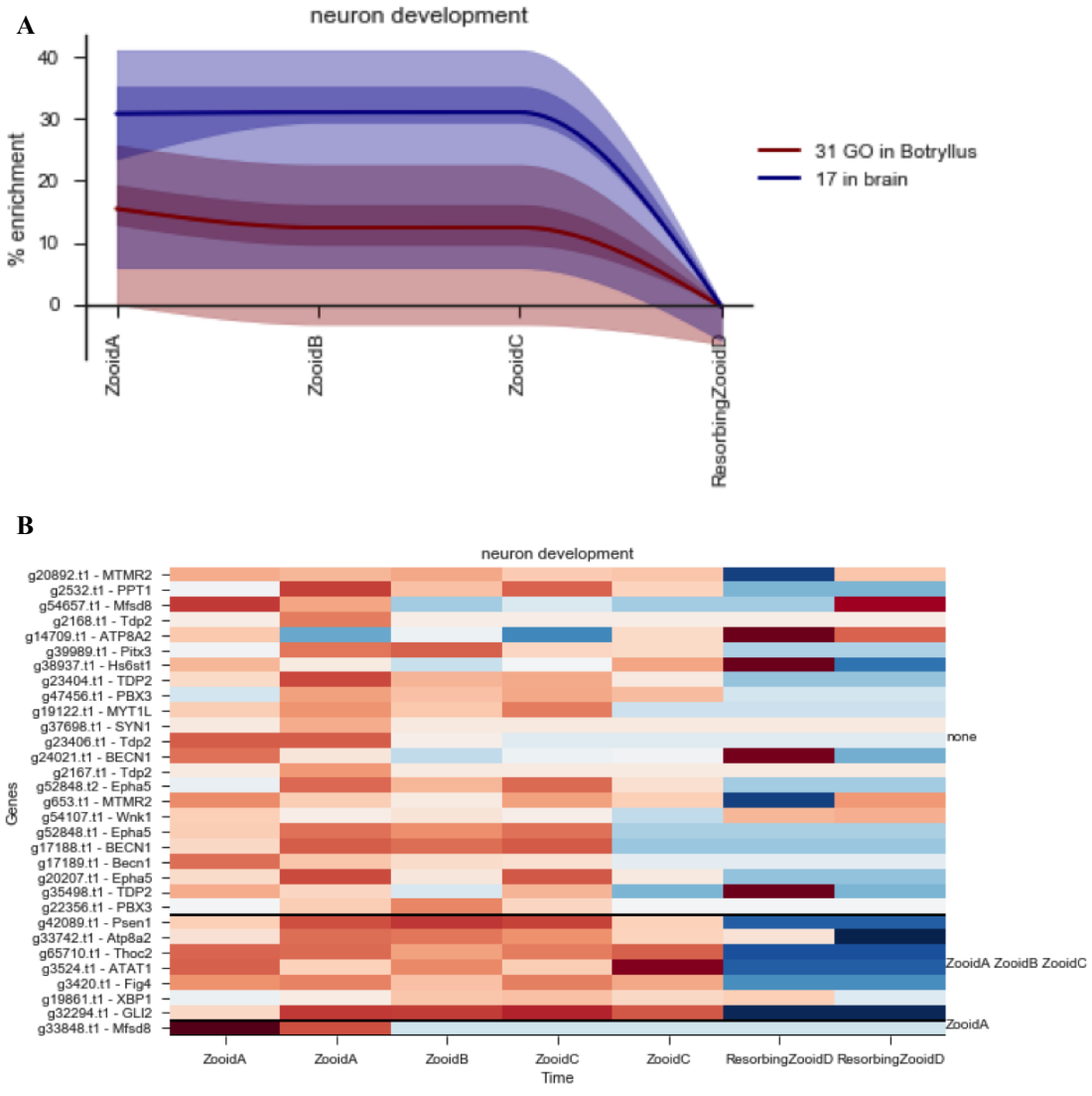

C

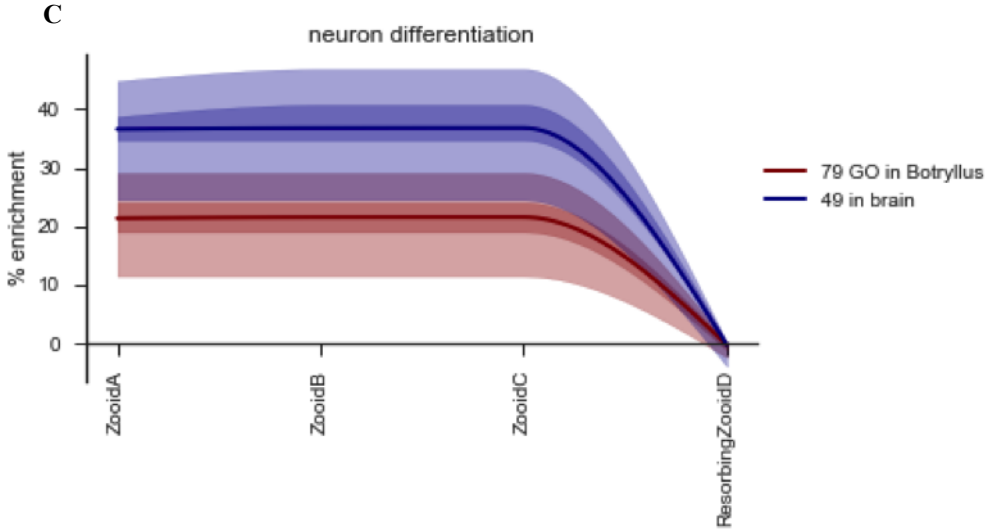
neuron differentiation
% enrichment
40
30
20
10
0
ZooidA
ZooidB
ZooidC
ResorbingZooidD
79 GO in Botryllus
49 in brain

D

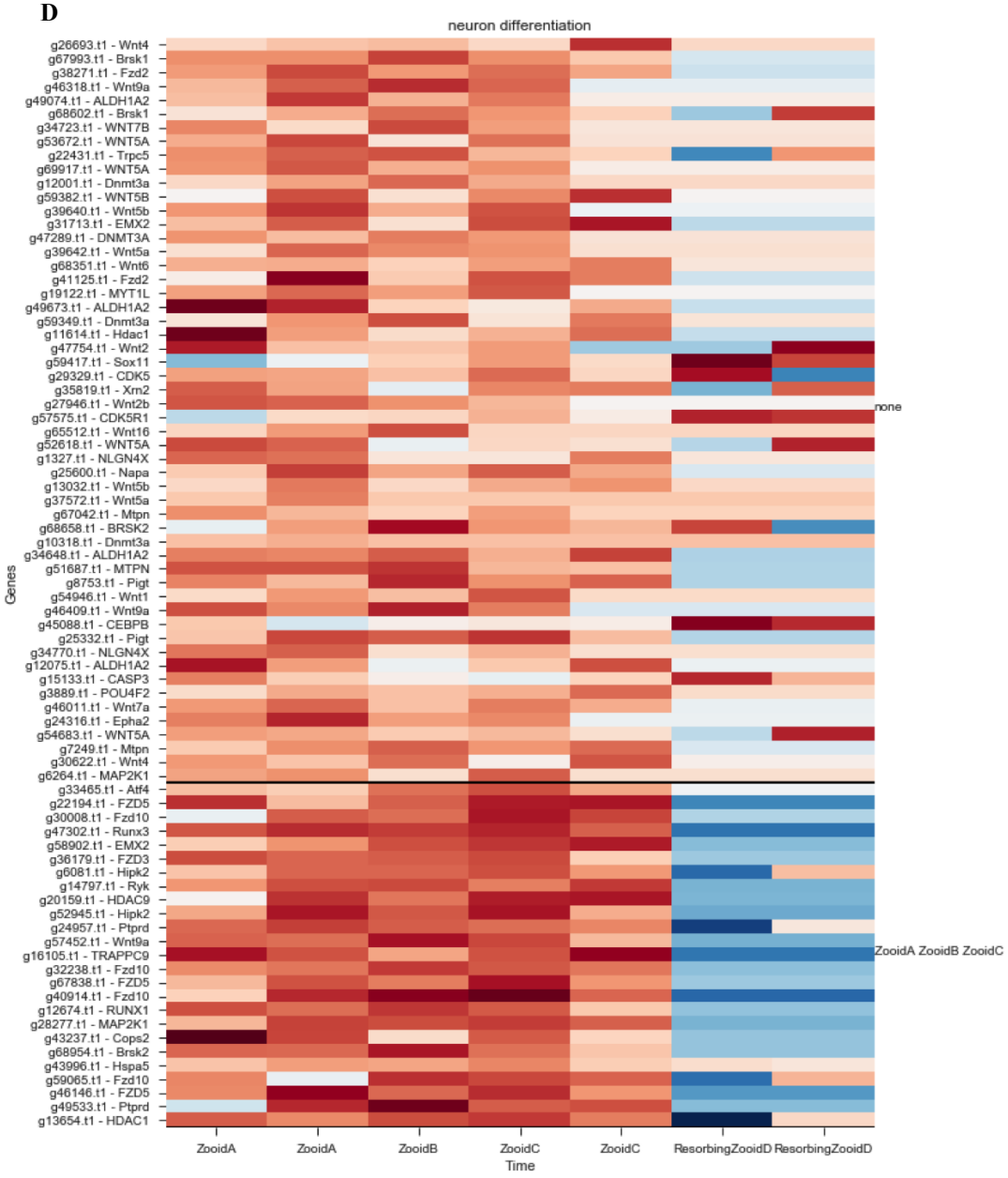
neuron differentiation
Genes
g26693.t1 - Wnt4
g67993.t1 - Brsk1
g38271.t1 - Fzd2
g46318.t1 - Wnt9a
g49074.t1 - ALDH1A2
g68602.t1 - Brsk1
g34723.t1 - WNT7B
g53672.t1 - WNT5A
g22431.t1 - Trpc5
g69917.t1 - WNT5A
g12001.t1 - Dnmt3a
g59382.t1 - WNT5B
g39640.t1 - Wnt5b
g31713.t1 - EMX2
g47289.t1 - DNMT3A
g39642.t1 - Wnt5a
g68351.t1 - Wnt6
g41125.t1 - Fzd2
g19122.t1 - MYT1L
g49673.t1 - ALDH1A2
g59349.t1 - Dnmt3a
g11614.t1 - Hdac1
g47754.t1 - Wnt2
g59417.t1 - Sox11
g29329.t1 - CDK5
g35819.t1 - Xrn2
g27946.t1 - Wnt2b
g57575.t1 - CDK5R1
g65512.t1 - Wnt16
g52618.t1 - WNT5A
g1327.t1 - NLGN4X
g25600.t1 - Napa
g13032.t1 - Wnt5b
g37572.t1 - Wnt5a
g67042.t1 - Mtpn
g68658.t1 - BRSK2
g10318.t1 - Dnmt3a
g34648.t1 - ALDH1A2
g51687.t1 - MTPN
g8753.t1 - Pigt
g54946.t1 - Wnt1
g46409.t1 - Wnt9a
g45088.t1 - CEBPB
g25332.t1 - Pigt
g34770.t1 - NLGN4X
g12075.t1 - ALDH1A2
g15133.t1 - CASP3
g3889.t1 - POU4F2
g46011.t1 - Wnt7a
g24316.t1 - Epha2
g54683.t1 - WNT5A
g7249.t1 - Mtpn
g30622.t1 - Wnt4
g6264.t1 - MAP2K1
g33465.t1 - Atf4
g22194.t1 - FZD5
g30008.t1 - Fzd10
g47302.t1 - Runx3
g58902.t1 - EMX2
g36179.t1 - FZD3
g6081.t1 - Hipk2
g14797.t1 - Ryk
g20159.t1 - HDAC9
g52945.t1 - Hipk2
g24957.t1 - Ptprd
g57452.t1 - Wnt9a
g16105.t1 - TRAPPC9
g32238.t1 - Fzd10
g67838.t1 - FZD5
g40914.t1 - Fzd10
g12674.t1 - RUNX1
g28277.t1 - MAP2K1
g43237.t1 - Cops2
g68954.t1 - Brsk2
g43996.t1 - Hspa5
g59065.t1 - Fzd10
g46146.t1 - FZD5
g49533.t1 - Ptprd
g13654.t1 - HDAC1
none
ZooidA ZooidB ZooidC
ZooidA
ZooidA
ZooidB
ZooidC
ZooidC
ResorbingZooidD
ResorbingZooidD
Time

SUPPLEMENTARY MATERIAL 2.2

Figures: Expression of neurodegenerative diseases associated genes in colonies of different ages. Upper panels: Venn diagram showing the number of genes associated with the titled disease with putative homologies and the number of these that are expressed in the brain. Lower panels: Heatmaps of gene expression of the brain-expressed genes in young (red) and old (blue) colonies. Values are log transformed and normalized (mean = 0, standard deviation = 1). Red = high, blue = low.

Parkinson Disease

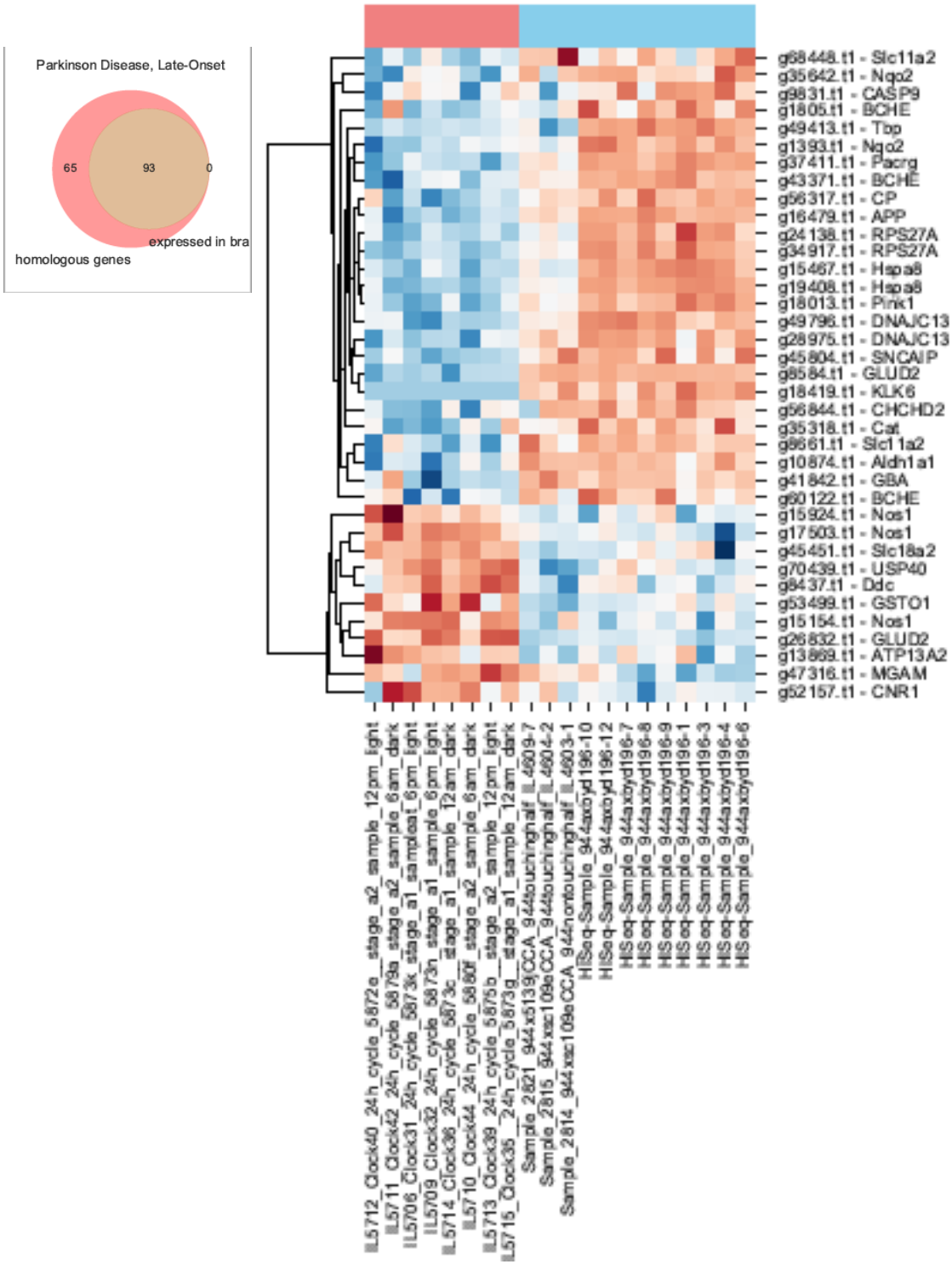

Muscolar Distrophy

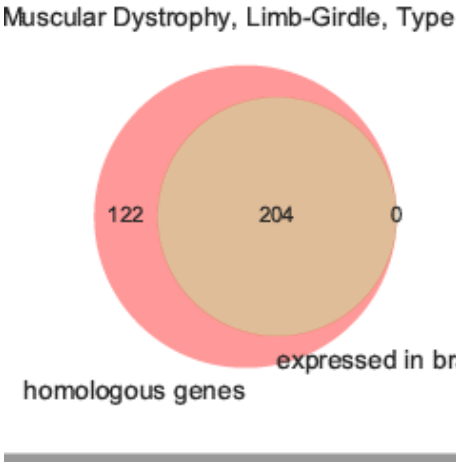

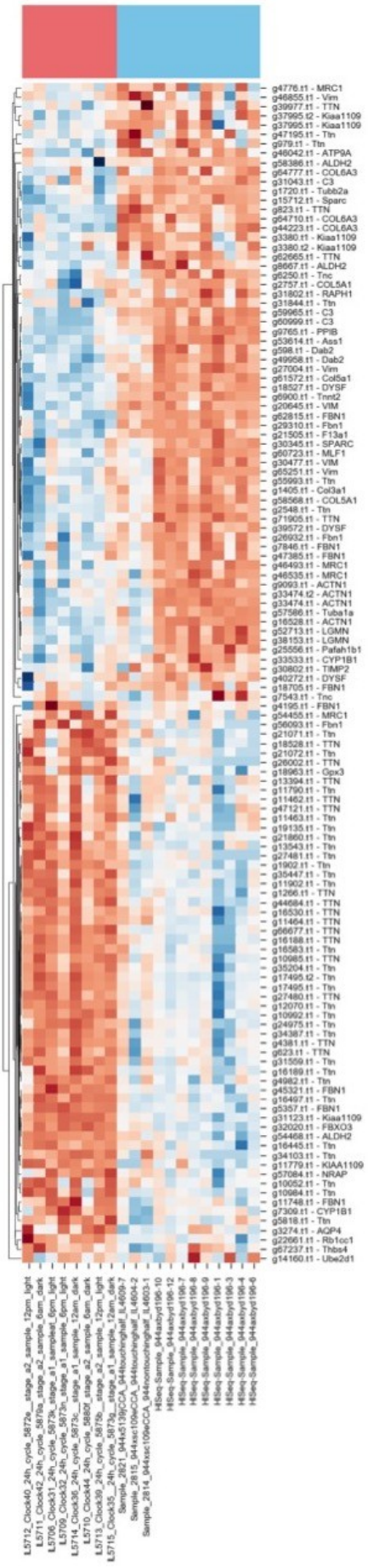

Hungtinton Disease

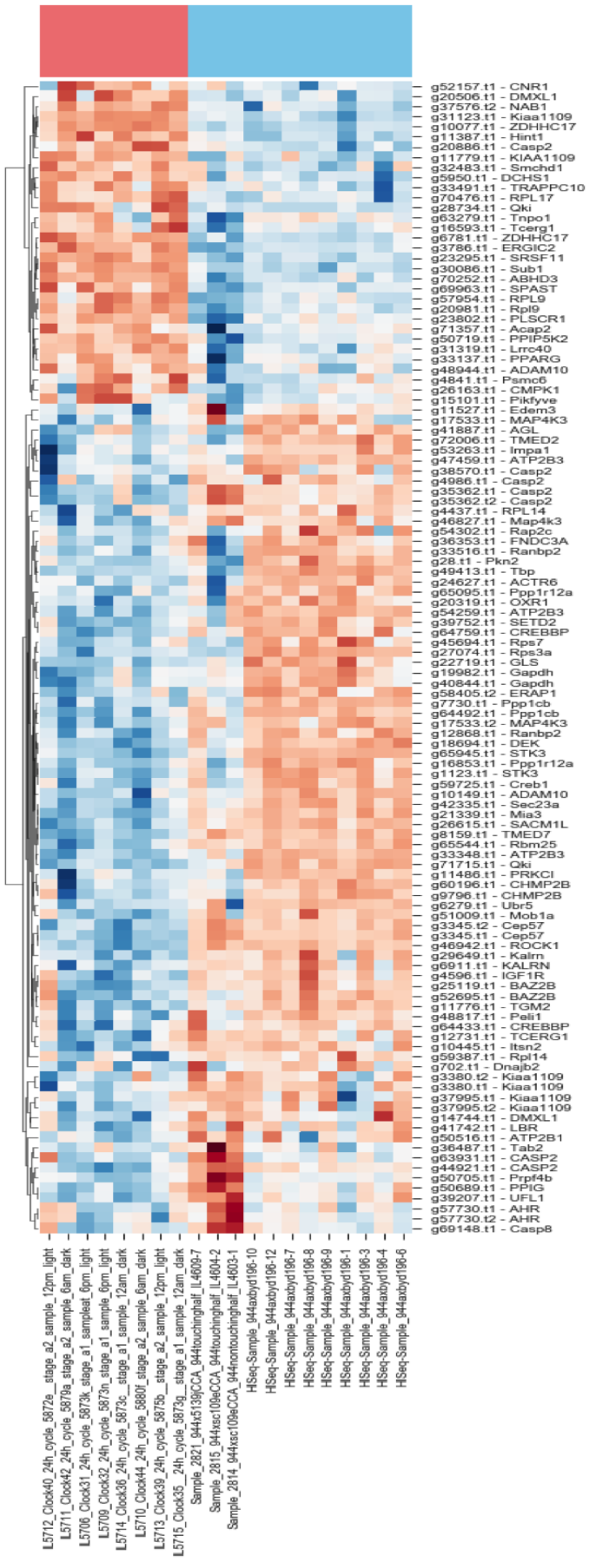

Amiotrophic Lateral Sclerosis

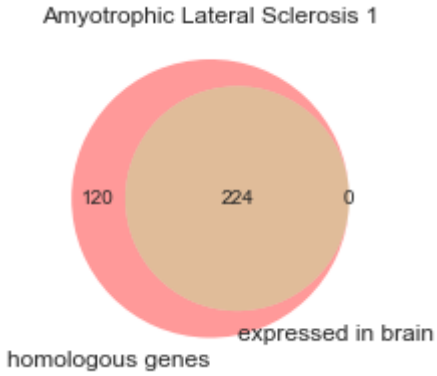

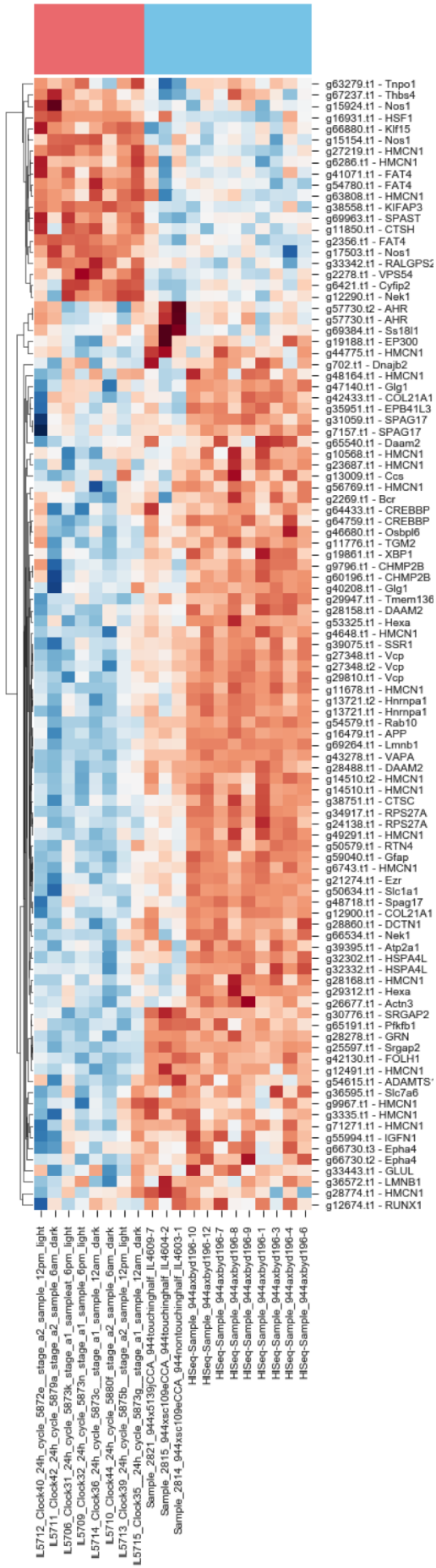

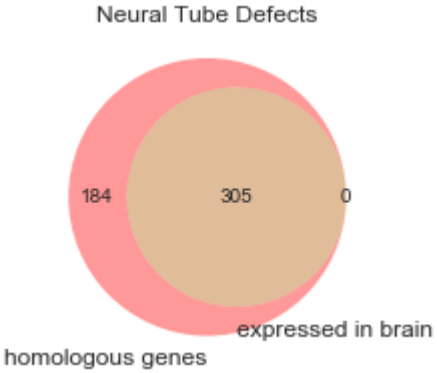
Neural Tube Defects
184
305
0
expressed in brain
homologous genes

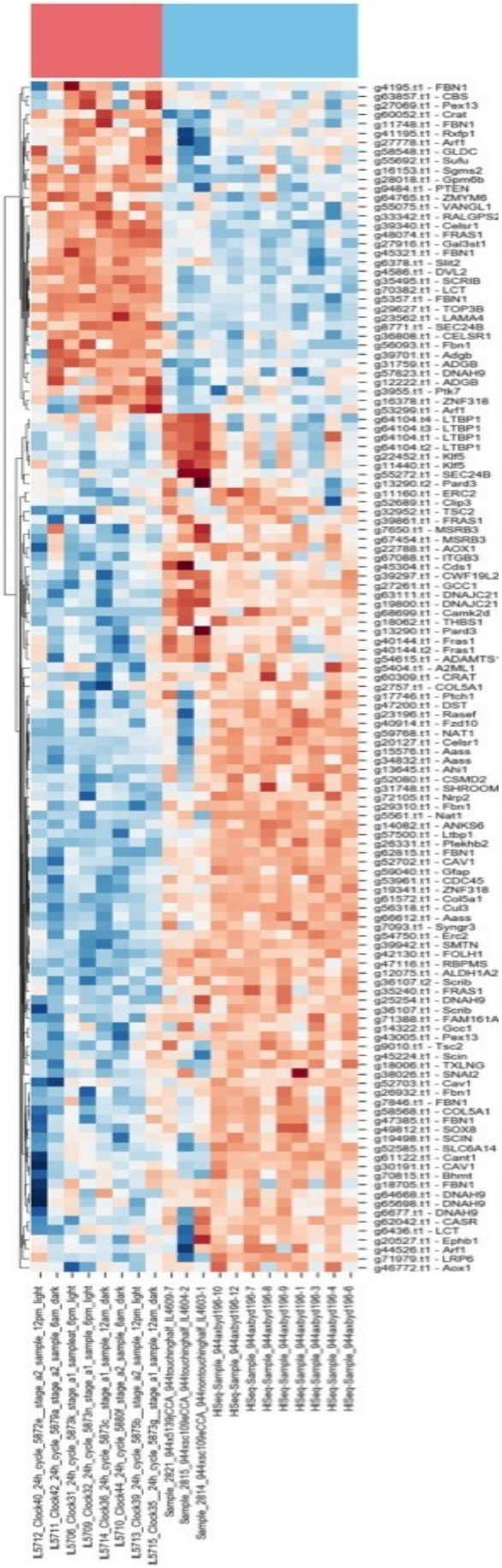

Hereditary Plastic Paraplegia

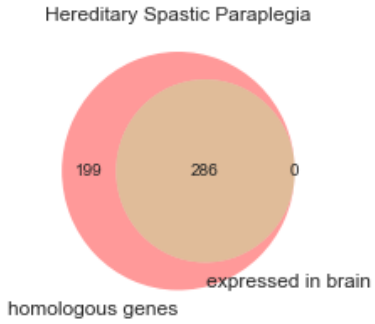

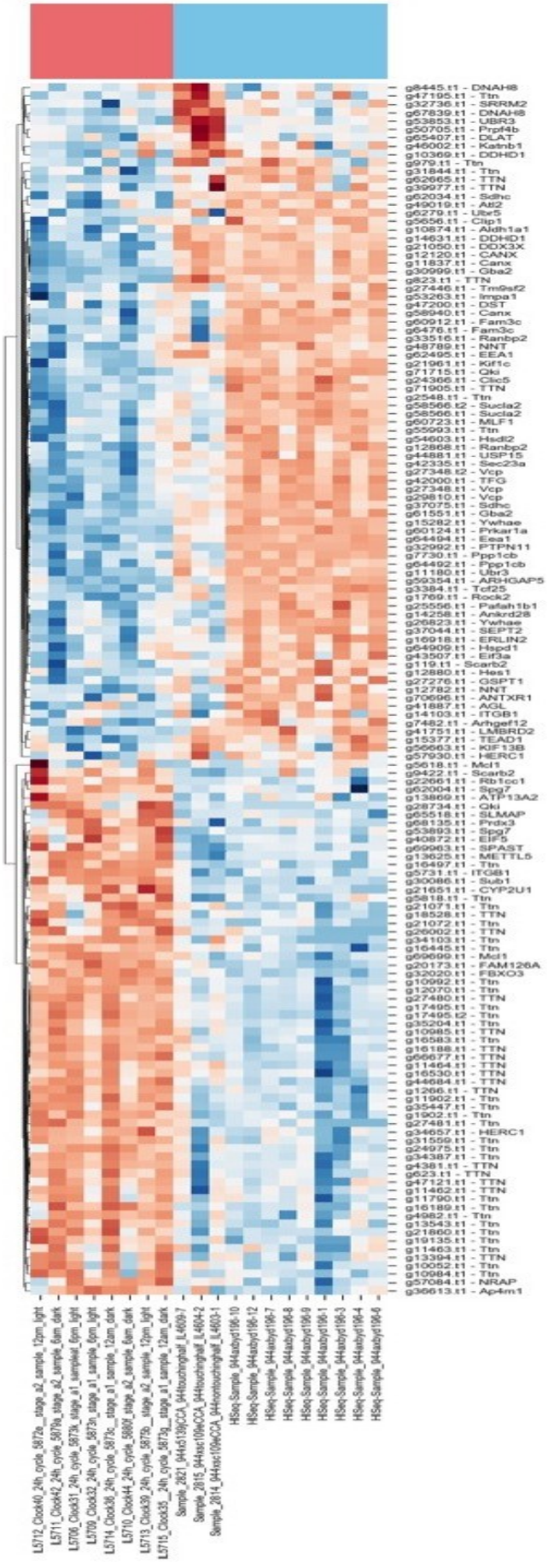

Microcephaly

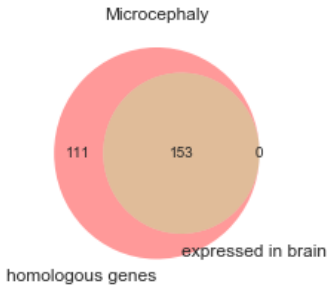

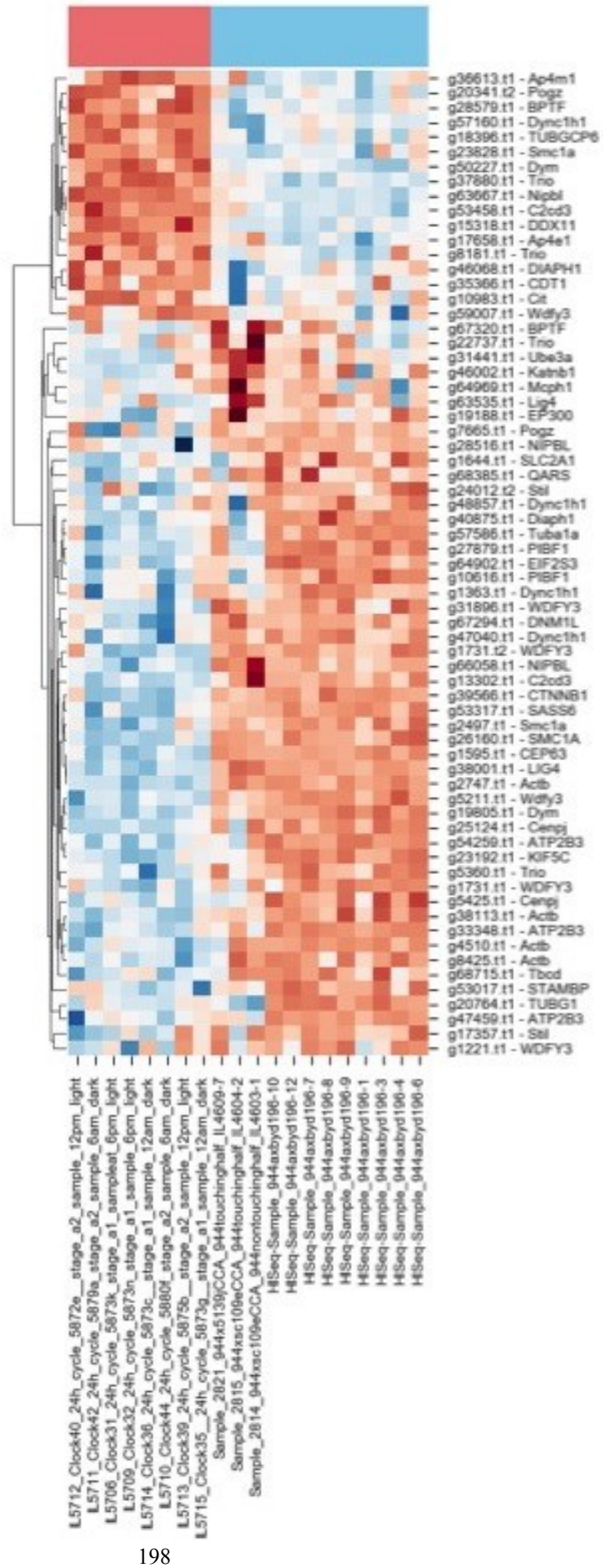

Schizophrenia

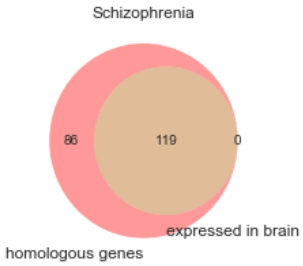

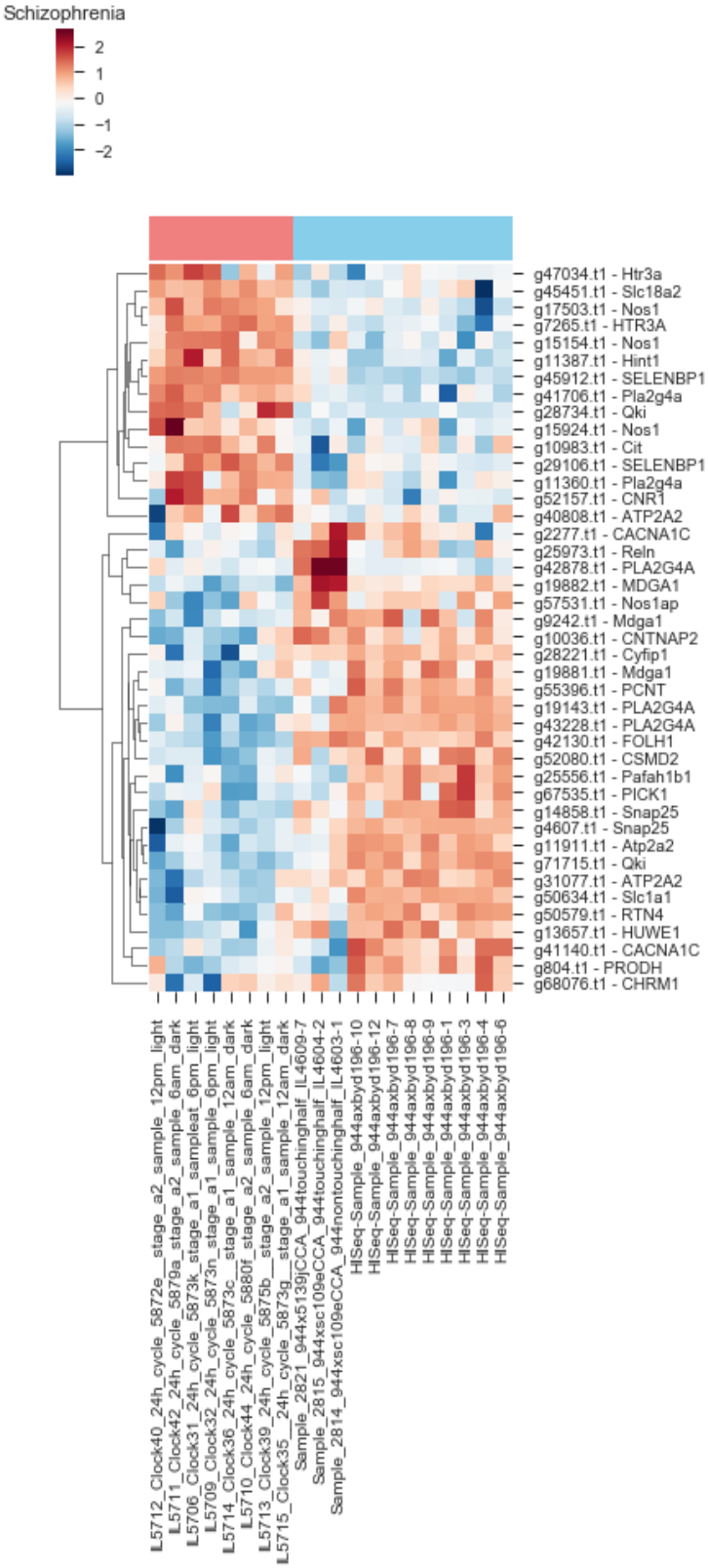

Myotonic Dystrophy

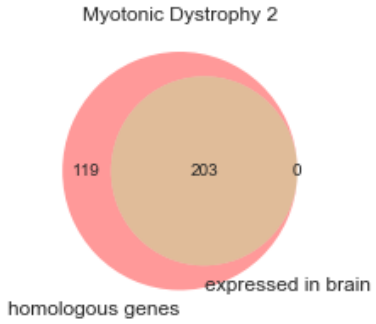

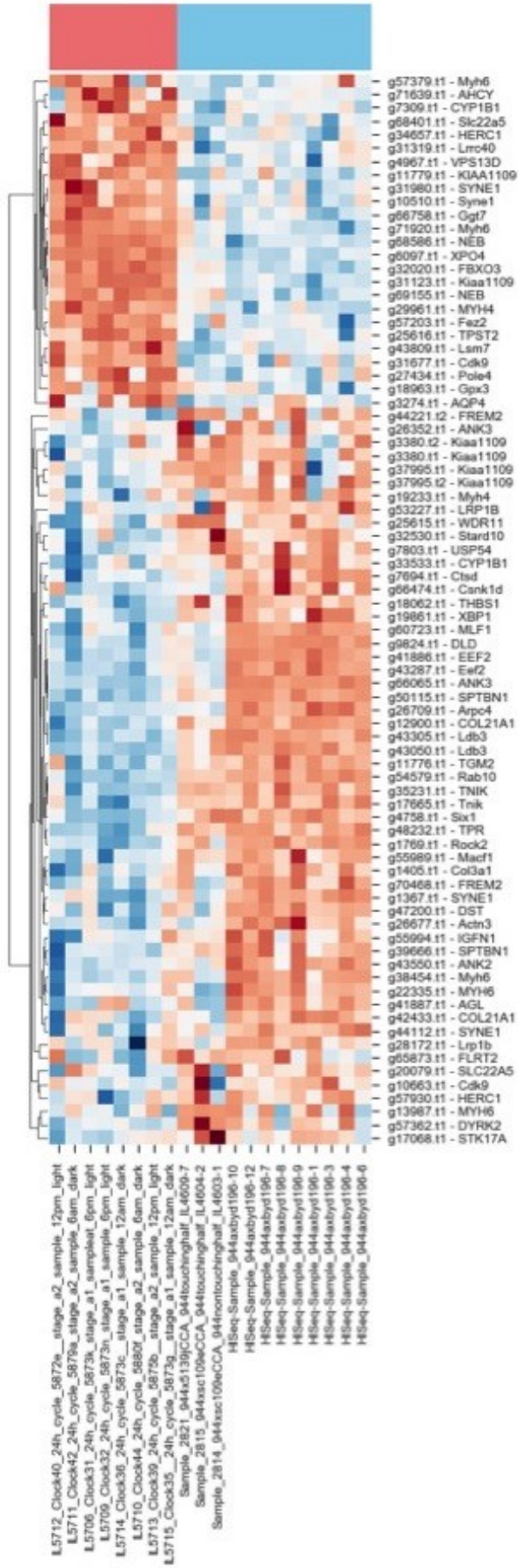

Dilated Cardiomyopathy

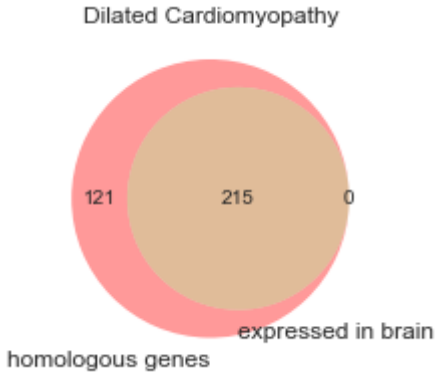

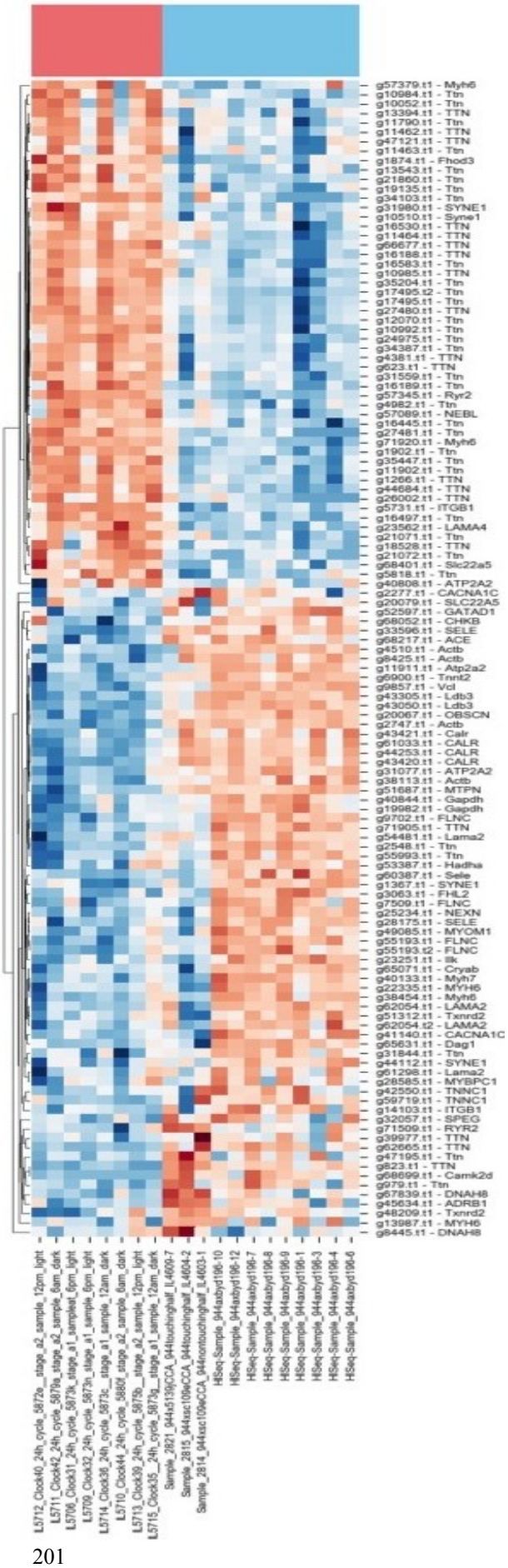

Joubert Syndrome

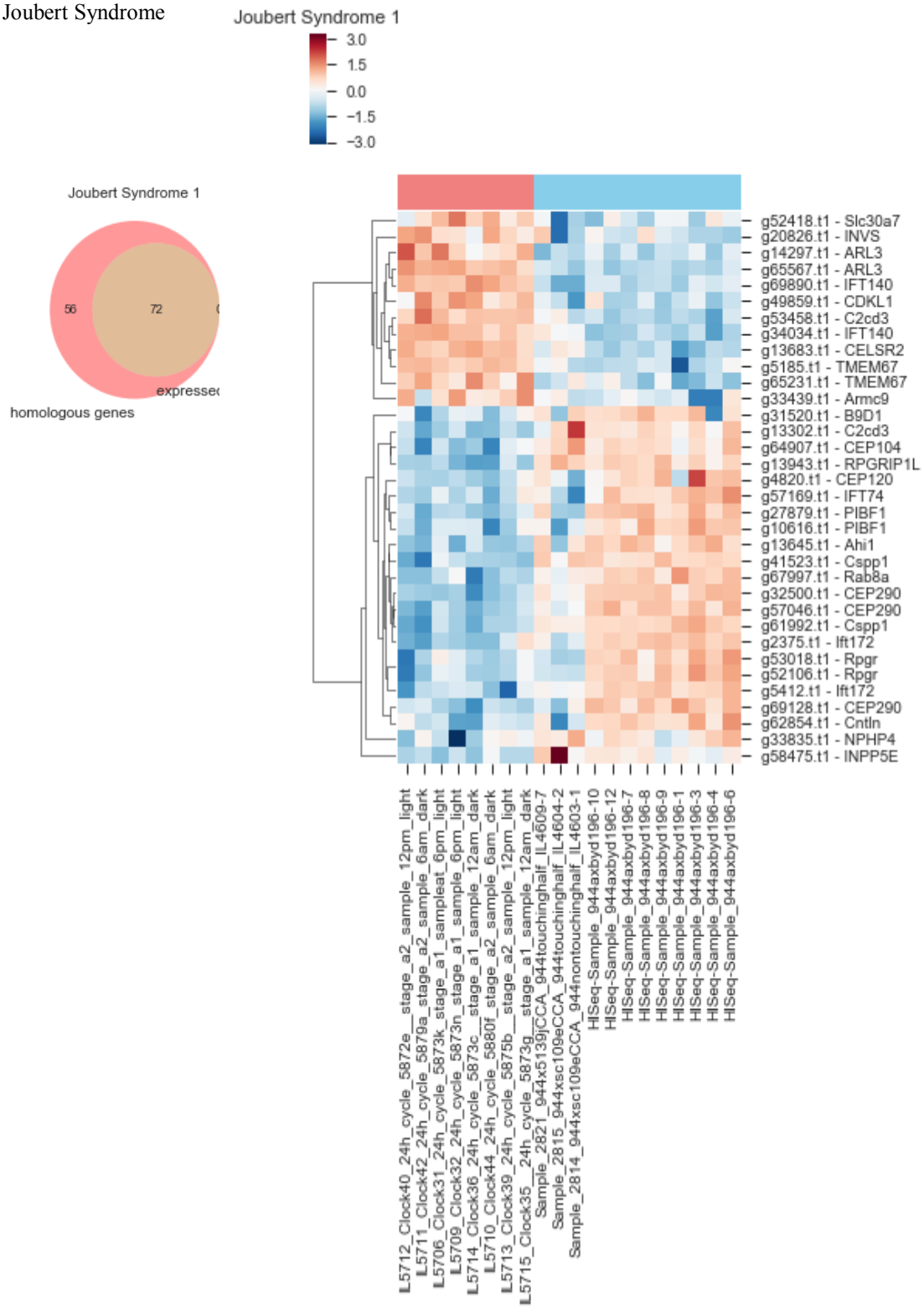

Ewing Sarcoma

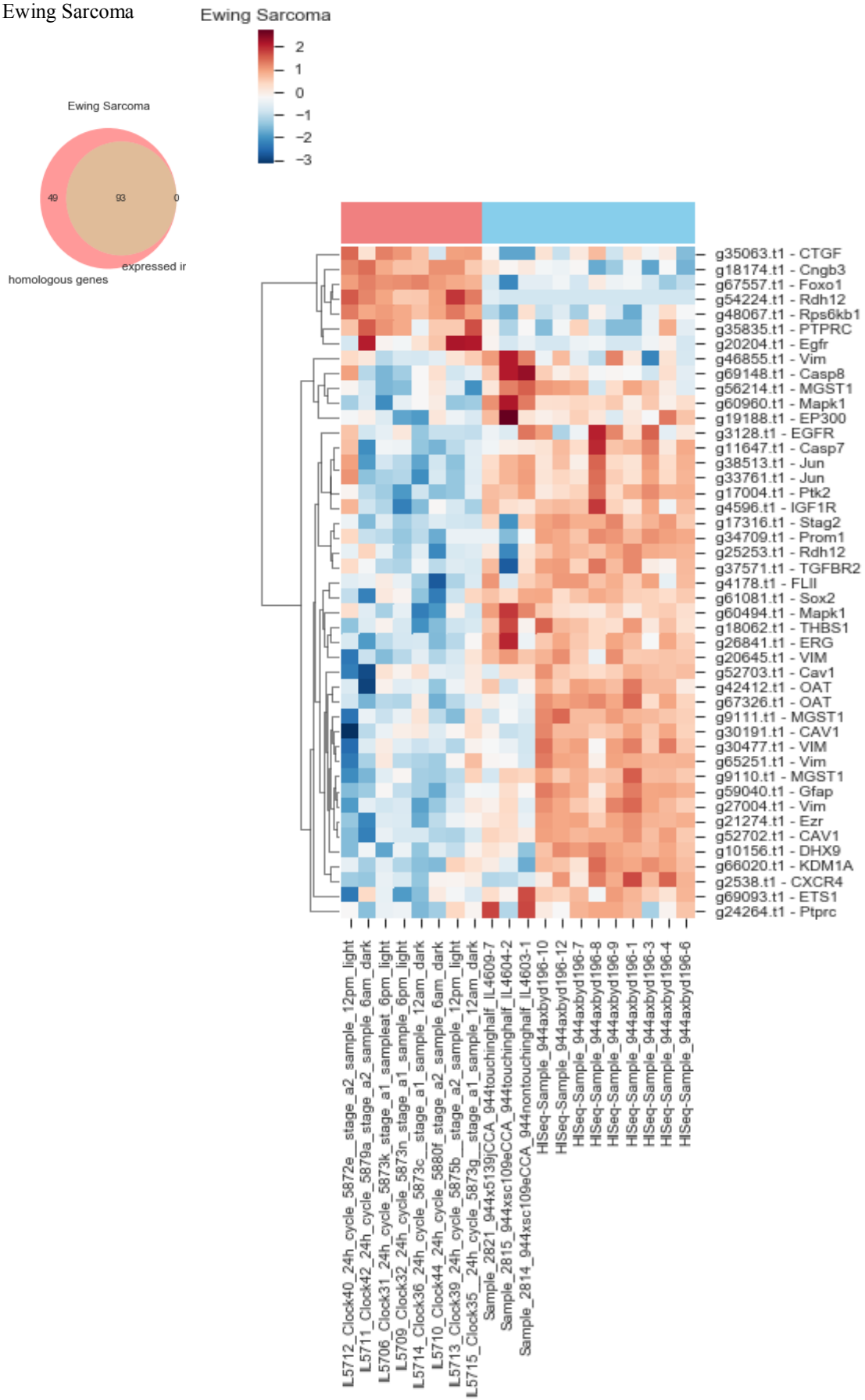

Tooth Disease

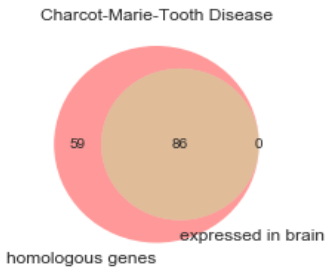

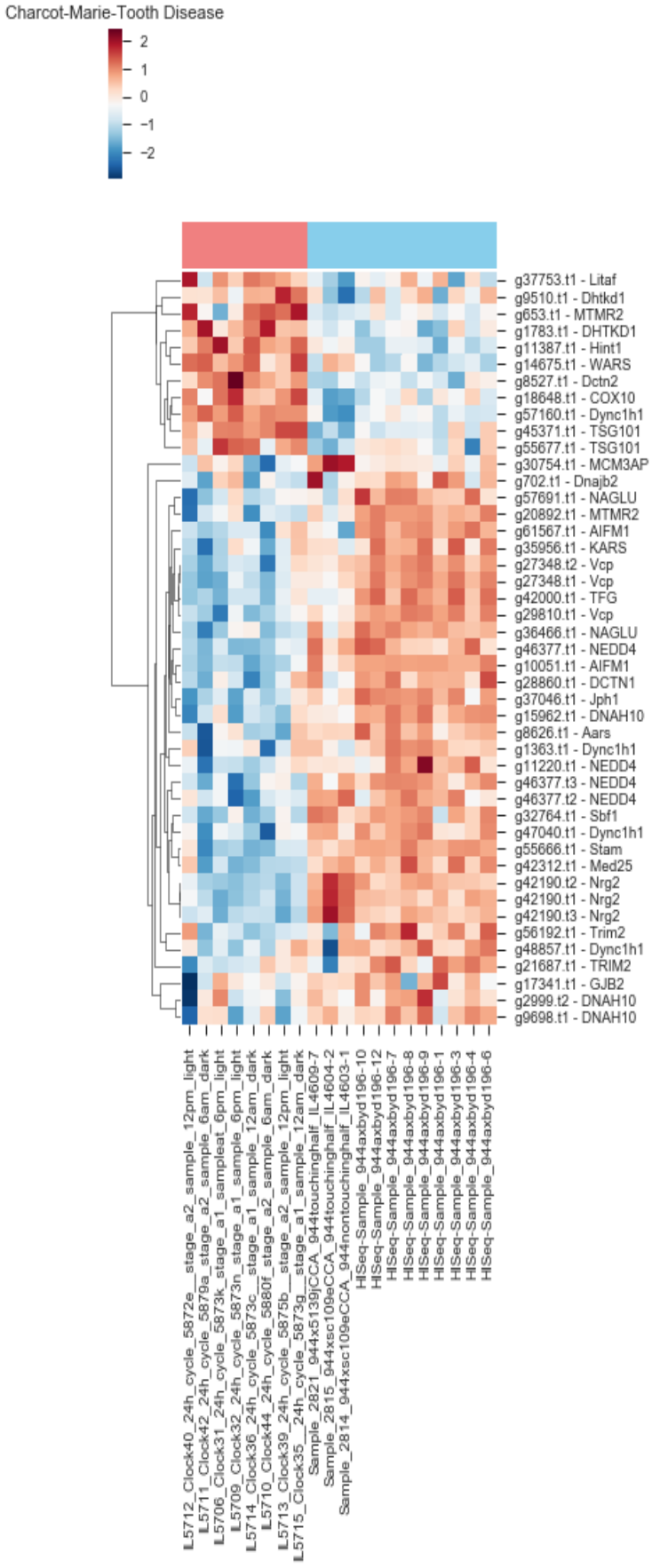

Emery-Dreifuss Muscolar Dystrophy

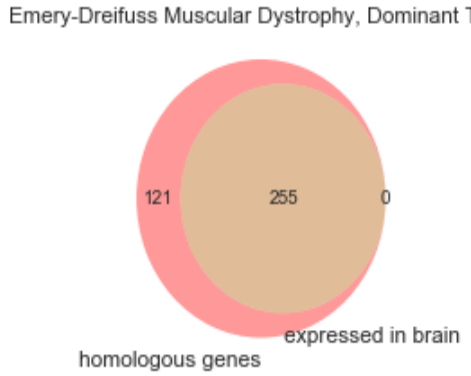

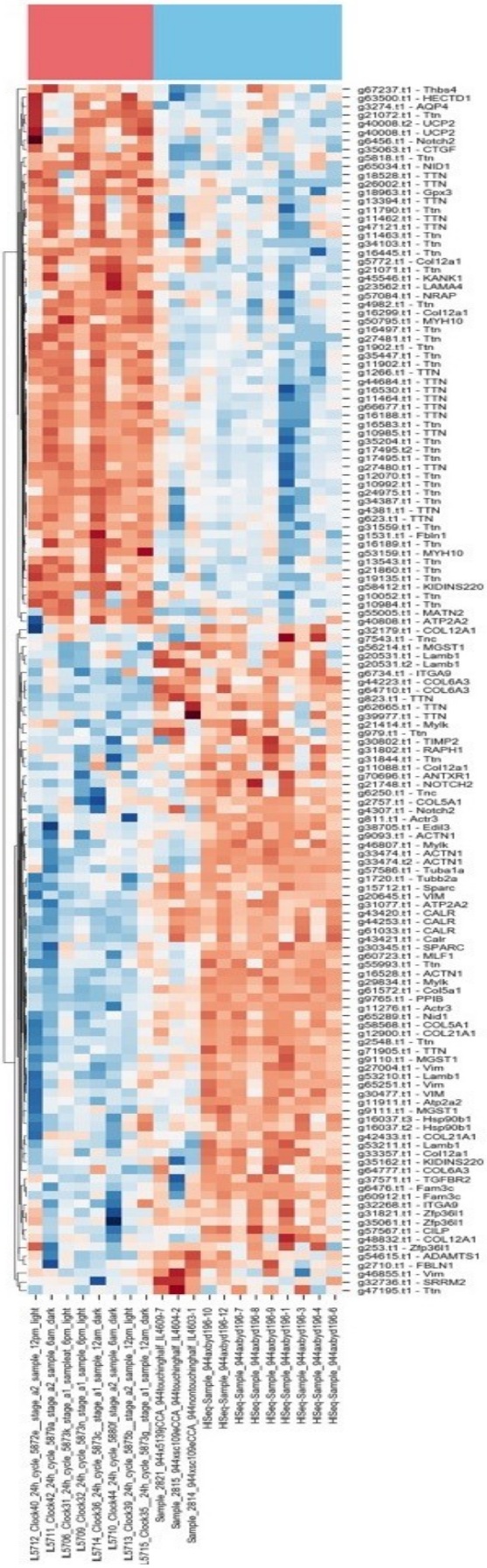

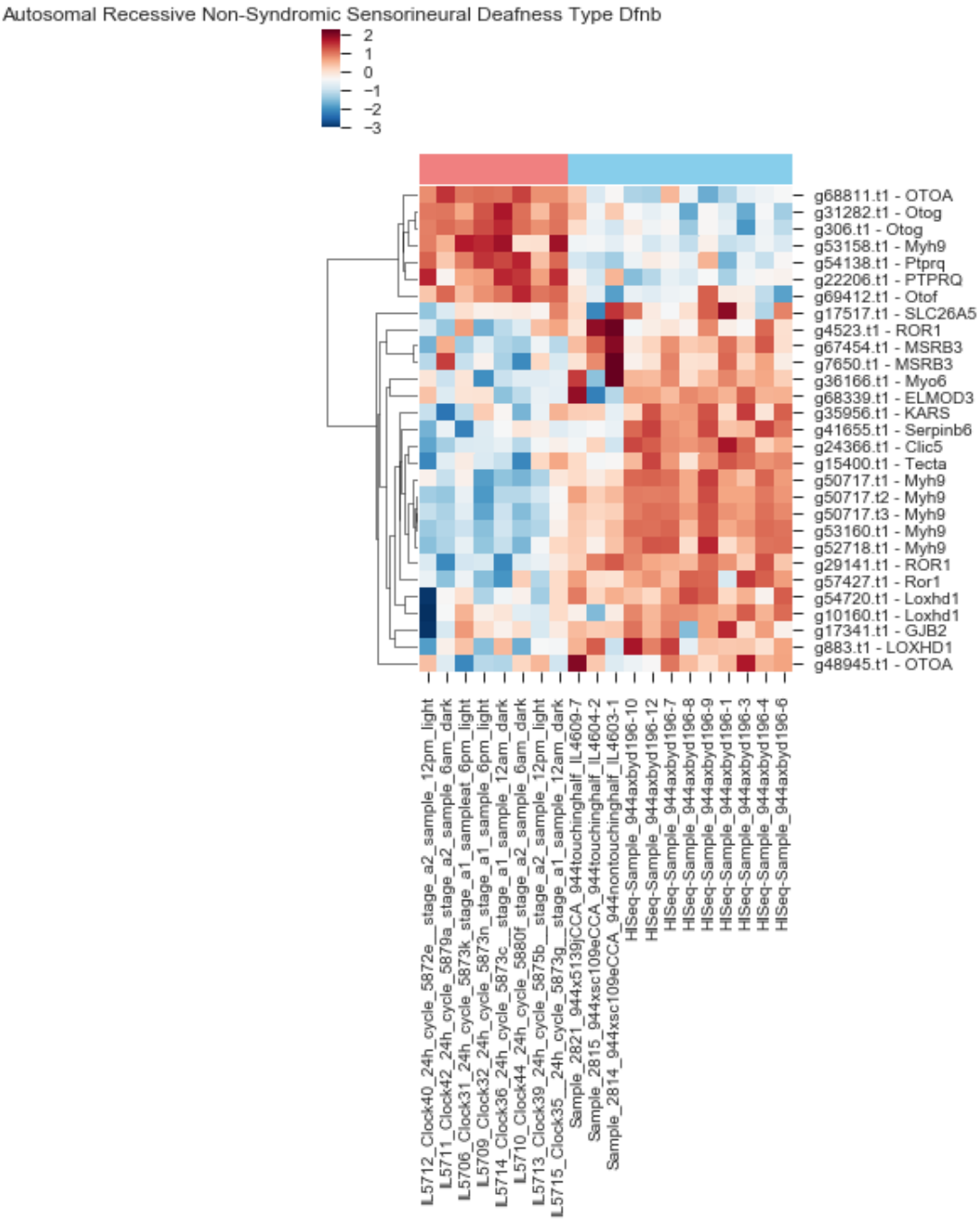
Autosomal Recessive Non-Syndromic Sensorineural Deafness Type Dfnb
2
1
0
−1
−2
−3
g68811.t1 - OTOA
g31282.t1 - Otog
g306.t1 - Otog
g53158.t1 - Myh9
g54138.t1 - Ptprq
g22206.t1 - PTPRQ
g69412.t1 - Otof
g17517.t1 - SLC26A5
g4523.t1 - ROR1
g67454.t1 - MSRB3
g7650.t1 - MSRB3
g36166.t1 - Myo6
g68339.t1 - ELMOD3
g35956.t1 - KARS
g41655.t1 - Serpinb6
g24366.t1 - Clic5
g15400.t1 - Tecta
g50717.t1 - Myh9
g50717.t2 - Myh9
g50717.t3 - Myh9
g53160.t1 - Myh9
g52718.t1 - Myh9
g29141.t1 - ROR1
g57427.t1 - Ror1
g54720.t1 - Loxhd1
g10160.t1 - Loxhd1
g17341.t1 - GJB2
g883.t1 - LOXHD1
g48945.t1 - OTOA
IL5712_Clock40_24h_cycle_5872e__stage_a2_sample_12pm_light
IL5711_Clock42_24h_cycle_5879a_stage_a2_sample_6am_dark
IL5706_Clock31_24h_cycle_5873k_stage_a1_sampleat_6pm_light
IL5709_Clock32_24h_cycle_5873n_stage_a1_sample_6pm_light
IL5714_Clock36_24h_cycle_5873c__stage_a1_sample_12am_dark
IL5710_Clock44_24h_cycle_5880f_stage_a2_sample_6am_dark
IL5713_Clock39_24h_cycle_5875b__stage_a2_sample_12pm_light
IL5715_Clock35__24h_cycle_5873g__stage_a1_sample_12am_dark
Sample_2821_944x5139jCCA_944touchinghalf_IL4609-7
Sample_2815_944xsc109eCCA_944touchinghalf_IL4604-2
Sample_2814_944xsc109eCCA_944nontouchinghalf_IL4603-1
HiSeq-Sample_944axbyd196-10
HiSeq-Sample_944axbyd196-12
HiSeq-Sample_944axbyd196-7
HiSeq-Sample_944axbyd196-8
HiSeq-Sample_944axbyd196-9
HiSeq-Sample_944axbyd196-1
HiSeq-Sample_944axbyd196-3
HiSeq-Sample_944axbyd196-4
HiSeq-Sample_944axbyd196-6

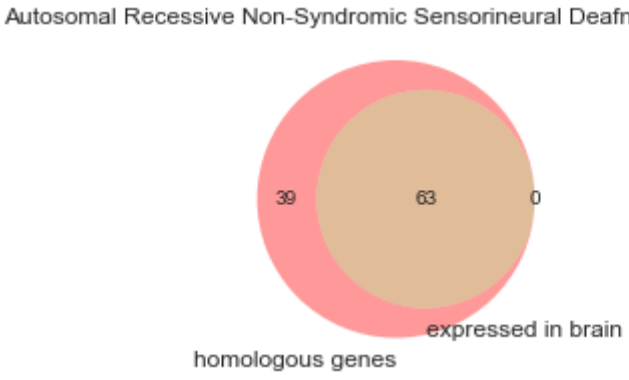
Autosomal Recessive Non-Syndromic Sensorineural Deafness Type Dfnb
39
63
0
expressed in brain
homologous genes

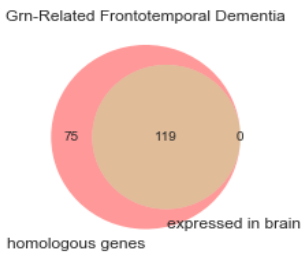
Grn-Related Frontotemporal Dementia
75
119
0
expressed in brain
homologous genes

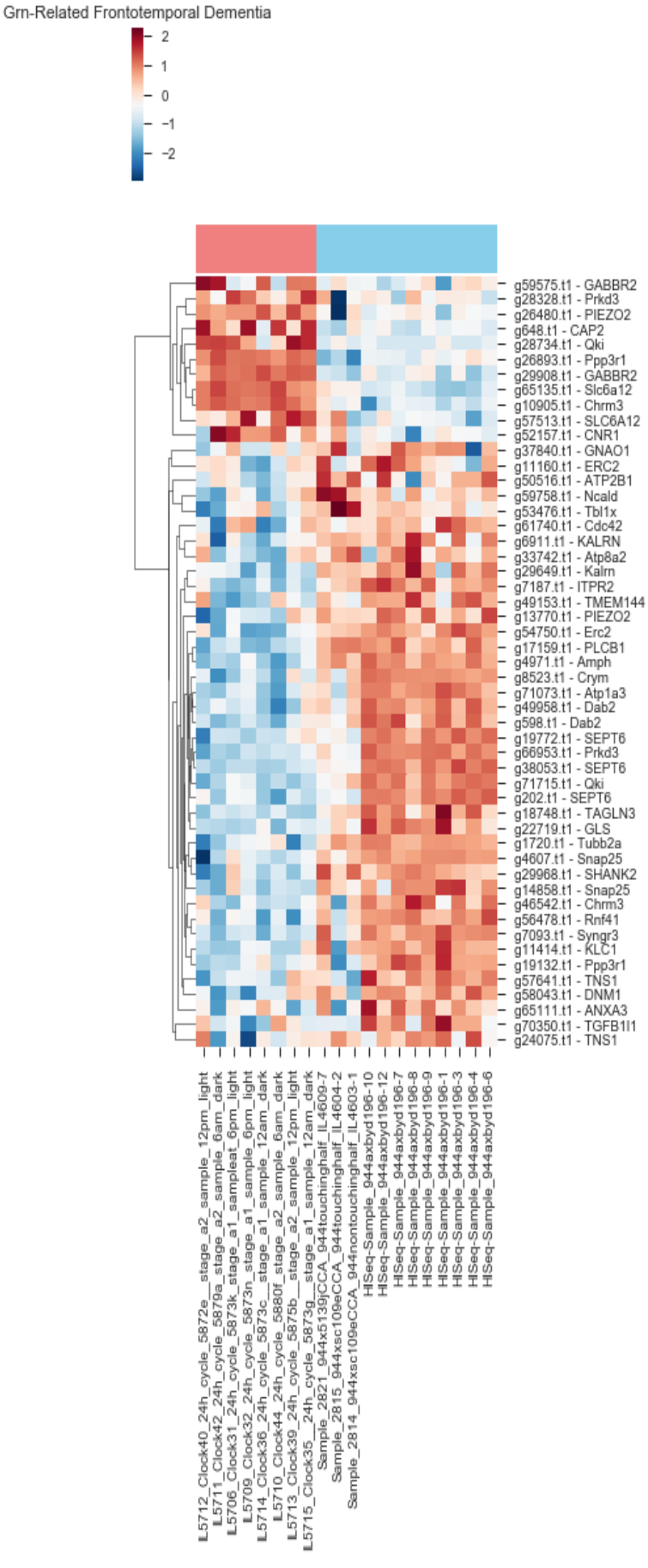
Grn-Related Frontotemporal Dementia
2
1
0
−1
−2
g59575.t1 - GABBR2
g28328.t1 - Prkd3
g26480.t1 - PIEZO2
g648.t1 - CAP2
g28734.t1 - Qki
g26893.t1 - Ppp3r1
g29908.t1 - GABBR2
g65135.t1 - Slc6a12
g10905.t1 - Chrm3
g57513.t1 - SLC6A12
g52157.t1 - CNR1
g37840.t1 - GNAO1
g11160.t1 - ERC2
g50516.t1 - ATP2B1
g59758.t1 - Ncald
g53476.t1 - Tbl1x
g61740.t1 - Cdc42
g6911.t1 - KALRN
g33742.t1 - Atp8a2
g29649.t1 - Kalrn
g7187.t1 - ITPR2
g49153.t1 - TMEM144
g13770.t1 - PIEZO2
g54750.t1 - Erc2
g17159.t1 - PLCB1
g4971.t1 - Amph
g8523.t1 - Crym
g71073.t1 - Atp1a3
g49958.t1 - Dab2
g598.t1 - Dab2
g19772.t1 - SEPT6
g66953.t1 - Prkd3
g38053.t1 - SEPT6
g71715.t1 - Qki
g202.t1 - SEPT6
g18748.t1 - TAGLN3
g22719.t1 - GLS
g1720.t1 - Tubb2a
g4607.t1 - Snap25
g29968.t1 - SHANK2
g14858.t1 - Snap25
g46542.t1 - Chrm3
g56478.t1 - Rnf41
g7093.t1 - Syngr3
g11414.t1 - KLC1
g19132.t1 - Ppp3r1
g57641.t1 - TNS1
g58043.t1 - DNM1
g65111.t1 - ANXA3
g70350.t1 - TGFB1l1
g24075.t1 - TNS1
IL5712_Clock40_24h_cycle_5872e__stage_a2_sample_12pm_light
IL5711_Clock42_24h_cycle_5879a_stage_a2_sample_6am_dark
IL5706_Clock31_24h_cycle_5873k_stage_a1_sampleat_6pm_light
IL5709_Clock32_24h_cycle_5873n_stage_a1_sample_6pm_light
IL5714_Clock36_24h_cycle_5873c__stage_a1_sample_12am_dark
IL5710_Clock44_24h_cycle_5880f_stage_a2_sample_6am_dark
IL5713_Clock39_24h_cycle_5875b__stage_a2_sample_12pm_light
IL5715_Clock35__24h_cycle_5873g__stage_a1_sample_12am_dark
Sample_2821_944x5139jCCA_944touchinghalf_IL4609-7
Sample_2815_944xsc109eCCA_944touchinghalf_IL4604-2
Sample_2814_944xsc109eCCA_944nontouchinghalf_IL4603-1
HiSeq-Sample_944axbyd196-10
HiSeq-Sample_944axbyd196-12
HiSeq-Sample_944axbyd196-7
HiSeq-Sample_944axbyd196-8
HiSeq-Sample_944axbyd196-9
HiSeq-Sample_944axbyd196-1
HiSeq-Sample_944axbyd196-3
HiSeq-Sample_944axbyd196-4
HiSeq-Sample_944axbyd196-6

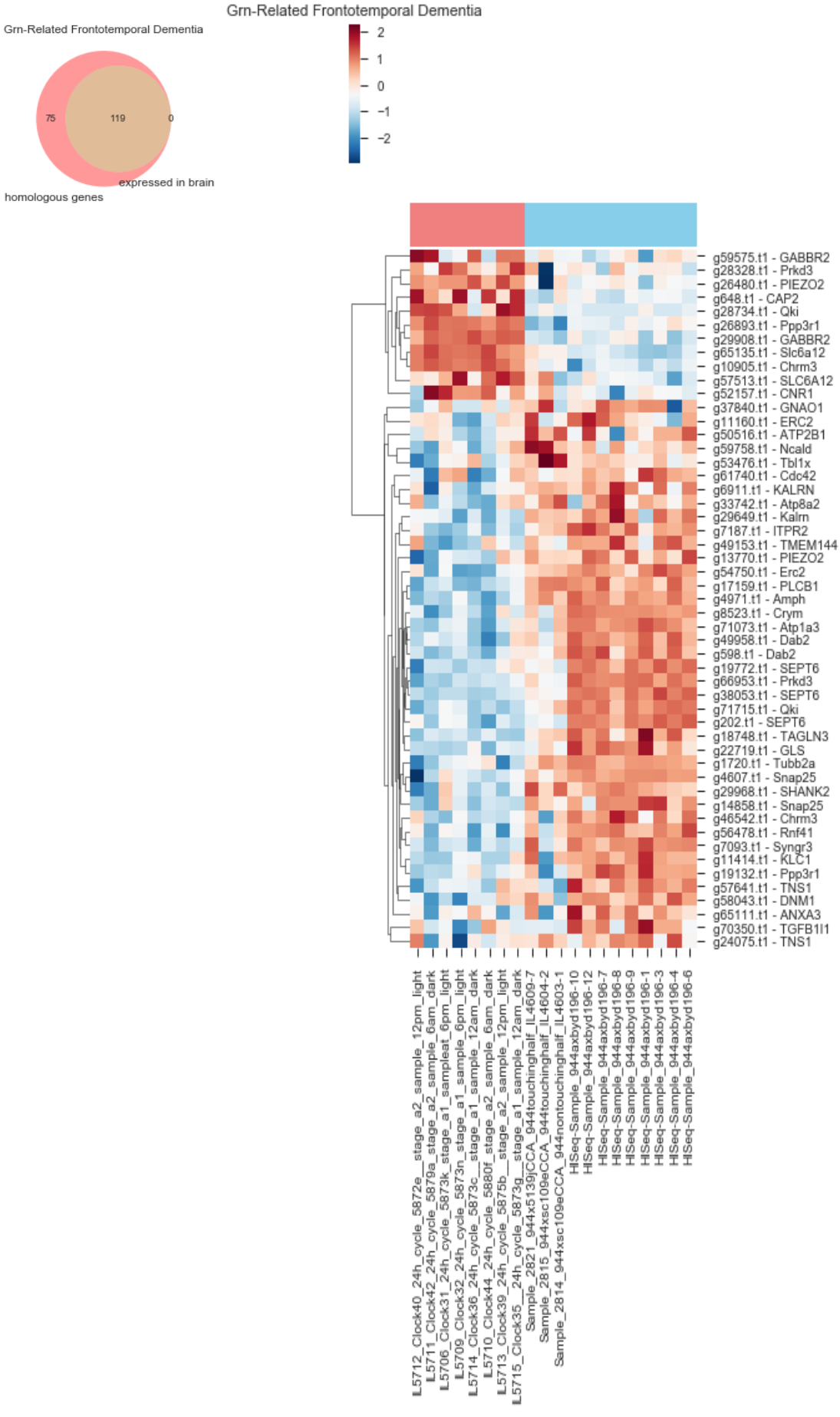
Grn-Related Frontotemporal Dementia
Grn-Related Frontotemporal Dementia
75
119
0
expressed in brain
homologous genes
2
1
0
−1
−2
g59575.t1 - GABBR2
g28328.t1 - Prkd3
g26480.t1 - PIEZO2
g648.t1 - CAP2
g28734.t1 - Qki
g26893.t1 - Ppp3r1
g29908.t1 - GABBR2
g65135.t1 - Slc6a12
g10905.t1 - Chrm3
g57513.t1 - SLC6A12
g52157.t1 - CNR1
g37840.t1 - GNAO1
g11160.t1 - ERC2
g50516.t1 - ATP2B1
g59758.t1 - Ncald
g53476.t1 - Tbl1x
g61740.t1 - Cdc42
g6911.t1 - KALRN
g33742.t1 - Atp8a2
g29649.t1 - Kalrn
g7187.t1 - ITPR2
g49153.t1 - TMEM144
g13770.t1 - PIEZO2
g54750.t1 - Erc2
g17159.t1 - PLCB1
g4971.t1 - Amph
g8523.t1 - Crym
g71073.t1 - Atp1a3
g49958.t1 - Dab2
g598.t1 - Dab2
g19772.t1 - SEPT6
g66953.t1 - Prkd3
g38053.t1 - SEPT6
g71715.t1 - Qki
g202.t1 - SEPT6
g18748.t1 - TAGLN3
g22719.t1 - GLS
g1720.t1 - Tubb2a
g4607.t1 - Snap25
g29968.t1 - SHANK2
g14858.t1 - Snap25
g46542.t1 - Chrm3
g56478.t1 - Rnf41
g7093.t1 - Syngr3
g11414.t1 - KLC1
g19132.t1 - Ppp3r1
g57641.t1 - TNS1
g58043.t1 - DNM1
g65111.t1 - ANXA3
g70350.t1 - TGFB1I1
g24075.t1 - TNS1
IL5712_Clock40_24h_cycle_5872e__stage_a2_sample_12pm_light
IL5711_Clock42_24h_cycle_5879a_stage_a2_sample_6am_dark
IL5706_Clock31_24h_cycle_5873k_stage_a1_sampleat_6pm_light
IL5709_Clock32_24h_cycle_5873n_stage_a1_sample_6pm_light
IL5714_Clock36_24h_cycle_5873c__stage_a1_sample_12am_dark
IL5710_Clock44_24h_cycle_5880f_stage_a2_sample_6am_dark
IL5713_Clock39_24h_cycle_5875b__stage_a2_sample_12pm_light
IL5715_Clock35__24h_cycle_5873g__stage_a1_sample_12am_dark
Sample_2821_944x5139jCCA_944touchinghalf_IL4609-7
Sample_2815_944xsc109eCCA_944touchinghalf_IL4604-2
Sample_2814_944xsc109eCCA_944nontouchinghalf_IL4603-1
HiSeq-Sample_944axbyd196-10
HiSeq-Sample_944axbyd196-12
HiSeq-Sample_944axbyd196-7
HiSeq-Sample_944axbyd196-8
HiSeq-Sample_944axbyd196-9
HiSeq-Sample_944axbyd196-1
HiSeq-Sample_944axbyd196-3
HiSeq-Sample_944axbyd196-4
HiSeq-Sample_944axbyd196-6

Medulloblastoma

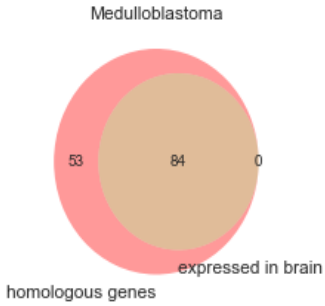

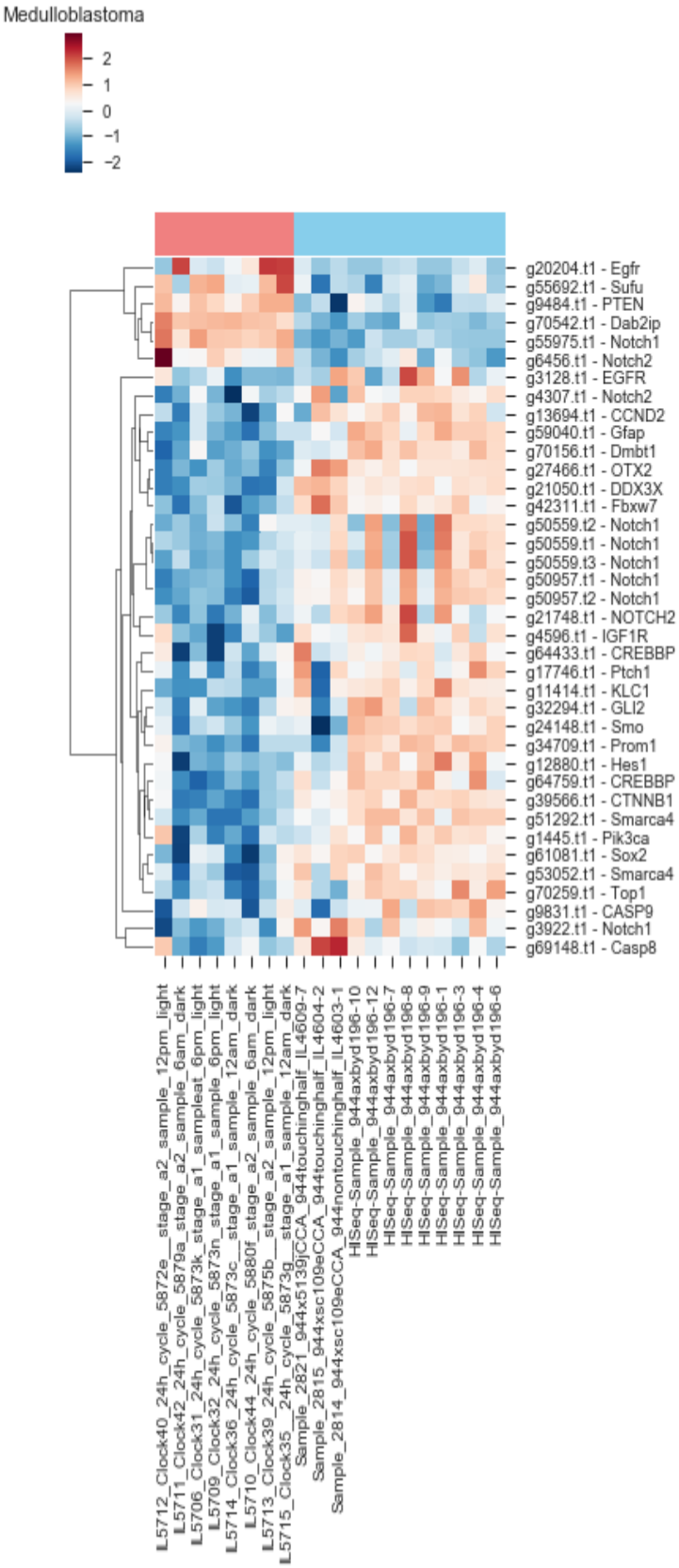

Chapter 4

Differentiation and induced sensorial alteration of the coronal organ in the asexual life of a tunicate

Lucia Manni[1]*, **Chiara Anselmi[1]***, Paolo Burighel[1], Margherita Martini[1], Fabio Gasparini[1]

[1]Dipartimento di Biologia, Università degli Studi di Padova

**Corresponding Authors*: Lucia Manni, Chiara Anselmi

Journal: Integrative and Comparative Biology

ABSTRACT

Tunicates, the sister group of vertebrates, possess a mechanoreceptor organ, the coronal organ, which is considered the best candidate to address the controversial issue of vertebrate hair cell evolution. The organ, located at the base of the oral siphon, controls the flow of seawater into the organism and can drive the "squirting" reaction, *i.e*., the rapid body muscle contraction used to eject dangerous particles during filtration. Coronal sensory cells are secondary mechanoreceptors and share morphological, developmental and molecular traits with vertebrate hair cells. In the colonial tunicate *Botryllus schlosseri*, we described coronal organ differentiation during asexual development. Moreover, we showed that the ototoxic aminoglycoside gentamicin caused morphological and mechanosensorial impairment in coronal cells. Finally, fenofibrate had a strong protective effect on coronal sensory cells due to gentamicin-induced toxicity, as occurs in vertebrate hair cells. Our results reinforce the hypothesis of homology between vertebrate hair cells and tunicate coronal sensory cells.

INTRODUCTION

Fifteen years ago, a novel mechanoreceptor organ, the coronal organ, was described in the oral siphon of the colonial tunicate *Botryllus schlosseri* (Burighel et al., 2003). Tunicates are marine, filter-feeding invertebrates that are considered to be the vertebrate sister group (Kocot et al., 2018). In this respect, coronal cells are of interest for researchers studying vertebrate evolution. Like vertebrate hair cells, coronal cells are receptor cells without own axons (referred here as secondary receptors) and thus they can contribute to the investigation of vertebrate hair cell evolution. The coronal organ is located at the base of the oral siphon and is responsible for the "squirting" reaction (Mackie et al., 2006): when cells are stimulated by contact with potentially dangerous particles that enter the siphon with seawater flow, the animal stops the inflowing current and contracts its body muscles to expel these particles. The organ is composed of one or a few more rows of sensory cells flanked by supporting cells, bordering the edge of the oral velum and tentacles (Caicci et al., 2010). Sensory cells are contacted at their base by neurites that come from elsewhere (*i.e.*, from the cerebral ganglion), as occurs in vertebrate hair cells innervated by afferents that derive from the ear (Dabdoub et al., 2016). Vertebrate hair cells are also innervated by efferent fibres (Sienknecht et al., 2014). Moreover, as in vertebrate hair cells, coronal cells possess a hair bundle, delimited by supporting cell apical protrusions, to detect the stimulus.

Hair cells of the ear and the lateral line system are mechanoreceptors that mediate vibrational and fluid-flow sensing that allow hearing, balance, and vibrational sensing (Chagnaud et al., 2017). Loss of hair cells is an important cause of deafness in humans because lost cells are typically not replaced (Burns and Stone, 2017). In mammals, this loss occurs because of age and/or use of therapeutics drugs, such as aminoglycoside antibiotics, which can destroy both hair cells and their innervating neurons. Hair cells and associated sensory neurons develop from cranial placodes, in particular, from otic and lateral line placodes, which are thickened areas of the cranial ectoderm expressing a particular set of developmental genes (Schlosser et al., 2014). As cranial placodes, together with neural crests, are classically considered to be exclusive to vertebrates and crucial for the evolution of their features (Gans and Northcutt, 1983; Northcutt and Gans, 1983). The discovery hair cell-like coronal cells raises the possible earlier evolution of placodes in tunicates (Manni et al., 2001).

Since the first coronal organ description, many steps have been taken. The coronal organ is now considered to be a tunicate synapomorphy (Caicci et al., 2013; Rigon et al., 2013). The organ has a complex connectivity system, with involvement in afferent, efferent, and reciprocal synapses with neurites (Burighel et al., 2011; Rigon et al., 2018). Moreover, axo-dendritic contacts and synapses between neurites and supporting cells are also recorded (Burighel et al., 2003). Sensory cells have diverse hair bundles in different species: mono-, bi- or pluri-ciliated bundles with microvilli or stereovilli, the latter of which are sometimes graded in length. Some neurotransmitters are localized in the coronal organ (Rigon et al., 2018), such as glutamate (which mediates afferent hair cell inputs) and acetylcholine, GABA and serotonin (which is involved in efferent stimulation to hair cells).

Morphological and molecular development of the coronal organ have been analyzed in the tunicate *Ciona* (Gasparini, Caicci, et al., 2013; Rigon et al., 2018). Sensory cells are first identified during larval metamorphosis, before tentacles form, as cells with short cilia and microvilli. Sensory cells undergo gradual differentiation, acquiring their definitive morphology in juveniles. Different from those in vertebrates, in *Ciona*, not only supporting cells, but also sensory cells can proliferate and accompany tentacle growth during the lifespan (Gasparini, Caicci, et al., 2013). Some of the genes involved in hair cell differentiation (*Atoh, Notch, Delta-like, Hairy-b* and *Musashi*) (Fritzsch and Elliott, 2017) are expressed in the developing coronal organ (Rigon et al., 2018). Moreover, the embryonic territory that is the origin of the oral siphon and therefore the tentacles and velum, is a thickened ectodermal epithelium (called "anterior proto-placode") expressing homologues of some placodal genes (Patthey et al., 2014). In *B. schlosseri*, placodal genes are also expressed in the territory that gives rise to the oral siphon in buds produced by asexual reproduction (Gasparini, Degasperi, et al., 2013)

Tunicates develop from an embryo in which the chordate body plan is recognizable. However, in colonial species, such as *B. schlosseri*, sexual reproduction is accompanied by asexual reproduction (blastogenesis), permitting colony growth (Manni et al. 2007; Gasparini et al., 2015). In *B. schlosseri*, three blastogenic generations coexist and synchronously develop in the colony: the adult, filter-feeding blastozooids, their buds, and budlets on buds. Cyclically, adult blastozooids regress and are substituted in filtration by their buds, which open their siphons (Cima et al., 2010). This cyclical event, called a change of generation (or takeover), is accompanied by the transformation

of budlets in buds and the formation of a new generation of budlets in the latter. Adult filtering individuals formed through the two developmental pathways are morphologically similar and can be used as correspondent experimental models (Manni and Burighel 2006; Brunetti et al., 2017). This feature extends comparisons between blastozooid and vertebrate structures, as in the case of the blastozooid and vertebrate pharynx, which are considered to be homologous. In this species, coronal sensory cells possess an immobile cilium surrounded or flanked by a corolla of short stereovilli (Burighel et al., 2003). A fibrillary fuzzy coat extends radially to establish connections between adjacent stereovilli and between the stereovilli and ciliary shaft. At their base, the plasmalemma forms a groove in which neurites are located.

From an evo-devo perspective, understanding coronal organ development and function could provide insights into the evolution of vertebrate hearing and balance, which will likely facilitate the development of new therapies for hair cell loss in humans. Here, we explore both the development of the coronal organ during blastogenesis and the effect of an ototoxic agent, the aminoglycoside gentamicin, on coronal organ morphology and functional mechano-receptivity in *B. schlosseri*.

MATERIALS AND METHODS

Animals and whole-mount preparation

Specimens of *Botryllus schlosseri* (family Styelidae, order Stolidobranchia) were collected from the lagoon of Venice and reared and staged according to Sabbadin's (1955) technique (reviewed (Manni et al., 2014; Cima et al., 2015)). Blastozooids are grouped in star-shaped systems around the common cloacal siphon.

Colonies were anesthetized with MS 222, fixed in Bouin's fluid, washed in 50% ethyl alcohol, rehydrated and stained with Mayer's hematoxylin. After washing in distilled water, colonies were dehydrated in alcohol and mounted with balsam. For the acetylcholinesterase (AChE) reaction, colonies were treated according to (Zaniolo et al., 2002). To control reaction specificity, the substrate was omitted, or the specific inhibitor 0.03 M neostigmine bromide (cat. No. N2001, Sigma-Aldrich) was added. Buds were studied with light microscopy.

Electron microscopy (EM)

Colonies were anesthetized, fixed, postfixed, dehydrated and embedded as described in (Franchi et al., 2016). For Transmission EM (TEM), thick sections (1 □m) were counterstained with toluidine blue; thin sections (60 nm) were contrasted with uranyl acetate and lead citrate. Micrographs were taken with a FEI Tecnai G12 electron microscope operating at 75 kV.

For Scanning EM (SEM), pieces of colony containing adult blastozooids were anesthetized and fixed as described for TEM, but not postfixed. After dehydration with ethanol, the pieces were dissected to expose the oral velum and tentacles. Specimens were air-dried after hexamethyldysilazane (Sigma-Aldrich, H4875) washes at increasing concentrations (30% and 70% in EtOH, and then two washes of 100%, 15 min each). Specimens were sputter-coated with gold-palladium and observed under a FEI Quanta 200 SEM.

Gentamicin and/or fenofibrate treatment and behavioral response

Colonies immediately after the takeover were treated with gentamicin (LFM, 80 mg/2 ml) and/or fenofibrate (Sigma-Aldrich, F6020). Colonies were immerged in a petri dish filled with one or both drugs in seawater as indicated in Table 1.

For SEM, eight colonies were treated with gentamicin solution (2 mg/ml x 2 h), and six control colonies were processed.

Before and after treatment with gentamicin and/or fenofibrate, the reaction of about 40 (34 to 45) zooids *per* colony to the tentacle stimulation test (TST) was tested. The colonies used were 32 in total. The test consisted of a single mechanical stimulation of the tentacle rim, gently touching it with a glass needle prepared with a Narishige PD-5 horizontal capillary puller mounted on a Singer Mk1 micromanipulator. The response repeatability to TST was verified during the phase of method development taking into consideration the following variables: operators, instruments, lot of reagents, elapsed time between TST implemented pre- and post-drug treatment, rearing temperature, stage of blastogenesis. During protocol development zooids responded consistently to repeated stimulation. Commonly the expected reaction of zooids to the TST is a typical squirting behavior consisting of sudden atrial siphon closure and vigorous body

contraction (Mackie et al. 2006). In our experiments, three primary different categories of reaction were observed: i) squirting behavior, ii) faint and anomalous reaction (*i.e.*, absence of atrial siphon closure and/or faint-to-absent body contraction), and iii) not perceptible reaction; for simplicity, we call these reactions "fast," "faint" and "null," respectively. The TSTs were performed under a Leica MZ6 stereomicroscope.

	Gentamicin				Fenofibrate	Fenofibrate + Gentamicin
N°. of colonies	4	8	2	6	5	7
N°. of zooids	169	334	86	255	204	286
Treatment	0.65mg/ml x 24 h	1.3 mg/ml x 24 h	2.6 mg/ml x 1 h	2 mg/ml x 2 h	50 µM x 45 min	[50 µM x 45 min] + [2 mg/ml x 2 h]

Table 1: Number of tested colonies and zooids, and implemented treatments.

Statistical analyses

Data on behavioral response were grouped in samples of percentages as follow (see Supplementary Material 01):

Type i) zooids *per* colony with absence of squirting reaction before treatment, and zooids *per* colony with absence of squirting reaction after treatment;

Type ii) zooids *per* colony changing behavior after the treatment.

Statistical analyses were performed using R Software Environment, version 3.4.3 (R Core Team 2017). Samples were visualized in box-and-whisker plots. For each dataset, the following statistical pipeline was used. The Shapiro test was used to determine whether each sample was normally distributed. Bartlett test or in case of normality violation, Fligner-Killeen test, was used to verify the homogeneity of variances among samples in each dataset. For each implemented treatment (Table 1), a dataset of paired samples (before and after treatment) was tested for the equality of the means with the non-parametric Wilcoxon signed-rank test. The non-parametric one-way ANOVA equivalent, Kruskal-Wallis rank sum test, was used to verify the null hypothesis of

equality of medians among samples; subsequently, in case of rejection of the null hypothesis, the Conover's test with Bonferroni p-value adjustment and quantiles corrected for ties (Pohlert, 2014) were used to calculate the pairwise multiple comparisons between samples.

Summarizing, the following two testing methods were applied:

Testing method 1. Comparison of the means for two samples of paired data (before and after each single treatment, "type i" samples);

Testing method 2. ANOVA and post-hoc test, using two different groups of samples:

Group a) A sample formed from data collected before treatments, and other samples each formed from data collected after a treatment ("type i" samples);

Group b) Samples formed from data of zooids *per* colony changing behavior after treatment ("type ii" samples).

For both testing methods, the statistical test pipeline was conducted twice, *i.e.*, using two datasets (dataset 1: samples obtained from only null reactions; dataset 2: samples from both null and faint reactions). In regard to the zooids that changed their behavior after treatments (Testing method 2, Group b), two datasets were obtained considering zooids with a decreased intensity of reaction after treatment (dataset 1: from fast to null reaction; dataset 2: from fast to faint reaction, plus from faint to null reaction, plus from fast to null reaction) (see Supplementary Material 01).

Statistics were considered significant when the values were < 0.05.

RESULTS

Development of tentacles and velum and coronal organ organization

The coronal organ in *B. schlosseri* is located at the base of the oral siphon, on the ring of tentacles and velum (Fig. 1A-E). The thin epithelial fold that connects the tentacles is the velum. Both the tentacles and velum form during bud development from a thickened epithelium at the base of the oral siphon rudiment (Fig. 1F-K). During their differentiation, the oral siphon is closed. The two lateral tentacles are first recognizable in the early bud as small projections departing from the velum (Fig. 1F-G), successively; in mid-cycle, the ventral and the dorsal tentacles also became visible (Fig. 1H-I). These four tentacles represent the first order tentacles; later, four smaller

tentacles, belonging to the second order, form alternate to those of the first order (Fig. 1J-K). When the zooid is completely developed, the siphon opens and filtration begins: the tentacles reach their typical length and the coronal organ is fully differentiated (Fig. 2A-D).

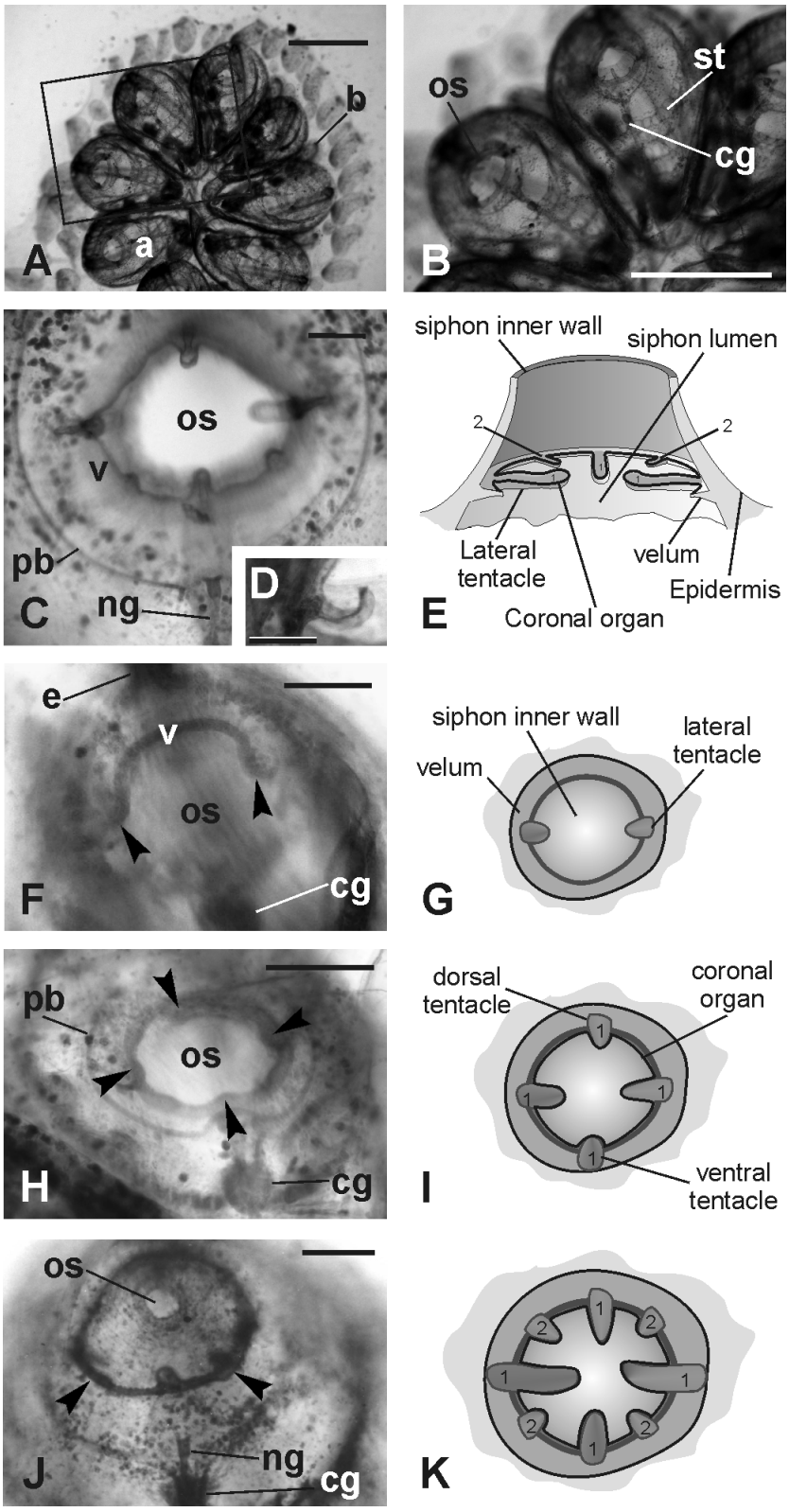

Fig. 1: Oral siphon development. Whole mounted colonies. **A-B**. Dorsal views of a colony in mid-cycle. The square area in A is enlarged in B to show the adult blastozooid organization. **C-D.** Oral siphon in an adult blastozooid in mid-cycle. The four first order tentacles and two of the second order tentacles are recognizable (the other two are out of focus). A thin velum (v) joins the tentacles. Note in D that the upper surface of the tentacle is spoon shaped. **E.** Schematic drawing of the oral siphon in adult blastozooid. **F-K.** Tentacles and velum development in buds; oral siphons closed. F, H, and J: whole mount specimens, dorsal view. G, I, and K: sketches of oral siphon rudiment (ventral view) corresponding to the stages shown in F, H, and I, respectively (*i.e.*, early, mid and late cycle buds, respectively). In F, lateral tentacles (arrowheads) and velum (v) are recognizable. In H, the four first order tentacles are visible (arrowheads). In J, two of the second order tentacles (arrowheads; 2 in K) are alternated with longer ones that belong to the first order (1). a: adult blastozooid; b: bud; cg: cerebral ganglion; ng: duct of the neural gland; os: oral siphon; pb: peripharyngeal band. Scale bars: A and B, 1 mm, C, D, F, H, and J, 100 μm.

Coronal organ differentiation

During early bud development, the oral siphon rudiment consists of two epithelial components: the outer component one is the epidermis; the inner component (called oral siphon inner epithelium) is a disk of tunic secreting cells facing the branchial chamber (Fig. 2E-F). The tunic represents a useful marker to distinguish the oral siphon inner epithelium from the adjacent cells of the forming branchial chamber. The oral siphon outer and the inner components approaches during bud development and eventually fuses together, permitting the siphon aperture. During siphon development, the two components are separated by the hemocoel in which hemocytes move and muscle cell precursors differentiate (Fig. 2 E-H). These precursors will form the sphincter muscle of the siphon (Degasperi et al., 2009). Posteriorly, the siphon rudiment is close to the neural complex rudiment. This is composed of the rudiments of a neural gland, which is opened into the branchial chamber by means of a duct, the dorsal organ and the cerebral ganglion.

The coronal sensory epithelium is derived from a ring of thickened epithelium that forms around the oral siphon inner epithelium. At the stage at which the heart begins beating (Fig. 2G-I), this epithelium (including the presumptive sensory area) forms from cylindrical cells resting on a basal lamina. Cells have a large nucleus with nucleolus and are rich in free ribosomes, whereas mitochondria and RER cisterns are rare. A thick glycocalyx covers the cell apical surface; the basal profile is smooth. Cells actively proliferate (Fig. 2I). At this stage, the first neurites close to the oral siphon rudiment are recognizable. With the localization of AchE, their path can be followed in detail (Fig.

2J). Nerves reach the oral siphon rudiment from a couple of primary nerves (anterior roots) emerging from the anterior cerebral ganglion. These two nerves, which divide repeatedly, are directed to the anterior tissues. Thin neurites at the base of the lateral tentacle rudiments are also visible (Fig. 2J), which form at this stage. TEM showed that small neurite sections are in the area of the forming coronal organ (Fig. 2I, inset).

At the mid-cycle stage, numerous neurites are close to the presumptive sensory area (Fig. 2K). The AchE reaction reveals the large pericoronal nerves encircling the siphon and located at the base of the peripharyngeal bands. Nerves split repeatedly into progressively smaller bundles, which eventually reach the numerous muscle fibers of the forming oral sphincter muscle and the differentiating coronal cells. The latter begin to emerge from the epithelium of the velum and tentacles (Fig. 2L-M) and are cylindrical, similar to the adjacent velum/tentacle cells, but they become recognizable for apical and basal features. Apically, sensory cells differentiate a cilium and some short stereovilli, both of which are surrounded by a fibrillary fuzzy coat, whereas the thick glycocalyx was no longer recognizable (Fig. 2L). Basally, the plasmalemma forms a slight groove into which neurites extend (Fig. 2L-M). Synaptogenesis occurs concurrently with coronal cell differentiation. The first synaptic contacts are both conventional contacts between neurites and sensory cells and contacts between adjacent neurites. Supporting cells are recognizable as C-shaped cells flanking and anchoring sensory cells. Apically, supporting cells exhibit a thick glycocalyx (inset in Fig. 2L) and partially cover the sensory cell apex, leaving only the area bearing the sensory hair bundle exposed to seawater. Basally, supporting cells limit the sensory cell groove in which the neurites are located.

In late bud, the velum is clearly recognizable as an epithelial fold at the base of the siphon, well separated by the close peripharyngeal band (Fig. 3A-B). The tunic covering the oral siphon inner epithelium extends to the velum. At this stage, the second order tentacles are formed, and tentacles begin to acquire a spoon shape. The coronal organ reaches the conventional adult configuration (Fig. 3C). Coronal sensory cells are cylindrical, with a round, large nucleus. Their cytoplasm has the features of differentiated cells: the Golgi apparatus is apical, with a field rich in vesicles; mitochondria are numerous; RER cisterns are close to the nuclear membrane; and some lipid droplets are recognizable (Fig. 3 D-E). The apical tuft is composed of numerous stereovilli filled with microfilaments, accompanying the cilium. The innervation pattern

increases in complexity. Sensory cell basal grooves are deeper than those in previous stages and contain more neurites (Fig. 3 F-G). The latter typically have microtubules, occasional mitochondria, and electron-dense vesicles (most likely neurotransmitter vesicles.

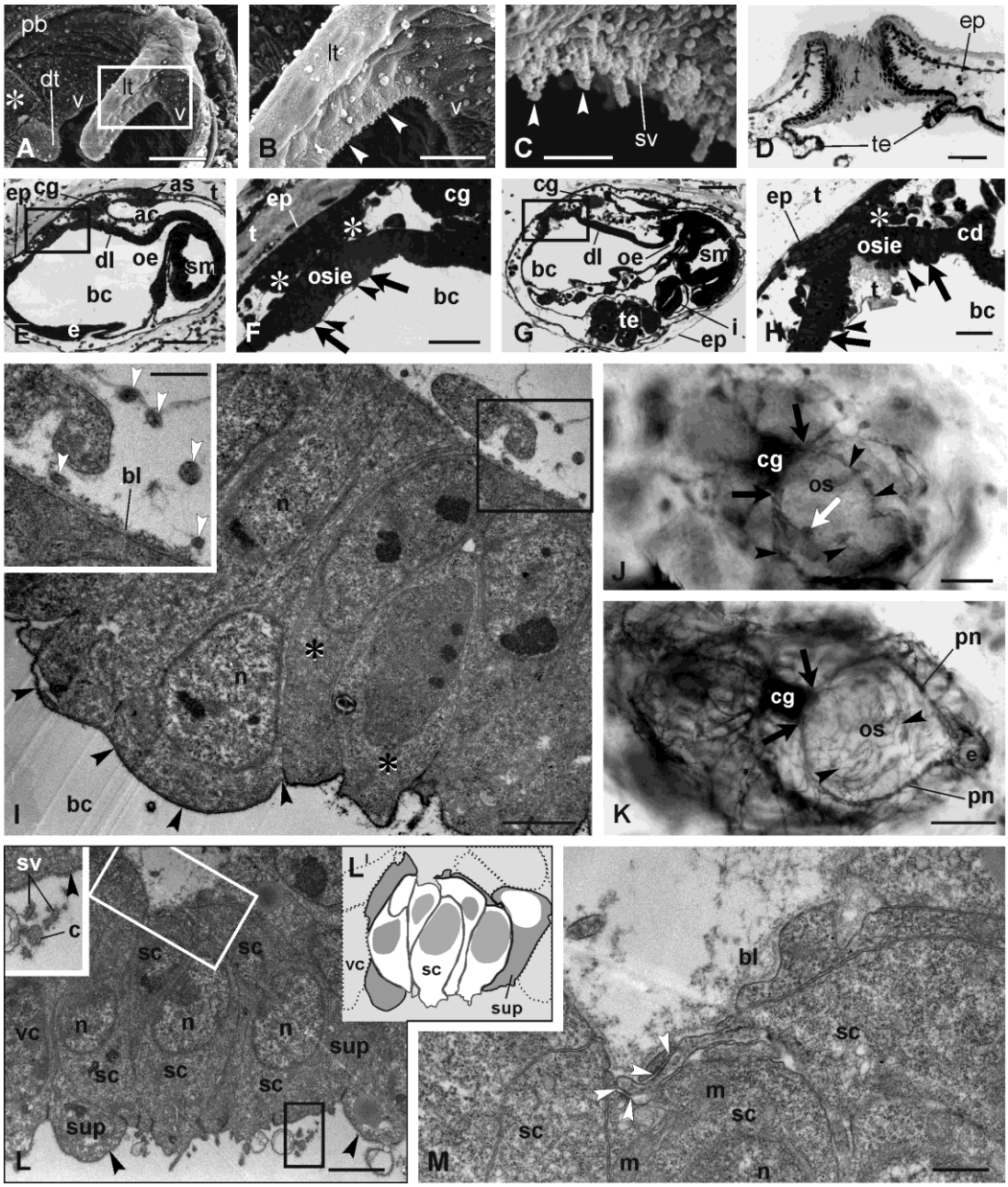

Fig. 2: Coronal organ in adult blastozooids and differentiation in early buds. **A-D**. Adult. A-C. SEM of part of the oral siphon viewed from the branchial chamber to show the coronal organ. The square area in A is enlarged in B. Arrowheads point to cilia of coronal sensory cells. Asterisk: ciliated area close to the dorsal tentacle (dt). D. Transverse section of an oral siphon; the tunic (t) lies on its inner side, partly covering the velum and tentacle (te) upper side. The section is tangential to the siphon wall so that the tunic appears to fill the siphon lumen. Toluidine blue. **E-H**. Sagittal medial sections of two early cycle buds at the beginning of the cycle (earlier stage in E-F). The square areas in E and G are enlarged in F and H, respectively, to show the details of the oral siphon rudiment. The oral siphon inner epithelium (osie, borders marked by arrowheads) and epidermis (ep) are covered by the tunic; asterisks: muscle cell precursors. Arrows: velum area. Toluidine blue. **I**. Mitotic cells (asterisks) within the velum/tentacles epithelium. Black arrowheads: thin tunic layer covering the apex of the oral siphon inner epithelium. The squared area is enlarged in the inset. White arrowheads: neurites close to the velum/tentacles area. TEM. **J-K**. Acetylcholinesterase reaction on a bud in early- (J) and mid-cycle (K) in dorsal view. Arrowheads: neurites reaching the oral siphon rudiment. The cerebral ganglion (cg) and nerves are marked. White arrow in J: forming right lateral tentacle marked by the acetylcholinesterase reaction. Black arrows: anterior nerve roots; pn: pericoronal nerves. Anterior at right-bottom. Whole mount bud. **L-M.** Detail of differentiating coronal cells in a mid-cycle bud. Oblique cut of the organ in L shows a few sensory cells (schematized in L^{I}; white cells: sensory cells; gray cells: supporting cells; dotted cells: velar cells). Black square, inset in L: stereovilli (sv) and a cilium (c) of a hair bundle, both of which are covered by the fibrillary fuzzy coat. Black arrowheads: thick glycocalyx cover supporting (sup) and velar (vc) cells. Sensory cells lack the covering. In M, the basal groove is enlarged with neurites (white square in L). White arrowheads: first recognizable synaptic contacts. ac: atrial chamber; as: atrial siphon; bc: branchial chamber; bl: basal lamina; cd: ciliated duct of the neural gland; dl: dorsal lamina; dt: dorsal tentacle; e: endostyle; ep: epidermis; i: intestine; lt: lateral tentacle; m: mitochondrion; n: nucleus; oe: esophagus; os: oral siphon; sc: sensory cell; sm: stomach; te: testis lobule; v: velum. Scale bars: A, D, and E, 50 µm; B, F, and G, 20 µm; C, I, and L, 2 µm; H, 5 µm; I (inset), 1 µm; J and K, 100 µm; M, 500 nm.

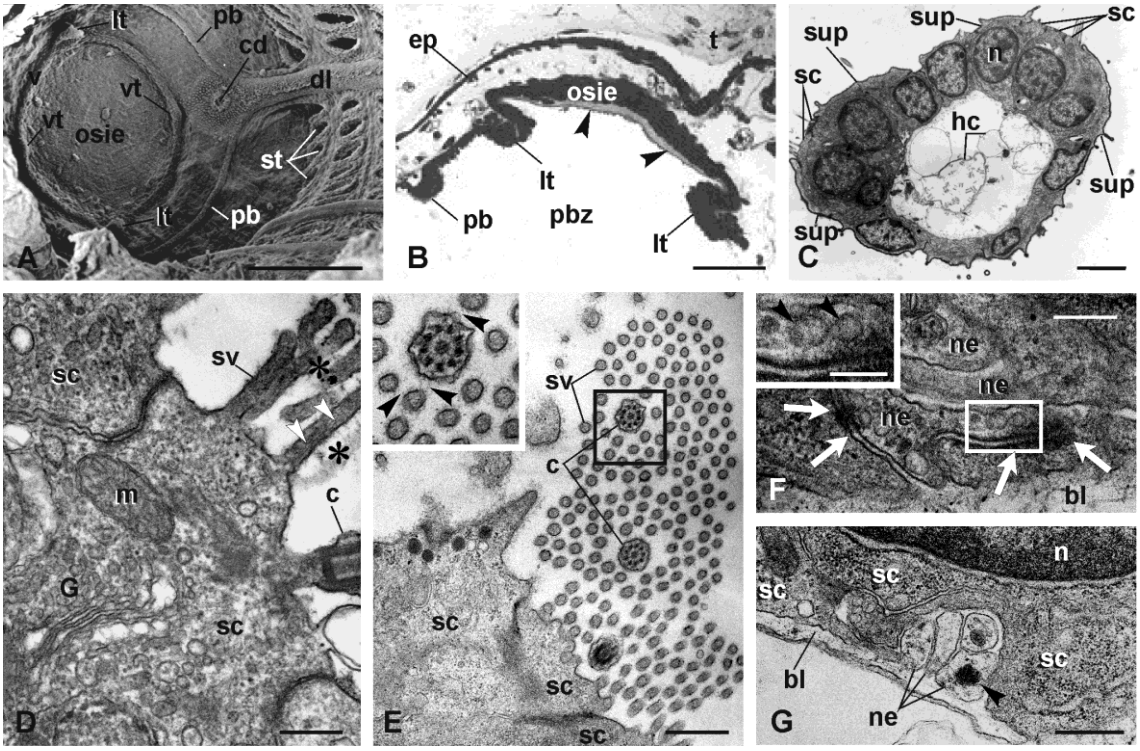

Fig. 3: Coronal organ differentiation in mid bud**. A**. SEM of the oral siphon rudiment viewed from the branchial chamber. The siphon is closed. The peripharyngeal band (pb) marks the border between the anterior prebranchial zone and posterior branchial zone of the pharynx. Developing velum (v) and first order tentacles are visible (lt: the two lateral ones; dt: the dorsal one; vt: the ventral one). cd: ciliated duct aperture of the neural gland; dl: dorsal lamina. Stigmata (st) are perforated. **B.** Transverse section of the oral siphon rudiment showing the relationships between the two lateral tentacles (lt), the peripharyngeal band (pb) and the oral siphon rudiment. Arrowheads: tunic produced by the oral siphon inner epithelium (osie). Toluidine blue. **C.** Transverse section of a tentacle belonging to a bud at a more advanced stage than that shown in A-B. Note the slightly spoon-shaped upper surface facing the inflowing seawater (upper, left). hc: hemocytes in the blood sinus. TEM. **D-E.** Details of the sensory bundle, cut longitudinally in D, transversely in E. Stereovilli and cilium are linked to one another by the fibrillary fuzzy coat (asterisks in D, black arrowheads in inset of E). White arrowheads in D: microfilaments in stereovilli. TEM. **F-G.** Details of sensory cell basal grooves containing neurites (ne) separated from the hemocoel by the basal lamina (bl). Some synaptic contacts are recognizable (white arrows in F). Some vescicles (arrowheads) are within neurites (enlarged in inset in F). TEM. Other symbols as in Fig. 2. Scale bars: A, 100 µm; B, 50 µm; C, 3 µm; D and F, 300 nm; inset in F: 150; E and G, 600 nm.

Morphological and sensorial effects of gentamicin and/or fenofibrate treatments on the coronal organ

SEM was used to investigate the morphology of the coronal organ of adult zooids in colonies treated with gentamicin compared with that of control colonies. Control colonies showed the typical coronal arrangement of a continuous ciliary row (see Fig. 2A-C), whereas in treated colonies, the continuity of this row was altered with scattered interruptions (Fig. 4A).

The three primary types of zooid reaction (fast, faint and null) were usually observed both in control and treated colonies.

Because some null and faint reactions could be due to some possible errors in touching and/or individual variation in sensitivity, the statistical test pipeline was conducted twice. The significance of the test was always confirmed in the two pipelines, except in a case of the two-sample comparisons (*i.e.*, fenofibrate followed by gentamicin treatment). The results of the statistical analyses are described below and are shown in Figure 4 B-C only for datasets with null plus faint reactions. Further details on the analyses can be found in Supplementary Materials 02-03.

The comparison before and after treatment with gentamicin for 24 h at 0.65 mg/ml indicated no significant effect on the behavioral response to the TST. By contrast, a double concentration of gentamicin (1.3 mg/ml) for the same period significantly increased the absence of the squirting reaction (Fig. 4B). To exclude that a 24 h treatment could overwhelm the protective effect of the fenofibrate pre-treatment, we tested reduced periods of gentamicin treatment. No effect was recorded in zooids from two colonies treated for 1 h at 2.6 mg/ml (data not shown), whereas a significantly altered behavior was observed after treatment for 2 h at 2 mg/ml (Fig. 4B).

The treatment with 50 µM fenofibrate for 45 min, followed by gentamicin at 2 mg/ml for 2 h, resulted in no significant effect on the TST, considering only null reaction data (Supplementary material 03), but a slight significance was recorded ($0.04 < p\text{-value} < 0.05$) when null and faint reactions were grouped together (Fig. 4 B). Finally, treatment with only fenofibrate did not affect zooid behavior.

ANOVAs and post-hoc tests showed that the results of treatments with fenofibrate and fenofibrate followed by gentamicin were not significantly different, and these two treatments were not different from the control. Additionally, the tests indicated that both

gentamicin treatments strongly affected the reaction to the TST compared with that of the other treatments and the control (Fig. 4C). Finally, the gentamicin treatment at 1.3 mg/ml for 24 h increased the absence of a fast reaction to the TST compared with that of the 2 mg/ml for 2 h treatment, but with strong significance only when the samples were compared with data from zooids that changed behavior after treatments (see Supplementary Materials 03).

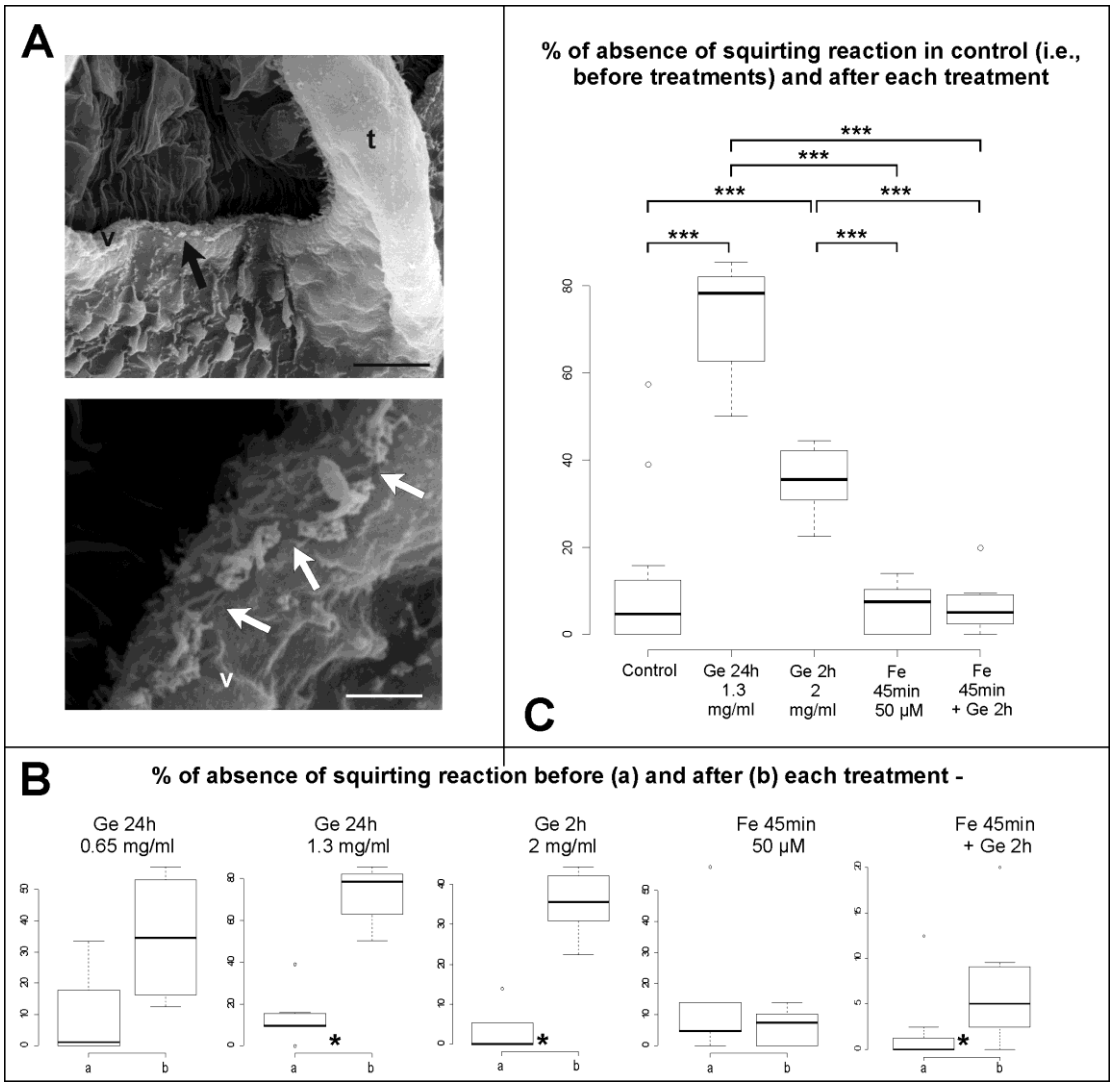

Fig. 4.: Gentamicin-induced morphological and mechanosensorial impairments on coronal organ. **A**. Colonies treated with gentamicin. SEM of part of the oral siphon viewed from the branchial chamber to show the coronal organ on the velum (v) and tentacles (t). Arrows point to some discontinuity of coronal apical tufts. **B-C**. Boxplots of datasets for the following: (B) comparison of means for two samples of paired data (before and after each single treatment) and (C) ANOVA and post-hoc test among treated samples (samples obtained from data after each treatment) and control (a sample obtained from all data before treatment). Boxplots from the datasets obtained from null plus faint reactions are shown. Ge: gentamicin, Fe: fenofibrate. Asterisks denote significance in the comparisons between samples as follow: * < 0.05, ** < 0.01, *** < 0.001. Scale bars in A: 10 μm (upper) and 2 μm (lower).

DISCUSSION

Coronal sensory cells of tunicates are considered to be putatively homologous to vertebrate hair cells based on recognized relationships at developmental, molecular, and morphological levels (Burighel et al., 2008, 2011; Gasparini, Caicci, et al., 2013; Gasparini, Degasperi, et al., 2013; Rigon et al., 2018).In this study, new information on coronal organ cytodifferentiation during asexual reproduction, which is associated with evidence on the morphological and mechanosensorial impairment caused by gentamicin, reinforces this hypothesis.

Coronal organ and innervation pattern development in blastozooids

In this study, we followed the coronal morphogenetic events during *B. schlosseri* asexual development. Differentiation of the organ was studied in sexual development in another species, *Ciona robusta*, previously called *Ciona intestinalis* type A (Brunetti et al., 2015; Pennati et al., 2015), in which differentiation occurs during metamorphosis and in early juveniles (Gasparini, Caicci, et al., 2013). Different from those of *B. schlosseri* buds, in *Ciona* early juvenile, coronal cells are morphologically recognizable before tentacle and velum development because of the precocious apical bundle appearance. Moreover, the bundle undergoes a deep rearrangement during differentiation, whereas in *B. schlosseri*, the bundle shows the definitive configuration as soon as it is recognizable.

In *Ciona* juveniles, mitoses are detected in both sensory and supporting cells (Gasparini, Caicci, et al., 2013). This finding suggests that the proliferative ability was found in the ancestors of both cell types but is now restricted to supporting cells in vertebrates and

limited in mammals to very small populations of multipotent stem/progenitor cells (Burns and Stone, 2017; Xu et al., 2017). Moreover, in *Ciona*, mitoses are hypothesized to sustain coronal organ elongation following the increase of the size and number of tentacles. This elongation is related to animal growth throughout its lifespan, which lasts several months.

In contrast to *Ciona*, *B. schlosseri* adult zooids have a shorter lifespan of few days and do not increase in size, either in tentacle number or length. Mitosis in *B. schlosseri* was recognized in early buds in the presumptive coronal organ territory but not in differentiated coronal cells. Additionally, in the congeneric *Botryllus primigenus* in which the proliferative activity was studied, mitoses were not specifically reported for the adult coronal organ (Kawamura et al., 2008). We hypothesized that the coronal proliferative ability decreases or ceases in botryllid differentiated coronal cells as an adaptation to their short cycle, which involves continuous regression and the formation of new individuals.

In *B. schlosseri*, neurites from the cerebral ganglion reached the presumptive coronal organ territory before coronal sensory cells were morphologically distinguishable. Although we could not exclude that neurites were involved in differentiating oral siphon muscle fibers, neurites within tentacle rudiments and their closeness to presumptive coronal cells strongly support a mutual relationship between coronal cells and associated brain sensory neurons during development. The precocious arrivals of neurites at differentiating organs has been observed in tunicates, also for coronal cells (Zaniolo et al., 2002; Gasparini, Caicci, et al., 2013): nerves spread among organs well before their cytodifferentiation and before the ganglion reaches its definitive configuration in terms of neuron number and nerves emanating from it. This nerve propagation apparently parallels development in mammal embryos (Elliott et al., 2017) in which segregation of afferent projections appears to develop before peripheral (hair cells) and central (cochlear nucleus neurons) target cell differentiation, although we do not know where the coronal sensory neurons are positioned in the cerebral ganglion nor when they become active. In this respect, both a precise neuronal map of the adult tunicate cerebral ganglion and a cell lineage analysis of sensory neurons would be very useful to refine the homology relationships between coronal sensory cells and vertebrate hair cells by including their sensory neurons.

Gentamicin impairs coronal sensory cells but fenofibrate prevents it

Gentamicin, like other aminoglycoside, is ototoxic, causing hair cell damage by first inducing disarray and disruption of the apical bundle followed by apoptosis (Huth et al., 2011). Research related to ototoxic effects of aminoglycosides primarily focuses on mammal vestibular hair cells, but the disruptive effect of these drugs on hair cells has also been demonstrated for fish lateral line mechanoreceptors (neuromasts) (Coffin et al., 2009; Fan et al., 2016) and electroreceptors (ampullary organs) (Fan et al., 2016). Despite some differences, the vertebrate vestibular and lateral line systems are considered to be two evolutionarily related sensory systems that share developmental, morphological, physiological, and molecular traits (Chagnaud et al., 2017). For this reason, the lateral line is currently used as a model to study both the normality of hair cells and pathophysiology of hearing defects because the position on the body surface simplifies experimental treatments *in vivo* (Whitfield, 2002) and the lateral line also grows after embryogenesis (Brignull et al., 2009). Similarly, the coronal organ is accessible and continuously formed throughout the lifespan. However, different from vertebrate hair cells, coronal sensory cells also form by non-self-renewal division (Gasparini, Caicci, et al., 2013) and during non-embryonic development (present work). In this respect, the coronal organ represents a suitable model for the study of the recovery of damaged secondary sensory cells. Moreover, statistical approaches take advantage of the experimental value of resorting colonial organisms for an appropriate analysis of out-coming data (Gasparini et al., 2014). Indeed, more than in isogenic strains, in *B. schlosseri*, each individual zooid in a colony is essentially a biological replicate that is not perturbed by intrinsic variables, as a clonal individual. Differences among individuals derive only from external perturbations (*e.g.*, experimental variations). Therefore, the statistically powerful results are strongly facilitated.

In this study, SEM analyses demonstrated for the first time the disruptive effect of gentamicin on this mechanoreceptor, showing a loss of coronal sensory cell continuity along the organ. Moreover, the TST on colonies after gentamicin correlated with the morphological analysis, demonstrating a significant decrease of the percentage of zooid with squirting response to the TST with respect to the same colonies before treatment. The treatment duration and concentration influenced animal responses. Therefore, these experiments suggested that the coronal organ not only has the same mechanosensorial

function as that of the lateral line/vestibular systems of vertebrates but has also a similar sensibility to gentamicin.

Fenofibrate is a peroxisome proliferator-activated receptor (PPAR) agonist. PPARs protect from reactive oxygen species (ROS) by increasing antioxidant enzymes in different tissues and organs (Yousefipour et al., 2010; Aleshin and Reiser, 2013; Ding et al., 2014). Fenofibrate was first recognized to protect kidneys from oxidative stress by increasing antioxidant enzymes, including catalase and superoxide dismutase (SOD)-1 (Hou et al., 2010). Recently, fenofibrate has been found to protect hair cells from gentamicin-induced toxicity, both in vestibular and lateral line systems of zebrafish (Park et al., 2017). In this study, we demonstrated that a loss in zooid squirting response did not occur when *B. schlosseri* colonies were preventively treated with fenofibrate, indicating a strong protective effect to coronal sensory cells, as occurs in vertebrate hair cells.

In conclusion, this investigation on coronal organ differentiation, function and induced damage during the asexual life cycle not only reinforces the hypothesized multi-level homology between secondary sensory cells in Vertebrata and its sister group Tunicata (Kocot et al., 2018) but also has an evo-devo relevance. The study allows us to gain insight into the depicted scenario of the co-option of both morphodynamic mechanisms and genetic pathways during the evolution of coloniality, which characterizes tunicates among chordates (Tiozzo et al., 2006; Gasparini et al., 2008, 2011; Gasparini, Degasperi, et al., 2013; Ricci et al., 2016).

FUNDING

This work was supported by grant the University of Padova - Progetti di Ricerca di Ateneo [Grant 2015 - CPDA153837] by LM.

ACKNOWLEDMENTS

The authors thank Mr. Filippo Ferraro for help in performing behavioral experiments.

REFERENCES

- Aleshin S., Reiser G. (2013). Role of the peroxisome proliferator-activated receptors (PPAR)-α, β/δ and γ triad in regulation of reactive oxygen species signaling in brain. Biol Chem 394:1553–70

- Brignull HR., Raible DW., Stone JS. (2009). Feathers and fins: non-mammalian models for hair cell regeneration. Brain Res 1277:12–23

- Brunetti R., Gissi C., Pennati R., Caicci F., Gasparini F., Manni L. (2015). Morphological evidence that the molecularly determined *Ciona intestinalis* type A and type B are different species: *Ciona robusta* and *Ciona intestinalis*. J Zoolog Syst Evol Res 53:186–93

- Brunetti R., Manni L., Mastrototaro F., Gissi C., Gasparini F. (2017). Fixation, description and DNA barcode of a neotype for *Botryllus schlosseri* (Pallas, 1766) (Tunicata, Ascidiacea). Zootaxa 4353:29–50

- Burighel P., Caicci F., Manni L. (2011). Hair cells in non-vertebrate models: lower chordates and molluscs. Hear Res 273:14–24

- Burighel P., Caicci F., Zaniolo G., Gasparini F., Degasperi V., Manni L. (2008). Does hair cell differentiation predate the vertebrate appearance? Brain Res Bull 75:331–34

- Burighel P., Lane NJ., Gasparini F., Tiozzo S., Zaniolo G., Carnevali MDC., Manni L. (2003). Novel, secondary sensory cell organ in ascidians: in search of the ancestor of the vertebrate lateral line. J Comp Neurol 461:236–49

- Burns JC., Stone JS. (2017). Development and regeneration of vestibular hair cells in mammals. Semin Cell Dev Biol 65:96–105

- Caicci F., Degasperi V., Gasparini F., Zaniolo G., Del Favero M., Burighel P., Manni L. (2010). Variability of hair cells in the coronal organ of ascidians (Chordata, Tunicata). Can J Zool 88:567–78

- Caicci F., Gasparini F., Rigon F., Zaniolo G., Burighel P., Manni L. (2013). The oral sensory structures of Thaliacea (Tunicata) and consideration of the evolution of hair cells in Chordata. J Comp Neurol 521:2756–71

- Chagnaud BP., Engelmann J., Fritzsch B., Glover JC., Straka H. (2017). Sensing external and self-motion with hair cells: a comparison of the lateral line and vestibular systems from a developmental and evolutionary perspective. Brain Behav Evol 90:98–116

- Cima F., Ballarin L., Caicci F., Franchi N., Gasparini F., Rigon F., Schiavon F., Manni L. (2015). Life history and ecological genetics of the colonial ascidian *Botryllus schlosseri*. Zoologischer Anzeiger - A Journal of Comparative Zoology 257:54–70

- Cima F., Manni L., Basso G., Fortunato E., Accordi B., Schiavon F., Ballarin L. (2010). Hovering between death and life: natural apoptosis and phagocytes in the blastogenetic cycle of the colonial ascidian *Botryllus schlosseri*. Dev Comp Immunol 34:272–85

- Coffin AB., Reinhart KE., Owens KN., Raible DW., Rubel EW. (2009). Extracellular divalent cations modulate aminoglycoside-induced hair cell death in the zebrafish lateral line. Hear Res 253:42–51

- Dabdoub A., Fritzsch B., Popper AN., Fay RR (Eds.). (2016). The primary auditory neurons of the mammalian cochlea, Springer handbook of auditory research New York: Springer

- Degasperi V., Gasparini F., Shimeld SM., Sinigaglia C., Burighel P., Manni L. (2009). Muscle differentiation in a colonial ascidian: organisation, gene expression and evolutionary considerations. BMC Dev Biol 9:48

- Ding L., Cheng R., Hu Y., Takahashi Y., Jenkins AJ., Keech AC., Humphries KM., Gu X., Elliott MH., Xia X., Ma J-X. (2014). Peroxisome proliferator-activated receptor α protects capillary pericytes in the retina. Am J Pathol 184:2709–20

- Elliott KL., Kersigo J., Pan N., Jahan I., Fritzsch B. (2017). Spiral ganglion neuron projection development to the hindbrain in mice lacking peripheral and/or central target differentiation. Front Neural Circuits 11:25

- Fan C., Zou S., Wang J., Zhang B., Song J. (2016). Neomycin damage and regeneration of hair cells in both mechanoreceptor and electroreceptor lateral line organs of the larval Siberian sturgeon (*Acipenser baerii*). J Comp Neurol 524:1443–56

- Franchi N., Ballin F., Manni L., Schiavon F., Basso G., Ballarin L. (2016). Recurrent phagocytosis-induced apoptosis in the cyclical generation change of the compound ascidian *Botryllus schlosseri*. Dev Comp Immunol 62:8–16

- Fritzsch B., Elliott KL. (2017). Gene, cell, and organ multiplication drives inner ear evolution. Dev Biol 431:3–15

- Gans C., Northcutt RG. (1983). Neural crest and the origin of vertebrates: a new head. Science 220:268–73

- Gasparini F., Burighel P., Manni L., Zaniolo G. (2008). Vascular regeneration and angiogenic-like sprouting mechanism in a compound ascidian is similar to vertebrates. Evol Dev 10:591–605

- Gasparini F., Caicci F., Rigon F., Zaniolo G., Burighel P., Manni L. (2013). Cytodifferentiation of hair cells during the development of a basal chordate. Hear Res 304:188–99

- Gasparini F., Caicci F., Rigon F., Zaniolo G., Manni L. (2014). Testing an unusual in vivo vessel network model: a method to study angiogenesis in the colonial tunicate *Botryllus schlosseri*. Sci Rep 4:6460

- Gasparini F., Degasperi V., Shimeld SM., Burighel P., Manni L. (2013). Evolutionary conservation of the placodal transcriptional network during sexual and asexual development in chordates. Dev Dyn 242:752–66

- Gasparini F., Manni L., Cima F., Zaniolo G., Burighel P., Caicci F., Franchi N., Schiavon F., Rigon F., Campagna D., Ballarin L. (2015). Sexual and asexual reproduction in the colonial ascidian *Botryllus schlosseri*. Genesis 53:105–20

- Gasparini F., Shimeld SM., Ruffoni E., Burighel P., Manni L. (2011). Expression of a Musashi-like gene in sexual and asexual development of the colonial chordate *Botryllus schlosseri* and phylogenetic analysis of the protein group. J Exp Zool B Mol Dev Evol 316:562–73

- Hou X., Shen YH., Li C., Wang F., Zhang C., Bu P., Zhang Y. (2010). PPARalpha agonist fenofibrate protects the kidney from hypertensive injury in spontaneously hypertensive rats via inhibition of oxidative stress and MAPK activity. Biochem Biophys Res Commun 394:653–59

- Huth ME., Ricci AJ., Cheng AG. (2011). Mechanisms of aminoglycoside ototoxicity and targets of hair cell protection. Int J Otolaryngol 2011:937861

- Kawamura K., Tachibana M., Sunanaga T. (2008). Cell proliferation dynamics of somatic and germline tissues during zooidal life span in the colonial tunicate *Botryllus primigenus*. Dev Dyn 237:1812–25

- Kocot KM., Tassia MG., Halanych KM., Swalla BJ. (2018). Phylogenomics offers resolution of major tunicate relationships. Mol Phylogenet Evol 121:166–73

- Mackie GO., Burighel P., Caicci F., Manni L. (2006). Innervation of ascidian siphons and their responses to stimulation. Can J Zool 84:1146–62

- Manni L., Burighel P. (2006). Common and divergent pathways in alternative developmental processes of ascidians. Bioessays 28:902–12

- Manni L., Gasparini F., Hotta K., Ishizuka KJ., Ricci L., Tiozzo S., Voskoboynik A., Dauga D. (2014). Ontology for the asexual development and anatomy of the colonial chordate *Botryllus schlosseri*. PLoS ONE 9:e96434

- Manni L., Lane NJ., Burighel P., Zaniolo G. (2001). Are neural crest and placodes exclusive to vertebrates? Evolution & Development 3:297–98

- Manni L., Zaniolo G., Cima F., Burighel P., Ballarin L. (2007). *Botryllus schlosseri*: a model ascidian for the study of asexual reproduction. Dev Dyn 236:335–52

- Northcutt RG., Gans C. (1983). The genesis of neural crest and epidermal placodes: a reinterpretation of vertebrate origins. Q Rev Biol 58:1–28

- Park C., Ji HM., Kim SJ., Kil SH., Lee JN., Kwak S., Choe SK., Park R. (2017). Fenofibrate exerts protective effects against gentamicin-induced toxicity in cochlear hair cells by activating antioxidant enzymes. Int J Mol Med 39:960–68

- Patthey C., Schlosser G., Shimeld SM. (2014). The evolutionary history of vertebrate cranial placodes--I: cell type evolution. Dev Biol 389:82–97

- Pennati R., Ficetola GF., Brunetti R., Caicci F., Gasparini F., Griggio F., Sato A., Stach T., Kaul-Strehlow S., Gissi C., Manni L. (2015). Morphological differences between larvae of the *Ciona intestinalis* species complex: hints for a valid taxonomic definition of distinct species. PLoS ONE 10:e0122879

- Pohlert T. (2014). The pairwise multiple comparison of mean ranks package (PMCMR). R package http://CRANR-project.org/package=PMCMR 27

- R Core Team. (2017). R: a language and environment for statistical computing. R Foundation for statistical Computing, Vienna, Austria http://wwwR-project.org/

- Ricci L., Chaurasia A., Lapébie P., Dru P., Helm RR., Copley RR., Tiozzo S. (2016). Identification of differentially expressed genes from multipotent epithelia at the onset of an asexual development. Sci Rep 6:27357

- Rigon F., Gasparini F., Shimeld SM., Candiani S., Manni L. (2018). Developmental signature, synaptic connectivity and neurotransmission are conserved between vertebrate hair cells and tunicate coronal cells. J Comp Neurol 526:957–71

- Rigon F., Stach T., Caicci F., Gasparini F., Burighel P., Manni L. (2013). Evolutionary diversification of secondary mechanoreceptor cells in tunicata. BMC Evol Biol 13:112

- Schlosser G., Patthey C., Shimeld SM. (2014). The evolutionary history of vertebrate cranial placodes II. Evolution of ectodermal patterning. Dev Biol 389:98–119

- Sienknecht UJ., Köppl C., Fritzsch B. (2014). Evolution and development of hair cell polarity and efferent function in the inner ear. Brain Behav Evol 83:150–61

- Tiozzo S., Ballarin L., Burighel P., Zaniolo G. (2006). Programmed cell death in vegetative development: apoptosis during the colonial life cycle of the ascidian *Botryllus schlosseri*. Tissue Cell 38:193–201

- Whitfield TT. (2002). Zebrafish as a model for hearing and deafness. J Neurobiol 53:157–71

- Xu J., Ueno H., Xu CY., Chen B., Weissman IL., Xu P-X. (2017). Identification of mouse cochlear progenitors that develop hair and supporting cells in the organ of Corti. Nat Commun 8:15046

- Yousefipour Z., Oyekan A., Newaz M. (2010). Interaction of oxidative stress, nitric oxide and peroxisome proliferator activated receptor gamma in acute renal failure. Pharmacol Ther 125:436–45

- Zaniolo G., Lane NJ., Burighel P., Manni L. (2002). Development of the motor nervous system in ascidians. J Comp Neurol 443:124–35

SUPPLEMENTARY MATERIAL 01
Samples used in R for statistical analyses.

The command lines to load the data are in red.

Data on the behavioral response were grouped in samples of percentages as follow:
Type i) zooids per colony with a lack of the squirting reaction before treatment, and zooids per colony with a lack of the squirting reaction after treatment;
Type ii) zooids per colony that changed behavior after the treatment.

Categories of reactions of a zooid to the tentacle stimulation test (TST):
i) squirting behavior (i.e., fast)
ii) faint and anomalous reaction (i.e., faint)
iii) not perceptible reaction (i.e., null)

Each statistical test pipeline (see Supplementary Material 02) was conducted twice, *i.e.*, using two datasets (dataset 1: samples obtained from only null reactions; dataset 2: samples from both null and faint reactions). In regard to the zooids that changed their behavior after treatments, the two datasets were obtained considering zooids with a decreased intensity of reaction after treatment (dataset 1: from fast to null reaction; dataset 2: from fast to faint reaction, plus from fast to faint reaction, plus from faint to null reaction, plus from fast to null reaction).

"Type i" samples
 # % of zooids per *colony with absence of squirting reaction*

 # GENTAMICIN TREATMENTS

```
## [24h at 0.65mg/ml]

### Dataset 1 (null reaction)
#### before treatment
Bs_CorOrg_971_Null_preGent24h05ml <- scan()
0 0 0 0.1

#### after treatment
Bs_CorOrg_971_Null_postGent24h05ml <- scan()
10 22.22 16.67 2.5


### Dataset 2 (not fast reactions: null + faint)
#### before treatment
```

```
Bs_CorOrg_971_NotFast_preGent24h05ml <- scan()
0 0 33.33 2.38

#### after treatment
Bs_CorOrg_971_NotFast_postGent24h05ml <- scan()
20 48.89 57.14 12.5
```

```
## [24h at 1.3mg/ml]
### Dataset 1 (null reaction)
#### before treatment
Bs_CorOrg_971_Null_preGent24h1ml <- scan()
0 0 2.44 0 2.38 0 0 2.27

#### after treatment
Bs_CorOrg_971_Null_postGent24h1ml <- scan()
38.1 46.34 39.02 25 51.28 48.78 22.5 47.73
```

```
### Dataset 2 (not fast reactions: null + faint)
#### before treatment
Bs_CorOrg_971_NotFast_preGent24h1ml <- scan()
9.52 14.63 39.02 9.09 9.52 0 10 15.91

#### after treatment
Bs_CorOrg_971_NotFast_postGent24h1ml <- scan()
80.95 85.37 82.93 52.27 76.92 73.17 50 79.55
```

```
## [2h at 2mg/ml]
### Dataset 1 (null reaction)
#### before treatment
Bs_CorOrg_971_Null_preGent2h2mg <- scan()
4.65 0 0 0 0 0

#### after treatment
Bs_CorOrg_971_Null_postGent2h2mg <- scan()
22.73 9.52 13.33 9.3 5 22.22
```

```
### Dataset 2 (not fast reactions: null + faint)
#### before treatment
Bs_CorOrg_971_NotFast_preGent2h2mg <- scan()
13.95 0 0 0 0 5.26

#### after treatment
Bs_CorOrg_971_NotFast_postGent2h2mg <- scan()
38.64 30.95 42.22 32.56 22.5 44.44
```

```
                    # FENOFIBRATE TREATMENT [45min at 50µM]

### Dataset 1 (null reaction)
#### before treatment
Bs_CorOrg_971_Null_preFen45m005ml <- scan()
0 2.33 15 0 2.33

#### after treatment
Bs_CorOrg_971_Null_postFen45m005ml <- scan()
0 0 5.6 0 0
```

```
### Dataset 2 (not fast reactions: null + faint)
#### before treatment
Bs_CorOrg_971_NotFast_preFen45m005ml <- scan()
0 4.65 57.5 4.55 13.95

#### after treatment
Bs_CorOrg_971_NotFast_postFen45m005ml <- scan()
0 10.26 13.9 0 7.5
```

 # FENOFIBRATE* [45min at 50µM] *followed by GENTAMICIN* [2h at 2mg/ml] *TREATMENT

Dataset 1 (null reaction)
before treatment
```
Bs_CorOrg_971_Null_preGentPlusFen <- scan()
0 0 0 0 0 2.5 0
```

after treatment
```
Bs_CorOrg_971_Null_postGentPlusFen <- scan()
0.1 0 0 0 0 0 0
```

Dataset 2 (not fast reactions: null + faint)
before treatment
```
Bs_CorOrg_971_NotFast_preGentPlusFen <- scan()
12.5 0 0 0 0 2.5 0
```

after treatment
```
Bs_CorOrg_971_NotFast_postGentPlusFen <- scan()
20 5 0 0 8.7 4.9 9.52
```

 # "BEFORE TREATEMENT" MERGED DATA

Dataset 1 (null reaction)
```
Bs_CorOrg_971_Null_PosContr <- scan()
0 0 2.44 0 2.38 0 0
4.65 0 0 0 0 0
0 2.33 15 0 2.33
0 0 0 0 0 2.5 0
```

Dataset 2 (not fast reactions: null + faint)
```
Bs_CorOrg_971_NotFast_PosContr <- scan()
9.52 14.63 39.02 9.09 9.52 0 10 15.91
13.95 0 0 0 0 5.26
0 4.65 57.5 4.55 13.95
12.5 0 0 0 0 2.5 0
```

"Type ii" samples
 # % of zooids per *colony changing behavior after the treatment*

Dataset 1 (from fast to null reaction)
gentamicin [24h at 1.3mg/ml] treatment
```
Bs_CorOrg_971_NullFromFast_Gent24h1ml <- scan()
35.71 43.9 24.39 20.45 48.72 48.78 20 43.18
```

gentamicin [2h at 2mg/ml] treatment
```
Bs_CorOrg_971_NullFromFast_Gent2h2mg <- scan()
18.19 9.52 13.33 9.3 5 19.44
```

fenofibrate [45min at 50µm] treatment
```
Bs_CorOrg_971_NullFromFast_Fen45m005ml <- scan()
0 0 0 0 7.5
```

fenofibrate [45min at 50µM] followed by gentamicin [2h at 2mg/ml] treatment
```
Bs_CorOrg_971_NullFromFast_GentPlusFen <- scan()
0 0 0 0 0 0 0.1
```

Dataset 2 [(from fast to null) + (from fast to faint) + (from faint to null)]
gentamicin [24h at 1.3mg/ml] treatment
```
Bs_CorOrg_971_FastToNull_FaintToNull_FastToFaint_Gent24h1ml <- scan()
71.43 70.73 63.41 50 71.79 73.17 47.5 72.73
```

gentamicin [2h at 2mg/ml] treatment

```
Bs_CorOrg_971_FastToNull_FaintToNull_FastToFaint_Gent2h2mg <- scan()
38.64 30.95 42.22 32.56 22.5 41.67

### fenofibrate [45min at 50µm] treatment
Bs_CorOrg_971_FastToNull_FaintToNull_FastToFaint_Fen45m005ml <- scan()
0 0 0 7.5

### fenofibrate [45min at 50µM] followed by gentamicin [2h at 2mg/ml] treatment
Bs_CorOrg_971_FastToNull_FaintToNull_FastToFaint_GentPlusFen <- scan()
20 5 0 0 8.7 4.9 9.52
```

SUPPLEMENTARY MATERIAL 02

test procedures performed in R (the command lines are in red)

Categories of reactions of a zooid to the tentacle stimulation test (TST):

i) squirting behavior (*i.e.*, fast)

ii) faint and anomalous reaction (*i.e.*, faint)

iii) not perceptible reaction (*i.e.*, null)

The testing methods applied were the following:

Testing method 1) Comparison of the means of two samples of paired data (before and after each single treatment) ("type i" samples, see Supplementary Material 01);

Testing method 2) ANOVA and post-hoc test using two different groups of samples:

Group a) A sample formed from data collected before treatments, and other samples formed from data collected after a treatment ("type i" samples).

Group b) Samples formed from data of zooids per colony changing behavior after treatment ("type ii," see Supplementary Material 01).

Each statistical test pipeline was conducted twice, *i.e.*, using two datasets (dataset 1: samples obtained from only null reactions; dataset 2: samples from both null and faint reactions) (see Supplementary Material 01). In regard to the zooids that changed their behavior after the treatments (Testing method 2, Group b), two datasets were obtained considering zooids with a decreased intensity of reaction after treatment (dataset 1: from fast to null reaction; dataset 2: from fast to faint reaction, plus from faint to null reaction, plus from fast to null reaction).

```
# 1) Comparison of the means for two samples for paired
     data (before and after each single treatment)

                              # GENTAMICIN TREATMENTS

                          ## GENTAMICIN [24h at 0.65mg/ml]
### Dataset 1 (null reaction)

      shapiro.test(Bs_CorOrg_971_Null_preGent24h05ml)      # Result p-value = 0.001241
(**)
      shapiro.test(Bs_CorOrg_971_Null_postGent24h05ml)     # Result p-value = 0.9461

      fligner.test                                                 # Result p-value =
```

```
0.02349 (*)

        wilcox.test

                # Result                        Wilcoxon signed rank test
                # Result                       V = 0, p-value = 0.06789
```

Dataset 2 (not fast reactions: null + faint)

```
        shapiro.test(Bs_CorOrg_971_NotFast_preGent24h05ml)   # Result p-value = 0.006754
(**)
        shapiro.test(Bs_CorOrg_971_NotFast_postGent24h05ml)  # Result p-value = 0.386

        fligner.test                                                        # Result p-
value = 0.424

        wilcox.test

                # Result                        Wilcoxon signed rank test
                # Result                       V = 0, p-value = 0.06789
```

GENTAMICIN [24h at 1.3mg/ml]

Dataset 1 (null reaction)

```
        shapiro.test(Bs_CorOrg_971_Null_preGent24h1ml)       # Result p-value = 0.000745
(***)
        shapiro.test(Bs_CorOrg_971_Null_postGent24h1ml)      # Result p-value = 0.1515

        fligner.test                                                # Result p-value =
0.001328 (*)

        wilcox.test

                # Result                        Wilcoxon signed rank test
                # Result                       V = 0, p-value = 0.01172 (*)
```

Dataset 2 (not fast reactions: null + faint)

```
        shapiro.test(Bs_CorOrg_971_NotFast_preGent24h1ml)    # Result p-value = 0.02124
(*)
        shapiro.test(Bs_CorOrg_971_NotFast_postGent24h1ml)   # Result p-value = 0.02795
(*)

        fligner.test                                                        # Result p-
value = 0.5648

        wilcox.test

                # Result                        Wilcoxon signed rank test
                # Result                       V = 0, p-value = 0.01172 (*)
```

GENTAMICIN [2h at 2mg/ml]

Dataset 1 (null reaction)

```
        shapiro.test(Bs_CorOrg_971_Null_preGent2h2mg)        # Result p-value = 2.073e-05
(***)
        shapiro.test(Bs_CorOrg_971_Null_postGent2h2mg)       # Result p-value = 0.2912

        fligner.test(data_Bs_CorOrg, group_Bs_CorOrg)        # Result p-value = 0.01911
(*)

        wilcox.test

                # Result                        Wilcoxon signed rank test
                # Result                       V = 0, p-value = 0.02771 (*)
```

Dataset 2 (not fast reactions: null + faint)

```
        shapiro.test(Bs_CorOrg_971_NotFast_preGent2h2mg)             # Result p-value =
0.003662 (**)
        shapiro.test(Bs_CorOrg_971_NotFast_postGent2h2mg)    # Result p-value = 0.7625
```

```
        fligner.test                                                    # Result p-
value = 0.2879

        wilcox.test

                # Result                        Wilcoxon signed rank test
                # Result                       V = 0, p-value = 0.02771 (*)
```

 # FENOFIBRATE TREATMENT [45min at 50µM]

Dataset 1 (null reaction)

```
        shapiro.test(Bs_CorOrg_971_Null_preFen45m005ml)      # Result p-value = 0.009481
(**)
        shapiro.test(Bs_CorOrg_971_Null_postFen45m005ml)     # Result p-value = 0.000131
(***)

        fligner.test                                                  # Result       p-
value = 0.3094

        wilcox.test

                # Result                        Wilcoxon signed rank test
                # Result                       V = 6, p-value = 0.1025
```

Dataset 2 (not fast reactions: null + faint)

```
        shapiro.test(Bs_CorOrg_971_NotFast_preFen45m005ml)   # Result p-value = 0.01965
(*)
        shapiro.test(Bs_CorOrg_971_NotFast_postFen45m005ml)  # Result p-value = 0.3554

        fligner.test                                                    # Result p-
value = 0.6319

        wilcox.test

                # Result                        Wilcoxon signed rank test
                # Result                       V = 8, p-value = 0.2733
```

 # FENOFIBRATE [45min at 50µM] *followed by GENTAMICIN* [2h at 2mg/ml] *TREATMENT*

Dataset 1 (null reaction)

```
        shapiro.test(Bs_CorOrg_971_Null_preGentPlusFen)      # Result p-value = 4.136e-06
(***)
        shapiro.test(Bs_CorOrg_971_Null_postGentPlusFen)     # Result p-value = 4.136e-06
(***)

        fligner.test(data_Bs_CorOrg, group_Bs_CorOrg)        # Result       p-value =
0.8252

        wilcox.test

                # Result                        Wilcoxon signed rank test
                # Result                       V = 2, p-value = 0.6547
```

Dataset 2 (not fast reactions: null + faint)

```
        shapiro.test(Bs_CorOrg_971_NotFast_preGentPlusFen)   # Result p-value = 9.159e-05
(***)
        shapiro.test(Bs_CorOrg_971_NotFast_postGentPlusFen)  # Result p-value = 0.2574

        fligner.test(data_Bs_CorOrg, group_Bs_CorOrg)                # Result p-value =
0.0926

        wilcox.test

                # Result                        Wilcoxon signed rank test
                # Result                       V = 0, p-value = 0.04311 (*)
```

 # 2) ANOVA and post-hoc tests

 # a) among control (i.e., before treatments) and after each treatment

```
## a: control    [before treatments]
## b: gentamicin  [24h at 1.3mg/ml]
## c: gentamicin  [2h at 2mg/ml]
## d: fenofibrate [45min at 50µM]
## e: fenofibrate [45min at 50µM] + gentamicin [2h at 2mg/ml]
```

Dataset 1 (null reaction)

```
        fligner.test

                # Result              Fligner-Killeen:med chi-squared = 25.854, df = 4,
p-value = 3.386e-05 (***)

        kruskal.test

                # Result              Kruskal-Wallis chi-squared = 35.82, df = 4, p-value
= 3.152e-07 (***)

        posthoc.kruskal.conover.test

#                       Pairwise comparisons using Conover's-test for multiple
#                                    comparisons of independent samples
#
#               a       b       c       d
#             b 1.1e-10 -       -       -
#             c 5.4e-06 0.70463 -       -
#             d 1.00000 3.6e-07 0.00038 -
#             e 1.00000 4.3e-09 1.4e-05 1.00000
#
#             P value adjustment method: bonferroni
#             Warning message:
#             In posthoc.kruskal.conover.test.default(data_Null, group_Null,  :
#               Ties are present. Quantiles were corrected for ties.
#
```

Dataset 2 (not fast reactions: null + faint)

```
        fligner.test

                # Result              Fligner-Killeen:med chi-squared = 1.0722, df = 4,
p-value = 0.8987

        kruskal.test

                # Result              Kruskal-Wallis chi-squared = 29.222, df = 4, p-
value = 7.047e-06 (***)

        posthoc.kruskal.conover.test

#                       Pairwise comparisons using Conover's-test for multiple
#                                    comparisons of independent samples
#
#             data:  data_NotFast and group_NotFast
#
#               a       b       c       d
#             b 1.1e-07 -       -       -
#             c 0.00075 1.00000 -       -
#             d 1.00000 0.00011 0.01966 -
#             e 1.00000 2.5e-05 0.01035 1.00000
#
#             P value adjustment method: bonferroni
#             Warning message:
#             In posthoc.kruskal.conover.test.default(data_NotFast, group_NotFast,  :
#               Ties are present. Quantiles were corrected for ties.
```

 # b) % of zooids per colony changing behavior after treatments

```
## a: gentamicin  [24h at 1.3mg/ml]
## b: gentamicin  [2h at 2mg/ml]
## c: fenofibrate [45min at 50µM]
## d: fenofibrate [45min at 50µM] + gentamicin [2h at 2mg/ml]
```

Dataset 1 (from fast to null reaction)

```
        shapiro.test(Bs_CorOrg_971_NullFromFast_Gent24h1ml)         # Result p-value =
0.09852
        shapiro.test(Bs_CorOrg_971_NullFromFast_Gent2h2mg)          # Result p-value =
0.6391
        shapiro.test(Bs_CorOrg_971_NullFromFast_Fen45m005ml)        # Result p-value =
0.000131 (***)
        shapiro.test(Bs_CorOrg_971_NullFromFast_GentPlusFen)        # Result p-value =
4.136e-06

        fligner.test

                # Result              Fligner-Killeen:med chi-squared = 16.179, df = 3,
p-value = 0.001042     (**)

        kruskal.test

                # Result              Kruskal-Wallis chi-squared = 21.079, df = 3, p-
value = 5.056e-05             (***)

        posthoc.kruskal.conover.test

#                       Pairwise comparisons using Conover's-test for multiple
#                                       comparisons of independent samples
#
#               data:  data_NullFromFast and group_NullFromFast
#
#                 a       b       c
#               b 0.00014 -       -
#               c 1.4e-09 8.9e-05 -
#               d 9.5e-11 8.6e-06 1.00000
#
#               P value adjustment method: bonferroni
#               Warning message:
#               In posthoc.kruskal.conover.test.default(data_NullFromFast,
group_NullFromFast,  :
#                 Ties are present. Quantiles were corrected for ties.
```

decreasing reaction dataset [(from fast to null) + (from fast to faint) + (from faint to null)]

```
        shapiro.test(Bs_CorOrg_971_FastToNull_FaintToNull_FastToFaint_Gent24h1ml)  #
Result p-value = 0.00862 (**)
        shapiro.test(Bs_CorOrg_971_FastToNull_FaintToNull_FastToFaint_Gent2h2mg)   #
Result p-value = 0.4613
        shapiro.test(Bs_CorOrg_971_FastToNull_FaintToNull_FastToFaint_Fen45m005ml) #
Result p-value = 0.001241 (**)
        shapiro.test(Bs_CorOrg_971_FastToNull_FaintToNull_FastToFaint_GentPlusFen) #
Result p-value = 0.2574

        fligner.test

                # Result              Fligner-Killeen:med chi-squared = 2.7868, df = 3,
p-value = 0.4257

        kruskal.test

                # Result              Kruskal-Wallis chi-squared = 21.079, df = 3, p-
value = 8.733e-05 (***)

        posthoc.kruskal.conover.test

#                       Pairwise comparisons using Conover's-test for multiple
#                                       comparisons of independent samples
#
#               data:  data_FastToNull_FaintToNull_FastToFaint and
```

```
group_FastToNull_FaintToNull_FastToFaint
#
#                a       b       c
#              b 0.00035 -       -
#              c 2.5e-09 2.6e-05 -
#              d 2.8e-09 0.00022 0.62596
#
#              P value adjustment method: bonferroni
#              Warning message:
#              In
posthoc.kruskal.conover.test.default(data_FastToNull_FaintToNull_FastToFaint,
group_FastToNull_FaintToNull_FastToFaint,  :
#                Ties are present. Quantiles were corrected for ties.
```

SUPPLEMENTARY MATERIAL 03

Boxplots of datasets for the following: **A)** comparison of the means for two samples of paired data (before and after each single treatment), **B)** ANOVAs and post-hoc tests among a control (sample formed from all data before treatment) and samples formed from data collected after treatments, **C)** ANOVAs and post-hoc tests among samples formed from data of zooids per colony changing behavior after treatment. Each test pipeline was conducted twice, i.e., using two datasets (dataset 1: samples obtained from only null reactions; dataset 2: samples obtained from both null and faint reactions). In regard to the zooids that changed their behavior after the treatments, in C, two data ets were obtained considering zooids with a decreased intensity of reaction after treatment (dataset 1: from fast to null reaction; dataset 2: from fast to faint reaction, plus from faint to null reaction, plus from fast to null reaction). Ge: gentamicin, Fe: fenofibrate. Asterisks denote significance in the comparisons between samples as follow: * < 0.05, ** < 0.01, *** < 0.001.

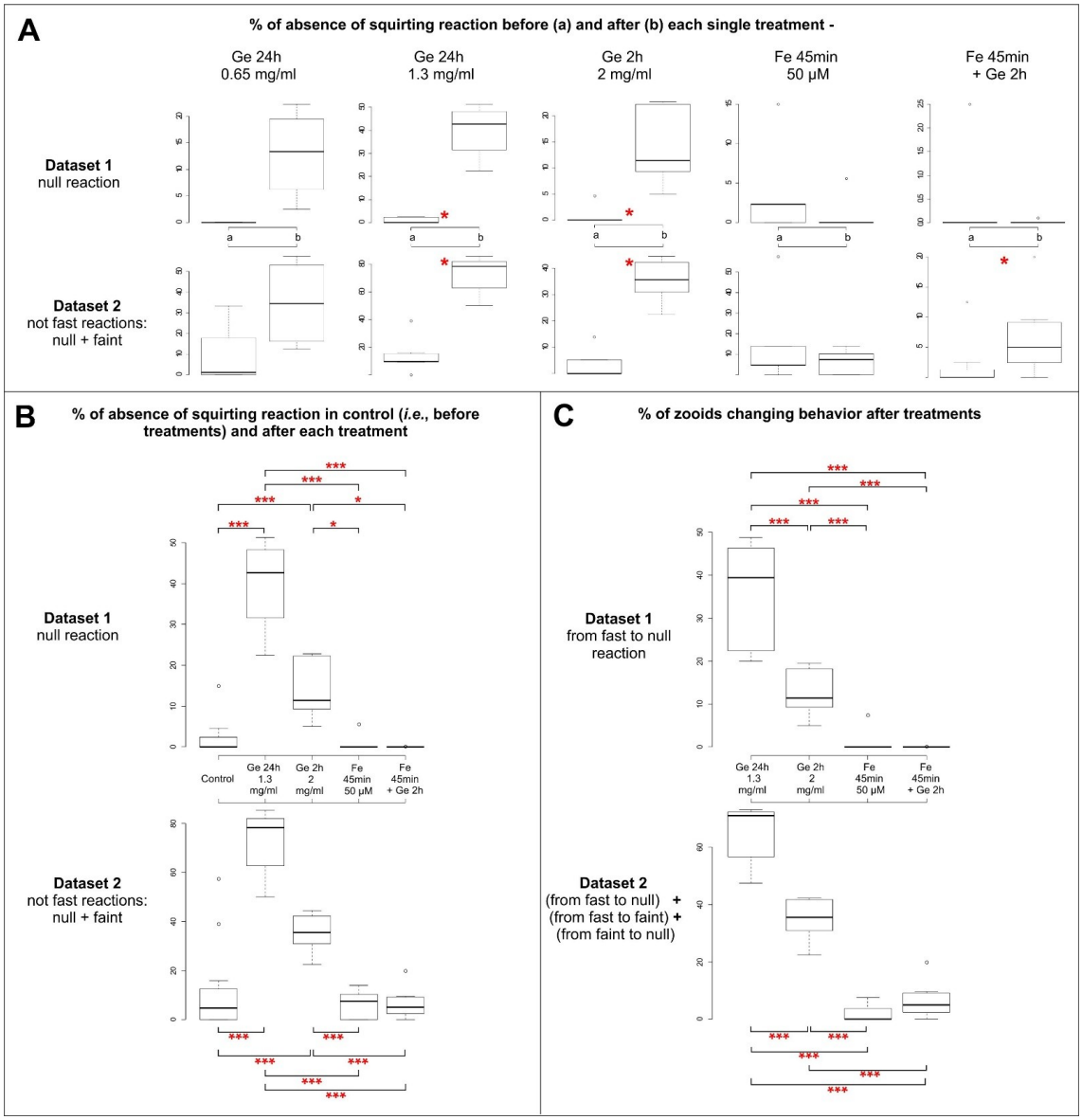
A
% of absence of squirting reaction before (a) and after (b) each single treatment -
Ge 24h 0.65 mg/ml
Ge 24h 1.3 mg/ml
Ge 2h 2 mg/ml
Fe 45min 50 µM
Fe 45min + Ge 2h
Dataset 1 null reaction
Dataset 2 not fast reactions: null + faint
a
b
B
% of absence of squirting reaction in control (i.e., before treatments) and after each treatment
Dataset 1 null reaction
Dataset 2 not fast reactions: null + faint
Control
Ge 24h 1.3 mg/ml
Ge 2h 2 mg/ml
Fe 45min 50 µM
Fe 45min + Ge 2h
C
% of zooids changing behavior after treatments
Dataset 1 from fast to null reaction
Dataset 2 (from fast to null) + (from fast to faint) + (from faint to null)

CONCLUSION

This doctoral research aimed to investigate the nervous and sensory system of the colonial ascidian *Botryllus schlosseri* during the development of embryos, buds, and in adult individuals belonging to young and old colonies.

Overall, I can summarize the results in the following points:

- 60 years of experimental study on *B. schlosseri* were reviewed and synthesized, analysing data published in Italian language studies during the 1950s and 1960s of that are not readily available to many researchers. I believe that the knowledge gained, as well as the methods and databases developed, throughout the years, render this animal an excellent model for the study of stem cell mediated regenerative processes, development, chimerism, and senescence. I suggest that recent technological advancements (*i.e*. modern molecular and gene manipulation techniques) could be used to productively investigate fundamental biological problems.
- I compared the development of the nervous system in the two different pathways, *i.e*. embryogenesis and blastogenesis. A method for culturing embryos was developed in order to study their development *in vitro*, producing the first description of the embryonic development of *B. schlosseri*, relying upon complementary information obtained from different technical approaches. The first 3D reconstructions of selected developmental stages were produced and transcriptomes for several stages of embryogenesis and blastogenesis, analysed considering the nervous system related genes, were sequenced. The molecular analyses well fitted the morphogenetic events during both the developmental pathways. I believe that the description of embryogenesis and the number of transcriptomes related to embryogenesis and blastogenesis represent an invaluable resource for future research.
- I showed that the central nervous system and sensory system change dynamically during the adult zooid life and during colony life. Surprisingly, the brain was found not stable in cell number. Cell number increases during the first phases of the cycle and then decreases before the brain is totally reabsorbed at takeover. This observation raises new questions about the presence of adult

neurogenesis and neurodegeneration. The relation between the brain and the others component of the neural complex (dorsal organ and neural gland) changes accordingly. These organs could have an active role in adult neurogenesis.

- The role of apoptosis plays in brain cell death was demonstrated during the entire blastogenetic cycle, not only during the takeover. A balance between brain cell death and neurogenesis could be responsible for the increase and subsequent decrease in brain cell number. Immunocytes around and within the cerebral ganglion were also investigated, finding that their number significantly increases during the cycle. This increase parallels an increase in the expression of genes associated with a kind of immunocyte, the morula cells. An important role during neurodegeneration has been hypothesize for immunocytes.
- Two behavioural experiments on *B. schlosseri* were performed for the first time: the siphon stimulation test and the tentacle stimulation test. These tests involved different sensory cells and different behavioural responses. Both indicated cyclical performance of individuals during the blastogenetic cycle, suggesting a possible correlation between the behavioural responses and the number of neurons in the brain. The highest responsiveness corresponds to the phase with the highest number of neurons and *vice versa*.
- This species was also found a useful model to analyse aging. This process of aging in *B. schlosseri* is relevant to the study of mammalian aging on account of the extensive number of brain genes homologue to human and mouse. Specifically, clear patterns of differentially expressed genes associated with 20 human neurodegenerative diseases were found in young and old colonies. Age-related phenotypes, namely a lower brain cell number, a lower sensory cell number, and decreased behavioural performances with respect to young colonies, were clearly documented in old colonies.
- Lastly, the blastogenetic development of the coronal cells, considered homologues to vertebrate hair cells, was documented together with both the morphological and mechanosensorial impairment caused by gentamicin. This investigation not only supports the hypothesized multi-level homology between secondary sensory cells in Vertebrata and its sister group, the Tunicata, but also has an evo-devo relevance. The study allows us to gain insight into the depicted scenario of the co-option of both morphodynamic mechanisms and genetic

pathways during the evolution of coloniality, which characterizes tunicates among chordates.

In conclusion, the research presented in this thesis show that *B. schlosseri* can be considered a useful model species to analyse both the development of the central nervous system and sensory system, and their degeneration as caused by drugs, metamorphosis, takeover, and aging. I believe that on account of its different developmental pathways, *B. schlosseri* allows interesting evolutionary comparison at morphological and molecular level that can help improve scientific understanding of the origin of the animal phenotype.

ACKNOWLEDGMENT

This period as PhD student has been a great experience for me, due to several reasons. First of all, I had the opportunity to work on some very interesting topics that really involved me improving many of my technical and non-technical skills. Secondly, not only my academic and scientific knowledge have increased, but my relationship within the researching group and team-work skills as well. Nevertheless, I grew up as a person, bettering day by day as a researcher, colleague, scientist also thank to the discussion and debate with great researchers, both during conferences and in our laboratory in Padua.

Therefore, I would like to thank the following people that, during last three years, helped me, being a great support for my work and my final thesis.

Immense and special gratitude goes to my supervisor Prof. Lucia Manni. She helped me all along my course of studies, research and my academic path with proficiency, availability and patience. I would like to thank her for passing down to me her passion for researching and the possibility she gave me to improve my knowledge in different universities as well. I thank her for having believed in me and my project.

Moreover, I would like to really thank Dr. Fabio Gasparini, with whom I shared much active work and for his help.

Furthermore, a sincere thank goes to the Ascidian Research Group in Padua, that shared their competences with me in order to better my thesis: Prof. Paolo Burighel, Prof. Giovanna Zaniolo, Prof. Loriano Ballarin, Prof. Francesca Cima and Dr. Federico Caicci (Electron Microscopy Service).

Appreciation goes to my PhD evaluators too. They stimulated me and helped me bettering my research: Prof. Elisa Greggio, Prof. Mauro Zordan and the whole College of the Science PhD School of Padova University.

A big thanks to all the students I worked with: Pierpaolo Sartori, Lisa Morin, Beatrice Meneghetti, Veronica Giusti, Arianna Targonato.

With deep gratitude, I would like to thank the Stanford groups of Prof. Weissman for their hospitality and the warm welcoming I received. In particular, thanks to Dr. Ayelet Voskoboynik and the great contribution she gave to my thesis, Mark Kowarsky for his accurate work, Kathi Ishizuka, Karla Palmeri and Dr. Benjamin Rosental.

Moreover, I would like to thank Dr. Kohji Hotta for sharing with me his results (in Chapter 2) and Prof. Hiroki Nishida, Prof. Joachim Kurtz and Dr. Thomas Stach for the helpful discussion I had with.

A kind thanks goes to Dr. Thomas Stach and Prof. Sebastian Shimeld with whom I worked before the PhD, and who's collaboration continues still.

A warm thanks to Tim and Isabella for helping me in the English revision.

Finally thanks to my beloved parents that always walked with me through out this experience.

FINAL REPORT OF ACTIVITIES

Period: 1 October 2015 – 30 September 2018

Cycle: 31 **Curriculum:** Cellular biology and physiology

PhD candidate: Anselmi Chiara

Supervisor: Manni Lucia

Publications (*Corresponding author):

Manni L., **Anselmi C.***, Burighel., Martini M., Gasparini F. 2018. Differentiation and induced sensorial alteration of the coronal organ in the asexual life of a Tunicate. Integr Comp Biol. doi: 10.1093/icb/icy044

Manni L., **Anselmi C**.*, Cima F., Gasparini F., Voskoboynik A., Martini M., Peronato A., Burighel P., Zaniolo G. Ballarin L. 2018. Sixty years of experimental studies on the blastogenesis of the colonial tunicate *Botryllus schlosseri.* Dev. Biol. https://doi.org/10.1016/j.ydbio.2018.09.009

Others publications (not related to PhD project):

Lara-Ramirez R., Perez-Gonzalez C., **Anselmi C**., Pattey C., Shimeld S. 2018. A Notch-regulated proliferative stem cell zone in the developing spinal cord is an ancestral vertebrate trait. Development. https://doi.org/10.1101/298877

Stach T., and **Anselmi C.** 2015. High-precision morphology: bifocal 4D-microscopy enables the comparison of detailed cell lineages of two chordate species separated for more than 525 million years. BMC biology, 13(1), 113. https://doi.org/10.1186/s12915-015-0218-1

Congresses:

Anselmi C., Kowarsky M., Gasparini F., Palmeri K., Ishizuka K., Martini M., Targonato A., Voskoboynik A., Manni L. An Evo-Devo approach to neurogenesis and neurodegeneration. European Evo-Devo Meeting. Galway (IRL). June 26-29 2018. INTERNATIONAL CONGRESS. Poster.

Anselmi C., Martini M., Targonato A., Gasparini F., Manni L. Cyclical neurogenesis and neurodegeneration in the colonial tunicate *Botryllus schlosseri*. GEI. L'Aquila. June 11-14 2018. NATIONAL CONGRESS. Oral communication.

Manni L., **Anselmi C.**, Pennati R., Mercurio S., Gasparini F. Development and function of secondary mechanoreceptor cells in tunicates. Annual Meeting of the Society for Integrative and Comparative Biology. San Francisco (CA-USA). January 3-7 2018. INTERNATIONAL CONGRESS.

Kowarsky M., Hotta, K., Manni L., **Anselmi C.**, Neff N., Ishizuka KJ., Palmeri KJ., Okamoto J., Quake SR., Weissman IL., Voskoboynik A. The molecular

signatures of development in *Botryllus schlosseri.* 9th International Tunicate Meeting. New York (USA) July 17-21, 2017. INTERNATIONAL CONGRESS. Poster.

Anselmi C., Hotta K., Kowarsky M., Manni L., Ishizuka KJ., Palmeri KJ., Quake SR., Weissman IL., Voskoboynik A. The *Botryllus schlosseri* embryogenesis timeline reveals heterochrony between solitary and colonial ascidian embryogenesis. 9th International Tunicate Meeting. New York (USA) July 17-21, 2017. INTERNATIONAL CONGRESS. Poster.

Anselmi C., Gasparini F., Manni L. Placodal, migratory piooner nerve cells contribute to brain growth during the adult phase of the invertebrate chordate *Botryllus schlosseri*. Neural Crest and Cranial Placodes Gordon Research Conference. Ventura (CA-USA) 5-10 February 2017. INTERNATIONAL CONGRESS. Poster.

Gasparini F., **Anselmi C**., Ballarini L., Manni L. "Regeneration and blastogenesis: successful strategies of survival in a colonial chordate". 1° Congresso Nazionale Congiunto SITE-UZI-SIB, Biodiversity: concepts, new tools and future challenges. 30 August - 2 September 2016, Università degli Studi di Milano Bicocca (IT). NATIONAL CONGRESS.

Manni L., **Anselmi C**., Gasparini F. "Environmental influences on the asexual development of the colonial ascidian *Botryllus schlosseri*". 1° Congresso Nazionale Congiunto SITE-UZI-SIB, Biodiversity: concepts, new tools and future challenges. 30 August - 2 September 2016, Università degli Studi di Milano Bicocca (IT). NATIONAL CONGRESS.

Anselmi C., Sartori P., Gasparini F., Manni L. "Insıde the brain of the colonial tunicate *Botryllus schlosseri*: when budding involves cyclical neurodegeneration". 1° Congresso Nazionale Congiunto SITE-UZI-SIB, Biodiversity: concepts, new tools and future challenges. 30 August - 2 September 2016, Università degli Studi di Milano Bicocca (IT). NATIONAL CONGRESS. Poster

Courses attended:

- Data analysis, manipulation and presentation in Biology: a primer in the use of R –Prof. Zordan
- Enhancing gender awareness in scientific research – Prof. Perini and Prof. Badaloni, Organizer: Prof. Manni
- Notes on Statistical analysis – Prof. Eidukevicious
- An eco-immunological approach to allorecognition – Prof. Kurtz, Organizer: Prof. Ballarin. 8h.
- Fund raising per la ricerca scientifica: quali opportunità?
- Basic of image analysis with Imagej. Prof. Argenton
- Stem cells of marine invertebrate: from basic research to innovative applications. March 9-10 2016, University of Padova. Workshop

Stays:

- Short-term scientific mission titled “Investigation on the developmental dynamics of stem cells during the blastogenesis of the colonial tunicates *Botryllus schlosseri*” at the Humboldt University (Berlin, DE) at the Thomas Stach’s laboratory, April 9-21 2018. Grant: COST ACTION CA16023 "MARISTEM Stem cells of marine/aquatic invertebrates: from basic research to innovative applications".
- Phd visiting student at Hopkins Marine Station (Stanford University, USA) in the Weissman laboratory, from February 15th to August 31st 2017. Fellowships: Fondazione Aldo Gini; Proposte di Cooperazione Internazionale-University of Padova

Teaching activities:

- Teaching Assistant in Laboratory of Comparative Anatomy at Padova University.
  November- December 2016-2017, and November-December 2017-2018